Ultrafast Electron Transfer in Solutions Studied by Picosecond Pulse Radiolysis

Jun Ma

NNT : 2015SACLS023

THESE DE DOCTORAT

DE L'UNIVERSITE PARIS-SACLAY
Préparée à l'Université Paris Sud

ÉCOLE DOCTORALE N°571
Sciences chimiques : molécules, matériaux, instrumentation et biosystèmes
Laboratoire de Chimie Physique (LCP)

Spécialité de doctorat : Chimie

Ultrafast Electron Transfer in Solutions Studied by Picosecond Pulse Radiolysis

Jun MA

Thèse présentée et soutenue à Orsay, le 9 Octobre 2015
Composition du Jury :

M. Yosuke Katsumura, Professeur, Japan Radioisotope Association, Rapporteur
M. Buntinx Guy, Université de Lille1, CNRS, Rapporteur
Mme Sophie Le Caer, Laboratoire de Radiolyse, CEA, Présidente du jury
M. Massoud Fattahi Vanani, Subatech Nantes, Examinateur
M. Mehran Mostafavi, Professeur, Université Paris-Sud, Directeur de thèse

Ultrafast Electron Transfer in Solutions Studied by Picosecond Pulse Radiolysis

Chapter 1 Introduction of Radiation Chemistry and Water Radiolysis

Chapter 2 Experimental Methodology: Picosecond Electron Pulse Radiolysis

Acknowledgements

Firstly, I would like to express my sincere gratitude to my advisor Prof. Mehran Mostafavi, for the continuous support of my Ph.D study and related research, for his patience, motivation, and immense knowledge. His guidance helped me in all the time of research and writing of this thesis. I could not have imagined having a better advisor and mentor for my Ph.D study.

Besides my advisor, I would like to thank Prof. Pascal Pernot, Prof. Pierre Archirel and Dr. Uli Schmidhammer, Dr. Abdel Karim EL OMAR for their strong support, collaboration and insightful encouragement for my Ph.D research. I really learnt a lot from their theoretical chemistry and optics physical knowledge.

I am also very grateful to Prof. Yosuke Kastumura, Prof. Buntinx Guy, Prof. Massoud FATTAHI VANANI and Prof. Sophie LE CAER for accepting the invitation to be the referees of my thesis.

My sincere thanks also goes to Prof. Jacqueline Belloni and Prof. Jean-Louis Marignier. Their personalities, curiosity to the science, the ways of doing research and great minds encouraged me to be a person like them.

I thank my fellow labmates Jean-Philippe, Audrey Gayral, Jeunesse Pierre, Anna Balcerzyk, and Furong Wang for the stimulating discussions, and for all the fun we have had in the last three years.

I take this opportunity to express gratitude to all of administration group in the lab for helping me focusing the research, they are Marie-Françoise Lecanu, Séverine Bourguignon, Anne Morel, Eve Ranvier

Last but not the least, I would like to thank my family: my parents for supporting me spiritually throughout writing this thesis and my life in general.

Chapter 1: An Introduction of Radiation Chemistry and Water Radiolysis

Chapter 1 An Introduction of radiation chemistry and water radiolysis

1.1 Introduction

Radiation chemistry is a subject that deals with the chemical changes induced by high energy radiation. The radiations usually used in radiation chemical studies are high energy photon (X−rays, γ rays) or charged particles (electrons, α particles, β particles, heavy ions *etc*)[1]. The energy of each particle in a high energy beam is much greater than the ionizing potential of a molecule. Thus they cause the ionizing of the medium in which they are absorbed, so they are also often named "ionizing radiation".

This "ionizing" makes radiation chemistry unique from photochemistry which concerns with the chemical effects caused by absorption of light. The light mainly refers to ultraviolet (200 nm to 400 nm), visible and infrared photon, whose preferred energies, in fact, are not usually aiming at knocking out an electron directly from a molecule but more interested in leading to the electronic or vibrational excitations of a molecule and its consequent processes *etc*. It also much differs from radiochemistry which is a subject of studying the chemical properties of radionuclides and reactions involving them and their isotopes.

In the action of charged particles or photon irradiation on condensed matter, it is instructive to consider several stages of overlapping time scales[1]. The stages, in ascending orders of time, are normally called the physical, physicochemical, chemical stages, biochemical and biological stages, respectively. Within each stage various events take place occupying their respective time scales. It is thus appeared that radiation chemistry "bridges" the radiation physical and biological stage. Similar to the role of chemistry played in science, radiation chemistry remains as a central disciple of the science when high energy radiation is present.

The subject of my thesis is to explore the ultrafast reactions occurring in solution using picosecond electron pulse radiolysis. The chemical events on the timescale of picoseconds or

sub-femtosecond actually are not far away from the initial stage, which is the process of energy transferred from incident high energy electrons into a liquid molecule. Therefore, the information on electron-liquid molecule collision and subsequent physicochemical effects, for example, on liquid water will be introduced in this chapter on the basis of many previous literatures and books.

1.2 Fundamental Processes in the Physical Stage

1.2.1 Interaction of radiation with matter

In the interaction of an incident particle with any molecules, there is an *inelastic* collision, where the kinetic energy of the particle is completely or partially transferred into the molecules. The way of radiation energy given to a molecule depends predominantly on the type of radiation[2,3]:

(1) Photon radiation (X-rays, γ rays, Extreme UV)

Three processes contribute to the absorption of energy from these photons; the (a) *Photoelectric effect*, *Compton scattering* and *pair production*.

Photoelectric effect-refers to the light that is mostly at photon energy < 0.1 MeV. In this case, one electron from an inner shell is ejected when it collides with a photon (**Figure 1.1**). The kinetic energy of the ejected electron (*T*) is equal to the photon energy (*hv*) minus the binding energy (ω) of the electron in the atom or molecule.

$$T = h\upsilon - \omega \tag{1.1}$$

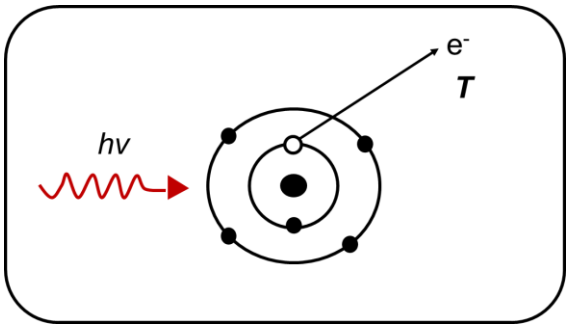

Figure 1.1 *Photoelectric absorption of photon hv by an inner electron shell of an atom.*

Compton effects become important for energies 0.1 MeV ~ 10 MeV. The photon collides with an electron and gives up part of its energy to the electron (**Figure 1.2**).

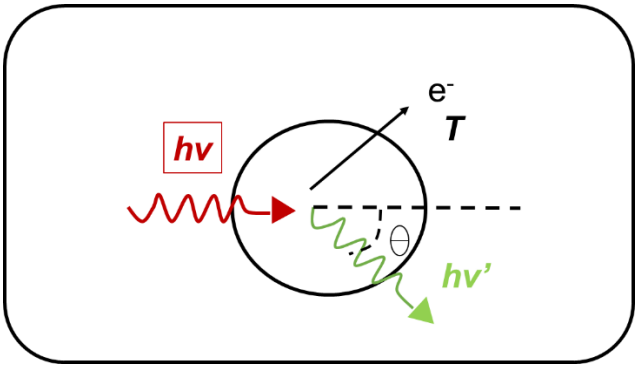

Figure 1.2 *Compton scattering of photon hv to photon hv' by an atom or a molecule.*

Pair production, in which an incident photon is absorbed when passing close to an atomic nucleus and a positron-electron pair is produced. Pair production occurs at very high energies and is unimportant compared with the two former processes in radiation chemistry.

(2) Charged Particles (electron, heavy ions and alpha particles)

Heavy charged particles lose energy mainly by inelastic collisions with electrons or secondary electron in their trajectory[2]. Other types of interactions are comparatively unimportant except at low energies where nuclear collisions and nuclear stopping are the dominant processes. A nuclear collision occurs when heavy charged particles interact with atomic nuclei. Emission of *Bremsstrahlung* takes place when the fast electron decelerated due to the coulomb interaction with molecular electron producing ionization and excitations[3].

1.2.3 Ionization and Excitation Phenomena

The fate of energy of fast charged particles or photon transferred to liquid, namely H_2O, is the ionization and excitation[1]. They have a common, raising the electronic level of an atom or molecule from its ground state to a state of higher energy.

The minimum energy *I* needed for ionization is called first ionization potential. (12.6 eV for H_2O, 15.8 eV for Ar). The *W* value is the average energy to produce a pair of ions in the medium. This value is commonly obtained through experimental measurements in which dividing the absorbed dose by the total number of ions. It varies with different molecule and the quality of radiation but normally two to three times higher than *I* value. For example the *W* value of H_2O is 30.5 eV which is 2.42 times higher than *I* of water (12.6 eV). The reasons for the additional energy required is that firstly, the production of excited states; second, the kinetic energy of ejected electron; and third, the removal of electrons with binding energy more than the minimum.

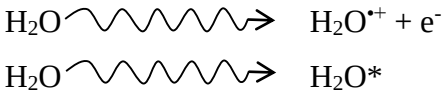

Excited states may be formed by many processes, typically (1) light absorption; (2) direct excitation by the impact of charged particle; (3) ion recombination; and other mechanism like chemical reaction or thermal process…

In radiolysis, the process (3) mentioned above plays a key role of producing the excited states. In water, the water excited states is mainly attributed from the recombination of the excess electron with water hole[4].

$$H_2O^{\bullet+} + e^-_{excess} \rightarrow H_2O^*.$$

Additionaly, the direct excitation by charged paricles (electron, heavy ions *etc*) also contributes electronic and vibartional excitation from the ground states. The latter excitation may have a very small cross section in this case but not negligiable. Although their total yield in radiolysis of water is small, several model of disscoiation are possible below the ionization threshold. The two models of disscoiation of excited states might gernerate $H^\bullet + OH^\bullet$ or $O^\bullet + H_2$.

$$H_2O^*_{vib.} \rightarrow H^\bullet + HO^\bullet$$

$$H_2O^*_{vib.} \rightarrow H_2 + O^\bullet\ (^1D)$$

$$H_2O^*_{vib.} \rightarrow 2H^\bullet + O^\bullet\ (^3P)$$

$$H_2O^*_{elec.} \rightarrow H^\bullet + HO^\bullet$$

$$H_2O^*_{elec.} \rightarrow H_2 + O^\bullet\ (^1D)$$

$$H_2O^*_{elec.} \rightarrow 2H^\bullet + O^\bullet\ (^3P)$$

1.3 Fundamental Processes in Physicochemical Stage

The earliest discernible time, in the physical stage, is obtained from the uncertainty principle corresponding the equation of $\Delta E\ \Delta t \sim h$, as $\sim 10^{-17}$s if we consider energy of the secondary electron is above 100 eV. Consequently, physicochemical processes in radiolysis which is a boundary stages between physical and chemistry have some significant features.

1.3.1 Track in liquids

The concept of spurs was developed to describe the events when the high energy particle passed through the liquids. It states that the ionizing events is, in fact, inhomogeneous and occur in clusters called spurs at the beginning. The distribution and evolution of spurs along the track could be very simplified as the pattern of a small stone (electron) skipping across on smooth surface of water pool. The "splashes" induced by "stone" are initially well-separated but as the elapse of the time the cycle rippers expand and eventually overlap with their neighbors to a homogenous distribution (see **Figure 1.3**)[5]. But this simple picture is not true in some cases. For instance, Fig.1.4 gives us a simulated track structure when the alpha particle comes into the water. The ionizing events occurs mainly around the trajectory axis of this incident radiation. Most of spurs are, however, not separated and the track has a cylinder structure. So, it is very important to learn that type of radiation or type particle would have a profound effect on the track structure and subsequent spur reactions as well.

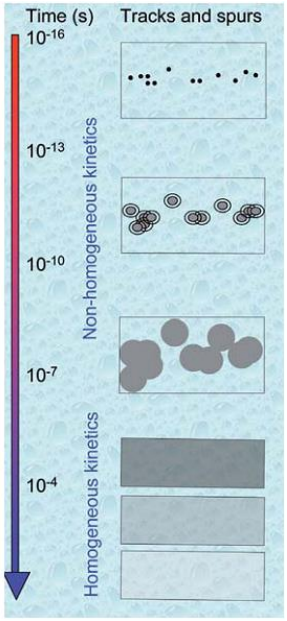

Figure 1.3 *Initial inhomogeneous spatial distribution of ionizing events and its evolution with time by diffusion and reactions until the formation homogenous distribution at* $\sim 10^{-7}$*s*[5]

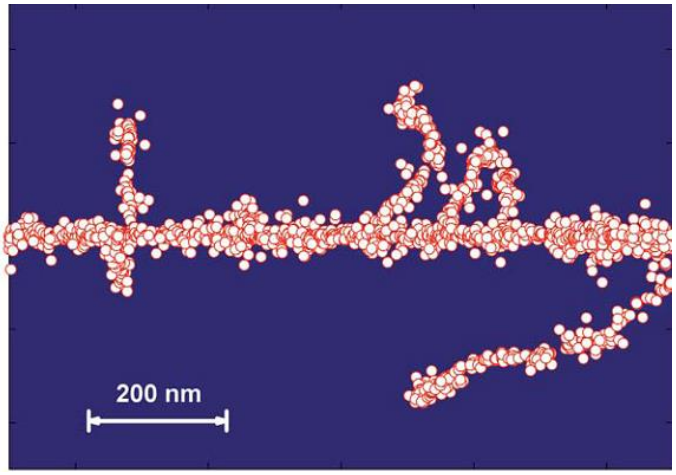

Figure 1.4 *Simulated ionization track due to an alpha ray of a few MeV of energy coming from the left side in the water continuum (blue). Each red cycle represent an ionizing event*[6].

1.2.2 Definition of LET

As mentioned above, the physical-chemical effect including the way of energy loss and track structure are strongly depending on the type of radiation and its energy. Historically, the term linear energy transfer (LET), keV μm^{-1}, was defined to help describe the local densities of energy transferred to the medium per unit length of particle track as expressed:

$$LET = -\left(\frac{dE}{dx}\right) \qquad (1.2)$$

The incident particle is characterized by plenty of physical parameters and the relation is illustrated below:

$$\beta = \sqrt{1-\left(\frac{Mc^2}{Mc^2+E}\right)} \qquad (1.3)$$

$$Z_{eff} = Z\left[1-\exp\left(125\beta Z^{\left(-\frac{2}{3}\right)}\right)\right] \qquad (1.4)$$

- Kinetic energy « E » ;
- Celerity « β » ;
- Effective charge « Z_{eff} ».
- M is the mass of incident ions ;

- Z is the atom number of incident ions ;
- c is the speed of light in vacuum.

The LET of photon or ion could be expressed as the equation of Bethe[1]:

$$\left(-\frac{dE}{dx}\right)_{ion} = \frac{4\pi e^4}{mc^2}\left(N_{target}Z_{target}\right)\left(\frac{Z_{eff}^2}{\beta^2}\right)\ln\frac{2mc^2\beta^2}{I} \qquad (1.5)$$

- m is the mass of electron ;
- e is the charge of electron,
- N_{target} is the atom density of the target;
- Z_{cible} is the atom number of the target;
- I is the average excitation potential of the target.

As shown in Figure 1.5, the amount of transient species and products of molecules is relied on the LET value[7]. With higher LET value such as alpha particles, due to the dense geometry of track formed by radiation, the initial spurs reaction become much fast and probability of recombination reactions of each species is accelerated to be higher.

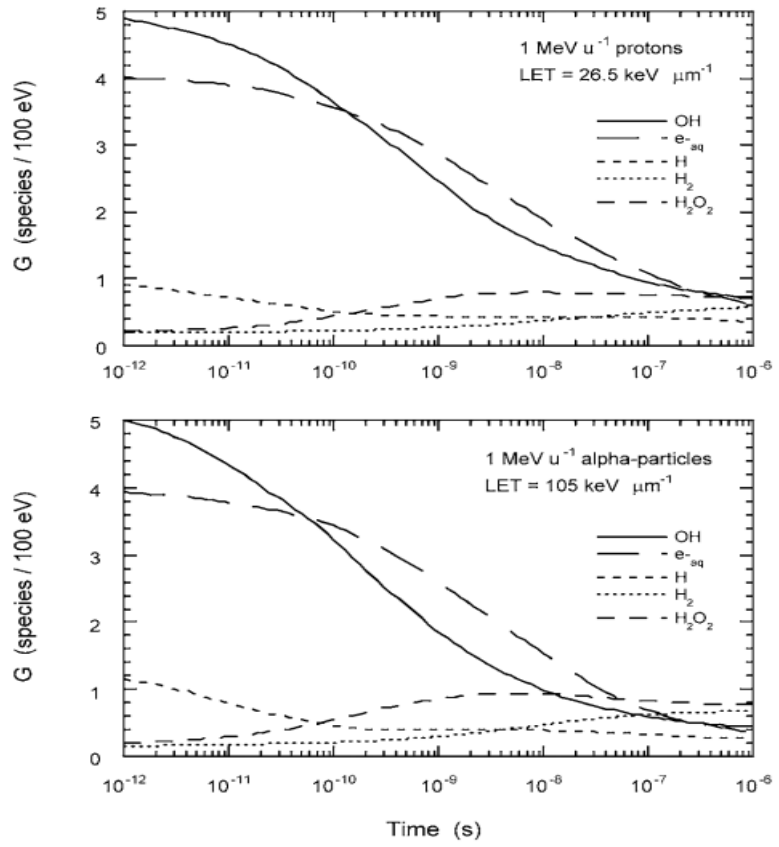

Figure 1.5 *Variation of radiolytic yield of species in water as a function of LET with different incident particles*[7].

1.3.2 Definition of Radiolytic yield

Radiolytic yield, $G_t(X)$, of transient species or products in liquids is a very important concept in the domain of radiation chemistry not only for fundamental interests of understanding chemical process but also constitutes a key parameter in nuclear reactors from a practice point of view. It is defined as the number of species formed or disappeared in the medium per unit absorbing energy at certain time (ps − ms) as followed:

$$G = \frac{\text{Number of species formed or disppeared}}{\text{100 eV absorbed}} \qquad (1.6)$$

Today, the commonly used unit of radiolytic yield is mol J^{-1}, and in the early literature the unit is more straightforward (molecules $(100\ eV)^{-1}$). They could be transferred into each other by:

$$1\ \text{molecule}\ (100\ eV)^{-1} = 1.036 \times 10^{-7}\ \text{mol}\ J^{-1}$$

For a given type of linear energy transfer (LET) corresponding to the type of ionizing radiation, the radiolytic yield is determinated by the time (t) after the energy deposited in the condensed medium.

$$G_t(X) = \frac{[X]_t}{\rho \times D} \qquad (1.7)$$

- $[X]_t$ is the concentration of species X (in mol L^{-1}) at a given time t ;
- ρ is the density of the solutions irradiated (in kg L^{-1}) ;
- D is the dose absorbed by the system (in J kg^{-1} or Gy).

According to the time stages, the radiolytic yield is often classified as three type:

(1) Initial radiolytic yield, which is noted as G°(X). This radiolytic yield refers to the yield of ions or excited states (X) in the end of physicochemical stage ~ 10^{-12} s. It is very difficult to measure directly this value.

(2) Primary radiolytic yield which is noted as g(X). g(X) is correspond to the transient species, radicals or molecules measured at the time when the homogenous distribution is achieved ~ 10^{-7} s after the passage of ionizing radiation. The value of g(X) is normally lower than G°(X) due to the spurs reactions.

(3) Global or apparent radiolytic yield which is noted as G(X). This yield represent some stable molecules which is measured using steady state method at relative longer time.

1.3.3 Solvation of electron in water

When the ionizing radiation deposits onto the liquid water, the electron is ejected from the parent molecule over certain length. Those with much high energy could further produce secondary electron. The electrons lose their kinetics energy in collision with surrounding water molecules. Because water has not electron affinity, the electron is able to undergo subsequently thermalization, relaxation, and reorganization of surrounding molecules and eventually they are becoming hydrated electron, the simplest reducing species.

Figure 1.6 *Schematic representation of the solvation of electron following water ionizing5.*

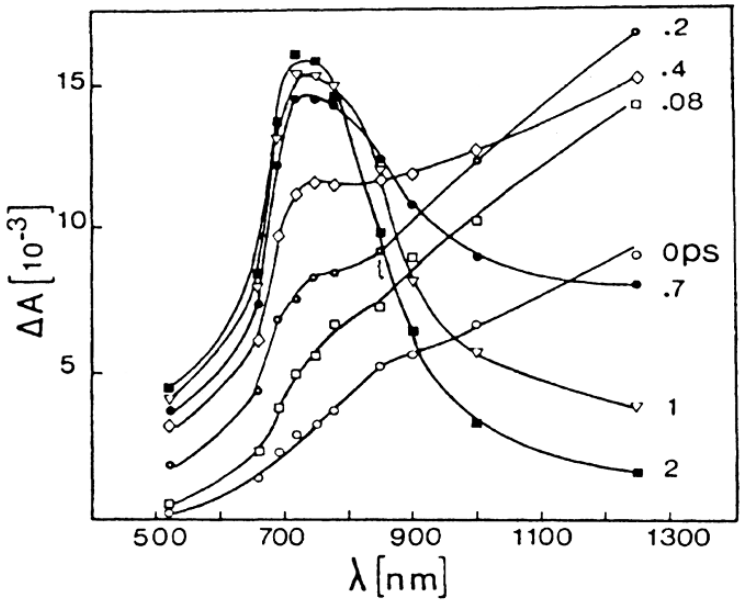

Figure. 1.7 *Time-dependent absorption spectrum of electron in water from photon-ionizing of liquid water at 21 °C[8].*

The solvation dynamic of electron was firstly studied using femtosecond pump probe method in the year of 1987[8], with better time resolution than that of pulse radiolysis. It showed the solvation process is complete in hundreds of femtoseconds and the precursors of hydrated electron absorb in the near infrared spectral domain (**Figure 1.7**). The continuous shift of absorption spectrum could be either interpreted as sequential stepwise relaxation cascades with each electron having its individual spectrum or solvent molecular reorientation around the electron as a function of dielectric relaxation time. Later, there have been tremendous work on the dynamic of electron solvation of relaxation using different time-resolved spectroscopy methods. [9,10,11,12]

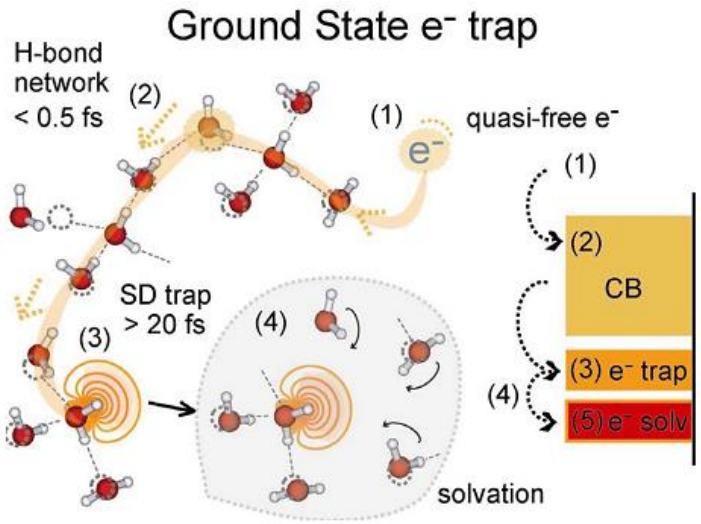

Figure 1.8 *Schematic diagram of electron trapping in liquid water: (1 & 2) an excess electron propagating along the H-bond network, (3) trapping at a weakly H-bonded OH group of a single-donor site followed by (4) electron solvation dynamics to reach the solvated electron (5)*[12]

It gradually came to clear that the quantum states of the hydrated electron consist of a localized *s* ground state, a three degenerate localized *p* state, and a delocalized conduction band (**Figure 1.8**). The generation of the *s* state involves multiply dynamics over a large temporal range: ultrafast librational dynamics (tens of femtoseconds, fs); localization of the electron in preexisting traps (100 fs); and solvation dynamics involving translational motion of surrounding water molecules.

It should be noted here that the ejected length and energy distribution of electron by high energy radiation (with energy rang from 1MeV-10 MeV) is not the same with that by photolysis (laser energy is below 50 eV). The way of energy deposition on the liquid is different. So, the relaxation of electron is supposed to have some unique features in radiolysis of water. But the

time resolution (electron pulse) of pulse radiolysis or heavy ions radiolysis is still limited us to address this issue by observing the changes of absorption bands or by other detection techniques.

1.4 Transient Species in Water radiolysis

The largest contribution of radiation induced chemical techniques to produce free radicals ($OH^{\bullet}$ $H^{\bullet}$ *etc*) have been made in liquid water because they provide a very convenient and clean way of generating a tremendous variety of highly reactive species (**Figure 1.8**). These species could not be produced by thermal or normal chemical method. In particular, pulse radiolysis is a well-established and this technique allows us to observe and study these short-lives transient species and the reactions not only between each other but also towards many other compounds (S).

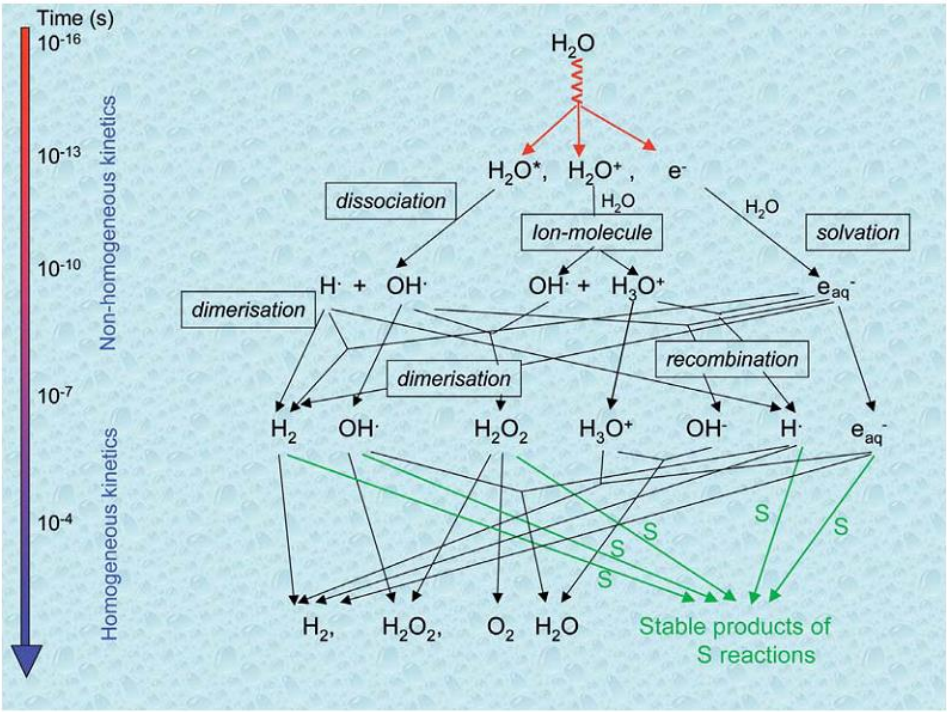

Figure 1.8 *Schematic representation of transient species produced by irradiation and their reactions with or without solutes*[5].

Here is a list of spurs reactions with the preferable rate constant values between the transient species induced by ionizing radiation. All of these reactions obey the second order reactions in neat water or diluted solutions. In pulse radiolysis coupled with optical detection system, the main absorbing species is hydrated electron because it has a very high molar extinction coefficient (ε_{715nm} = 19130 L mol^{-1} cm^{-1}) and broad spectrum range. In order to obtain more

information concerning the other species ($OH^{\bullet}$ $H^{\bullet}$ *etc*), scavenging method is commonly used not only to select a solute (N_2O) to react with electron, but also with other solutes converting the $OH^{\bullet}$ or $H^{\bullet}$ radicals into absorbing radicals for observation.

$e^-_{hyd} + H_3O^+ \rightarrow H^{\bullet} + H_2O$	$k_1 = 2.3 \times 10^{10}$ L mol^{-1} s^{-1}
$e^-_{hyd} + HO^{\bullet} \rightarrow HO^-$	$k_2 = 3.0 \times 10^{10}$ L mol^{-1} s^{-1}
$H_3O^+ + OH^- \rightarrow 2H_2O$	$k_3 = 14 \times 10^{10}$ L mol^{-1} s^{-1}
$e^-_{hyd} + e^-_{hyd} + 2H_2O \rightarrow H_2 + 2HO^-$	$k_4 = 1.1 \times 10^{10}$ L mol^{-1} s^{-1}
$e^-_{hyd} + H^{\bullet} + H_2O \rightarrow H_2 + HO^-$	$k_5 = 2.5 \times 10^{10}$ L mol^{-1} s^{-1}
$H^{\bullet} + H^{\bullet} \rightarrow H_2$	$k_6 = 1.55 \times 10^{10}$ L mol^{-1} s^{1}
$H^{\bullet} + HO^{\bullet} \rightarrow H_2O$	$k_7 = 1.5 \times 10^{10}$ L mol^{-1} s^{-1}
$HO^{\bullet} + HO^{\bullet} \rightarrow H_2O_2$	$k_8 = 1.1 \times 10^{10}$ L mol^{-1} s^{-1}
$e^-_{hyd} + H_2O_2 \rightarrow HO^{\bullet} + HO^-$	$k_9 = 1.1 \times 10^{10}$ L mol^{-1} s^{-1}
$e^-_{hyd} + S_1 \rightarrow P_1$	
$HO^{\bullet} + S_2 \rightarrow P_2$	
$e^-_{hyd} + P_2 \rightarrow S_2$	
$HO^{\bullet} + P_1 \rightarrow S_1 + HO^-$	

1.4.1 Hydrated electron

The first observation of hydrated electron was made in the year of 1962 using pulse radiolysis technique, by *Keene*, *Hart* and *Boag*[13,10] in different labs but almost at the same time (see **Fig.1.9**). The hydrated electron (e_{hyd}^-) display a very broad spectrum peaking around 715 nm with a long tail at higher energy. Since then the reactivity and nature picture of e_{hyd}^- has been a great issue both in experimental and theoretical interests. Theoretical simulations suggested that the absorption spectra observed is mainly attributed the transitions from *s* like ground states to three non- degenerate *p* like states[11]. The traditional cavity model can give us a picture that the electron is surrounded with four or six water molecules with different configurations even the model of e_{hyd}^- has been a very controversial issue.

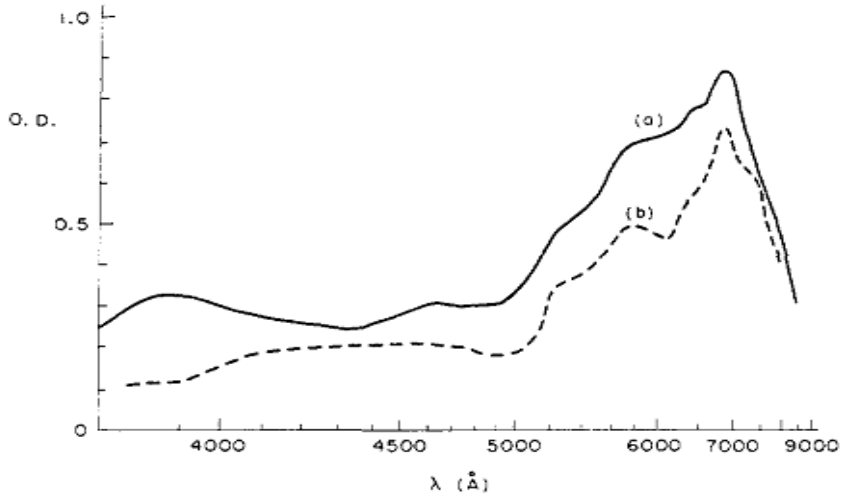

Figure 1.9 *First absorption spectrum of hydrated electron observed in sodium carbonate aqueous solution (0.05 mol L^{-1}) (a) and in neat water (b)*[14].

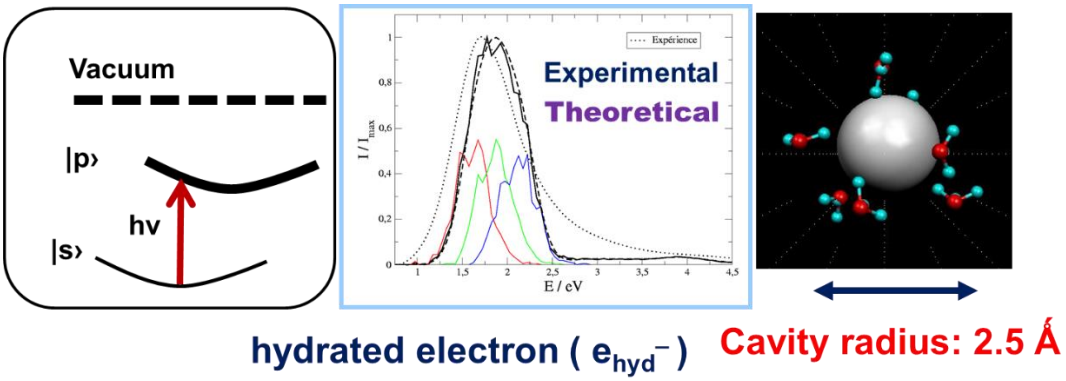

Figure 1.10 *Theoretical model of hydrated electron and simulation concerning the absorption spectrum*[15].

In pulse radiolysis, the radiolytic yield of hydrated electron is determined based on the absorbance in the spectrum either by direct observation or chemical dosimetry. The equation below is the most basic one for calculating the yield:

$$A(t) = \varepsilon \times l \times c(t) = \varepsilon \times l \times \rho \times D \times G(t) \quad (1.8)$$

- l: is the optical path in the sample cell in cm ;
- ρ: is the electron density of solutions in kg L^{-1} ;
- D: is the dose absorbed by the solution, in Gy;
- ε: is the molar extinction coefficient of hydrated electron.

Therefore, it can been seen that the ε is an important parameter in precisely determining the *G* value of e_{hyd}^-. **Fig. 1.11** give the ε value of hydrated electron at different wavelengths. The maximum ε value is at 715 nm with the value of ε_{715nm} = 19130 L mol^{-1} cm^{-1} at ambient temperature[16,17]. Even this classic ε value is on the debate[18,19], but it is taken in my thesis for analysis particular for the dose.

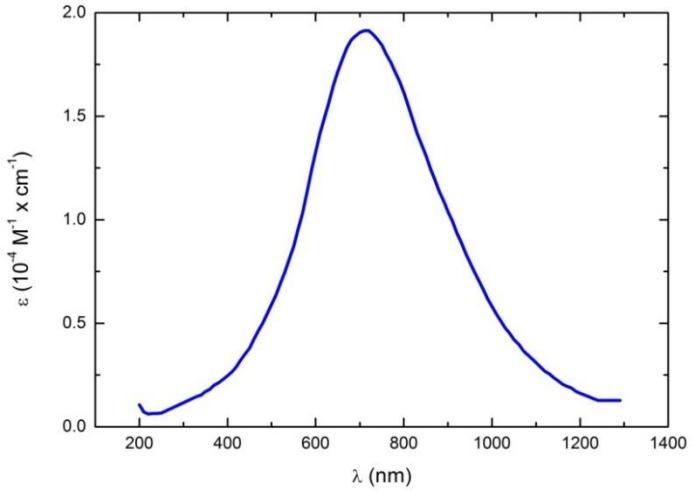

Figure 1.11 *Molar extinction coefficient value of hydrated electron at ambient condition[16,17].*

The first study of radiolytic yield of e_{hyd}^- in the year of 1973 by *Wolf et al.* [20]gives us the value $G(e_{hyd}^-) = 4.0 \pm 0.2$ molecules x (100 eV) $^{-1}$ at 30 ps after the passage of ionizing radiation. In the same year, *Jonah et al.* [21]used the same method and found the value is $G(e_{hyd}^-) = 4.1 \pm 0.1$ molecules x (100 eV) $^{-1}$ at 200 ps.

Meanwhile, different groups use scavenged method to measure the radiolytic yield of e_{hyd}^- at ~10^{-7} s when the solutions becomes homogenous after the irradiation. The well-accepted value is ($G\ e_{hyd}^-$ = 2.7 molecules × (100 eV) $^{-1}$).

Bartels *et al*[22]. re-evaluated the value of G e^-_{hyd} on the time scale from 100 ps to 1 μs, and they reported by extrapolation of their results, the value is G $(e^-_{hyd}) = 4.0 \pm 0.2$ molecules × (100 eV)$^{-1}$ at time zero, initial yield « G° (e^-_{hyd}) ». This value was later confirmed by Muroya *et al.* [23]in 2005 by the laser driven ultrafast pulse radiolysis. Their value is G$(e^-_{hyd}) = 4.1 \pm 0.2$ molecules x (100 eV) $^{-1}$ at 20 ps after the ionizing radiation. This value is believed to be the most reliable one and it is taken in my thesis for dose calculation at 15 ps.

The initial yield of electron, however, is still under debate due to the time resolution of pulse radiolysis. It varies from 4.2 to 5.2 molecules × (100 eV) $^{-1}$ from the predictions of Monte-Carole simulations[19].

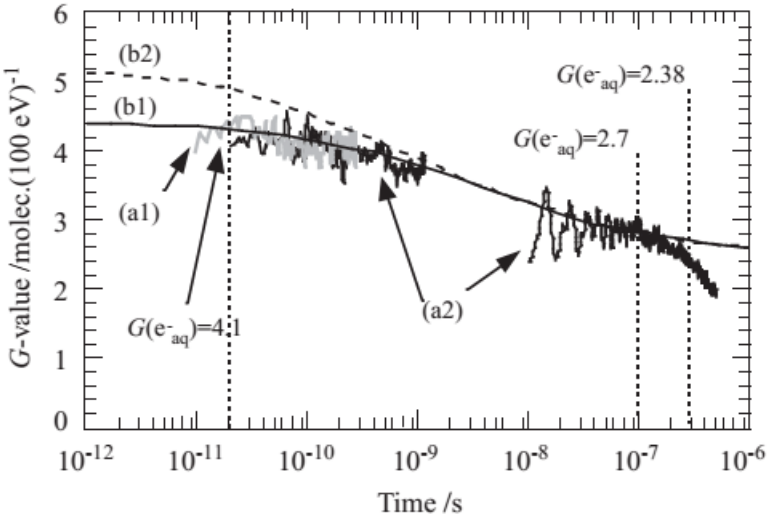

Figure 1.12 *Time-dependent radiolytic yield of hydrated electron (a1 and a2) with the predictions from Monte-Carole simulations (b1 and b2)[19].*

The lifetime of hydrated electron in neat water in relatively long, even up to several milliseconds and its decay from 15 ps to 3.5 ns will be given in Chapter 2 measured by picosecond pulse radiolysis in ELYSE. The decay on this timescale is mainly attributed to the reaction of e_{hyd}^- with H_3O^+ and $OH^\bullet$.

1.4.2 $OH^{\bullet}$ radicals

The ionization and excitation of water by high energy radiation produce the excited states of water and positive holes $H_2O^{\bullet+}$. They subsequently introduce the $OH^{\bullet}$ radicals in the liquid water via dissociation and proton transfer. $OH^{\bullet}$ radicals is acting as a highly oxidizing species towards many organics or inorganics. It has a very high redox potential + 2.7 V_{NHE} in acidic aqueous solutions and + 1.8 V_{NHE} in neutral solutions. In basic solutions, the $OH^{\bullet}$ radicals rapidly converted into its basic form $O^{\bullet-}$.

$$HO^{\bullet} + HO^{-} \underset{k= 1.7 \times 10^{6}\ s^{-1}}{\overset{k= 1.2 \times 10^{10}\ L\ mol^{-1}\ s^{-1}}{\rightleftharpoons}} H_2O + O^{\bullet-} \qquad (1.9)$$

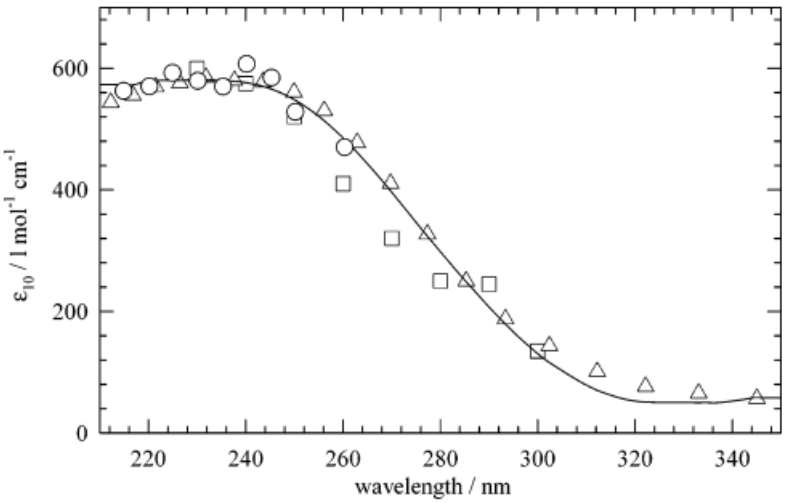

Figure 1.13 *Absorption spectrum of $OH^{\bullet}$ radicals in neat water, (-): Hesper and Hermann, (□): Jayson et al., (○): Nielsen et al., (Δ) completed by Hartmut Herrmann*[24,25,26].

The absorption spectrum of $OH^{\bullet}$ radicals from the literatures are presented in **Fig.1.13**. It absorbs in deep UV from 200 nm to 300 nm with very low molar extinction coefficient value (λ_{max} = 580 L mol^{-1} cm^{-1}). *Karim et al* [27]recently using picosecond pulse radiolysis directly measured the time dependent yield and its value at 15 ps is 4.85 mol J^{-1}. The decay of $OH^{\bullet}$ radicals from 15 ps to 3.5 ns in neat water will be given in Chapter 3.

In ionized water, $OH^{\bullet}$ also reacts with other transient species as the list below:

$HO^{\bullet} + e^{-}_{hyd} \rightarrow HO^{-}$ $\qquad$ $k_{10}= 3 \times 10^{10}$ L mol^{-1} s^{-1}

$HO^{\bullet} + H^{\bullet} \rightarrow H_2O$ $\qquad$ $k_{11} = 1.5 \times 10^{10}$ L mol^{-1} s^{-1}

$HO^{\bullet} + HO^{\bullet} \rightarrow H_2O_2$ $k_{12}= 1.1 \times 10^{10}$ L mol^{-1} s^{-1}

$HO^{\bullet} + H_2 \rightarrow H_2O + H^{\bullet}$ $k_{13}= 4.2 \times 10^{7}$ L mol^{-1} s^{-1}

$HO^{\bullet} + H_2O_2 \rightarrow H_2O + HO_2^{\bullet}$ $k_{14} = 2.7 \times 10^{7}$ L mol^{-1} s^{-1}

$HO^{\bullet} + O_2^{\bullet-} \rightarrow HO^{-} + O_2$ $k_{15} = 8.0 \times 10^{9}$ L mol^{-1} s^{-1}

$HO^{\bullet} + O^{\bullet-} \rightarrow HO_2^{\bullet-}$ $k_{16} < 2 \times 10^{10}$ L mol^{-1} s^{-1}

1.4.3 $H^{\bullet}$ radicals

The $H^{\bullet}$ radicals like $OH^{\bullet}$ radicals absorbs in deep UV region with a very low absorbance. In 1976, Nielson *et al*[20]. found the absorption spectrum of $H^{\bullet}$ radicals as shown in **Figure 1.14** with ε_{188nm} = 1647 L mol^{-1} cm^{-1}. $H^{\bullet}$ radicals is a short-lived reducing species and it could react with many other transient species in ionized water (see below)

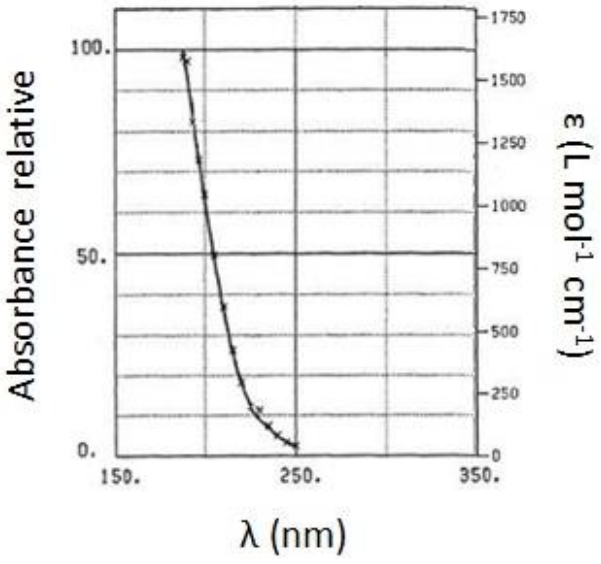

Figure 1.14 *Absorption spectrum of $H^{\bullet}$ radical in solutions containing 3.39 × 10^{-4} mol L^{-1} of $HClO_4$, 2.82 × 10^{-2} mol L^{-1} de H_2 and 4.5 × 10^{-5} mol L^{-1} de H_2O_2*[20].

$H^{\bullet} + e^{-}_{hyd} + H_2O \rightarrow H_2 + HO^{-}$ $k_{17} = 2.5 \times 10^{10}$ L mol^{-1} s^{-1}

$H^{\bullet} + H^{\bullet} \rightarrow H_2$ $k_{18} = 1.55 \times 10^{10}$ L mol^{-1} s^{-1}

$H^{\bullet} + HO^{\bullet} \rightarrow H_2O$ $k_{19} = 1.5 \times 10^{10}$ L mol^{-1} s^{-1}

$k_{20} = 2.0 \times 10^{10}$ L mol^{-1} s^{-1}

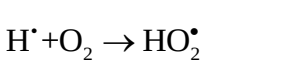

$k_{21} = 2.1 \times 10^{10}$ L mol^{-1} s^{-1}

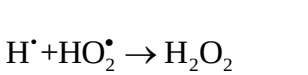

$k_{22} = 8.5 \times 10^{9}$ L mol^{-1} s^{-1}

$k_{23} = 4.2 \times 10^{7}$ L mol^{-1} s^{-1}

$k_{24} = 2.2 \times 10^{7}$ L mol^{-1} s^{-1}

1.5 Concluding remarks

This first chapter presents a very brief introduction of the interactions between high energy charged particles and photons with matter, and the subsequent physic-chemical effects based on many references and books. Some definitions in radiation chemistry was also given in this chapter. The ionized matter is dedicated to the liquid water and some properties of the main transient species (hydrated electron, OH radicals and $H^{\bullet}$ radicals) generated from water radiolysis are presented.

The reason to focus on water is that my thesis research concerns on the reactivity of $H_2O^{\bullet+}$ and electron, which is the initial ionized species of water molecule; The reactions involving them are ultrafast, occurring on the time scale of femtosecond, a boundary time region of physical and chemical processes. From a practical view of point, the water as the cooling agent plays a key role in nuclear reactors and spent nuclear fuel process as the solvent. The new understandings of water radiolysis and the reactivity of transient species from it has many implications in radiotherapy and radiobiology.

References

[1] Hatano, Y.; Mozumder, A. Introduction. In *Charged Particle and Photon Interactions with Matter;* Eds.; CRC Press: 2003, 1-8.

[2] Larry, T. Ionization and Secondary Electron Production by Fast Charged Particles. In *Charged Particle and Photon Interactions with Matter;* Mozumder, A.; Hatano, Y.; Eds.; CRC Press: 2003, 31-74.

[3] Belloni, J.; Marignier, J. L. Electron-Solvent Interaction: Attachment Solvation Competition. *Int. J. Radiat. Appl. Instrum., Part C., Radiat. Phys. Chem.,* **1989**, 34(1), 157-171.

[4] Gauduel, Y.; Pommeret, S.; Migus, A.; Antonetti, A. Femtosecond Dynamics of Geminate Pair Recombination in Pure Liquid Water. *J. Phys. Chem.,* **1989**, 93(10), 3880-3882.

[5] Buxton G.V. An overview of the radiation chemistry of liquids. *From Basics to Applications in Material and Life Sciences;* Spotheim-Maurizot, M.; Mostafavi, M.; Douki, T.; Belloni, J.; Eds.; EDP SCIENCES: 2008, 35-52.

[6] Gérard B and Bernard H; Water radiolysis under extreme condition. Application to nuclear industry *From Basics to Applications inMaterial and Life Sciences;* Spotheim-Maurizot, M.; Mostafavi, M.; Douki, T.; Belloni, J.; Eds.; EDP SCIENCES: 2008, 35-52.

[7] Uehara, S.; Nikjoo, H. Monte Carlo Simulation of Water Radiolysis for Low-Energy Charged Particles. *Journal of radiation research,* **2006**, 47(1), 69-81.

[8] A. Migus, Y. Gauduel, J. L. Martin, and A. Antonetti. Excess electrons in liquid water: First evidence of a prehydrated state with femtosecond lifetime*Phys. Rev. Lett*. 58, 1499 (**1987**)

[9] R. Laenen, T. Roth, and A. Laubereau, Novel precursors of solvated electrons in water: evidence for a charge transfer process. Phys. Rev. Lett. 85, 50 (2000).

[10] M.F. Emde, A. Baltuska, A. Kummrow, M.S. Pshenichnikov, D.A. Wiersma, "Ultrafast Librational Dynamics of the Hydrated Electron," *Phys. Rev. Lett*. 80, 4645-4648 (**1998**).

[11] M. H. Elkins, H. L. Williams, A. T. Shreve, D. M. Neumark. Relaxation Mechanism of the Hydrated Electron. *Science*. 342, 1496-1499, **2013.**

[12] D. Nordlund, H. Ogasawara, H. Bluhm, O. Takahashi, M. Odelius, M. Nagasono, L. G. M. Pettersson, and A. Nilsson. Probing the Electron Delocalization in Liquid Water and Ice at Attosecond Time Scales. *Phys. Rev. Lett.* 99, 217406 (**2007**).

[13] Keene, J. P. Absorption Spectra in Irradiated Water and Some Solutions: Optical Absorptions in Irradiated Water. *Nature,* **1963**, 197(4862), 47-48.

[14] Hart, E. J.; Boag, J. W. Absorption Spectrum of the Hydrated Electron in Water and in Aqueous Solutions. *J. Am. Chem. Soc.,* **1962**, 84(21), 4090-4095.

[15] Nicolas, C.; Boutin, A.; Levy, B.; Borgis, D. Molecular Simulation of a Hydrated Electron at Different Thermodynamic State Points. *J. Chem. Phys.,* **2003**, 118(21), 9689-9696.

[16] Jou, F.-Y.; Freeman, G. R. Shapes of Optical Spectra of Solvated Electrons. Effect of Pressure. *J. Phys. Chem.,* **1977**, 81(9), 909-915.

[17] Hug, G. L. Optical Spectra of Nonmetallic Inorganic Transient Species in Aqueous Solution. *Natl. Stand. Ref. Data Ser. (U. S., Natl. Bur. Stand.),* **1981**, NSRDS-NBS 69, 52.

[18] Hare, P. M.; Price, E. A.; Bartels, D. M. Hydrated Electron Extinction Coefficient Revisited. *J. Phys. Chem. A*, **2008**, 112(30), 6800-6802.

[19] Torche, F. *Contribution À L'étude Des Électrons Solvatés Dans L'eau Et Les Alcools Et Des Processus Radiolytiques Dans Les Carbonates Organiques Par Radiolyse Impulsionnelle Picoseconde.* Ph.D. Thesis, Université Paris-Sud 11, **2012**.

[20] Wolff, R. K.; Bronskill, M. J.; Aldrich, J. E.; Hunt, J. W. Picosecond Pulse Radiolysis. Iv. Yield of the Solvated Electron at 30 Picoseconds. *J. Phys. Chem.*, **1973**, 77(11), 1350-1355.

[21] Jonah, C. D.; Hart, E. J.; Matheson, M. S. Yields and Decay of the Hydrated Electron at Times Greater Than 200 Picoseconds. *J. Phys. Chem.*, **1973**, 77(15), 1838-1843.

[22] Bartels, D. M.; Cook, A. R.; Mudaliar, M.; Jonah, C. D. Spur Decay of the Solvated Electron in Picosecond Radiolysis Measured with Time-Correlated Absorption Spectroscopy. *J. Phys. Chem. A,* **2000**, 104(8), 1686-1691.

[23] Muroya, Y.; Lin, M.; Wu, G.; Iijima, H.; Yoshii, K.; Ueda, T.; Kudo, H.; Katsumura, Y. A Re-Evaluation of the Initial Yield of the Hydrated Electron in the Picosecond Time Range. *Radiat. Phys. Chem.*, **2005**, 72(2-3), 169-172.

[24] Nielsen, S. O.; Michael, B. D.; Hart, E. J. Ultraviolet Absorption Spectra of Hydrated Electrons, Hydrogen, Hydroxyl, Deuterium, and Hydroxyl-D Radicals from Pulse Radiolysis of Aqueous Solutions. *J. Phys. Chem.*, **1976**, 80(22), 2482-2488.

[25] Herrmann, H. Kinetics of Aqueous Phase Reactions Relevant for Atmospheric Chemistry. *Chem. Rev.*, **2003**, 103(12), 4691-4716.

[26] Thomas, J. K.; Rabani, J.; Matheson, M. S.; Hart, E. J.; Gordon, S. Absorption Spectrum of the Hydroxyl Radical1. *J. Phys. Chem.*, **1966**, 70(7), 2409-2410.

[27] El Omar, A. K.; Schmidhammer, U.; Jeunesse, P.; Larbre, J.-P.; Lin, M.; Muroya, Y.; Katsumura, Y.; Pernot, P.; Mostafavi, M. Time-Dependent Radiolytic Yield of OH• Radical Studied by Picosecond Pulse Radiolysis. *J. Phys. Chem. A,* **2011**, 115(44), 12212-12216.

Chapter 2: Experimental Methodology: Picosecond Electron Pulse Radiolysis

Chapter 2 Experimental Methodology: Picosecond Electron Pulse Radiolysis

2.1 Introduction

Radiation chemists have been trying to understand the chemical changes of ionizing radiation on matter. The first or proud thing for them, therefore, is always to make the suitable and unique radiation sources available in a controlled way for exploring the chemical process on the timescale from femtosecond to days; in the condition from ambient temperature to high temperature, high pressure; on the effect induced from high LET (heavy ion or α particles) to low LET (electron beam or γ rays) sources *etc*. This trend still continues today. It has to be added that, some of them also take advantages of theoretical simulations combined with experiments for better understanding the initial yield of radiolytic ions and structure of tracks formed in the physico-chemical processes. Therefore, the various stages of radiation chemistry could be briefly summarized according to the radiation sources:

(1) Observations in the period of natural isotopic sources

In the early twentieth century, the radioactive elements were the newly found matters. It was soon recognized that these elements like radium or radon sources produce primarily alpha rays and beta rays, which induce the darkening of glass, the formation of gas (H_2 and O_2) in water and changes in form of some minerals *etc*. Quantification of these observations was difficult because on the one hand, the penetrating ability of these particles into condensed media is low, on the other hand, radioactive radium or radon gas were not often separated from the irradiated substances and it was suspected that the radioactive element itself also participate the reactions other than the reactions induced by emitted radiation. For example, the radiation source used for water radiolysis was actually water dissolved radium or radon gas.

The first quantification work was probably done by *Lind* [1] who used conductivity experiments to determinate the number of ions formed in gas radiolysis. He defined a "yield" as the ratio *M* / *N*, where *M* was the yield of products and *N* was the number of ions that were formed by radiation. It was then learned from these observations that the amount of ionizing radiation played an important role and that it was closely related to the yield of chemical products.

(2) Experiments using X-rays generators and artificial isotopic sources

X-rays found by *Roentgen* was firstly generated by a vacuum tube that uses a high voltage to accelerate the electrons towards a metal target. The energy of X-rays depends on the energy of incident electrons which is equal to the voltage on the tube times and the electron charge. Therefore, the powerful X-rays generators made it possible to deliver the hard X-rays (5-10 keV) which would penetrate container and evenly irradiate a reasonable physical volume of liquid or aqueous solutions.

Quantitative radiolysis experiments of liquid came after the great invention of Fricke dosimeter by *Hugo Fricke* which is still widely used today. The principle is based on the deposit of energy in the water solvent that passes subsequently to the ferrous ions. The yield of Fe^{3+} ions is used as a reference to determine the total amount of radiation. However, at that time, the water decomposition by radiation was not known in depth. The induced transient species before the formation of hydrogen and oxygen in water was not proposed.

This situation was not changed until the war time when much research effort made use of radiation sources that were available[2]. Among those, the cobalt-60 or Cs-137 sources were proven to be relatively simple, less expensive and could be used in many university environments. Nowadays, they are still commonly equipped in many facilities worldwide for radiation researches and also turn out to be one of the main sources for industrial radiation process. The knowledge of chemical process induced by high energy radiation since then has been greatly expanded in liquids especially in water. As a consequence, radiation chemistry christened by *Milton Burton* came into a branch discipline of chemistry, which was independent but much related to nuclear science[3].

(3) Pulse radiolysis / heavy ions radiolysis / theoretical simulations

Early steady-state measurements had already suggested that water radiolysis involves many short-lived species including $H^{\bullet}$, $OH^{\bullet}$, e_{hyd}^{-} *etc* that were highly reactive towards many compounds. The new chapter of radiation chemistry was written, however, by time-resolved

pulse radiolysis. Since the first observation of hydrated electron in 1962 by *Keene*, *Hart* and *Boag*[4,5], a wealth of radiation-induced reactions have been studied in detail and the rate constant or reduction redox potential values of many intermediates were so numerous that they were eventually summarized as several databases in *Notre Dame Radiation laboratory*[6]. The principle of pulse radiolysis is to generate the short-lived species using a pulse of electrons that should be much shorter than the time constants of the subsequent reactions and to be detected these species by time-resolved optical or conductivity techniques. From this time on, radiation chemists were not only able to gain a further insight into the properties and reactivity of various transient species in real time induced by ionizing radiation, but also to explore some elementary chemical process in general with strong impact to other domains such as Marcus theory of electron transfer[7,8] or oxidizing reaction in biological system[9].

Heavy ions radiolysis provided an excellent complementary radiation source to study the effects induced by high LET particles[10]. The various types of ionizing radiation that exist in real radiation environment can have significant difference of radiation effects due to their variation in track structure. The radical – radical or radical – molecule reactions in the spurs formed by heavy charge particles would be greatly different compared with those by the fast electron. Meanwhile, theoretical simulations like stochastic models were emerging as a tool to find a picture of early events from the inelastic collisions to the formation of track structure as well as the initial yields of radiolytic ions[11]. They were developed as a helpful method in terms of having a good prediction on the new homogenous liquid phase or interfacial system as well.

(4) Picosecond electron pulse radiolysis

Undoubtedly, as shorter electron pulse sources and more elaborated detection methods became available, more and more sophistical even controversial questions could be posed and answered. In the past decades, there have been a continuous global effort on constructing picosecond pulse radiolysis. The first picosecond pulse (30 ps) was reported by Hunt *et al.* in 1968[12], in which the Cerenkov light was used as the probing light. The reactivity of precursor electron towards many ions or organic compound was studied based on the decrease of its initial absorbance after the pulse. Shortly after that, the generation of a single 20 picosecond electron pulse in Argonne National Laboratory[13], and a 10 picosecond pulse from the S-band linear accelerator in University of Tokyo Nuclear Engineering Research Laboratory (NERL)[14] were realized in 1971 and 1979 respectively. The latter was further improved as a "Twin Linac" with one linac as the pulse sources and the other as the Cerenkov sources in the 1980s[15].

Subsequently, picosecond linacs were also installed in Osaka University where a femtosecond laser was firstly synchronized with electron pulse[16,17]. In the 1990s, laser-driven electron gun accelerators namely the LEAF facility at Brookhaven National Laboratory[18], the ELYSE facility at University of Paris Sud[19] and the facilities at Tokyo University[20], at Osaka University[21], at Sumitomo Heavy Industries[22] and Waseda University[23], were constructed in their own paces and many of them have already reached the full capacities for picosecond pulse radiolysis measurements.

Recently, a femtosecond single bunched linac for pulse radiolysis based on laser wakefield acceleration is also under optimization at Osaka University[24] and it is a promising technique that might allow the radiation chemists to enter an entirely new continent.

2.2 Femtosecond laser source

2.2.1 Laser basics

Laser is the abbreviation from "Light amplification by stimulated emission of radiation" which is the basic building block of the generation techniques of short light pulses. In 1905, Albert Einstein told us that electromagnetic energy is quantitated. So according to his theory, three different elementary processes can take place during the interaction of light with matter, that is, absorption (**Figure 2.1a**), spontaneous emission (b) and stimulated emission (c).

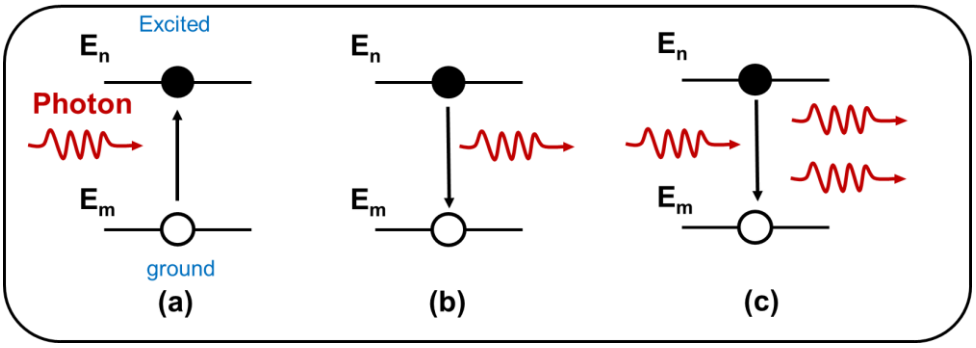

Figure 2.1 *The three elementary electron photon interaction processes in atoms: (a) absorption, (b) spontaneous emission, (c) stimulated emission*

When a photon with energy of $h\nu = E_n - E_m$ passes by an excited atom as shown in **Figure 2.1c**, it may stimulate the emission of a twin photon by this atom. These two photons have the same energy, the same direction of propagation, the same polarization state and the same phase as the original inducing photon. In an elementary stimulated emission process the net optical gain is two, so it is very similar to a chain reaction for growing the photon number. Light is amplified. In this case, more excited atoms than atoms in the ground state are needed; the population is said to be "inverted". Unfortunately, this "population inversion" cannot be reached in a two electronic level because the distribution of photons obeys Fermi-Dirac statistical distribution which shows more ground atom than excited ones.

Optical pumping was then proposed in 1958 by Alfred Kastler to realize inverted populations of electrons. Real electronic structures are rather complicated series of states and for the sake of simplicity, an example of three-level system is given in **Figure 2.2**. Electrons are pumped or promoted from state 1 to state 3 with a probability per unit of time W_P. From state 3, electrons can decay either to state 2 with probability of W_{32} or the ground state 1 with probability of W_{31}. If the transition probability from state 3 to state 2 is much larger than to state 1 ($W_{32} >> W_{31}$), and the pumping rate is large enough to overcome the spontaneous emission between state 2

and 1 ($W_p >> W_{21}$), then the average number of atoms in state 2 can be larger than state 1. The population inversion is reached as the similar gain medium of chromium ions dissolved in alumina (ruby) using flash lamp as the optical pumping.

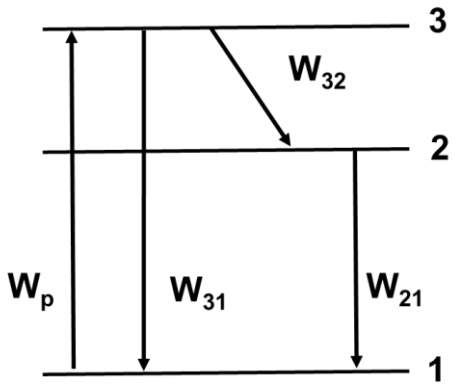

Figure 2.2. *Three-level system used here to model the population inversion in optical pumping*

An oscillator is basically made of an amplifier / gain medium and a feedback. The feedback includes an optical cavity—a pair of mirrors on either end of the gain medium. Light in the optical cavity bounces back and forth between the mirrors, passing through the gain medium and being amplified by stimulated emission each time to overcome the losses.

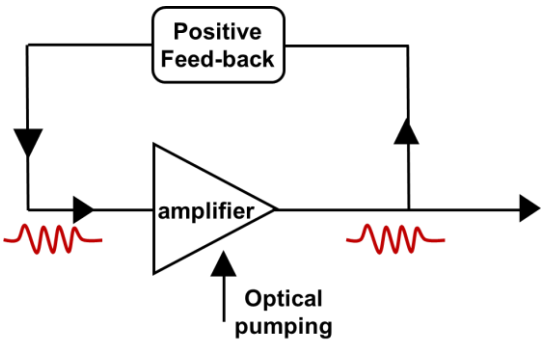

Figure 2.3*. An oscillator includes a gain medium and a feedback to ensure a constructive interference between the input and amplified waves.*

Therefore, three conditions must be fulfilled in order to obtain a laser, (1) optical pumping to excited the electrons to higher states; (2) a gain medium like three or four level system, to realize the electronic population inversion; (3) An optical cavity to enlarge the intensity of electromagnetic wave after each round trip of light.

2.2.2 Laser source in Elyse

The commercial laser source is installed in a separated room vertically above the accelerator room with the purpose of delivering a femtosecond laser to drive the accelerator as well as partly being converted into the probing light in the direct line of the accelerator ("V0"). The ultra-short laser pulses of 100 fs duration delivered at 780 nm have an energy of 2 nJ after frequency doubling of the oscillator. The energy of these original pulses is too low to reach the charge per pulse requirement. They are therefore amplified by a regenerative amplifier based on the chirped pulse amplification (CPA) techniques. Shortly, as shown in **Figure 2.4**, in CPA, the femtosecond laser pulse is stretched out before the gain medium (amplifier) using a pair of gratings. The gratings expand the incident laser beam spectrally so that the low-frequency component of the laser pulse travels a shorter path than the high-frequency component does. As a result, the high-frequency component lags behind the low-frequency component, and the overall pulse has longer pulse duration than the original. By this pulse stretching, the laser pulse can be safely amplified without causing damages on the internal optics. After amplification, the stretched pulse is then recompressed back to the original pulse width through the reversal process of stretching to reach a higher energy. Finally, the amplified femtosecond laser pulse has the energy of 2.3 mJ for radiolysis and the same for photolysis.

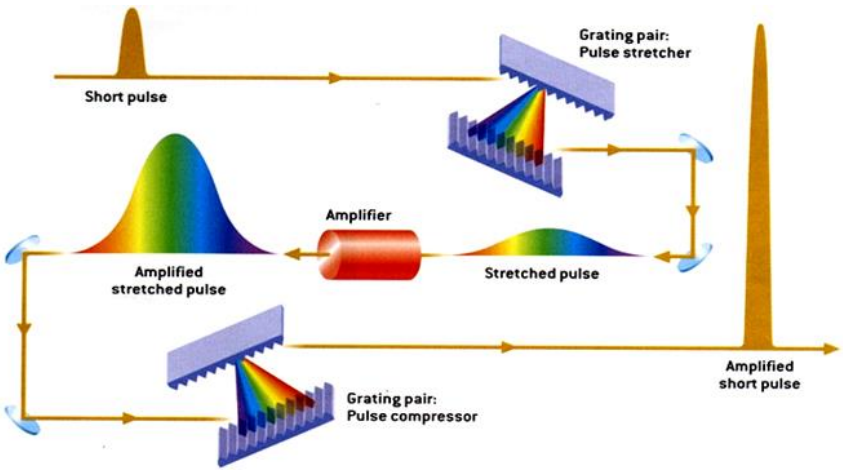

Figure 2.4 *Schematic illustration of chirped pulse amplification for the generation of femtosecond laser pulses with mJ energy.*

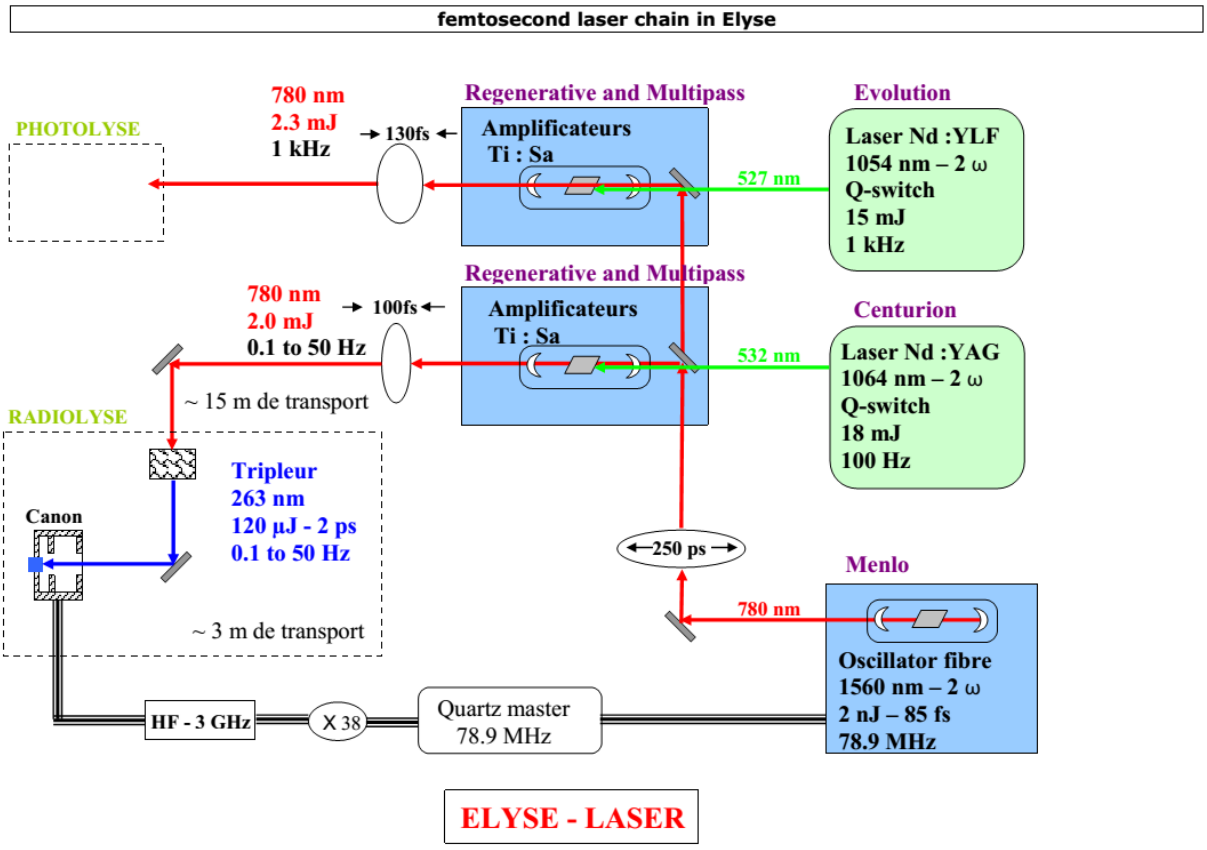

Figure 2.5 *Schematic diagram illustrating the femtosecond laser chain in Elyse*[25].

Precise synchronization between laser and electron beam is achieved by the quartz master-oscillator with frequency of 79.8 MHz. The laser beam at a repetition rate of 20 Hz is transferred down to the accelerator room through a hole in the lead shielding. At this output, the laser is divided into two different pathways by an optical beam splitter. The main part is then converted into 263 nm by third harmonic generation and directed almost perpendicularly onto a photocathode in a vacuum chamber almost perpendicularly by a laser entrance mirror (LEM) in the accelerator. The almost normal incident of the laser onto the photocathode guarantees a time structure of the initial photoelectron pulse close to the one of 260 nm pulse. The other fraction of laser pulse travels a series of optical mirrors and is used to generate the analyzing light. Two cameras are used to monitor the position of laser by two small beam portions split off from the main beam. With these spatial references and the remote control of two mirrors, spatial drifts of the laser beam can be corrected during experiments, when the lead door of accelerator room is closed.

As the energy of laser pulse is also an important parameter that could influence the radiation dose as well as the supercontinuums probe, a joulemeter is thus daily used to measure the energy. In addition, the whole facility is thermally stabilized, especially the temperature of laser and accelerator room is kept constant at 22.5 ˚C.

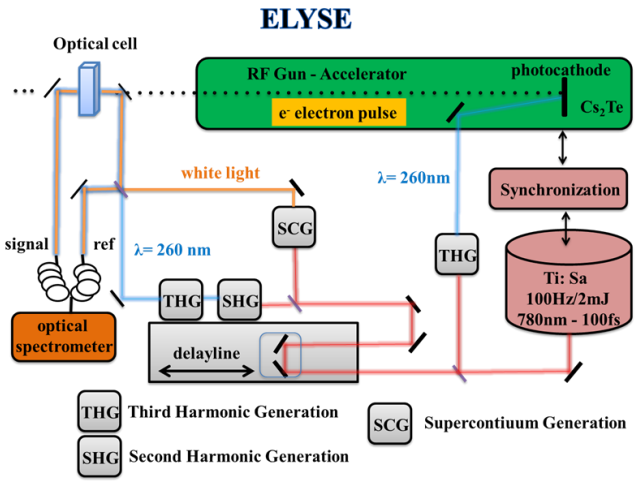

Figure 2.6 *The two laser pathways for producing electron beam and the conversion of the probing light*

2.3 Laser photocathode electron gun accelerator

2.3.1 Design of the accelerator

The electron accelerator is the core part of pulse radiolysis facility. The general design of Elyse accelerator and the meaning of each components are illustrated in **Figure.2.7**. The electrons are extracted out of Cs_2Te photocathode material. The radiofrequency gun is used to initially provide an electron beam of 4 MeV for an input power 8.3 MW and it is subsequently accelerated up to 8 MeV by the four cell boosters. The radiofrequency power for the gun and booster is provided by a klystron and a modulator. The function of Triples (TR1) is to make the bunch more focused and delivered it to the target. Once the energy and charge of the electron beam reach a desirable value (7 MeV, 3.5-5 nC), it could be transported to any of three experimental areas by the magnetic field. V0 located at the straight line of beam, whereas V1 and V2 are at 30 ˚C and 60 ˚C respectively. All the areas have the same time resolution of electron beam (7 ps), but the detection system is different. Pulse-probe technique is applied in V0 for the time window from several picoseconds up to 3.5 nanoseconds, which is the main platform for my measurements.

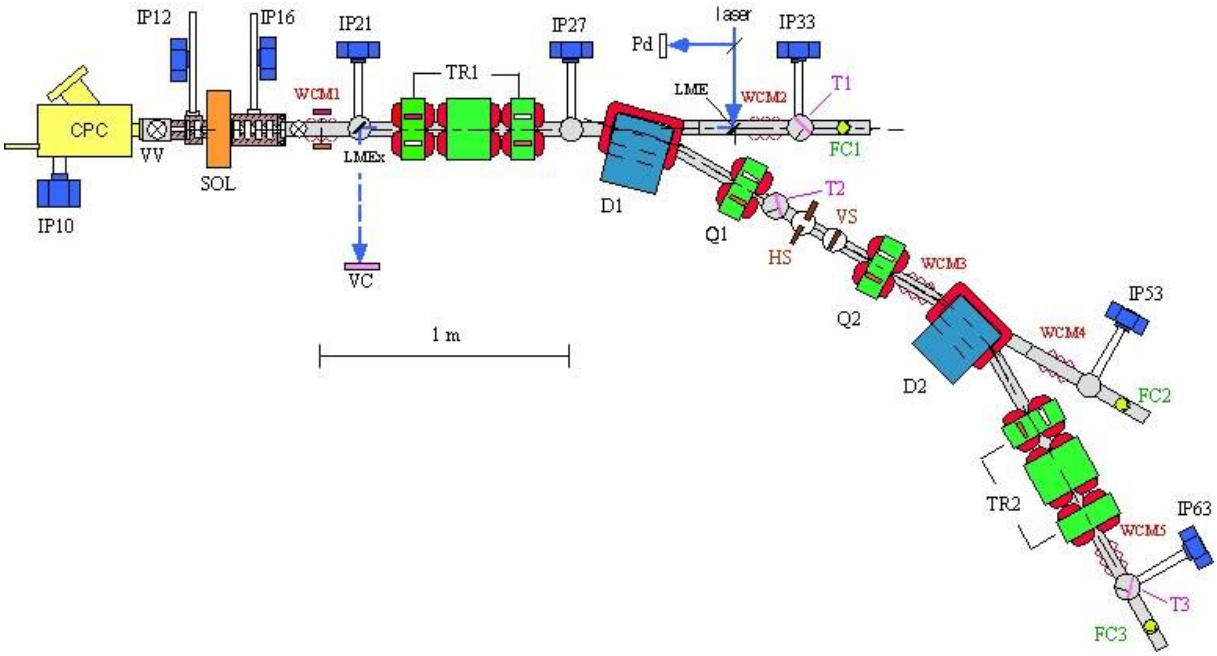

Figure 2.7 *A general schematic for radiofrequency gun accelerator in Elyse. IP: ion vacuum pump; CPC: cathode prepare chamber; SOL: solenoid; VV: vacuum valve; D: dipole; TR1 and 2: triples; Q: quadrupole; WCM: wall current monitor; FC: Faraday cup; T: translator for Cerenkov light emitter and visualization screen; LME: laser entrance mirror; LEMx: laser exit mirror; VC: virtual cathods; HS: horizontal slit; VS: vertical slits*[19].

2.3.2 Photocathode

The photocathode used in laser driven accelerator can be metal, like Mg, Cu or semiconductor such as Cs_2Te, NaKSb. The metal photocathode has the advantages of easy preparation and low cost but its quantum efficiency is low (< 0.01 %). Semiconductor photocathode have a much higher quantum efficiency (~ 0.25 %), but they are very sensitive to oxidation by air. So they are prepared either *in situ* in a vacuum preparation chamber like in ELYSE or in a separated chamber with a vacuum transport system. The photon charge per pulse of electron beam is influence by the quantum efficiency, it can be given by:

$$Q = 2.1 \times E_\lambda \times \eta \qquad (2.1)$$

Where, Q is photon charge in nC, E_λ is the charge per laser pulse at 263 nm (in µJ) and η is quantum efficiency of the photocathode (in %).

The principle of producing photoelectrons is based on photoelectric effect which is the absorbed energy of a quantum light causes electron emission. According to the band theory, Cs_2Te is a semiconductor containing valence band and conduction band with a very small band gap (E_G = 3.3 eV) between these two bands as shown in **Figure 2.8** (left). When the valence electrons receive enough energy (photon), they may escape valence band and jump to the conduction band where they move freely throughout the crystal lattice. The threshold energy is 3.5 eV, so the electron affinity is calculated as $E_T - E_G$ = 0.2 eV. The emission electron could be detected when the photon is above 3.5 eV and the quantum efficiency increase with the photon energy up to 6.6 eV as presented in **Figure 2.8** (right).

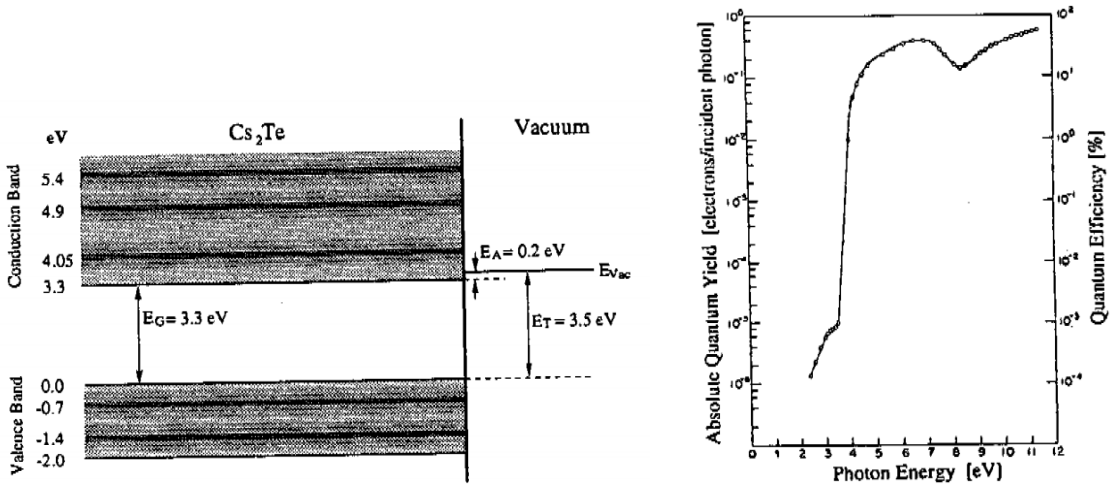

Figure 2.8. *Schematic band structure of Cs_2Te (left) and the quantum efficiency plotted as a function of incident photon energy*[26].

Another effect that can change the charge is the position and spot diameter of the laser beam on the photocathode. It is regularly optimized for obtaining high charge and thus a higher radiation dose. Cs_2Te photocathode is coated on the Cu metal plate as shown in **Figure 2.9**. After a few months, the photocathode is damaged either due to the possible impurity in the accelerator or by accumulation of high energy laser injections. The consequence is that the dose dramatically decrease and become instable during the measurements. Therefore, after certain time, it is re-prepared in the preparation vacuum chamber by the technicians.

Figure 2.9. *Cs_2Te Photocathode installed in the accelerator: from left to right the metal cooper photocathode, fresh coated Cs_2Te; from up to bottom: fresh prepared one and used one after several months.*

2.3.3 Characterizations of electron beam

The energy of the electron beam have been of great importance for time resolution because of the beam scattering of the electron beam in irradiated sample. At ELYSE, the delivered electron pulse typically has the energy of 7 MeV with time resolution of 7 picosecond in working condition. If the electron beam with an energy of 5 MeV passes a sample, the scattering of the beam becomes significant over 1 cm and radiolytic dose is spread over a large cross section. In addition, due to the zigzag trajectory of the beam, the time duration of the pulse is longer in this case. However, electron beams with energies over 10 MeV begin to cause some photonuclear radioactivation of the components. Therefore, higher energy (10 MeV – 20 MeV) of the pulse is only available in the specially equipped labs like Osaka University and Tokyo University where the electron beam can provide sufficient penetration for specific high temperature and high pressure flowing cell with thick windows. For ELYSE and LEAF, the energy of 7- 9 MeV is the best compromise.

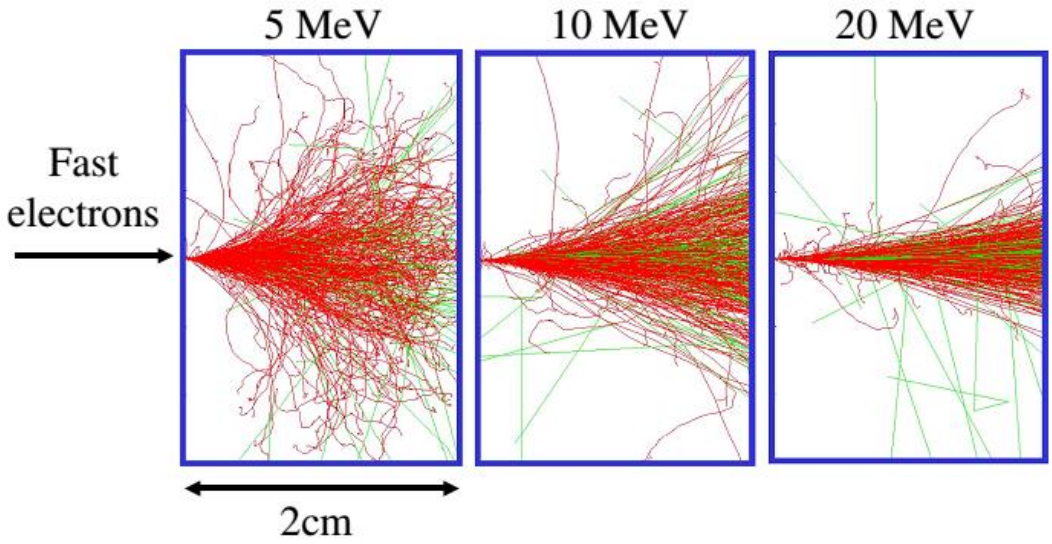

Figure 2.10. *Penetration of 5, 10,20 MeV electron beam through a 2 cm water cell calculated by the Monte Carlo code (EGS5 code); red and green lines show the trajectories of electrons and secondary X-ray photon*[9].

The shape of the beam cross-section close to the exit windows of the accelerator may be visualized by the image of the emitted light produced by the electron beam on a YAG/Ce slide located close to the entrance window of the sample. At direct line of Elyse, it can be seen from **Figure 2.11 top**, the cross section becomes greater as scatter of the electron beam passing the cell. The radius of beam in the output of accelerator is around 0.5 cm, which turn out to be 1

cm at the exit of the sample. In order to minimize the divergence resulting from the electron beam scattering by the exit window, the cell is fixed as close as possible to this window.

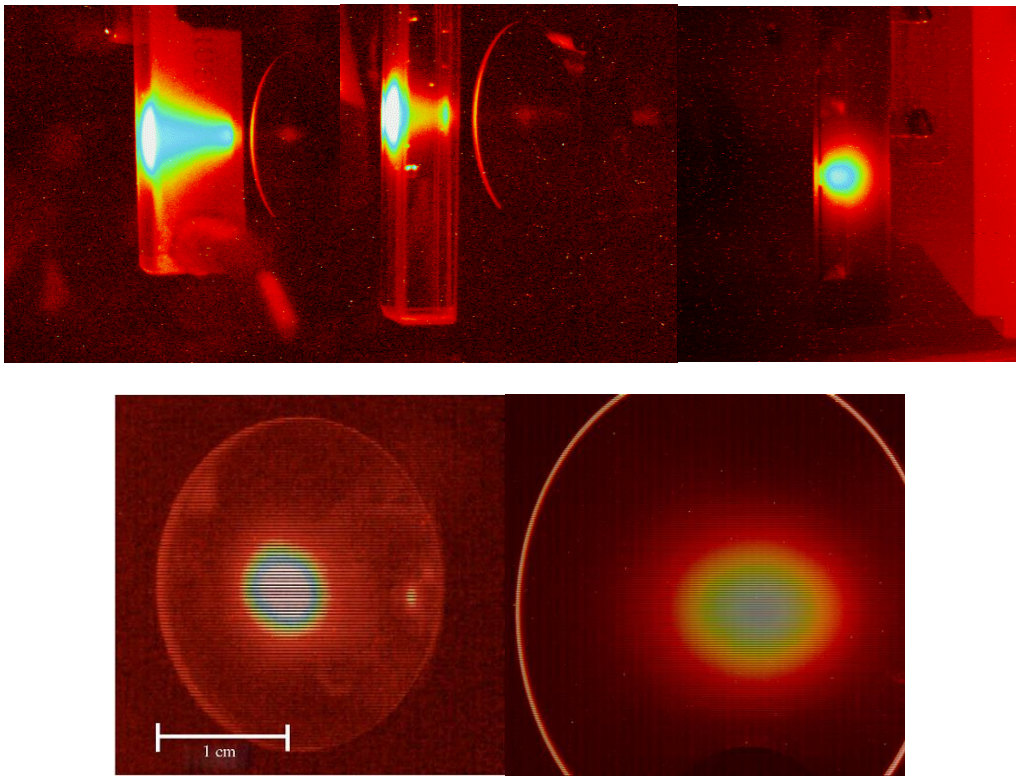

Figure 2.11. *Top: Images in different angles when the electron beam passing the sample cell. Bottom: imaging of the electron beam section as visualized at 45 ˚C incidence angle by the Cerenkov light emitted on a YAG/Ce slide located at the entrance window of the sample cell*[19].

The duration of the pulse is also measured using the Cerenkov light pulse emitted by sapphire screens moved across the electron beam. An oscilloscope is used to monitor the parameters of the laser and electron beam as shown in **Figure 2.12**.The pulse width for 9 MeV electrons is 6 and 3.6 ps, respectively as shown in **Figure 2.13**. The dark current is negligible using the Cs_2Te photo-cathode. Wall current monitors (WCM) are commonly used to observe the time profile of electron beams. The general principle is that the image current, which accompanying with the beam along the inside of the vacuum pipe develops a voltage across the resistor and eventually reflected in the oscilloscope.

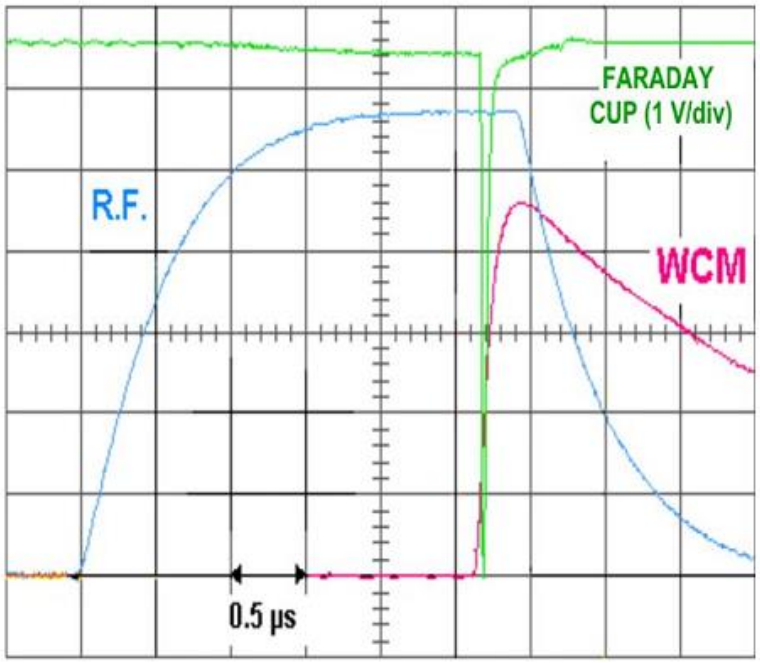

Figure 2.12. *Oscillograms showing (left to right): the RF filling of the gun, the laser pulse and the electron pulse. Signals with Cs_2Te photo-cathode (the dark current is negligible)*[25].

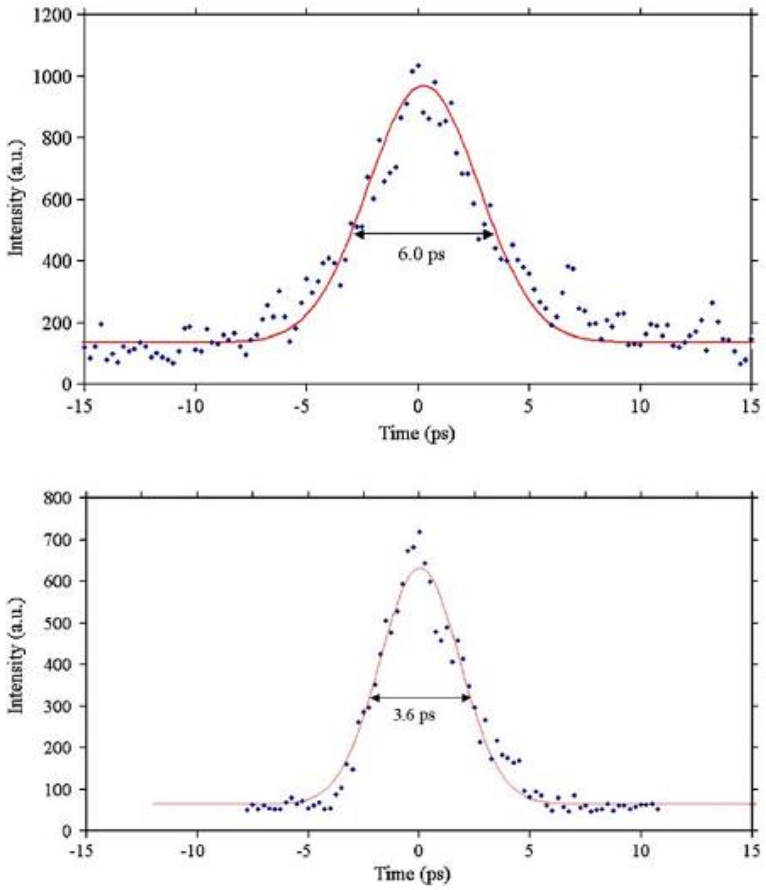

Figure 2.13. *Pulse duration measured using Cerenkov light at the direct line V0 and streak camera at V3 region of ELYSE. The pulse energy is 9 MeV, the charge is 5 nC*[25].

2.4 Pulse-probe optical detection

2.4.1 Absorbance

The interaction of high energy irradiation with liquids in the measuring cell produces short-lived species of various types which are to be detected and the changes in their concentration are to be recorded. Optical detection methods are commonly used because many transient species have an absorption spectrum of its own. In other words, to be detected by the optical method, the intermediates must absorb light in the detection range. The basic principle is the law of a Lambert-Beer:

$$A = \varepsilon c l = \log_{10} \frac{I_0}{I} \tag{2.2}$$

Where A is the absorbance, ε is the molar extinction coefficient, c is the molar concentration of species, l is the path length of the light beam through the sample and I_0, I are the intensive power of analyzing light before and after sample.

At V0 of ELYSE, to generate this analyzing light, thirty percent of the laser energy is available, split off from the main laser beam that is used to generate the electron pump pulse. As shown in **Figure 2.14**, the corresponding laser pulse passes a 380 cm long delay line and is subsequently used to generate the probe, either a spectrally broad source or selected wavelength[27]. In the latter case, the third harmonic generation is used in an orthogonal direction of the supercontiuum device with the purpose of transferring the probe laser at 780 nm into the light at 260 nm. This single wavelength of 260 nm enables us to observe, for example, the kinetics of $OH^{\bullet}$ radicals in aqueous solutions which absorbs in deep UV region. The initial probing white light is divided into the reference light which directly focuses into the optical reference fiber, and signal light that is coupled with electron pulse in parallel through the sample. In time-resolved pulse-probe technique, three types of data acquisitions are recored during the measurements to obtain the change of absorbance or optical density as follow:

$$A_t = \varepsilon c_t l = \log_{10} \left(\frac{I_{ref}^0 - I_{obs}}{I_{sig}^0 - I_{obs}} \Big/ \frac{I_{ref} - I_{obs}}{I_{sig} - I_{obs} - I_{Cer}} \right)$$

(1) I^0_{ref} and I^0_{sig} are the reference and signal in the absence of electron beam.

(2) I_{ref} and I^0_{sig} are the reference and signal in the presence of electron beam.

(3) I_{obs} is measured in the condition that both of probe and electron pulse are absent. It is the signal produced probably by the environment background.

The detected Cerenkov light is subtracted from the acquired data as the change of absorbance recorded before the time zero.

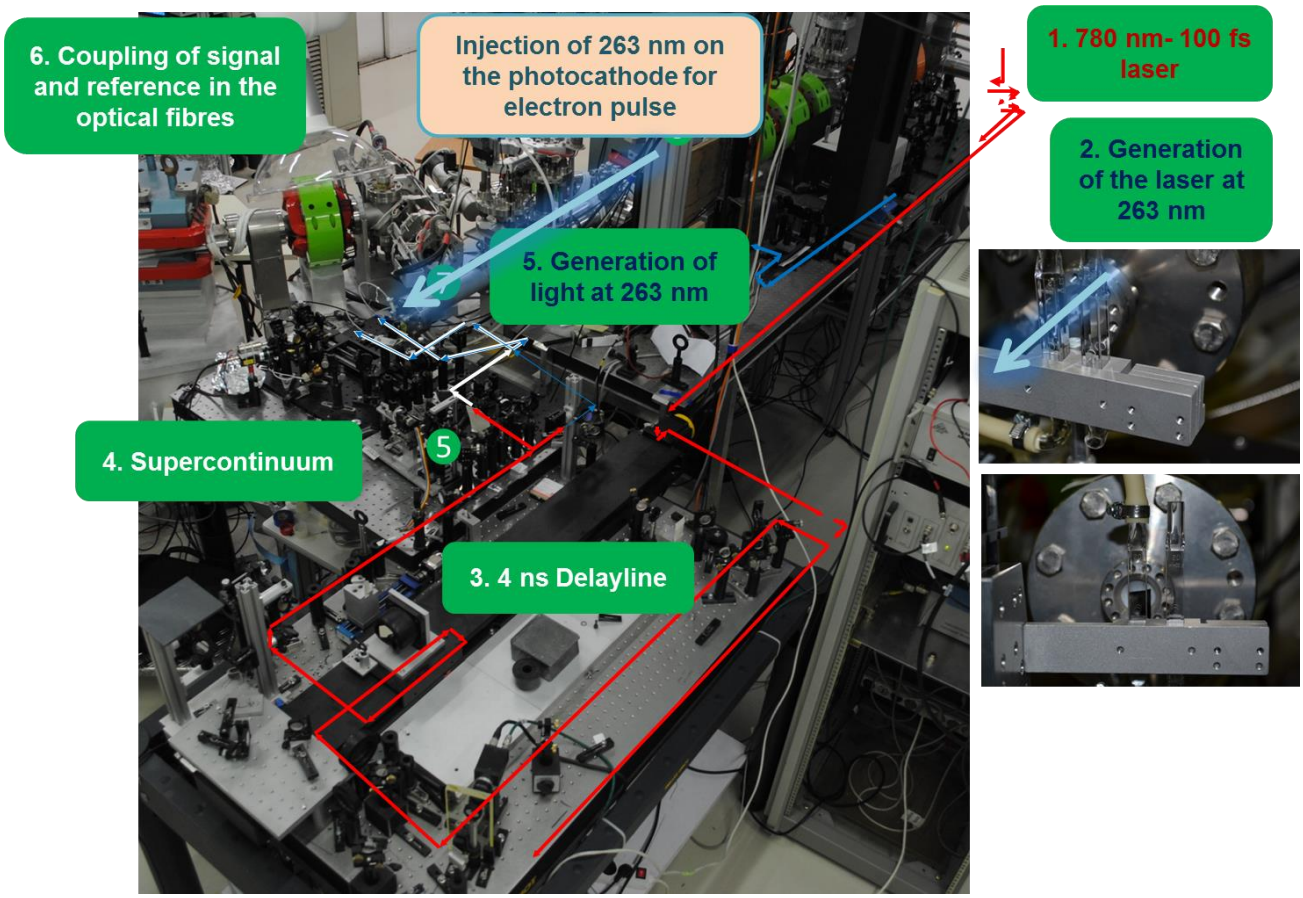

Figure 2.14. *Photo of pulse-probe optical detection system in Elyse. The red line indicates the beam path of the laser at 780 nm that is used to produce the probe light pulse and the dark blue line is the beam at 260 nm that is used to generate the electron pump pulse. The light blue arrow indicates the electron beam propagation.*

2.4.2 Dose determination

Determination of the radiation dose (Gy) deposited on the liquids is an indispensable measurement before starting the new samples that need to be studied. Unlike the cases in nanosecond or microsecond pulse radiolysis, in which, thiocyanate dosimetry is commonly used, in ELYSE, the transient absorption of hydrated electron in pure water in the visible or near-infrared is used as reference for dosimetry. In detail, the initial absorbance of hydrated electron at 15 ps at selected wavelength is taken directly from the kinetics as presented in **Figure 2.15**. The dose can be calculated as the equation:

$$A_t = \varepsilon(e_{hyd}^-)\ c_t l = \varepsilon(e_{hyd}^-) Dose G_t(e_{hyd}^-)\rho l \qquad (2.3)$$

Where ε (e_{hyd}^-) is the molar extinction coefficient of hydrated electron, l is the optical path (0.5 cm), ρ is the density of water at ambient temperature, and G_t (e_{hyd}^-) is time-dependent radiolystic yield of hydrated electron.

Although the value of ε (e_{hyd}^-) and G_{15ps} (e_{hyd}^-) has been a controversial issue, G_{15ps} (e_{hyd}^-) = 4.25×10^{-7} mol / J [28]and ε (e_{hyd}^-) = 18960 at 730 nm[29] are preferable in my thesis. The amount of dissolved O_2 in neat water is low and it is not likely to react with hydrated electron on the time scale of picosecond. So the pumping of N_2 or Ar into the solutions is no longer necessary.

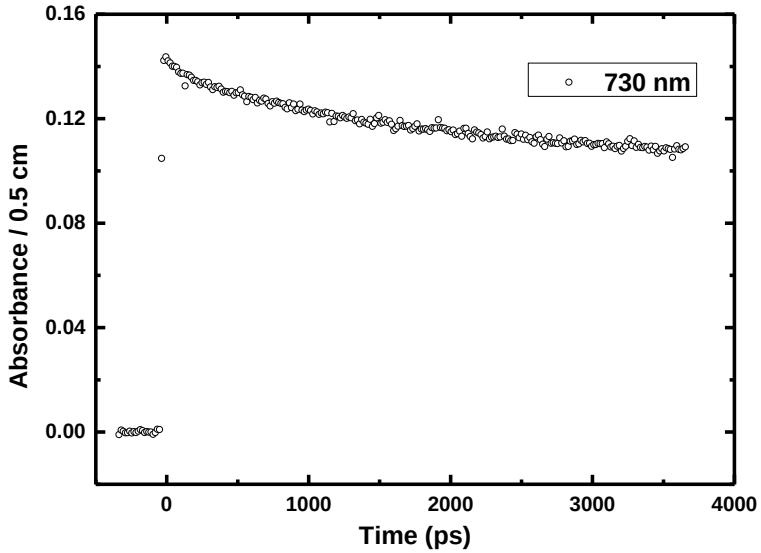

Figure 2.15. *Decay of hydrated electron in pure water at wavelength of 730 nm. The dose is calculated to be 35.8 Gy per pulse*

2.4.3 Supercontiuum

The function of supercontiuum generation is sort of device that broadens the narrow-band pulsed laser into continuous spectrum without destroying the spatial coherence of the laser light as shown in **Figure.2.16**. In combination with a spectrometer and a multichannel detection system, the probe light from supercontinuum generation is able to acquire entire UV-visible or near-infrared transient spectra independently of the shot-to-shot fluctuations and possible long-term drifts of the electron source. Therefore, it is a particular versatile tool that is widely used in time-resolved spectroscopy measurements at ELYSE. The covered spectra range of supercontiuum light depends on the crystals inside the device as well as the type of fundamental pulsed laser. In Elyse, two supercontiua are commonly used, one is commonly used crystal CaF_2, covering the smooth UV-visible light from 350 nm to 800 nm, the other is 4 mm yttrium aluminum garnet (YAG) crystal disk for the near-infrared regions ranging from 700 nm to 1500 nm

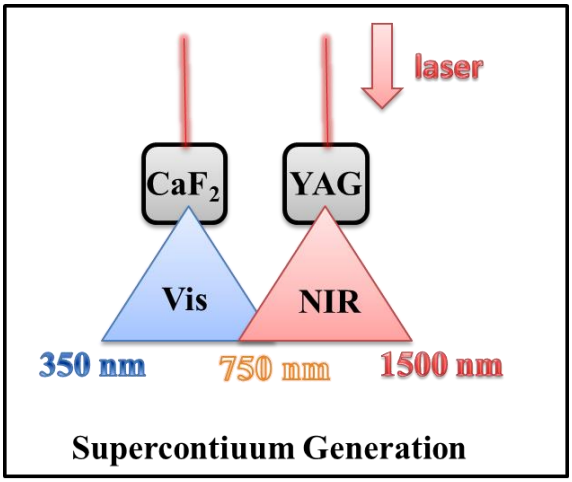

Figure 2.16. *Schematic diagram of supercontiuum gernerations in Elyse.*

The spectra and stability of supercontinuum light is scanned at the beginning of each manipulation and compared with those obtained in different dates; if necessary the continuum generation is optimized to the actual laser conditions. The stability of the peak output power and the shape of spectra over the time are critical and these parameters are strongly related to the energy and position of the pulsed laser delivering on the input of the device.

Figure.2.17 shows typical probe spectra of supercontinua that generated by the femtosecond laser pulse and detected with the transient absorption setup at ELYSE. The shape peak locating around 780 nm corresponds to the fundamental laser.

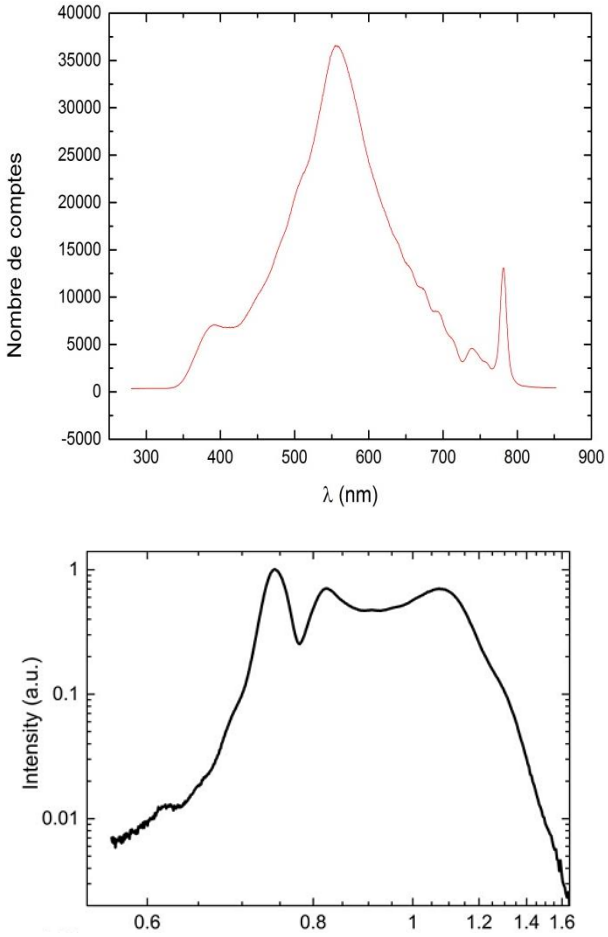

Figure 2.17. *Spectra of the supercontinua used in pulse-probe method. Top: spectrum of the UV-visible supercontinuum generated in a crystal CaF_2. Bottom: logarithmic display of the intensity of distribution of the probe supercontinuum detected by the fiber-coupled spectrometer with single-shot referencing for pulse radiolysis. The fundamental wavelength was adjusted by a notch filter. The near-infrared supercontinua generated in a crystal of YAG.*

2.4.4 Transition absorption of fused silica empty cell

In order to shorten the time duration of the measurements in picosecond pulse radiolysis setups, the analyzing light is coupled with electron beam in the parallel direction into a fused silica cell containing the solutions that are to be studied. It is known that highly energetic radiation of light or relativistic particles can modify the materials. A good example is the phenomenon of a transparent glass tube turning out be brown and dark after certain periods of radiation due to the change of color center in crystal region. So, in the measurements of ELYSE, the electron pulse with high energy (7 MeV) also induced some short-lived species (unknown defects in solid) in fused silica which absorb light. These species have some absorption contribution over the wavelength from UV-visible to near infrared that could influence the results we observe. The transition absorption of fused silica empty cell is then carefully studied using the same pulse-probe method in the same condition as a "blank experiment" for eliminating the optical contribution from the empty cell[30]. It can be seen that from **Figure 2.18**, with the electron pulse of 22.5 Gy, the fuse silica windows exhibit a broad absorption spectrum in visible regions peaking at 600 nm. The maximum absorbance is ~ 6 millioptical density (mOD), which is ten time lower than that of hydrated electron (~ 60 m OD) at the same wavelength. However, at single wavelength of 260 nm, the contribution of cell is relative higher (8 m OD). Therefore, it becomes a "must" that additional subtraction of this contribution is supposed to be made when observing some absorbing short-lived species with lower molar extinction coefficient, like $OH^{\bullet}$, $SO_4^{-\bullet}$, $H_2PO_4^{\bullet}$ radicals.

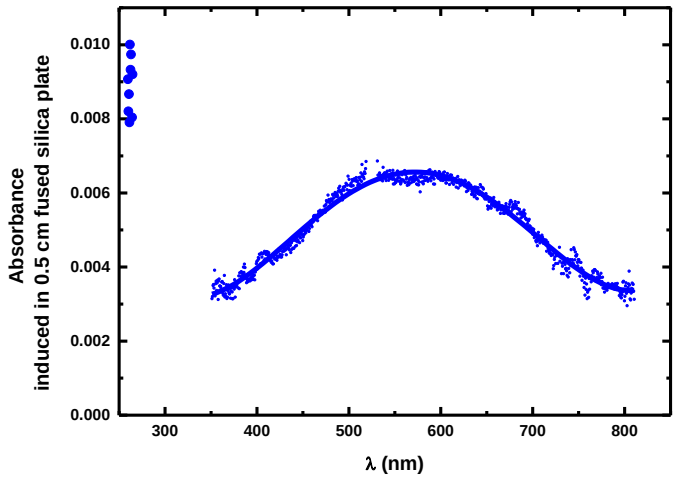

Figure 2.18. *Transition absorption spectrum in the fused silica optical cell 50 ps after picosecond electron of 22.5 Gy per pulse excitation.*

The first observation of empty cell signal was in a fused silica windows with thickness of 1 cm as shown in **Figure 2.19** (left). Because it causes many inconvenience of precise data treatments, it was proposed to shorter the thickness of window by 5 times to 200 µm or use a jet to overcome the problem of undesirable signal contribution. The thinner flowing cell (200 µm) was then specially made as shown in **Figure.2.19** (right). The kinetics observed at 260 nm are compared in **Figure 2.20** with these two different irradiation cells. The initial absorbance of the thinner one is around five times less than that of the previous one as expected.

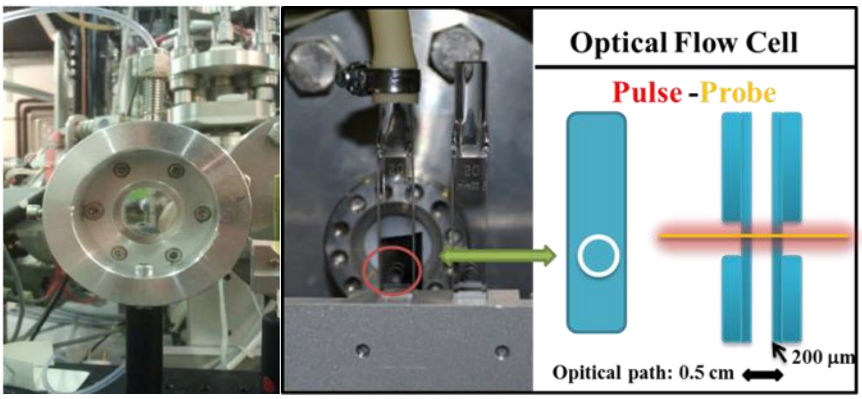

Figure 2.19. *Fused silica empty cell used in direct line of picosecond pulse radiolysis for circulating solutions to avoid accumulation of the radiolytic products.*

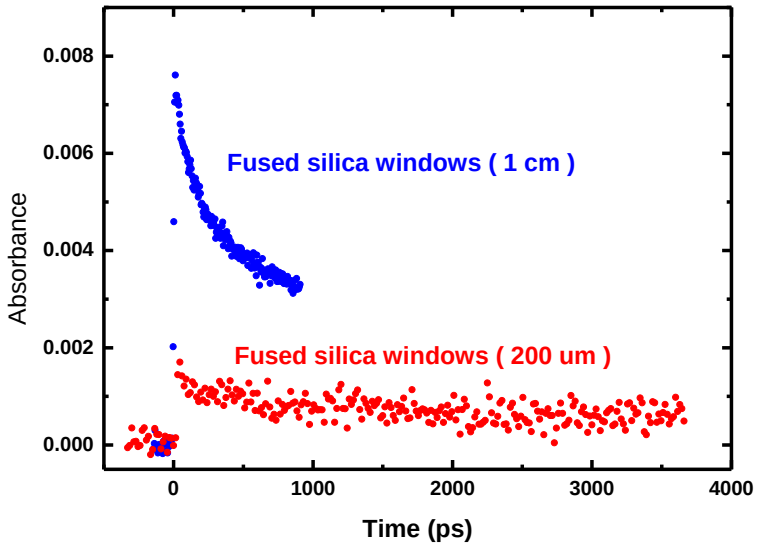

Figure 2.20. *Knetics at λ = 260 nm observed in the fused silica optical cell with a window of 1 cm and compared to that with 200 µm, respectively.*

2.5 Chemicals

All the chemicals are purchased from sigma-Aldrich. Water for dilution or dosimetry was purified until the value of conductivity reaches 18 MΩ.cm by passage through a Millipore purification system. THF for dissolving the inorganic compounds is anhydrous with purity *>99.9 %*. The water containing in THF is *<0.002%*. $HClO_4$ is the commonly used acid but it is dangerous to put any organic compounds into this acid solutions particularly at higher concentration. There would be an explosive accident. H_2SO_4 should be mixed with water much slowly with stirring. Do not put water directly into the acid. There would be an explosive accident.

2.5.1 Acids

Table 2.1 *A list of parameters of acids purchased from sigma-Aldrich chemical products company.*

Acids	*grade*	*Purity*	*Density*	*Mass fraction*	*Concentration*
$HClO_4$	*ACS reagent*	*>99.9 %*	*1.664 g/mL*	*70 %*	*11.6 mol* L^{-1}
H_2SO_4	*ACS reagent*	*>99.9 %*	*1.84 g/mL*	*95-98 %*	*18.4 mol* L^{-1}
H_3PO_4	*ACS reagent*	*>99.9 %*	*1.68 g/mL*	*85 %*	*14.6 mol* L^{-1}
HCl	*ACS reagent*	*>99.9 %*	*1.2 g/mL*	*37 %*	*12.1 mol* L^{-1}
HBr	*ACS reagent*	*>99.9 %*	*1.49 g/mL*	*48 %*	*8.89 mol* L^{-1}

2.5.2 Inorganic salts

Table 2.2 *A list of parameters of inorganic compounds purchased from sigma-Aldrich chemical products company.*

Acids	*grade*	*impurity*	*Density*	*Mole Mass*	*Appearance*
$LiClO_4$	*ACS reagent*	*≤0.005%*	*2.42 g/mL*	*106.4* g/mol	*Powder*
$Mg(ClO_4)_2$	*ACS reagent*	*≤0.005%*	*2.21 g/mL*	*223.3* g/mol	*Powder*
$Ca(ClO_4)_2$	*ACS reagent*	*≤0.005%*	*1.68 g/mL*	*238.9* g/mol	*Powder*
$Sr(ClO_4)_2$	*ACS reagent*	*≤0.005%*	*1.2 g/mL*	*286.5* g/mol	*Powder*

2.6 Summary and Perspectives

Picosecond pulse radiolysis technique has been a very powerful method to study the ultrafast reactions occurring in homogenous liquids induced by ionizing radiation. High temperature and high pressure setup coupled with picosecond accelerator further relate these studies to be more realistic for the application in nuclear reactors by considering the temperature-dependent effect. The principle of this technique is to use femtosecond laser driven electron accelerator to deliver a 7 ps electron pulse on the sample and use probe light to detect the chemical changes induced by the pulse. With this tool, the questions of the reactivity of short-lived water cations ($H_2O^{\bullet+}$) and presolvated electron are partially answered in my thesis but they still require a more sophisticate electron pulse (10-100 fs) to be clarified.

Another important issue is the interfacial radiation-induced chemical reactions. There have been many stead-state measurements concerning how the presence of the surface (PuO_2, ZrO_2 *etc*) modify the radical's reactions and their yields in aqueous. And also some simulation methods are establishing gradually for addressing this issue. Unfortunately, the fundamental time-resolved techniques has so far not been applied in radiation induced reactions taking place in the surface. It would be very exciting to study the reactivity of some interfacial transient species like water hole or hydrated electron which was only observed in pulse radiolysis of liquids phase. Probably, in the near future, free electron laser techniques with pump probe method could be a good option to at least show something different.

References

[1] Lind SC. (1928) The Chemical Effects of Alpha Particles and Electrons. American Chemical Society Monograph Series, No. 2, the Chemical Catalog Company, New York.

[2] Allen AO. (1968) Radiation chemistry today. *J Chem Ed* 45: 290–295.

[3] Mozumber A. (1999) Fundamentals of Radiation Chemistry. Academic Press, New York.

[4] Keene JP. (1960) Kinetics of radiation-induced chemical reactions. *Nature* 188:843–844.

[5] Boag JW, Hart EJ. (1963) Absorption spectra of 'hydrated' electron. *Nature* 197: 45–47.

[6] Mallard, W. G.; Ross, A. B.; Helman, W. P. (1998). NDRL-NIST Solution Kinetics Database: Ver3. Notre Dame Radiation Laboratory and National Institute of Standards and Technology: Notre Dame, IN and Gaithersburg, MD.

[7] Miller JR. (1973) Fast electron transfer reactions in a rigid matrix. Further evidence for quantum mechanical tunneling. *Chem Phys Lett* 22: 180–182.

[8] Closs GL, Calcaterra LT, Green NJ, Penfield KW, Miller JR. (1986) Distance, stereoelectronic effects, and the Marcus inverted region in intramolecular electron transfer in organic radical anions. *J Phys Chem* 90: 3673–3683.

[9] J.F Wishart and BSM Rao eds. (2009) Recent Trends in Radiation Chemistry. World Scientific.

[10] Mozumber A. Hatano Y. (2004). Charged Particle & Photon Interactions with Matter. MARCEL DEKKER, INC. New York.

[11] Kuppermann A. (1967) Diffusion model of the radiation chemistry of aqueous solutions. In: Silini G. (ed.), Radiation Research North-Holland Publishing Company, Amsterdam, pp. 212–234.

[12] Bronskill MJ, Taylor WB, Wolff RK, Hunt JW. (1970) Design and performance of a pulse radiolysis system capable of picosecond time resolution. *Rev Sci Instrum* 41: 333–340.

[13] Jonah CD. (1975) Wide-time range pulse radiolysis system of picosecond time resolution. *Rev Sci Instrum* 46: 62–66.

[14] Tagawa S, Katsumura Y, Tabata Y. (1979). The ultra-fast process of picosecond time-resolved energy transfer in liquid cyclohexane by picosecond single-pulse radiolysis. *Chem Phys Lett* 64: 258–260.

[15] Tabata Y, Kobayashi H, Washio M, Tagawa S, Yoshida Y. (1985) Pulse radiolysis with picosecond time resolution. *Radiat Phys Chem* 26: 473–479.

[16] Kozawa T, Nagahara S, Yoshida Y, Tagawa S, Watanabe T, Yamashita Y. (1997)Radiation-induced reactions of chemically amplified X-ray and electron beam resists based on deprotection of tetra butoxycarbonyl groups. *J Vac Sci Tech* B15:2582–2586.

[17] Yoshida Y, Mizutani Y, Kozawa T, Saeki A, Seki S, Tagawa S, Ushida K. (2001) Development of laser synchronized picosecond pulse radiolysis system. *Radiat Phys Chem* 60: 313–318.

[18] Wishart JF., Cook AR, Miller JR. (2004) The LEAF picosecond pulse radiolysis facility at Brookhaven National Laboratory. *Rev. Sci. Instrum*.75: 4359–4366.

[19] Belloni J, Monard H, Gobert F, Larbre JP, Demarque A, De Waele V, Lampre I,Marignier JL, Mostafavi M, Bourdon JC, Bernard M, Borie H, Garvey T, Jacquemard B, Leblond B, Lepercq P, Omeich M, Roch M, Rodier J, Roux R. (2005) ELYSE — A picosecond electron accelerator for pulse radiolysis research.*Nucl Instrum Meth* A539: 527–539.

[20] Muroya Y, Lin M, Han Z, Kumagai Y, Sakumi A, Ueda T, Katsumura Y. (2008) Ultra-fast pulse radiolysis: A review of the recent system progress and its application to study on initial yields and solvation processes of solvated electrons in various kinds of alcohols. *Radiat Phys Chem* 77: 1176–1182.

[21] Saeki A, Kozawa T, Tagawa S. (2006) Picosecond pulse radiolysis using femtosecond white light with a high S/N spectrum acquisition system in one beam shot. *Nucl Instrum Meth* A556: 391–396

[22] Aoki Y, Nakajyo T, Tsunemi A, Yang JF, Okada Y, Yorozu M, Hirose M, Sakai F, Endo A. (2001) Performance of compact pulse radiolysis system using a photocathode RF gun. Res Chem Intermediat 27: 689–697.

[23] Nagai H, Kawaguchi M, Sakaue K, Komiya K, Nomoto T, Kamiya Y, Hama Y, Washio M, Ushida K, Kashiwagi S, Kuroda R. (2007) Improvements in time resolution and signal-to-noise ratio in a compact pico-second pulse radiolysis system. *Nucl Instrum Meth B* 265: 82–86.

[24] Yang J, Kondoh T, Norizawa K, Yoshida Y, Tagawa S. (2009) Breaking time resolution limits in pulse radiolysis. *Radiat Phys Chem*78: 1164–1168.

[25] Marignier, J. L.; de Waele, V.; Monard, H.; Gobert, F.; Larbre, J. P.; Demarque, A.; Mostafavi, M.; Belloni, J. Time-Resolved Spectroscopy at the Picosecond Laser-Triggered Electron Accelerator Elyse. *Radiat. Phys. Chem.*, **2006**, 75(9), 1024-1033.

[26] Flöttmann, K. (1997). *Estimation of the Thermal Emittance of Electrons Emitted by Cesium Telluride Photocathodes*. Paper presented at the FEL conference, Beijing, China.

[27] Schmidhammer, U.; Jeunesse, P.; Stresing, G.; Mostafavi, M.; *Appl. Spectrosc.* **2014**,*68*,1137-1147.

[28] Muroya, Y.; Lin, M. Z.; Wu, G. Z.; Iijima, H.; Yoshi, K.; Ueda, T.; Kudo, H.; Katsumura, Y. A Re-evaluation of the Initial Yield of the Hydrated Electron in the Picosecond Time Range *Radiat. Phys. Chem.* **2005**, *72*, 169–172.

[29] Fielden, E.M.; Hart, E.J. Activation energy of the hydrated electron water reaction and the ultra-violet absorption spectrum of the hydrated electron. *Trans. Faraday Soc*. 63(12): 2975-82 (**1967**); 64: 3158

[30]Schmidhammer, U.; El Omar, A. K.; Balcerzyk, A.; Mostafavi, M., Transient Absorption Induced by a Picosecond Electron Pulse in the Fused Silica Windows of an Optical Cell. *Radiat. Phys. Chem.* **2012**, *81*, 1715–1719.

Chapter 3: Experimental Evidence for the Reactivity of $H_2O^{\bullet+}$ in Aqueous Solutions

Chapter 3 Experimental Evidence for the Reactivity of $H_2O^{\bullet+}$ in Aqueous Solutions

3.1 State of the art

The interaction of energetic particles with water results in the excitation and ionization of water molecules (**Figure 3.1**). The ionization process (R1) refers to the generation of the excess electrons detached from their parent molecules and leaving behind the positive hole (denoted as $H_2O^{\bullet+}$). This occurs on the timescale of an electronic transition ~10^{-15}s. The earliest chemical processes of $H_2O^{\bullet+}$ followed water ionizing in bulk still remain relative little known and constitute a challenging subject in radiation chemistry. It was generally assumed that, $H_2O^{\bullet+}$ is an extremely unstable charged species, which reacts with a neighboring water molecule on the timescale of a few molecular vibrations (<100 fs) via the proton transfer (R3), forming the H_3O^+ ion and the OH radical. It also recombines back with excess electron at the holes site before the relaxation of the electron, yielding the excited states of water (R2). Therefore, over the past decades, it is $OH^{\bullet}$ radical, instead of $H_2O^{\bullet+}$, that has been thought as the main oxidizing intermediates in indirectly radiation induced damage of moist materials or hydrated biomolecules including DNA and numerous kinetic studies have been devoted to elucidate the reactions process involving $OH^{\bullet}$ radical. However, the reactivity of this radical cation $H_2O^{\bullet+}$, precursor of the $OH^{\bullet}$ radicals towards the matter other than surrounding water, has been a long-term controversial issue and is not yet fully understood.

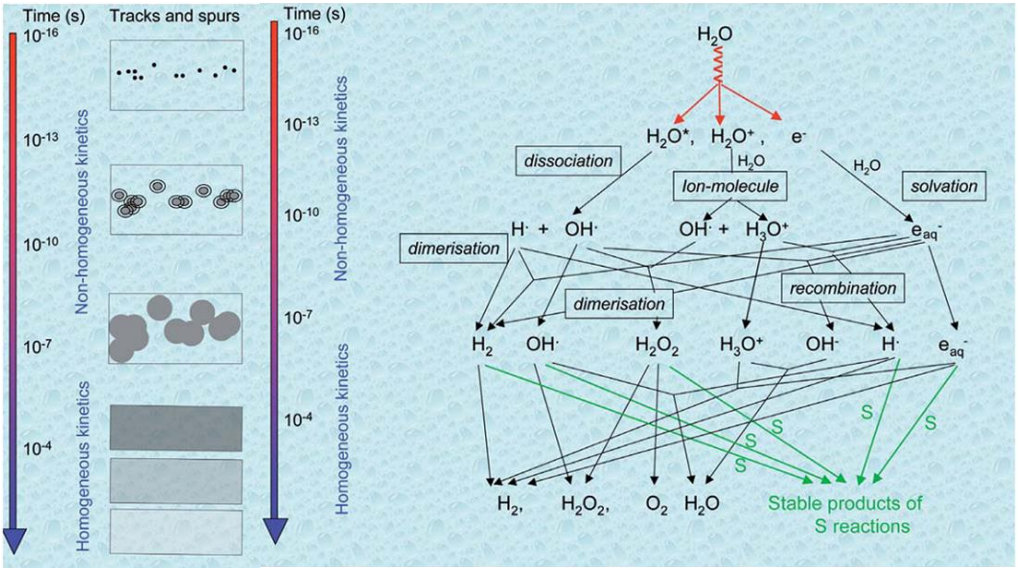

Figure.3.1 *Scheme of reactions of transients species in the spurs or homogenous distribution state produced by irradiated in water with or without a dilute solute acting as a radical scavenger.*

In the last few years, because of the advancement of femtosecond laser technology, many attempts have been made to chase experimentally this cationic species, $H_2O^{\bullet+}$, in different ways. In bulk liquid water, *Gaudel et al.*[1] reported for the first time using the ultraviolet femtoseconds pulses photoionization, that this water radical cation presents a transient absorbance in the ultraviolet spectral domain (460 ~ 410 nm) as shown in **Figure 3.2**. The evolution time of this ion molecule reaction (R3) was estimated as 100 fs in light water aganist 170 fs in heavy water. However, the charge localization step of $H_2O^{\bullet+}$ towards water molecules is suggested as < 40 fs by a theoretical simulation (**Figure 3.3**)[2]. Besides, a followed transient absorption experiment using a 30 fs pulse with the energy of 11 eV was carried out by *Marsalek et al*[2] but they did not see any optical signature of reaction in the visible and deep UV. It was then argued that the first photolysis used by *Gaudel et al.* at 8 eV is, in fact, not sufficient to generate the $H_2O^{\bullet+}$ directly. The induced absorbance at 100 fs is most likely attributed to the simultaneous absorption of one pump and one probe when the two laser pulses are overlapped in time. Nevertheless, very recently, a polarization anisotropy measurement by *Li et al*[3] estimated the lifetime of this transient species as long as 195 ± 5 fs. Additionally, the nature of $H_2O^{\bullet+}$ after the ultrafast X-ray core ionization of water is suggested by *Winter et al*[4] as a doubly charged species, but with the two positive charges located on different water units, $[H_2O^{\bullet+} \ldots H_2O^{\bullet+}]_{aq}$. The molar extinction coefficient for localized $H_2O^{\bullet+}$ is crudely predicated as 80-100 M^{-1} cm^{-1} at peak and a blue shift from 540 nm to 200 nm at the initial stage (<100 fs) is expected to occur as $H_2O^{\bullet+}$ relaxes to $OH^{\bullet}$ radicals. These

pioneering works both using experimental and theoretical methods has gained insight into this electronic signature of this positive radical and initialed the continuous interests to probe it using a more sophistical dynamic technology with time resolution of several femtoseconds or even higher.

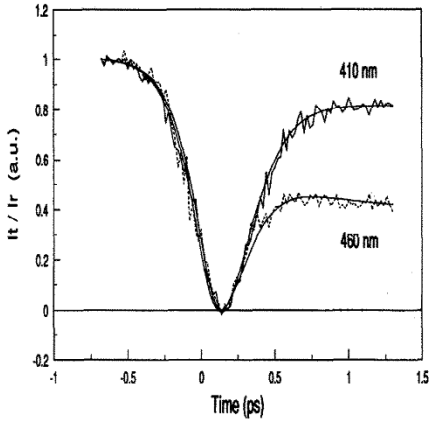

Figure.3.2 *Time-dependence of the induced absorbance at 460 and 410 nm following the femtosecond photoionization of pure liquid water by 100 fs ultraviolet pulse (310 nm). The incomplete recovery of the signal is due to the contribution of hydrated electron. The smooth lines represent the computed best fits of the experimental traces. The fits include the combination of the appearance time of the hydrated electron as measured in the red spectral region and in the near infrared*[1].

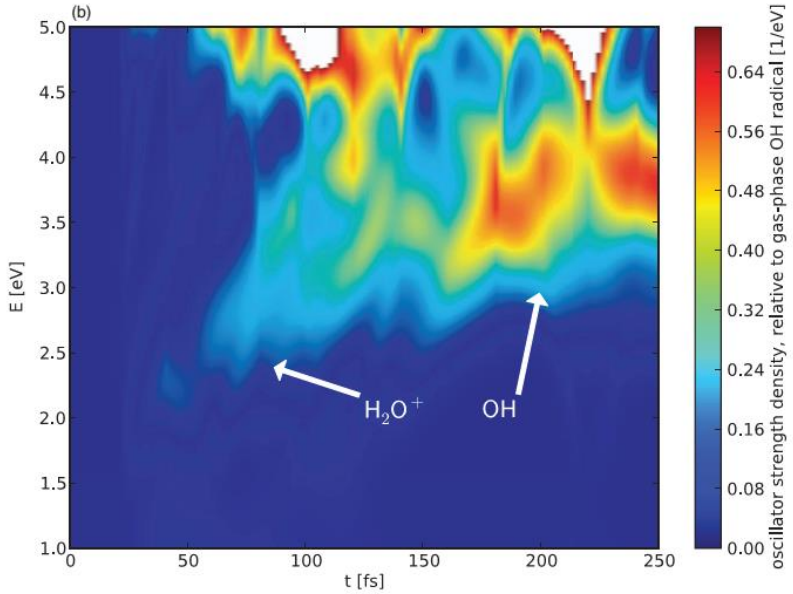

Figure.3.3 *Theoretical spectral simulation of ion molecule reaction of $H_2O^{\bullet+}$ for ionized bulk water*[2]

Despite the difficulties in directly observing this short-lived species, the possibilities concerning the reactivity of $H_2O^{\bullet+}$ with other ions or molecules have been proposed much

earlier. Not long after the discovery of hydrated electron in 1962, it was assumed by *Hamill et al.* [5,6] that hole in water could be trapped prior to hydration using sufficiently high concentrations of appreciated solutes such as NaX (Cl, Br, F, I) or sulfate salts. The measured yield of secondary radicals $Cl_2^{\bullet-}$ or $SO_4^{\bullet-}$ from steady state scavenger using γ rays or time resolved nanosecond pulse radiolysis is attributed to electron transfer from $H_2O^{\bullet+}$ to anions with some contribution from the direct effect of solutes. They added, capturing this "dry" charge species cannot be described by conventional kinetics, *e.g* (rate) =*k* [S], since translation cannot occur for molecular species at $t < 10^{-11}$s. Although this viewpoint is still almost true today, with nanosecond or microsecond pulse in those very early years, it is, unfortunately, not quite distinguishable to exclude the possibility of $OH^{\bullet}$ radicals which can also participate in this oxidizing reaction.

In gas phase, this water cation has been successfully identified with an observed absorption and emission spectra in the range 350 nm-660 nm[7]. The reactivity of $H_4O_2^{\bullet+}$ dimer towards a series of substances has been also studied in the gas phase using a Fourier transform ion cyclotron resonance (FT-ICR). By detecting the ions products from the reactions, it appears that the water dimer cation radical reacts with organic compounds via three competing processes: electron transfer, proton transfer and dissociative electron transfer[8].

In biological system, meanwhile, it was indicated by using ESR method [9] at low temperature that water hole transfer occurs from the inner hydration layer to DNA after γ rays. For the first layer of nine water/nucleotide, no signature of $OH^{\bullet}$ radicals was found, suggesting efficient hole transfer to DNA for these nine waters. As the hydration water /nucleotide increase up to 21, substantial amount of $OH^{\bullet}$ radicals was found, suggesting little charge transfer to the DNA. When the level of hydration over 21 water/nucleotide are reached, the yield of $OH^{\bullet}$ radicals in glass ice are very close to the value found for pure ice. This implies that the $H_2O^{\bullet+}$ towards the matter other than H_2O operated only over relatively short distances, length of several water molecules **(Figure 3.4)**.

Nevertheless, these early time-resolved measurements were limited to the microsecond and nanosecond range. The yields of the direct effect given in the published works were limited to these time windows and the spur reactions of the radicals produced by direct effect were often ignored or not discussed. Therefore, the reactivity of short lived radical cation, $H_2O^{\bullet+}$ in condensed phase was evoked without deducing a firm conclusion about its contribution on the oxidation mechanism of the solute.

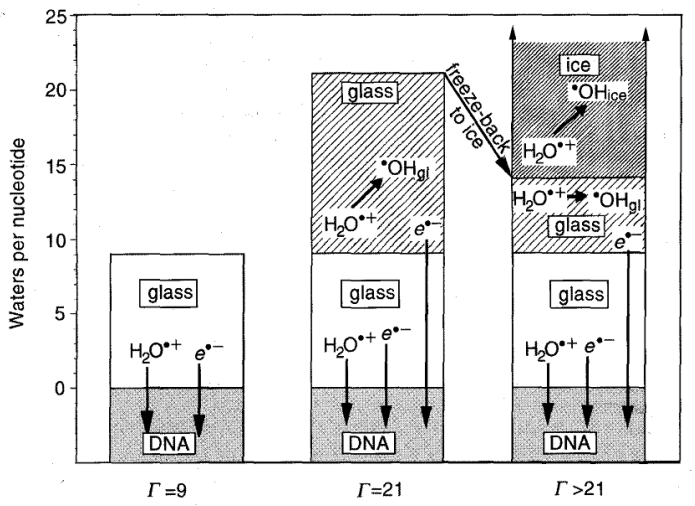

Figure.3.4 *Schematic radiological behavior of the water hydration of DNA*

Picosecond pulse radiolysis is a powerful method allowing us to measure the yields at ultrashort times when the spur reactions are still negligible. Lately, the time-dependent radiolytic yield of $OH^{\bullet}$ radicals in pure water was measured directly by picosecond pulse radiolysis with electron pulse-probe method.

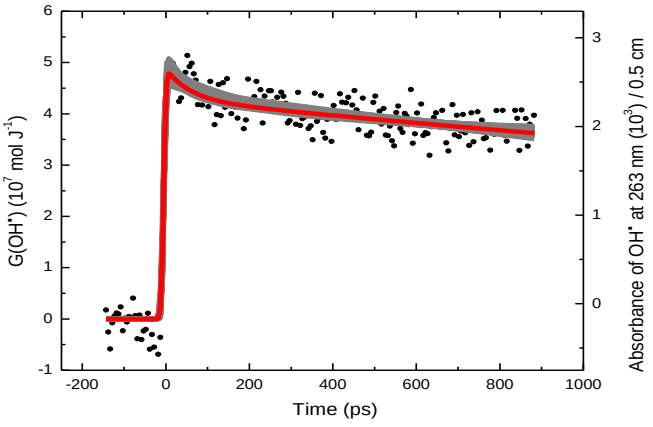

Figure.3.5 *The time-dependent radiolytic yield of the $OH^{\bullet}$ radical obtained by picosecond pulse radiolysis of neat water at 263 nm. The absorbance contribution of hydrated electron and empty cell has been subtracted. The red line is the best fit to the data and the gray area stands for the uncertainty of the fit by a bi-exponential function.*

At 15 ps, the *G* value of $OH^{\bullet}$ radicals was found to be $4.80 \pm 0.12 \times 10^{-7}$ mol J^{-1} (see **Figure 3.5**) by assuming the yield of the hydrated electron at 20 ps equals to 4.25×10^{-7} mol

J^{-1}, and on the basis of the values of the extinction coefficients of e_{aq}^- and $OH^\bullet$, at 782 nm ($\varepsilon_{\lambda=782\ nm}$ = 17025 M^{-1} cm^{-1}) and at 263 nm, ($\varepsilon_{\lambda=263\ nm}$ = 460 M^{-1} cm^{-1}), respectively[10]. The $OH^\bullet$ radicals in neat water after irrdiation orginated from the ion molecule of $H_2O^{\bullet+}$ with water as well as from the dissociation of excited state H_2O^* on the timescale of subpicosecond, but the contruibution from the latter is thought to be low. Gemination recombination of $H_2O^{\bullet+}$ also takes place in parallel with proton transfer. Therefore, it is reasonable that the initial yield of $H_2O^{\bullet+}$, precursor of $OH^\bullet$ radicals are expected to be higer than 4.8×10^{-7} mol J^{-1}.

Several studies in highly concentrated Br^-, Cl^- and HNO_3 solutions were performed with the purpose of capturing the $H_2O^{\bullet+}$.[11-15] For example, as shown in **Figure 3.6**, the kinetics at 370 nm that corresponds after data treatment to the $ClOH^{\bullet-}$ and $Cl_2^{\bullet-}$ radicals. The amount of $ClOH^{\bullet-}$ and $Cl_2^{\bullet-}$ formation within the electron pulse increases notably with increasing Cl^- concentration. This increase is too large to be due to normal water radiolysis. Decomposition of Cl^- due to direct energy absorption is responsible for some of the observed product formation. Additional Cl^- oxidation must occur by its ultrafast reaction within the pulse with a very short lived water decomposition transient, $H_2O^{\bullet+}$.

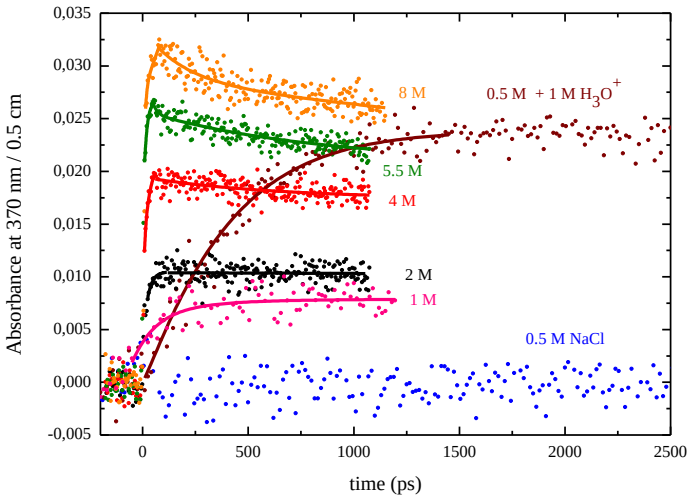

Figure.3.6 *Transient absorption of the product of oxidation of Cl^- in different aqueous solution at 370 nm. The contribution of the hydrated electron absorption and the transient signal of the irradiated fused silica cell at 370nm are subtracted.*

Molecular dynamics simulations were also performed on some of these systems to understand exactly the pre-irradiation configuration of the various components in these highly

concentrated salt solutions. The water local structure is clearly modified by salt addition. The intensity of the first peak (around 2.8 Å) as presented in **Figure 3.7**, which corresponds to H-bonded molecules, decreases with increasing salt concentration. The coordination number of water molecules, computed between $r = 0$ and the first local minimum at $r = r_{min}$ of the water-water radial distribution functions, decreases from 4.41 in pure water to 2.76 at 5.5 M concentration, showing that the probability of finding two water molecules in close proximity decreases with increasing salt concentration. Therefore, it can be concluded that this perturbation of the water local shell by solutes will affect the probability of proton transfer between the radiation produced $H_2O^{\bullet+}$ and the water molecule.

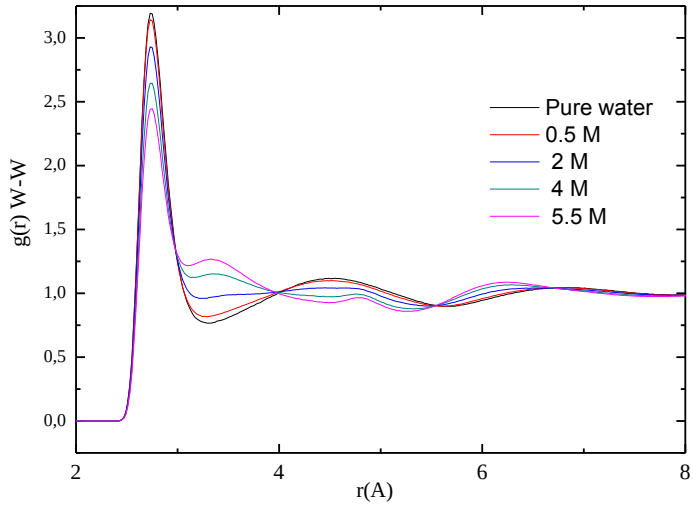

Figure.7 *Water-water radial distribution functions for different NaCl concentration. g(r) for pure water has been added for comparison.*

It may be pointed out that highly concentrated (multi-molar) sulfuric and phosphoric acid solutions are two appropriated, perhaps the best model systems to elucidate the occurrence of the different mechanisms by picosecond pulse radiolysis. The study of these two acid solutions can be motivated by several reasons: 1) several simulations of water/H_2SO_4 or water/H_3PO_4 mixtures were reported showing that the separation in two phases by clustering does not exist in these solutions[16,17]. Therefore, these solutions can be considered as a homogenous system even at high concentrations. This point is critical because if a non-homogenous distribution of water molecules occurs, the observed kinetics becomes meaningless, 2) in contrast to the halides and acid nitric solutions, the rate constant of the reactions of solutes in sulfuric acid or phosphoric solution with $OH^{\bullet}$ is rather low. These

reactions are unlikely in the picosecond time scale even at very high concentration. In fact if the oxidation reaction by $OH^{\bullet}$ radical occurs at short time it becomes very difficult to distinguish between $OH^{\bullet}$ and its precursor contribution on the oxidation mechanism, 3) usually the following relation is used for the experimental yield:

$$G_{\exp} = f_s G_{\mathrm{dir}} + f_w G_{in\mathrm{dir}} \tag{3.1}$$

Where G_{dir} is the yield of direct ionization of solutes, f_w is fraction of water electron density. The yield of reaction produced by the water radical is denoted G_{indir}. In the case of these acid solutions, the following relationship between the electron fractions and the molar ratio of solvent and solutes can be considered.

$$f_s = 1 - f_w = \frac{50 \times [SO_4^{2-}]}{10 \times [H_2O] + 50 \times [SO_4^{2-}]}$$

$$f_s = 1 - f_w = \frac{50 \times [H_2PO_4^{-}]}{10 \times [H_2O] + 50 \times [H_2PO_4^{-}]} \tag{3.2}$$

SO_4^{2-} or $H_2PO_4^{-}$ represent the sulfur or phosphorus compounds including the anions and the non-dissociated molecule. In both case of acid solutions it is possible to study almost neat liquid sulfuric and phosphoric acid and thereby, to eliminate the contribution of water radiolysis. The radiolytic yield of the oxidation via the direct effect of radiation on the solutes can be obtained (f_s almost 1). This important point could not be found in NaBr, NaCl and HNO_3 solutions due to the lower solubility at room temperature. In fact the determination of the yield of direct effect at the picosecond range is decisive. 4) The uncertainty of the radical yield depends on the uncertainty of the extinction coefficient of the secondary radical; The molar absorption extinction coefficient of $SO_4^{\bullet-}$ and $H_2PO_4^{\bullet}$ are well established by different radiolysis[30] or photolysis[18,19] methods and can be used for the precise determination of the radiolytic yield, 5) Contrary to the metal cation such as K^+, Na^+, the counter ions H^+ are not involved in the direct effect. This point is also very important because the metal cations could lose their electron by direct ionization, even if this process is ultrafast, the further electron transfer mechanism is more complicated, 6) the reduction potential of the couple $SO_4^{\bullet-}/SO_4^{2-}$ and $H_2PO_4^{\bullet}/H_2PO_4^{-}$ are estimated to be as high as 2.5 V_{NHE}. If a chemical species can oxidize $H_2PO_4^{-}$ or SO_4^{2-} its reduction potential can be considered to be even higher. For above six reasons, H_2SO_4/H_2O together with H_3PO_4/H_2O constitute two suitable model systems to study the direct effect of ionizing radiation and to show the possible oxidizing reactivity of $H_2O^{\bullet+}$.

3.2 Physicochemical properties of sulfuric and phosphoric acid aqueous solutions

Knowledge of thermodynamics and chemical compositions of concentrated H_2SO_4 and H_3PO_4 solutions is essential to an understanding of the radiation induced reactions involved in these systems.

Sulfuric acid is a strong diprotic acid and dissociates when dissolved in water[20] described as following equilibriums:

$$H_2SO_4 + H_2O \overset{K_{a1}}{\rightleftharpoons} HSO_4^- + H_3O^+$$
$$HSO_4^- + H_2O \overset{K_{a2}}{\rightleftharpoons} SO_4^{2-} + H_3O^+ \qquad (K_{a1}= 2.4 \times 10^6,\ \ K_{a2}=1.0 \times 10^{-2}) \quad (3.3)$$

The concentration of each species changes as the total concentration changes but HSO_4^- anion is observed over the entire concentration range as shown in Fig.3.8.

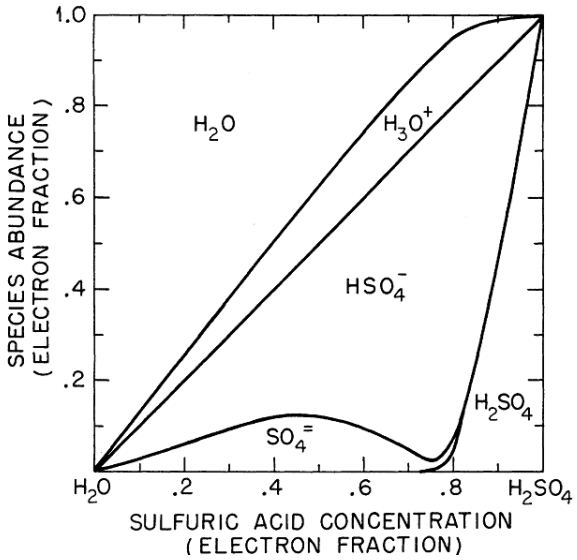

Figiure.3.8 *Relationship of species (anions and undissociated sulfuric acid) abundance with sulfuric acid concentration or electron fraction*[2]

Phosphoric (V) acid, like most polyprotic inorganic oxoacids, is characterized by dissociation constants rising by about 5*pKa* units in each consecutive dissociation step (2.16, 7.21, and 12.32).

$$H_3PO_{4\,(l)} + H_2O_{\,(l)} \rightleftharpoons H_2PO_4^{-}{}_{(aq)} + H_3O^+{}_{(aq)} \qquad PK_{a1} = 2.16$$
$$H_2PO_4^{-}{}_{(aq)} + H_2O_{(l)} \rightleftharpoons HPO_4^{2-} + H_3O^+{}_{(aq)} \qquad PK_{a2} = 7.21 \qquad (3.4)$$
$$HPO_4^{2-}{}_{(aq)} + H_2O_{(l)} \rightleftharpoons PO_4^{3-} + H_3O^+{}_{(aq)} \qquad PK_{a3} = 12.32$$

In diluted solutions, all protons can be dissociated and interact with water molecules through H-bond, leaving the anions behind. At high concentration, as the second and third dissociation constant is so small, the further dissociation process might be disregarded making H_3PO_4 essentially "monoprotic". The established thermodynamic model demonstrated that the ions ($H_2PO_4^-$) further interact with the undissociated phosphoric acid molecules, introducing the dimer species ($H_5P_2O_8^-$) through H bond as described by following chemical equilibrium:

$$H_2PO_4^-{}_{(aq)} + H_3PO_{4(aq)} \rightleftharpoons H_5P_2O_8^-{}_{(aq)} \qquad (3.5)$$

Therefore, it is postulated that, the main species presented in phosphoric acid aqueous solution are $H_2PO_4^-$, H^+, H_3PO_4 and $H_5P_2O_8^-$ over concentrations range from dilute to 15 mol L^{-1}. Other dimeric species involving $H_6P_2O_8$, $H_4P_2O_8^-$, and $H_3P_2O_8^{3-}$ are omitted as they are less stable and the amount is small.

Table.3.1. *Molar distribution of the species in phosphoric acid solutions.*

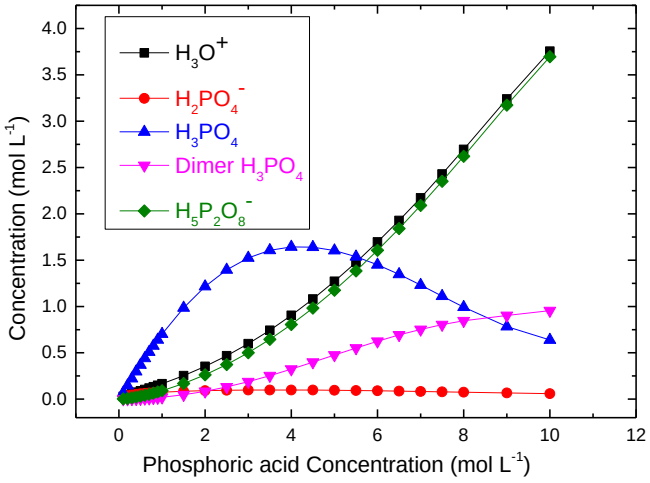

The degree of dissociation seems limited especially when the concentration is above 4 mol L^{-1}. The non-dissociated H_3PO_4 molecule domains in phosphoric acid solution followed by the species H_3O^+ (simplest form) and $H_5P_2O_8^-$. Although the dissociation process was proven to be complex and multistep, on the basis of this model, the primary species could be estimated after the energy deposited on each component in the solutions. More detail information about the distribution of each species in phosphoric acid solutions from dilute to 10 mol L^{-1} is given in **Table 3.1**.

It is also important to note that the neat phosphoric acid is the crystal like state at ambient condition. By giving a heat to 60 °C for several minutes, this solid melts becoming transparent liquid, and then it remains a super cooled liquid for several days at ambient temperature.

3.3 Dose calculation

The energy deposited in concentrated acidic solutions D_{sol} is increased relative to neat water by direct radiolysis of the solutes. The effective dose considering this contribution can be derived from the reference dose in pure water D_{water} as follows:

$$D_{sol}(J\ L^{-1}) = FD_{water}(J\ kg^{-1}) \tag{3.6}$$

With

$$F = d_{sol}(Z_{PO_4^{3-}} p / A_{PO_4^{3-}} + Z_{water}(100-p)/A_{water})(Z_{water}100/A_{water})^{-1}$$

$$F = d_{sol}(Z_{SO_4^{2-}} p / A_{H_2SO_4} + Z_{water}(100-p)/A_{water})(Z_{water}100/A_{water})^{-1} \tag{3.7}$$

Where d_{sol} is the density of the solution, Z is the number of electrons, A is the mass number, and p is the weight fraction of the solute percent. The estimate F and other relevant properties for aqueous solutions of sulfuric acid and phosphoric acid are given in **Table 3.2** and **3.3**.

Table.3.2 *Concentration of sulfuric acid solutions and their corresponding parameters: Electron density fraction of solute f_s, electron density fraction of water f_w, dose factor F, and solution density d_{sol}.*

C [mol L^{-1}]	f_s	f_w	F (g/cm^3)	d_{sol} (g/cm^3)	$[H_2O]/[H_2SO_4]$
1	0.085	0.915	1.05	1.06	53.6
2	0.16	0.84	1.11	1.12	25.7
4	0.30	0.70	1.20	1.23	11.7
6	0.42	0.58	1.29	1.34	7.0
8	0.53	0.47	1.38	1.44	4.58
10	0.62	0.38	1.46	1.54	3.10
12	0.70	0.30	1.55	1.65	2.06
14	0.79	0.21	1.64	1.74	1.33
16	0.88	0.12	1.67	1.80	0.68
18	0.96	0.04	1.69	1.83	0.23

Table.3.3 *Concentration of phosphoric acid solutions and their corresponding parameters: Electron density fraction of solute f_s, electron density fraction of water f_w, dose factor F, and solution density d_{sol}.*

C [mol L^{-1}]	f_s	f_w	***F*** **(g/cm^3)**	d_{sol} **(g/cm^3)**	**$[H_2O]/[H_3PO_4]$**
2	0.17	0.83	1.09	1.11	25.3
4	0.31	0.69	1.17	1.20	11.2
6	0.43	0.57	1.24	1.29	6.5
8	0.54	0.46	1.33	1.39	4.2
10	0.68	0.32	1.45	1.55	2.4
12	0.77	0.23	1.51	1.62	1.46
14.7	0.84	0.16	1.57	1.68	0.96
19	1	0	1.73	1.88	0

3.4 Primary radiation induced reactions involved in H_2SO_4/H_2O and H_3PO_4/H_2O systems

In this section, the possible primary reactions induced by ionizing radiation in aqueous solutions of sulfuric and phosphoric acid are summarized in **Table 3.4.** A brief history of radiolysis of these two acids has been given as follow:

Radiolysis of sulfuric acid aqueous solutions has been extensively investigated over the past decades because it is commonly used in Fricke and Ceric sulfate dosimeter.[21,22] Several observations showed that the yields of the radicals and molecular products in aqueous solutions containing sulfuric acid strongly depend on the solute concentrations.[23,24,25] Early in 1950s, it was postulated that the formation of molecules $H_2S_2O_8$ and H_2SO_5 under ^{60}Co source irradiation provides an evidence that the radicals from water radiolysis interact with the sulfuric acid molecule.[26] The OH· radicals acting as the oxidizing intermediates were considered to attack the molecules H_2SO_4 or its anions.[27] This view was further supported by determining the relative rate constant of the reaction between OH· radicals and sulfate anions in Ce^{III} salt system.[28] In the beginning of 1960s, yields of all the postulated intermediates in sulfuric acid solutions have been established by Boyle over the concentration from 0.4 mol L^{-1} to 18 mol L^{-1}.[24,25] It was pointed out that some of the primary excitations and ionizations are expected to occur in dissociated sulfuric molecules and ions species if the electron fraction is high enough. Although at that moment no direct proof was given on the oxidizing radicals generated by water radiolysis attacking the solutes or the direct oxidizing of solutes, both of these two processes were believed to be valid.[25] With the advent of the pulse radiolysis

technique in 1960s, the formation and yield measurement of sulfate radical ($SO_4^{\bullet-}$ or $HSO_4^{\bullet}$) became a central issue because it was identified as one of the major transients in radiolysis of sulfuric acid. [29] It was also shown that the yields of observed $SO_4^{\bullet-}$ within a 12 ns electron pulse is linearly proportional with the electron fraction over the range from ~0.01 to 0.3, giving a clear evidence of $SO_4^{\bullet-}$ formation by direct ionization of sulfuric acid anions (R5). [30] When diluted solutions of sulfuric acid are irradiated, the H-abstraction reaction takes place between HSO_4^- anion and $OH^{\bullet}$ radical forming the sulfate radical (R7). As the acid aqueous solution becomes concentrated, the amount of non-dissociated sulfuric acid is not negligible and participates in reacting with $OH^{\bullet}$ with a relatively higher rate constant (R8). In radiolysis of a neutral lithium sulfate aqueous solution, the additional sulfate radical formation is not observed in the kinetics apart from the contribution of fast direct action of radiation. Consequently, it was concluded that $OH^{\bullet}$ is not likely to react with sulfate anions SO_4^{2-}.

However, the possibility of electron transfer from solutes to the primary positive holes $H_2O^{\bullet+}$ in aqueous systems as another mechanism was also evoked without a consistent conclusion.

In parallel, several studies have been also carried out on pulse radiolysis and flash photolysis of phosphoric acid and phosphate anions.[31-35] The radical $H_2PO_4^{\bullet}$ in acidic forms has been identified as the main intermediate in radiolysis of H_3PO_4 aqueous solutions; this radicals has an absorption band with a maximum around 520 nm using nanosecond pulse radiolysis.[31,32,33] It was found that the *G* value of direct electron detachment on H_3PO_4 (R16) is 3.4×10^{-7} mol J^{-1}. The rate constant for the reaction between $OH^{\bullet}$ radical and H_3PO_4 or $H_2PO_4^-$ was determined (R18 and R19) by varying the concentration of the phosphate. It was shown that the rate constant of this reaction is 4.2×10^4, 2.0×10^4 mol^{-1} L s^{-1}, which is quite low.

From above, therefore, only the following chemical processes are believed to take place within 7 ps picosecond electron pulse.

$$H_2O \rightarrow H_2O^{\bullet+} + e^-$$

$$e^- + H_2O^{\bullet+} \rightarrow H_2O^{**}$$

$$H_2O + H_2O^{\bullet+} \rightarrow H_3O^+ + OH^{\bullet}$$

$$SO_4^{2-} \rightarrow SO_4^{\bullet-} + e^-$$

$$PO_4^{3-} \rightarrow PO_4^{\bullet2-} + e^-$$

Table 3.4 *Primary radiation induced reactions*	k (L mol^{-1} s^{-1})	
$H_2O \rightarrow H_2O^{\bullet+} + e^-$		(R1)
$e^- + H_2O^{\bullet+} \rightarrow H_2O^{**}$		(R2)
$H_2O + H_2O^{\bullet+} \rightarrow H_3O^+ + OH^\bullet$	8.0×10^{12}	(R3)
$e_{hyd}^- + H_3O^+ \rightarrow H^\bullet + H_2O$	2.3×10^{10}	(R4)
Reactions (H_2SO_4 / H_2O)	k (L mol^{-1} s^{-1})	
$SO_4^{2-} \rightarrow SO_4^{\bullet-} + e^-$		(R5)
$H_2SO_4 + H_2O^{\bullet+} \rightarrow H_3O^+ + HSO_4^\bullet$		(R6)
$OH^\bullet + H_2SO_4 \rightarrow HSO_4^\bullet + H_2O$	1.4×10^7	(R7)
$OH^\bullet + HSO_4^- \rightarrow SO_4^{\bullet-} + H_2O$	4.7×10^5	(R8)
$SO_4^{\bullet-} + H^\bullet \rightarrow HSO_4^-$	1.0×10^{10}	(R9)
$SO_4^{\bullet-} + SO_4^{\bullet-} \rightarrow S_2O_8^{2-}$	7.6×10^8	(R10)
$SO_4^{\bullet-} + OH^\bullet \rightarrow HSO_5^-$	1.0×10^9	(R11)
$SO_4^{\bullet-} + S_2O_8^{2-} \rightarrow S_2O_8^- + SO_4^{2-}$	6.6×10^5	(R12)
$SO_4^{\bullet-} + HO_2 \rightarrow O_2 + HSO_4^-$	3.5×10^9	(R13)
$H^\bullet + S_2O_8^{2-} \rightarrow SO_4^{\bullet-} + HSO_4^-$	2.5×10^7	(R14)
$H^\bullet + HSO_5^- \rightarrow SO_4^{\bullet-} + H_2O$	2.2×10^8	(R15)
Reactions (H_3PO_4 / H_2O)	k (L mol^{-1} s^{-1})	
$PO_4^{3-} \rightarrow PO_4^{\bullet2-} + e^-$		(R16)
$H_3PO_4 + H_2O^{\bullet+} \rightarrow H_3O^+ + H_2PO_4^\bullet$		(R17)
$OH^\bullet + H_3PO_4 \rightarrow H_2PO_4^\bullet + H_2O$	4.2×10^4	(R18)
$OH^\bullet + H_2PO_4^- \rightarrow HPO_4^{\bullet-} + H_2O$	2.0×10^4	(R19)
$H_2PO_4^\bullet + H^\bullet \rightarrow H_3PO_4$	1.3×10^{10}	(R20)
$H_2PO_4^\bullet + H_2PO_4^\bullet \rightarrow H_4P_2O_8$	2.5×10^9	(R21)
$H_2PO_4^\bullet + OH^\bullet \rightarrow H_3PO_5$	4.0×10^9	(R22)
$H_2PO_4^\bullet + HO_2^\bullet \rightarrow H_3PO_4 + O_2$	3.0×10^9	(R23)
$H_2PO_4^\bullet + H_2O_2 \rightarrow H_3PO_4 + HO_2^\bullet$	3.5×10^9	(R24)

3.5 Absorption spectra of transients

3.5.1 Sulfuric acid aqueous solutions

The transient absorption spectra for different solutions (1 to 18 mol L^{-1} sulfuric acid) observed around 15 ps are presented in **Figure 3.9**.

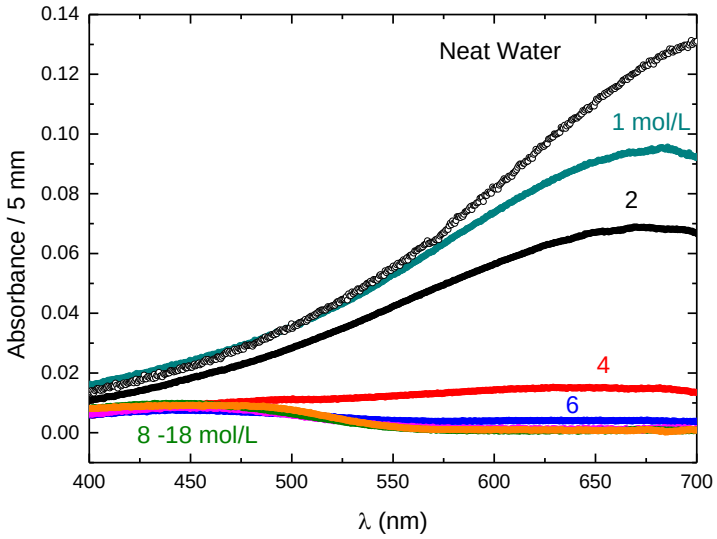

***Figure 3.9**. Transient absorption spectra recorded directly after the picosecond electron pulse (15 ps after time zero) in 1-18 mol L^{-1} H_2SO_4.The contribution of transient absorption induced in the cell windows is subtracted. The radiation dose deposited in neat water is 31Gy per pulse.*

For lower concentrations from 1 to 4 mol L^{-1}, the spectrums show the contribution of solvated electron with its typical large absorption centered in the red region, which is attributed mainly to the solvated electron pair, $(e_{hyd}^-, H_3O^+)_{hyd}$; H^+ effectively reacts with the electron and produce radical $H^\bullet$ in the spurs. The $H^\bullet$ atom absorbs far in the UV with very low contribution. The detail description of reaction R4 will be given in next chapter.

For the solutions containing higher concentrations, as the presolvated or dry electron could be also scavenged by hydronium ions H_3O^+, another absorption band with a maximum around 350-500 nm becomes more obvious compared to those in dilute solutions. From the 6 mol L^{-1} of sulfuric acid, absorbing signal of electron in visible is completely diminished.

Under our experiment conditions, the pulse-probe absorption measurements contain not only the absorbance contribution of $SO_4^{\bullet-}$ (or $HSO_4^{\bullet-}$) but also that of transient species induced in empty cell as well as that of non-scavenged solvated electron in the case of less concentrated sulfuric acid solutions. The absorption spectrum for each concentration are

obtained after careful subtraction of the contributions of the transients induced in empty cell and of the solvated electron (see **Figure 3.10**).

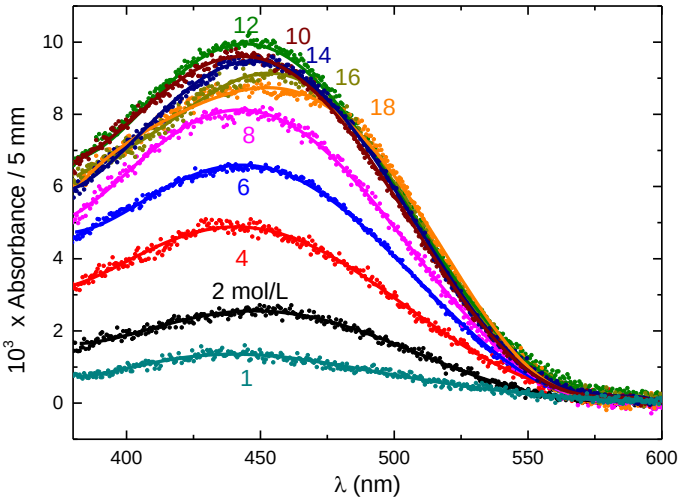

Figure.3.10 *Transient absorption spectra of the radical ($HSO_4^{\bullet}$ and $SO_4^{\bullet-}$) recorded at 15 ps in 1 to 18 mol L^{-1} H_2SO_4 .The contribution of solvated electron and the signal of empty cell in 1 to 6 mol L^{-1} H_2SO_4 is subtracted from the signal.*

An absorption band is clearly observed around 450 and 460 nm which is in excellent agreement with the identical spectrum of $SO_4^{\bullet-}$ in the literatures produced by radiolysis[30] or photolysis[18,19] both in diluted and concentrated solutions up to 10 mol L^{-1}.

It is important to note that the absorption spectrum of $SO_4^{\bullet-}$ gradually has a red shift to 460 nm when the concentration is increasing from 12 mol L^{-1} up to 18 mol L^{-1}. This is attributed to the protonation of this $SO_4^{\bullet-}$ as the non-dissociated H_2SO_4 molecules are the predominate species in very highly acid concentration:

$$SO_4^{\bullet-} + H^+ \rightarrow HSO_4^{\bullet} \qquad (3.8)$$

In order to determinate the radiolytic yield of $SO_4^{\bullet-}$ this radical, the reported molar extinction coefficient (ε, L mol^{-1} cm^{-1}) of $SO_4^{\bullet-}$ at 450 nm were given in **Table.3.5** below:

Table. 3.5 *Molar extinction coefficient of radicals $SO_4^{\bullet-}$ at 450 nm using different methods*

Technique	Reference[29,30,36]	ε, L mol^{-1} cm^{-1}
Laser Photolysis	W. John McElroy *et al.*	1600 ± 100

Laser Photolysis	C. George *et al.*	1600
Laser Photolysis	E. Hayon *et al.*	450± 45
Laser Photolysis	Treinin *et al.*	1100
Pulse radiolysis	B. Lesigne *et al.*	1000
Pulse radiolysis	Heckel *et al.*	1050
Pulse radiolysis	Y. Katsumura *et al.*	1600

In our picosecond pulse radiolysis study, the value of molar extinction coefficient of sulfate radicals is taken as most reliable one as 1600 L mol^{-1} cm^{-1} and it is assumed that this value remain constant and is not concentration dependent for each sulfuric acid solutions, though we realized that this value is supposed to be slightly changed in different solutions.

3.5.2 Phosphoric acid aqueous solutions

Transient absorption spectra of phosphoric acid aqueous solutions (2-19 mol L^{-1} obtained at the time delay of 15 ps) are presented in **Figure 3.11**. Similar to sulfuric acid system, the species that exhibits a broad and featureless band across the visible and near-IR is the transient pair of the solvated electron and hydronium cation (H_3O^+).

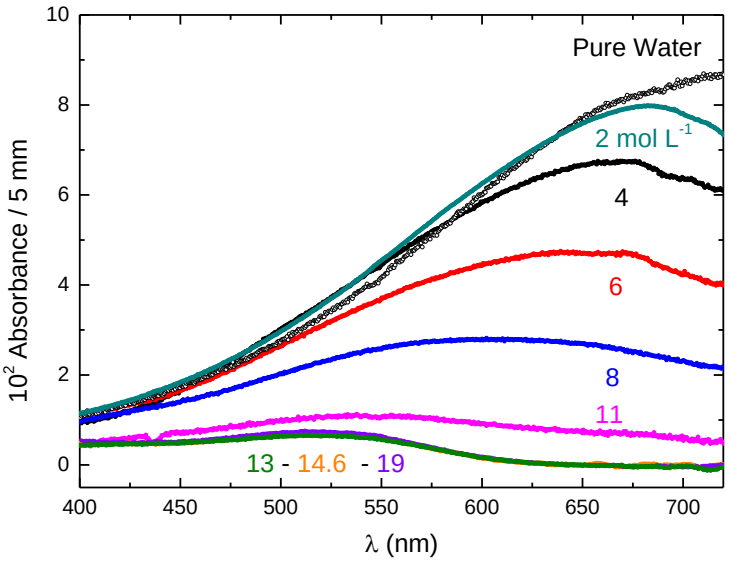

Figure.3.11 *Transient absorption spectra obtained 15 ps after the picosecond electron pulse in 2-19 mol L^{-1} H_3PO_4. The contribution of transient absorption induced in the cell windows has been subtracted. The radiation dose deposited in neat water is 22 Gy.*

Of great interest for the present study is another absorption band that is located in the UV-visible, which becomes more prominent as the solvated electron is scavenged by H_3O^+ ions in these acidic solutions.

In order to identify this intermediate, the contribution of the hydrated electron is subtracted and the difference spectra are presented in **Figure 3.12**. A feature in these resulting absorption spectrum that exhibits a maximum at 520 nm is attributed to the protonated form of the phosphate radical ($H_2PO_4^{\bullet}$), which is in agreement with several previous observations using photolysis and radiolysis on the time scale of microsecond.[31,32,33,35] In radiolysis of sulfuric acid, the spectrum of the sulfate radical ($HSO_4^{\bullet}$) undergoes red shift in 12-18 mol L^{-1} solutions due to the protonation of the radical, while the spectra of the phosphate radical are not much influenced in 2 to 19 mol L^{-1} H_3PO_4 solutions (see **Figure 3.12**). The reason is that the value of *pKa* (5.7) of $H_2PO_4^{\bullet}$ is much higher than that of ($HSO_4^{\bullet}$); so the phosphate radical stays protonated form even in relatively more dilute solutions (1-6 mol L^{-1}).[36]

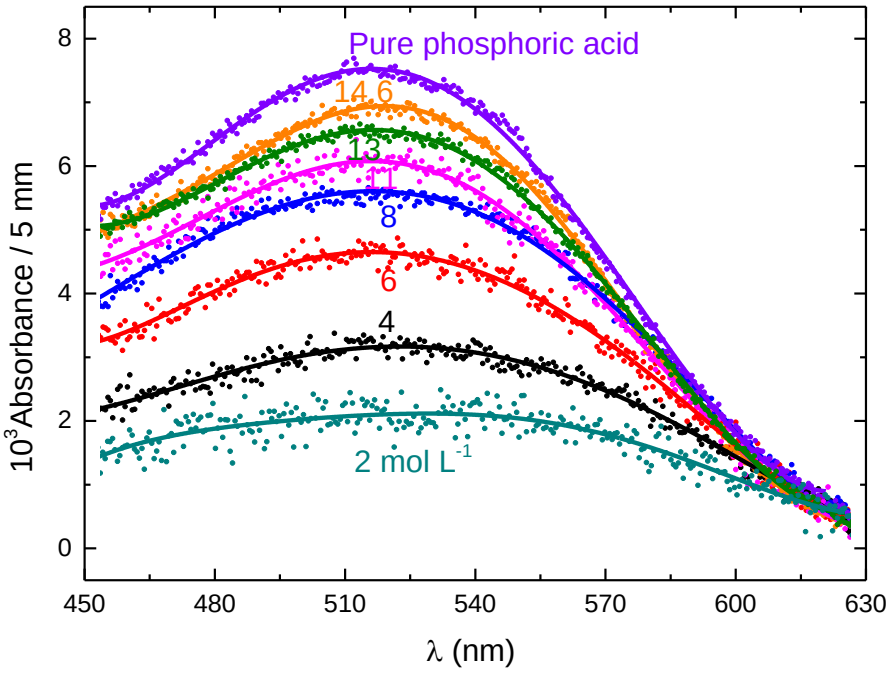

Figure.3.12 *Transient absorption spectra of the radical ($H_2PO_4^{\bullet}$) observed at t=15 ps in 2 to 19 mol L^{-1} H_3PO_4. The contribution of solvated electron in 2 to 11 mol L^{-1} H_3PO_4 was subtracted from the signal.*

In fact, the radical $H_2PO_4^{\bullet}$ in solutions has three acid-base form strongly depended on the acidity (pH) in the solutions. Each radical has its corresponding peak located at different wavelengths with discrepancy of 10 nm and the maximum extinction coefficient of $H_2PO_4^{\bullet}$, $HPO_4^{\bullet-}$, and $PO_4^{\bullet 2-}$ is 1850 $M^{-1}cm^{-1}$, 1550 $M^{-1}cm^{-1}$ and 2150 $M^{-1}cm^{-1}$, respectively[33].

$$H_2PO_4^{\cdot}{}_{(aq)} \underset{}{\overset{K_1=5.7}{\rightleftharpoons}} HPO_4^{\cdot -} \underset{}{\overset{K_2=8.9}{\rightleftharpoons}} PO_4^{\cdot 2-} \tag{3.9}$$

Radicals	$H_2PO_4^{\bullet}$	$HPO_4^{\bullet 2-}$	$PO_4^{\bullet 3-}$
λ_{max} (nm)	520 nm	510 nm	530 nm
ε_{max} (L mol^{-1} cm^{-1})	1850	1550	2150

As in phosphoric acid solutions that we studied, $H_2PO_4^{\bullet}$ form of radical is the only intermediate species from direct or indirect effect of phosphate anions or molecules. The value of molar extinction coefficient is taken as 1850 L mol^{-1} cm^{-1} for the further analysis. The distribution for each phosphate radicals formed is therefore not considered.

3.5 Kinetics analysis

3.5.1 Sulfuric acid system

The kinetics at 450 nm and 730 nm are selected for studying the reactions involving $SO_4^{\bullet-}$ in concentrated solutions. At 730 nm, the slow decay observed for pure water is accelerated by increasing the acid concentration. H^+ effectively reacts with the both solvated and presolvated electron yielding radical $H^{\bullet}$ in the radiation induced tracks as initial absorbance around 730 nm is decreased dramatically by increasing the concentration of acid. This decrease of the initial absorbance is also partly due to the shift of the absorption band of solvated electron which is depending on the concentration of sulfuric acid (see **Chapter 4**). In contrast, the kinetic at 450 nm is very different from those observed at 730 nm. For lower concentrations (1, 2 and 4 mol L^{-1}) a fast decay as at 730 nm is observed but the decay is never end and reaches a plateau within the delay time window (250 ps). For higher concentration the kinetics at 450 nm is very slow. The amplitude of the absorbance at this wavelength is, however, increasing with increasing acid concentration up to 12 mol L^{-1} and then it undergoes a decrease for the highest concentration (14, 16 and 18 mol L^{-1}). The decay observed at 450 nm is due to the spur reactions, mainly with $H^{\bullet}$ atom very similar to the reactions reported for $OH^{\bullet}$ radical in neat water.[37]

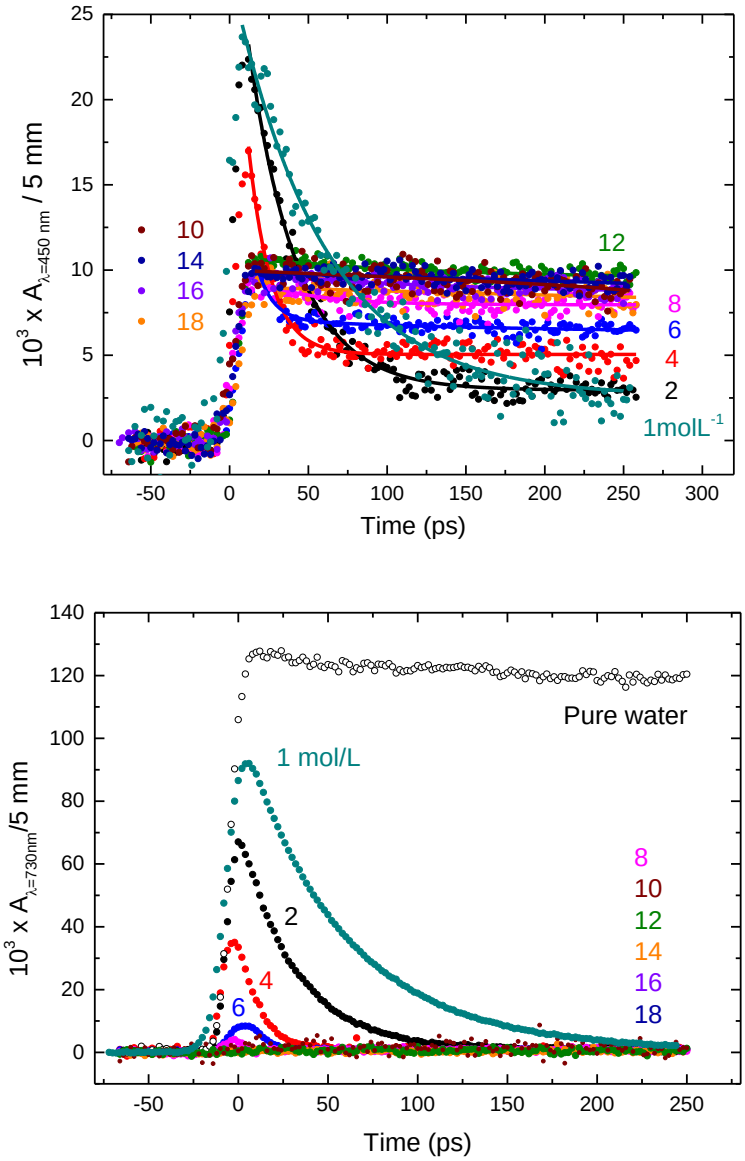

***Figure.3.13**.a) Kinetics at 450 nm (top) on the picosecond scale for solutions containing H_2SO_4 with different concentrations. b) Kinetics at 730 nm for pure water, and solutions containing H_2SO_4 with different concentrations (bottom). In a) and b) the transient absorbance amplitude was corrected by the factor F to consider the density effect (see text).*

In order to elucidate the detailed formation process of $SO_4^{\bullet-}$, the contribution of solvated electron is subtracted from kinetics presented in **Figure 3.13(a)(b)** and summarized as **Figure 3.14** to show the kinetics of $SO_4^{\bullet-}$ and its initial absorbance, respectively.

The detail subtraction process is described below:

The absorbance signal at certain time is attributed to two species, sulfate radicals $SO_4^{\bullet-}$ and electron pairs (e_s^-, H_3O^+).

At 450 nm:

$$A_{450\,nm}(t) = A_{(SO_4^{\bullet-})450\,nm}(t) + A_{(e_{hyd}^-, H_3O^+)450nm}(t) + A_{cell}(t) \qquad (3.10)$$

With the purpose of finding the kinetics of $SO_4^{\bullet-}$, the signal of (e_s^-, H_3O^+) at 450 nm is needed and it can be obtained from the kinetics at 730 nm.

$$n = A_{(e_{hyd}^-, H_3O^+)730nm}(t) \,/A_{(e_{hyd}^-, H_3O^+)450nm}(t) = \varepsilon_{730nm}/\varepsilon_{450nm} \qquad (3.11)$$

The ratio of the solvated electron absorption between 730 nm and 450 nm in neat water is known according to the well-established extinction coefficients of hydrated electron. However, in highly concentrated acid solutions, the band of electron has a strong blue shift while keeping the similar shape. Therefore, this ratio is much related to the acid concentration by taking the shift into account.

For example, for sulfuric acid solutions of 2 mol L^{-1}, the peak of electron turn to the lower wavelength from 715 (1.72 eV) nm to 680 (1.82 eV) nm. In this case, the ratio changed and was supposed to be take the value of ε (765 nm) / ε (485 nm) or in energy (eV) form to be more precisely.

$$n = A_{(e_{hyd}^-, H_3O^+)730nm}(t) \,/A_{(e_{hyd}^-, H_3O^+)450nm}(t) = \varepsilon_{765nm}/\varepsilon_{485nm} \qquad (3.12)$$

The absorption of empty cell during the ionizing radiation is not negligible, and this part of contribution after dose correction can be simply by deduced as the reference line on the basis of kinetics in silica cell previously described.

Figure 3.14 show the kinetics of $SO_4^{\bullet-}$ and its initial optical density, respectively. Interestingly, the initial absorbance at 15 ps of $SO_4^{\bullet-}$ increases in the first series of solutions as expected, but it reaches a maximum value at 12 mol L^{-1} and then drops down slightly (see **Fig. 3.14**). This observation points out that a second parallel mechanism must be involved in the generation of the sulfate radicals.

Figure 3.15 presented the long kinetic of $SO_4^{\bullet-}$ in 10 mol L^{-1} sulfuric acid solution up to 3.5 nanosecond. The slow decay is mainly attributed to the reaction of $SO_4^{\bullet-}$ with reducing $H^{\bullet}$ radicals in the spurs. As in 10 mol L^{-1} acid solutions, most of $H_2O^{\bullet+}$ is scavenged efficiently within the electron pulse, the amount of $OH^{\bullet}$ from the proton transfer is low. The rate constant of $OH^{\bullet}$ with H_2SO_4 is 1.4×10^7 L mol^{-1} s^{-1}. Hence, even in this highly concentrated acid

solution, on the timescale of several nanoseconds, it is not likely to observe the formation of $SO_4^{\bullet-}$ from the oxidizing reaction of $OH^{\bullet}$ radical.

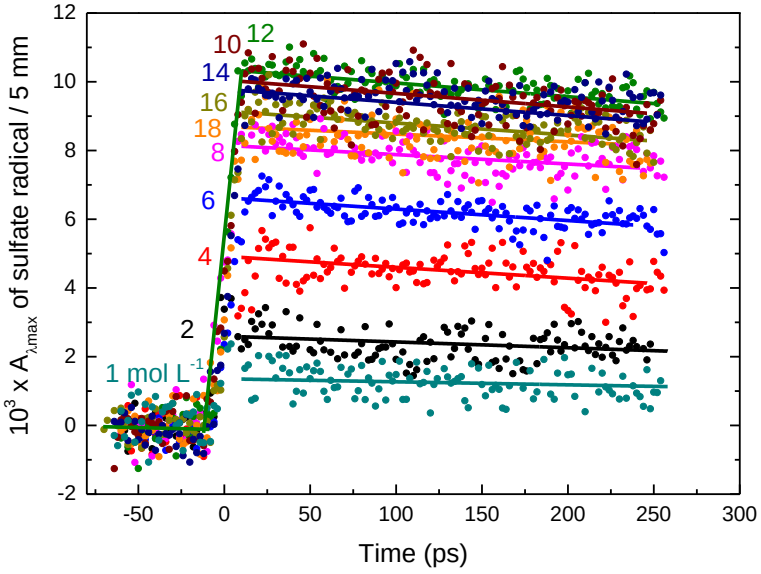

Figure.3.14 *Kinetics of radical ($HSO_4^{\bullet}$ traced at 460 nm or $SO_4^{\bullet-}$ traced at 450 nm) in 1 to18 mol L^{-1} H_2SO_4. The contribution of solvated electron in 1 to 6 M H_2SO_4 is subtracted from the signal.*

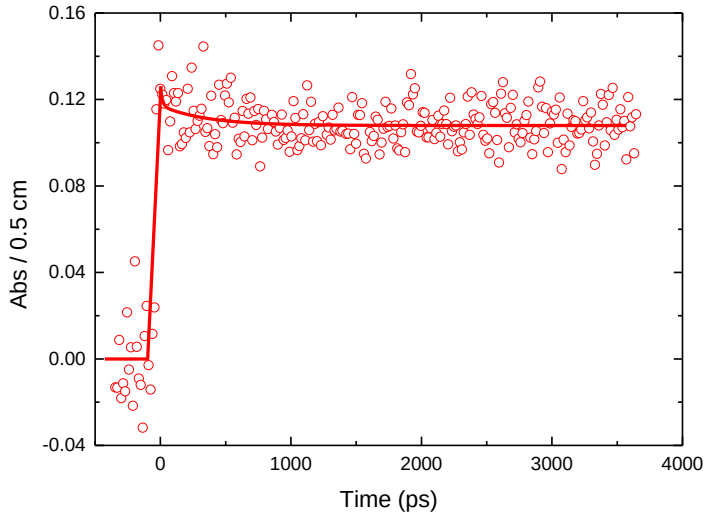

Figure.3.15 *Long decay of $SO_4^{\bullet-}$ radical in 10 mol L^{-1} H_2SO_4 solution up to 3.5 ns.*

3.5.1 Phosphoric acid system

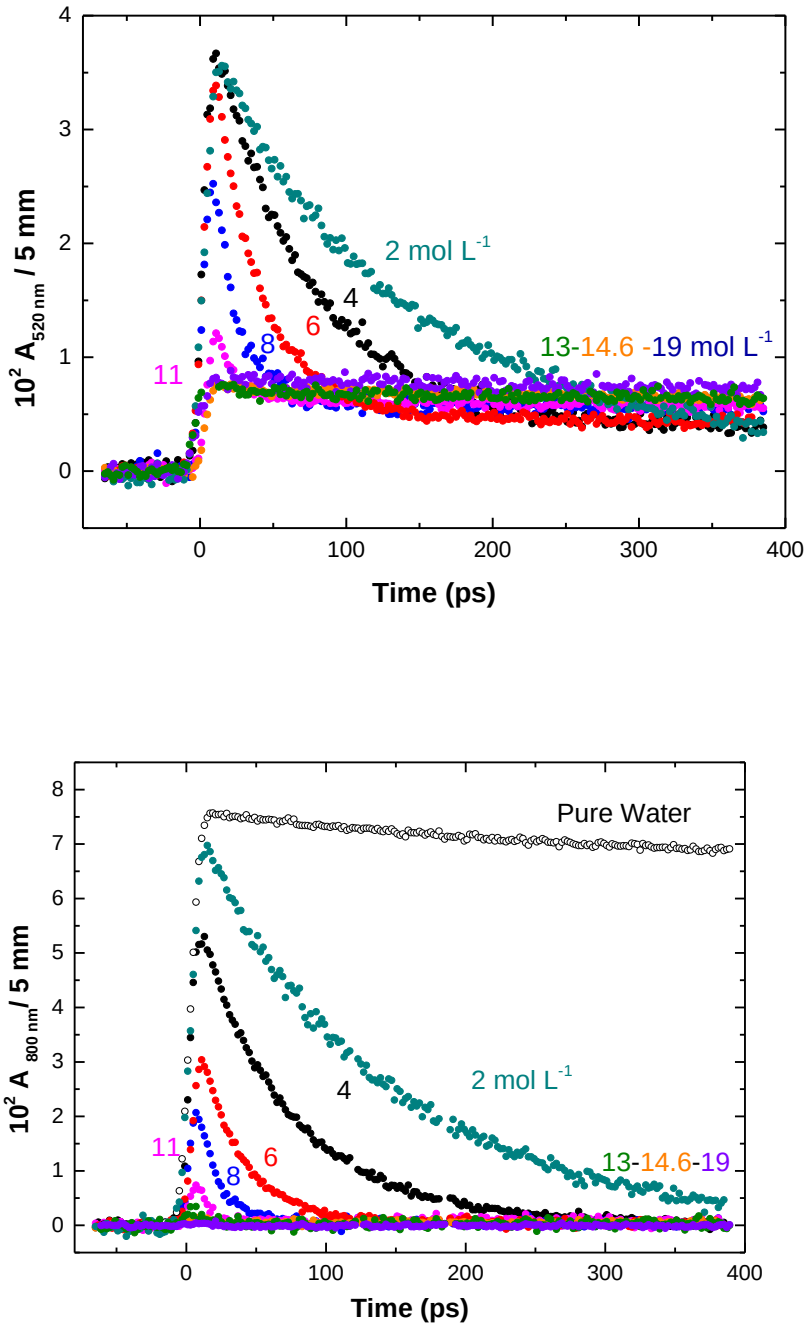

Figure.3.15 *a) Decay of absorbance for solutions containing H_3PO_4. The concentrations are given in the plot. b) Decay of absorbance for solutions containing H_3PO_4. In a) and b) The transient absorbance in this plot was divided by the factor F to take into account the direct radiolysis (see text).*

Figure 3.15 b) shows decay kinetics of the hydrated electron in phosphoric acid solutions of different concentrations observed at 800 nm. This decay becomes faster with increasing concentration of H_3PO_4 leading to a complete decay of the absorbance on the picosecond time scale. It is known that the decay of the transient pair $(e_s^-, H_3O^+)_{hyd}$ involves the hydronium cation; so the increase of H_3O^+ concentration due to the dissociation of H_3PO_4 in water accelerates the decay. Moreover, the initial transient absorption at 800 nm substantially decreases as the rapid reaction of presolvated electron with H_3O^+ occurs in concentrated solutions. The kinetic behavior at 520 nm differs considerably from the one observed at 800 nm. The rapid decay is followed by a plateau after a certain delay time that varies with the acid concentration (see **Figure 3.15a**). In fact, both the (paired) solvated electron and $H_2PO_4^{\bullet}$ absorb at this wavelength in dilute solutions; the rapid decay component is apparently due to the solvated electron. In concentrated acid solutions (11-19 mol L^{-1}), the scavenging of the electron is completed within the electron pulse, and the slow decay corresponds to the kinetics of $H_2PO_4^{\bullet}$. The initial absorption increases as the concentration of phosphoric acid increases.

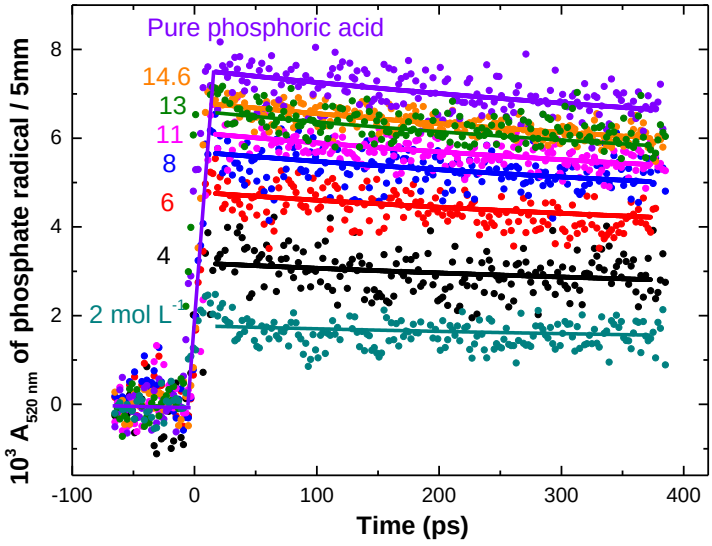

Figure 3.16 *Kinetics of the ($H_2PO_4^{\bullet}$) radical in aqueous H_3PO_4. The contribution of solvated electron in 2 to 11 mol L^{-1} H_3PO_4 has been subtracted as described in the text. The nominal concentrations of the phosphoric acid are indicated in the plot.*

The optical contribution of electron pair as well as empty cell was subtracted as mentioned above which is very similar to sulfuric acid system, and the kinetic of the ($H_2PO_4^{\bullet}$) radical in aqueous solutions is shown in **Figure 3.16**.

Similar to sulfuric acid system, **Figure 3.17** gives the long kinetic of $H_2PO_4^{\bullet}$ in 13 M sulfuric acid solution up to 3.5 nanosecond. The slow decay is due to the reaction between $H_2PO_4^{\bullet}$ and $H^{\bullet}$ radicals which seems a little faster than that in sulfuric acid solution as the rate constant is estimated relatively higher.

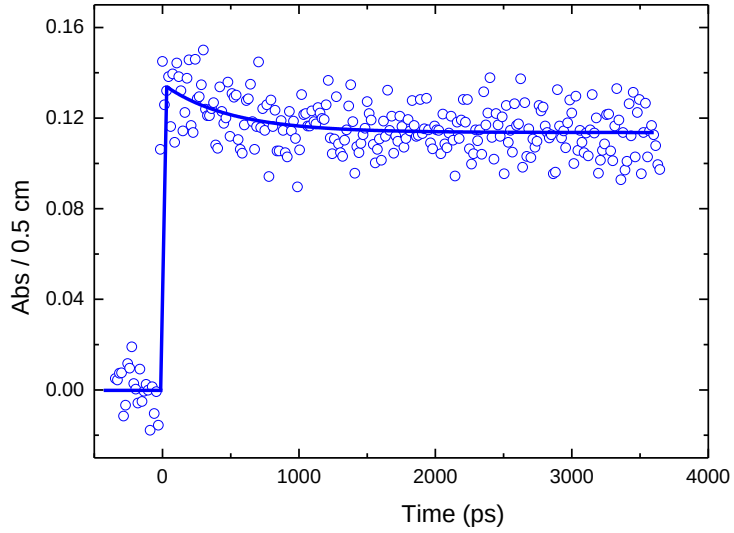

Figure.3.17 *Long decay of the ($H_2PO_4^{\bullet}$) radical in 13 mol L^{-1} aqueous H_3PO_4 to 3.5 ns. The contribution of solvated electron has been subtracted as described in the text.*

3.6 Yield and redox potential of $H_2O^{\bullet+}$

3.6.1 Yield of $H_2O^{\bullet+}$ in sulfuric acid solutions

To obtain the yields of $SO_4^{\bullet-}$ based on the optical measurements in our experiment, the value of molar absorption coefficient, ε ($SO_4^{\bullet-}$, 450 nm) =1600 $dm^3\ mol^{-1}\ cm^{-1}$ is considered as mentioned before.

Assuming that ε ($SO_4^{\bullet-}$, 450 nm, $HSO_4^{\bullet-}$ 460 nm) remains unchanged from 1 to 18 mol L^{-1}, the experimental yield of $SO_4^{\bullet-}$ (and $HSO_4^{\bullet-}$) is calculated and listed in Table 3.6 and Fig. 3.17. When the concentration of sulfuric acid is 18 mol L^{-1}, the amount of water molecule is very rare and unlikely to produce the $H_2O^{\bullet+}$. The experimental yield G_{exp} value obtained for 18 mol L^{-1} is considered to be almost the radiolytic yield of the direct effect ((G_{dir} = 3.5 ± 0.1) × 10^{-7} mol J^{-1}). With this critical value, the linear slope is plotted in Fig 3.17 denoting the contribution of the direct effect on the oxidation as a function of electron fraction. This line shows clearly that the direct effect alone cannot be response alone for the ultrafast built up of the oxidation products of sulfuric acid.

$$G_{\text{exp}} = f_{\text{s}}G_{\text{dir}} + f_{\text{w}}G_{\text{indir}}$$

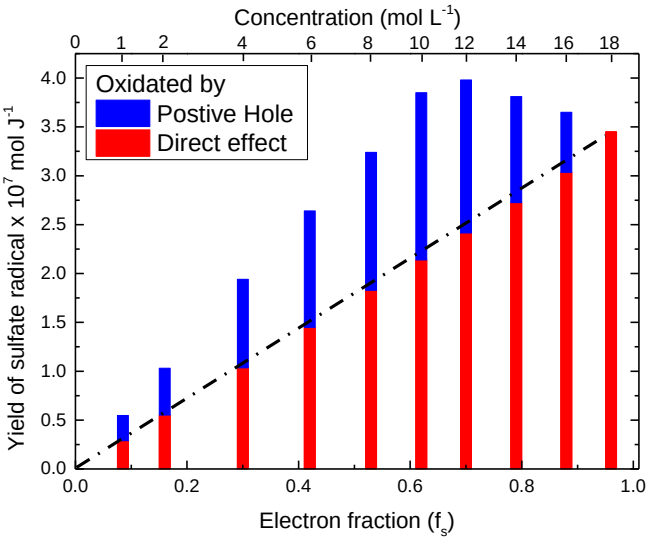

Figure 3.17 *Yield of sulfuric acid radical formation versus electron fraction of the solute. The value at 18 M is considered as the direct effect yield and is linearly extrapolated to the zero concentration. The supplementary yield is considered to be due to the electron transfer reaction with radical cation $H_2O^{\bullet+}$.*

For instance, in the case of 1 mol L^{-1} sulfuric acid solution (f_s = 0.085), if we consider only the direct effect for its formation, the value of direct effect yield must be 6.5 × 10^{-7} mol J^{-1}, which is too large compared to the values usually reported for the direct effect yield (lower

than 5×10^{-7} mol J^{-1}). Therefore, the observed yield cannot be explained only by the direct effect.

As the rate constant of $OH^{\bullet}$ radical with solutes is low and the reaction is unlikely on the timescale of picosecond range, the only reaction that can explain the additional formation of this radical is due to the reaction (R6).

$$H_2O^{\bullet+} + SO_4^{2-} \rightarrow SO_4^{\bullet-} + H_2O$$

This contribution is not linear with the electron fraction and reaches its maximum for f_s = 0.6 – 0.7 (see **Figure 3.17**). In fact, for the lowest concentrations (1 and 2 mol L^{-1}) the amount of water is important and still majority of the radical cation $H_2O^{\bullet+}$ reacts also with surrounding water molecule to form $OH^{\bullet}$ radical. For highest concentrated solutions the amount of water is negligible and then the contribution of the proton transfer reaction (R3) is insignificant.

C [mol L^{-1}]	f_s	f_w	$A_{SO_4^{\bullet-}} \times 10^3$ (t = 15 ps)	$G_{SO_4^{\bullet-}\ 10\ ps} \times 10^7$ mol J^{-1}
1	0.085	0.915	1.38	0.55
2	0.16	0.84	2.58	1.03
4	0.30	0.70	4.87	1.94
6	0.42	0.58	6.59	2.64
8	0.53	0.47	8.12	3.24
10	0.62	0.38	9.64	3.85
12	0.70	0.30	10.01	3.98
14	0.79	0.21	9.55	3.81
16	0.88	0.12	9.14	3.65
18	0.96	0.04	8.64	3.45

From the data of **Figure 3.18**, the yield of radical cation $H_2O^{\bullet+}$ scavenged by sulfuric acid is shown. It is interesting to note that the scavenged yield increases with the concentration of sulfuric acid and reaches a plateau with value around 5.2×10^{-7} (see **Figure 3.11**). Especially interesting thing is the behavior observed at concentrations of 12, 14 and 16 mol L^{-1}, at which the amount of water is so low that reaction (R3) is almost suppressed and $H_2O^{\bullet+}$ scavenging occurs within a few tens of femtoseconds. For these three solutions, the yield of scavenged $H_2O^{\bullet+}$ is found to be about $(5.2 \pm 0.2) \times 10^{-7}$ mol J^{-1} which is larger than the yield of hydrated electron at 1 ps (4.7×10^{-7} mol J^{-1}).[38] That means that the reactions (R3) and (R6) are also in competition with the following geminate recombination (R2):

$$H_2O^{\bullet+} + e^- \rightarrow H_2O$$

Therefore, it can be considered that the yield of ionized water from the electron ionizing radiation at the time ~10^{-15} s is no less than the value of 5.1 ± 0.2 × 10^{-7} mol J^{-1}, within the experimental uncertainty.

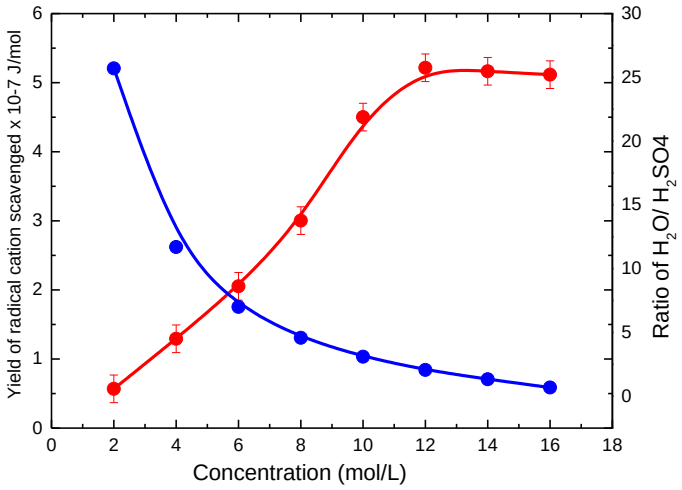

Figure.3.18 *Yield of scavenged radical cation $H_2O^{\bullet+}$ is obtained from the equation:* $G_{scv} = \frac{G_{exp} - f_s G_{dir}}{f_w}$ *(left) and the ratio of H_2SO_4 and water (right) as a function of sulfuric acid concentration in the aqueous solution.*

Finally, the picosecond experimental yield of sulfuric acid radical formation plotted as a function of electron fraction is compared with the data given in the literature based on nanosecond pulse radiolysis (**Figure 3.19**). Obviously the observed yield is dependent on the accessible times scale, in other words, the duration of electron pulse. To be best comparable with our condition, we report only the fast component of sulfuric radical yield which is formed within the nanosecond pulses (duration 12 or 100 ns) from the previous works. In this case, a possible contribution of $OH^{\bullet}$ radical is excluded. The experimental yield achieved by picosecond pulse radiolysis is distinctly higher than those obtained with nanosecond resolution. The data from Boyle are given over a large concentration range as in our work. His results obtained by using the scavenging method at 100 ns are also lower than those measured in this work due to the spur reactions of the secondary radical. But it is very interesting that both of data is sharing the same trend, and an invert region of the yield at highest concentrations, was also observed by Boyle.[24,25]

At the end, the role of excited states should be discussed in these processes. In fact, a part of energy is absorbed by forming excited states. It is known that the yield of H_2O^{**} channel forming $^{\bullet}O^{\bullet}$, $H^{\bullet}$ and $OH^{\bullet}$ is lower than that of ionization in neat water. Nevertheless, the amount of solvated electron was also measured and it is found that this amount (after

correction with the factor *F*) is not increased by increasing the solute concentration. Consequently, the channel involving the following reaction is not significant in our system:

$$H_2O^{**} + SO_4^{2-} \rightarrow H_2O + SO_4^{\bullet-} + e^-$$

In addition, the excited state of SO_4^{2-**} is also formed by electron pulse. These states can relax to the ground states, form new radicals or auto-ionize into the secondary radical $SO_4^{\bullet-}$.We considered this process as the direct effect even if a ultrashort-lived transient excited state can be involved for the formation of $SO_4^{\bullet-}$.

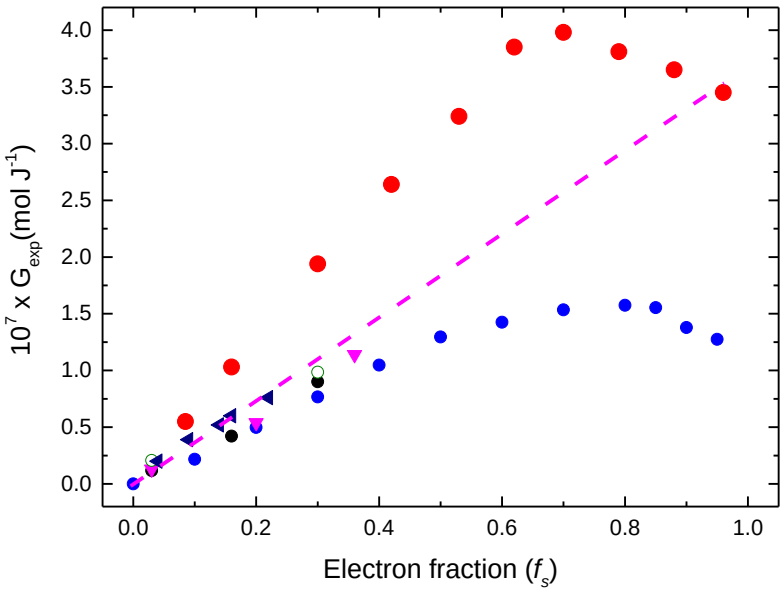

Figure.3.19 *Experimental yield of sulfuric acid radical formation determined on different time scales versus electron fraction of the solute. For the studies using nanosecond pulses only the yield of formation within the 10 ns or 100 ns electron pulse is reported in the literature; we corrected these data for comparison by using the same extinction coefficient* $\varepsilon_{450\ nm}$ *= 1600* mol^{-1} *L* cm^{-1}. ● *This work, within 10 ps pulse;* ●*Lesign et al.*[30] *within 12 ns pulse,* ● *Boyle*[24] *scavenging at 100 ns,* ▼*Katsumura el al. within 100 ns pulse,* ○*Sworski el al. 100 ns pulse* [28] , ◀*Katsumura et al 100 ns pulse using* $LiSO_4$ *solutions instead of* H_2SO_4*.. Dashed line is expressed to show the direct effect yield estimated in this work.*

3.6.2 Yield of $H_2O^{\bullet+}$ in phosphoric acid solutions

Special attention has been paid to radiolysis of pure phosphoric acid, which enabled us to determine the direct radiolytic yield, G_{dir}, of $H_2PO_4^{\bullet}$. As the same absorption spectra is observed in neat acid, it can be considered that in neat phosphoric acid, the electron detachment is followed by deprotonation, which is very rapid; consequently only $H_2PO_4^{\bullet}$ is formed within the duration of the electron pulse. The molar extinction coefficient of $H_2PO_4^{\bullet}$ was estimated as 1850 L mol^{-1} cm^{-1} in this study as the most reliable value. The yield of $H_2PO_4^{\bullet}$ observed as a function of the electron density fraction is presented in **Fig 3.20**. The direct effect is proportional to the electron density fraction that was estimated from the radiolytic yields in the neat phosphoric acid. As the oxidation of H_3PO_4 by $OH^{\bullet}$ radical is too slow to occur on the picosecond time scale, the supplementary yield, G_{indir}, observed for each concentration is thought to be the scavenging of $H_2O^{\bullet+}$ by rapid electron transfer reaction (R17).

Table 3.8 *Concentration of phosphoric acid solutions and relevant parameters: Electron density fraction of solute f_s, electron density fraction of water f_w, dose factor F, and solution density d_{sol}. The absorbance of $H_2PO_4^{\bullet}$ at 15 ps is obtained from $A_{H_2PO_4^{\bullet}}$. (t = 15 ps, λ = 520 nm) = A_{obs}(t = 15 ps, λ=520 nm) – $A_{solvated\ electron}$(t = 15 ps, λ= 520 nm) – A_{cell} (t = 15 ps, λ= 520 nm). The value of the absorbance due to the transient species induced in the windows of the cell around 520 nm, A_{cell} (15 ps), is 6.11 ×10^{-4} based on the work reported in ref.*

C [mol L^{-1}]	f_s	f_w	$A_{H_2PO_4^{\bullet}} \times 10^3$ (t = 15 ps)	$G_{H_2PO_4^{\bullet}\ 15\ ps} \times 10^7$ mol J^{-1}
2	0.17	0.83	1.76	0.86
4	0.31	0.69	3.16	1.55
6	0.43	0.57	4.75	2.33
8	0.54	0.46	5.65	2.77
11	0.68	0.32	6.08	2.98
13	0.77	0.23	6.56	3.21
14.6	0.84	0.16	6.77	3.32
Neat	1	0	7.49	3.67

The observed yield, G_{exp}, after the electron pulse obeys the same equation as in sulfuric acid

$$G_{\exp} = f_s G_{\mathrm{dir}} + f_w G_{in\mathrm{dir}}$$

We have demonstrated that in the sulfuric acid system the electron transfer from the solute to $H_2O^{\bullet+}$ competes with proton transfer reaction (R3) as the solute disturbs water molecules in

the first solvation shell. This reaction is the predominate reaction that involves $H_2O^{\bullet+}$ and it also competes with the geminate recombination of the $H_2O^{\bullet+}$ and the excess electron (R2).

In Figure 3.21, the yield of $H_2O^{\bullet+}$ scavenging in phosphoric acid is compared with sulfuric acid. The value of the scavenged yield increases as the concentration increases to 6 mol L^{-1} reaching a constant level of 1.5×10^{-7} mol J^{-1}. For scavenging of $H_2O^{\bullet+}$ by phosphoric acid, this plateau values is much lower than for sulfuric acid. In the latter case, the yield of scavenged $H_2O^{\bullet+}$ increases up to 12 mol L^{-1} reaching a constant level of 5.1×10^{-7} mol J^{-1}. Therefore, it appears that the charge transfer in the phosphoric acid system is less efficient than in the sulfuric acid system.

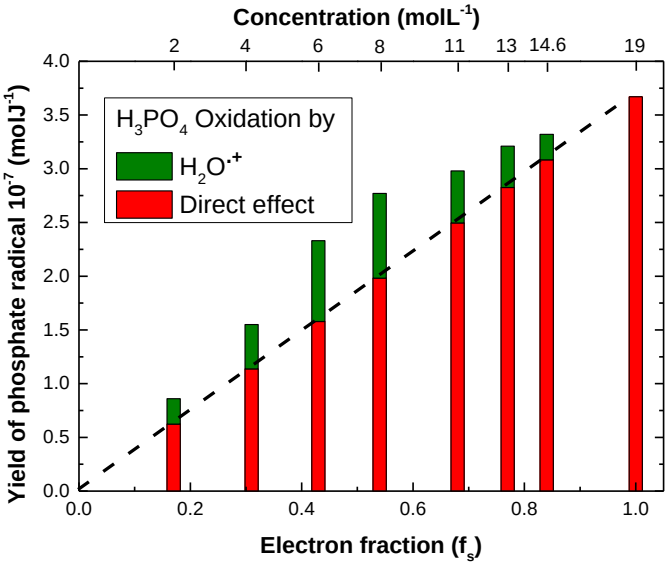

Figure 3.20 *Radiolytic yield of phosphoric acid radical vs. the electron fraction of the solute. The obtained yield at 19 mol L^{-1} is considered as the direct effect yield that is linearly extrapolated to the zero (dash line). The superliner contribution (green bars) is due to the charge transfer reaction involving water radical cation $H_2O^{\bullet+}$.*

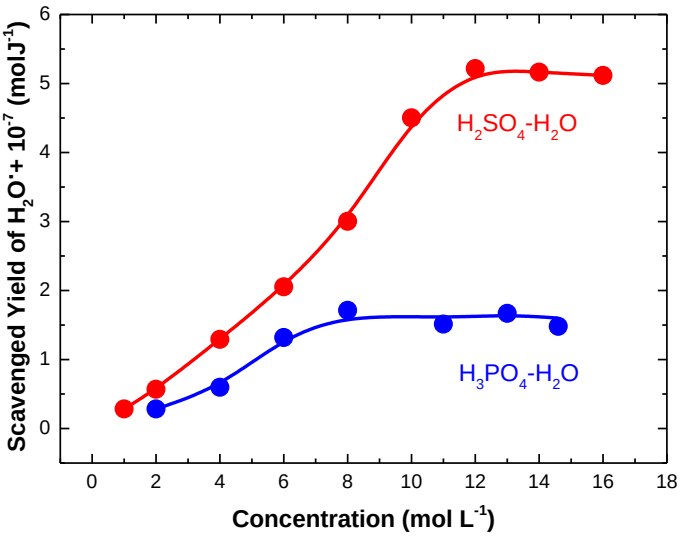

Figure 3.21 *The end of pulse radiolytic yield of scavenged radical cation $H_2O^{\bullet+}$ in aqueous sulfuric and phosphoric acid solutions.*

Phosphoric acid, exhibits dissociation constants that increase 5 *pK* units in each consecutive dissociation step. In dilute solutions, all protons can dissociate and interact with water molecules by forming H-bonds, leaving the anion behind. At high concentration of the acid, as the second and third dissociation constant decrease, the further dissociation can be disregarded. The established speciation model indicates that ($H_2PO_4^-$) anions further interact with undissociated acid yielding ($H_5P_2O_8^-$) anions by forming an H-bond. Therefore, the main species in phosphoric acid solution over the concentrations range below 14.6 mol L^{-1} are H^+, $H_2PO_4^-$, H_3PO_4 and $H_5P_2O_8^-$. The formation of dimers at high concentration changes the ratio between the number of water molecules interacting with the solute, decreasing the probability that a phosphoric species is in contact with a water molecule[39,40]. The geometry of hydrogen bond in the first solvation shell of water in H_3PO_4 is distinct from that in H_2SO_4. We believe that the radical cation of water, $H_2O^{\bullet+}$ can be involved in a charge transfer reaction provided that it forms a contact with the charge acceptor. For concentrated phosphoric acid, due to dimer formation, the concentration of H_3PO_4 is almost two times lower than the nominal concentration of the phosphoric acid. For example, at 10 mol L^{-1} the species H_3PO_4, $H_2PO_4^-$, $H_5P_2O_8^-$ and $H_4P_2O_8^{2-}$ are present at concentrations of 0.64, 0.06, 3.7 and 0.9 mol L^{-1}, respectively. Consequently, $H_2O^{\bullet+}$ cannot efficiently react with some of these species. In contrast, such dimers species have not been reported for sulfuric acid before. This can explain why the hole scavenging efficiency in phosphoric acid solutions is lower than in sulfuric acid solutions.

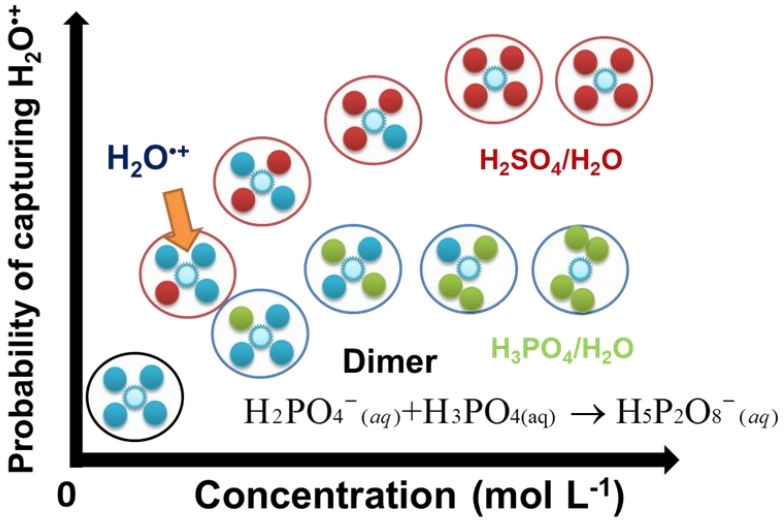

Figure.3.22 *Illustration of less efficiency of charge transfer from $H_2O^{\bullet+}$ to solutes in phosphoric acid and sulfuric acid solutions.*

3.6.3 Estimated redox potential of $H_2O^{\bullet+}$ in neat water

It is important to have an idea about the thermodynamic of the electron transfer by crudely estimating the redox potential of the couple $H_2O^{\bullet+}/H_2O$ in liquid water, even if the radical cation $H_2O^{\bullet+}$ is not a simple stable species at all. For this purpose the thermodynamic cycle is used with the ionization potential of water molecule in the gas phase, the hydration energy for water molecule and the ionized water molecule denoted $H_2O^{\bullet+}$ (**Figure 3.23**). According to this thermodynamic cycle the ionization potential of H_2O in water can be found as follows:

$$IP(H_2O)_{sol} = IP(H_2O)_{gas} + \Delta G_{solv}(H_2O^{\bullet+}) - \Delta G_{solv}(H_2O) \qquad (3.12)$$

The ionization potential of water molecule in the gas phase and the hydration energy of water molecule are experimentally known (12.6 eV[41,42] and - 0.27 eV[43], respectively). The main source of error for the estimation of the ionization energy of H_2O in water is the hydration energy of the positive radical hole. In fact, the value of hydration energy depends on the delocalization of the positive charge. In very first approximation, it can be assumed that the positive charge is localized only on one water molecule. Consequently, the hydration energy of the hole might be very close to the one of H_3O^+. The hydration energy of H_3O^+ is known experimentally to be equal to - 4.4 eV.[43] By considering that the positive charge is localized on one water molecule and that the size of $H_2O^{\bullet+}$ is slightly smaller than H_3O^+, the hydration energy of H_2O^+ could be around 10% larger than that of H_3O^+ (- 4.8 eV). Therefore, by using the absolute electrode potential (4.44 ± 0.02 V at 25 °C),[44,45] the redox potential of the couple $H_2O^{\bullet+}/H_2O$ versus hydrogen normal electron is:

$$E^{\circ}\left(\frac{H_2O^{\bullet+}}{H_2O}\right) = eIP_{sol}\left(H_2O\right) - 4.4 = (0.27 + 12.6 - 4.8) - 4.4 = 3.6\ V_{NHE}$$

This value is very high and larger enough to oxidize sulfuric and phosphoric acid. In fact, this thermodynamic cycle calculation is oversimplified. If the positive charge is delocalized on several water molecules, denoted as $(H_2O)_n\ H_2O^{\bullet+}$ the value of the redox potential would be different from 3.6 V_{NHE}. Molecular simulations are needed to obtain a more accurate value. However, this very primary estimation shows that the hole is a very oxidizing species.

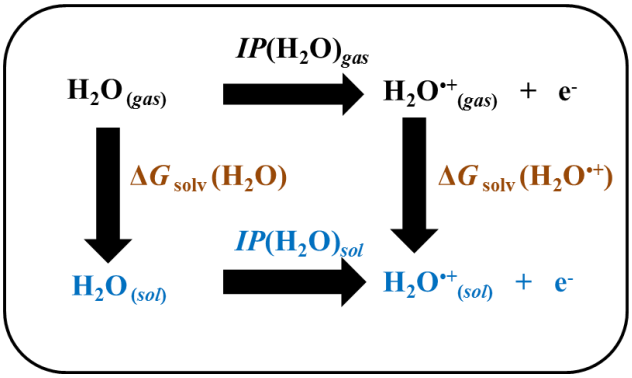

Figure.3.23 *Thermodynamic cycle used in the estimation of reduction potential of $H_2O^{\bullet+}/H_2O$ in neat water.*

3.8 Conclusion and perspective

3.8.1 Conclusion

The pulse-probe measurements reported in this work show clearly that the radical of sulfuric and phosphoric acid can be formed via two mechanisms: direct electron detachment by the electron pulse and oxidation by the radical cation of water $H_2O^{\bullet+}$. This latter has a very short life time in neat water, i.e. less than 100 fs. But in highly concentrated solution when another molecule is in contact with $H_2O^{\bullet+}$, the electron transfer becomes competitive against proton transfer with surrounding water molecule. Though often discussed in the past, the role of $H_2O^{\bullet+}$ in oxidation processes of irradiated systems was mostly a subject of controversy and speculation. Here, it has been clearly and quantitatively demonstrated by the picosecond pulse radiolysis of highly concentrated phosphoric and sulfuric acid that $H_2O^{\bullet+}$ may act as an extremely strong oxidant. Moreover, the radiolytic yield of $H_2O^{\bullet+}$ in H_2SO_4 is found to be 5.1 $\pm$ 0.2 $\times$ 10^{-7} mol J^{-1}. This value is reasonable and is higher than the radiolytic yield of solvated electron published at very short time (1 ps). In fact, within the first ps, geminate recombination between presolvated electron and radical cation $H_2O^{\bullet+}$ occurs and reduce the yield of hydrated electron. In addition to irradiation of concentrated solutions of strong or even weak electron donors, the direct oxidation phenomenon by $H_2O^{\bullet+}$ can actually take place anywhere where the probabilities of its nearest neighbors being H_2O or another molecule are comparable. That is the case in interfaces when irradiated water molecules are in contact with other molecules. However, phosphate radical formation through water hole scavenging depends on the concentration of the phosphoric acid; in general it is lower than the oxidation yield in sulfuric acid solutions of the same concentration. The main reason for this difference is attributed to the formation of dimer species in the concentrated phosphoric acid, in other words the geometry of hydrogen bond in first solvation shell of H_3PO_4. Up to now, in the oxidation mechanism only $OH^{\bullet}$ and H_2O_2 are evoked but our results clearly show that even if $H_2O^{\bullet+}$ is short lived, its involvement in oxidation mechanisms should be taken into account.

In addition to irradiation of concentrated H_2SO_4 or H_3PO_4 solutions, the direct oxidation by the $H_2O^{\bullet+}$ is expected to take place in other chemical environment where the probabilities of its nearest neighbors being H_2O or another molecule. Some examples are given below:

- Radiotherapy and radiobiology: It is known that large amounts of hydrating water molecules are in direct contact with biomolecules like DNA or proteins. When ionizing radiation is present, part of the radiation energy is absorbed directly by DNA and breaks the bonds of the sugars, phosphates and nucleobases, while some of the radiation is also absorbed

by the water adjacent to the DNA. In that case, the generated $H_2O^{\bullet+}$ radical cations may induce a chemistry different from $OH^{\bullet}$ radicals and the consequence is producing the secondary biomolecule radicals which has not been yet considered before.[46,47]

- Treatment and storage of fuel in the nuclear industry: Spent nuclear fuel is processed in highly concentrated nitric acid aqueous solutions and in this case, the radical cation $H_2O^{\bullet+}$ may react with nitrate ions to yield the $NO_3^{\bullet}$ radical which is also a highly oxidizing species. Alternatively, when radioactive waste of low and medium level is coated by cement or any other porous material, the interface effect is extensive and the formation of radical cation $H_2O^{\bullet+}$ and its oxidation reactions should be taken into account.

- When the core of a nuclear power plant comes into contact with water, as happened during the Fukushima accident in Japan, the amount of radiation deposited at the interface of the exposed fuel/water is important. Although we do not provide any evidences, the present work suggests that, in this situation, metal corrosion by $H_2O^{\bullet+}$ may be involved.

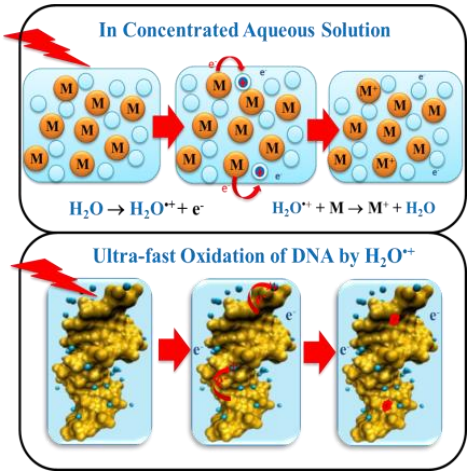

3.8.2 Perspective

(1) In the near future, the first attempt is still to directly find the spectroscopy observation of this radical cation $H_2O^{\bullet+}$ probably in UV region on the time scale of femtosecond. It would be a very challenging topic as a more sophisticated pulse (<30 fs) with sufficient energy (>11.4 eV) is necessary. X-rays pulse or laser with better time resolution maybe the great choices. Moreover, the micro-jet of heavy water is strongly suggested during the measurement to prevent the induced signal from fused silica. Excited state of water may also have absorption in this region. Therefore, it is also very important to exclude this possible signal by carefully analysis or experiment design.

(2) In heavy water, the ejection length and the probability of recombination reaction differ from that in light water. The proton transfer of $D_2O^{\bullet+}$ to D_2O molecule is thought to be less efficient than that of $H_2O^{\bullet+}$ while the electron transfer of water hole to solutes is less affected. The yield of hydrated electron in D_2O is also not clear due to its unknown value of molar extinction coefficient. Hence, it is interesting to discover the isotopic effect of the reactivity of $D_2O^{\bullet+}$ in highly concentrated acid solutions, for example sulfuric acid.

(3) Radiation enhanced corrosion of metal surface plays an important role in storage of spent nuclear fuel as well as in the running nuclear power plant. When the fuel /water interface is under exposition of radiation, the corrosion of metal involved $H_2O^{\bullet+}$ is proposed, but not proven yet. In which situation this oxidizing process might take place and the yield of $H_2O^{\bullet+}$ can participate this reaction still remain unexplored. Using the ESR method at low temperature or stead state measurement instead of time-resolved optical method seems more realistic to study this oxidizing reaction.

(4) Theoretical simulations would be very helpful to better understand the nature of $H_2O^{\bullet+}$ in liquid concerning the solvation coordinate number of $H_2O^{\bullet+}$. Delocalization of this positive charge of this water cation over several water molecules has not yet been probed by the simulations. The ejected electrons could either be valence electrons or the ones from core orbitals of H_2O molecule depending on the energy of radiation. By fast electron or laser radiation with the energy below 200 eV, the valence electrons are mainly knocked out to form the hole. However, in the latter case when the radiation energy is around 400-550 eV, $H_2O^{\bullet+}$ might be the complex species since the Auger decay and interatomic columbic decay (ICD) are believed to take place from the ejecting the core-level electrons. The cross section of each events should be also concerned and discussed in the future.

References

[1] Gauduel Y., Pommeret S., Migus A., Antonetti A.Some Evidence of Ultrafast H_2O^+ - Water Molecule Reaction in Femtosecond Photoionization of Pure Liquid Water. *J. Chem. Phys.* **2011**, *135*, 1-14.

[2] Marsalek, O.; Elles, C. G.; Pieniazek, P. A.; Pluharova, E.; VandeVondele, J.; Bradforth, S. E.; Jungwirth, P. Chasing Charge Localization and Chemical Reactivity Following Photoinozation in Liquid Water. *J. Chem. Phys.* **2011**, *135*, 1-14.

[3] Li, J. L.; Nie, Z. G.; Zheng, Y. Y.; Dong, S.; Loh, Z. H., Elementary Electron and Ion Dynamics in Ionized Liquid Water. *J. Phys. Chem. Lett.* **2013,** *4*, 3698-3703.

[4] Thurmer, S.; Oncak, M.; Ottosson, N.; Seidel, R.; Hergenhahn, U.; Bradforth, S. E.; Slavicek, P.; Winter, B. On the Nature and Origin of Dicationic Charge-separated Species Formed in Liquid Water on X-ray Irradiation. *Nature* Chem. **2013**, *5*, 590-596.

[5] Khorana, S.; Hamill. W.H. Electronic processes in the pulse radiolysis of aqueous solutions of halide ions. *J. Phys. Chem.* 75(20): 3081-8 (1971)

[6] Kim, K. J.; Hamill, W. H. Direct and Indirect Effects in Pulse Irradiated Concentrated Aqueous Solutions of Chlorides and Sulfate Ions. *J. Phys. Chem.* **1976***, 80*, 2320-2325.

[7] Das B. and Farley, J. W. Observation of the visible absorption spectrum of H_2O^+. *J. Chem. Phys.* **95**, 8809 (1991).

[8]. Dutuit, O. Tabche-Fouhaile, A. Nenner, I. Frolich. H and Guyon P.M. Photodissociation Processes of Water Vapor Below and Above the Ionization Potential. *J. Chem. Phys*. **83**, 584 (1985)

[9] La Vere T, Becker D, Sevilla M.D. Yields of OH in Gamma-irradiated DNA as a Function of DNA Hydration: Hole transfer in Competition with OH Formation. *Radiat Res.* **1996**.145(6):673-80.

[10] El Omar, A. K.; Schmidhammer, U.; Jeunesse, P.; Larbre, J.-P.; Lin, M.; Muroya, Y.; Katsumura, Y.; Pernot, P.; Mostafavi, M. Time-Dependent Radiolytic Yield of OH• Radical Studied by Picosecond Pulse Radiolysis. *J. Phys. Chem. A*, **2011**, 115(44), 12212-12216.

[11] Balcerzyk, A.; Schmidhammer, U.; El Omar, A. K. ; Jeunesse, P. ; Larbre J. P., Mostafavi. M. Direct and Indirect Radiolytic Effects in Highly Concentrated Aqueous Solutions of Bromide. *J. Phys. Chem. A*. **2011**, *115*, 4326−4333.

[12] El Omar, A. K. ; Schmidhammer, U. ; Rousseau, B. ; LaVerne, J. ; Mostafavi, M. Competition Reactions of H_2O^+ Radical in Concentrated Cl^- Aqueous Solutions: Picosecond Pulse Radiolysis Study. *J. Phys. Chem. A.* **2012**, *116*, 11509−11518.

[13] Balcerzyk, A.; LaVerne, J.; Mostafavi, M. Picosecond Pulse Radiolysis of Direct and Indirect Radiolytic Effects in Highly Concentrated Halide Aqueous Solutions. *J. Phys. Chem. A.* **2011**, *115*, 9151−9159.

[14] Balcerzyk, A.; El Omar, A. K.; Schmidhammer, U.; Pernot, P.; Mostafavi. M. Picosecond Pulse Radiolysis Study of Highly Concentrated Nitric Acid Solutions: Formation Mechanism of $NO_3^{\bullet}$ Radical. *J. Phys. Chem A*. **2012***, 116*, 7302−7307.

[15] El Omar, A. K. ; Schmidhammer, U. ; Balcerzyk, A.; LaVerne, J.; Mostafavi, M. Spur Reactions Observed by Picosecond Pulse Radiolysis in Highly Concentrated Bromide Aqueous Solutions. *J. Phys. Chem. A*. **2013**, *117*, 2287−2293.

[16] Choe, Y. K. ; Tsuchida, E. ; Ikeshoji T. First Principles Molecular Dynamics Study on Aqueous Sulfuric Acid Solutions, *J. Chem. Phys*. **2007**, *126*, 154510-1-154510-8.

[17] Kameda, Y. ; Hosoya, K. ; Sakamoto, S. ; Suzuki,H.; Usuki, T.; Uemura, O. Hydrogen-Bonded Structure in Aqueous Sulfuric Acid Solutions, *J. Mol. Liquds*, **1995**, *65/66*, 305-308.

[18] Tang, Y.; Thorn, R. P.; Mauldin, R. L.; Wine, P. H. Kinetics and Spectroscopy of the SO_4^{-} Radical in Aqueous Solution. *J. Photochem. Photobiol. A.* **1988**, *44*, 243−258.

[19]Hayon, E.; Treinin, A.; Wilf, J. Electronic Spectra, Photochemistry, and Autoxidation Mechanism of the Sulfite-bisulfitepyrosulfite Systems. The SO_2, SO_3, SO_4, and SO_5, Radicals. *J. Am. Chem. Soc.* **1972**, *94*, 47−57.

[20] Marziano, N. C.; Tomasin, A.; Tortato, C.; Isandelli, P., The problem of acidity in concentrated aqueous solutions of sulfuric acid J Chem Soc Perk T 2 1998, (11), 2535-2540.

[21] Allen, A. O. The Yields of Free H and OH in the Irradiation of Water. *Radiat Res.* **1954**, *1*, 85−96.

[22] Nathaniel F. Barr , R. H. S., The Dependence of Radical and Molecular Yields on Linear Energy Transfer in the Radiation Decomposition of 0.8 N Sulfuric Acid Solutions. *J. Phys. Chem*. **1959**, *63*, 808−813.

[23] Hochanadel, C. J. Ghormley, J. A. Sworski, T. J. The Decomposition of Sulfuric Acid by Cobalt γ-Rays. *J. Am. Chem. Soc*. **1955**, *72*, 3215−3215.

[24] Boyle, J. W. The Decomposition of Aqueous Sulfuric Acid Solutions by Cobalt Gamma Rays: I. Radical and Molecular Product Yields from Ce(IV) Solutions in 0.4 to 18 M Acid. *Radiat Res*. **1962**, *17*, 427−449.

[25] Boyle, J. W. The Decomposition of Aqueous Sulfuric Acid Solutions by Cobalt Gamma Rays II.Yields of Solvent Decomposition and Reducing Radicals from Fe(II) Solutions in 0.4 to 18 M Acid. *Radiat Res*. **1962**, *17*, 450−464.

[26] Daniels, M.; Lyon, J.; Weiss, J. The Formation of Peroxymonosulphuric Acid and Peroxydisulphuric Acid in Solutions of Sulphuric Acid Irradiated by ^{60}Co Radiation. *J. Chem. Soc*. **1957**, 4388−4390

[27] Bibler, N.E. Radiolysis of 0.4 M Sulfuric Acid Solutions with Fission Fragments from Dissolved Californium-252. Estimated Yields of Radical and Molecular Products that Escape Reactions in Fission Fragment Tracks. *J. Phys. Chem*. **1975**, *79*, 1991−1995.

[28] Sworski, T. J. Relative Rate Constants for Reaction of OH Radical with Sulfuric Acid, Formic Acid and Cerous ions. *J. Am. Chem. Soc.* **1956**, *78*, 1768−1769.

[29] Heckel. E. Pulsradiolytische Untersuchung Des Radikal-anions SO_4^-. *Ber. Bunsenges. Phys. Chem.* **1966**, *70*, 149-54.

[30] Lesigne, B.; Ferradini, C.; Pucheault, J. Pulse Radiolysis Study of the Direct Effect on Sulfuric Acid. *J. Phys. Chem.* **1973**, *77*, 2156−2158.

[31] Grabner, G.; Getoff, N.; Schworer, F. Znt. Pulsradiolyse von H_3PO_4, $H_2PO_4^-$, HPO_4^{2-} und $P_2O_7^{4-}$ in wässriger Lösung—I. Geschwindigkeitskonstanten der Reaktionen mit den Primärprodukten der Wasserradiolyse. *J. Radiat. Phys. Chem.* **1973**, *5*, 393-403.

[32] Grabner, G.; Getoff, N.; Schworer, F. Pulsradiolyse von H_3PO_4, $H_2PO_4^-$, HPO_4^{2-} und $P_2O_7^{4-}$ in wässriger Lösung—II. Spektren und Kinetik der Zwischenprodukte. *J. Radiat. Phys. Chem.* **1973**, *5*, 405-417.

[33] Maruthamuthu, P.; Neta, P. Phosphate Radicals. Spectra, Acid-base Equilibriums, and Reactions with Inorganic Compounds. *J. Phys. Chem.* **1978**, *82*, 710-713.

[34] Black, E. D.; Hayon, E. Pulse Radiolysis of Phosphate Anions $H_2PO_4^-$, HPO_4^{2-}, PO_4^{3-}, and $P_2O_7^{4-}$ in Aqueous solutions. *J. Phys. Chem.* **1970**, *74*, 3199-3203.

[35] Robert H. J.; Hayon, E. Flash Photolysis in the Vacuum Ultraviolet Region of the Phosphate Anions in Aqueous Solutions. *J. Phys. Chem.* **1968**, *11*, 3820-3827.

[36] Jiang, P. Y.; Katsumura, Y.; Nagaishi, R.; Domae, M.; Ishikawa, K.; Ishigure, K.; Yoshida, Y. Pulse Radiolysis Study of Concentrated Sulfuric Acid Solutions. Formation Mechanism, Yield and Reactivity of Sulfate Radicals. *J. Chem. Soc. Faraday. Trans.* **1992**, *88*, 1653-1658.

[37] El Omar, A. K.; Schmidhammer, U.; Jeunesse, P.; Larbre, J-P.; Lin, M.; Muroya, Y.; Katsumura, Y.; Pernot, P.; Mostafavi, M. Time-dependent Radiolytic Yield of $OH^{\bullet}$ Radical Studied by Picosecond Pulse Radiolysis. *J. Phys. Chem. A.* **2011**, *115*, 12212−12216.

[38] Yang, J. F.; Kondoh, T.; Yoshida, Y. Ultrafast Pulse Radiolysis. *Nuc. Instru. Meth. Phys. Res. A.* **2011**, *629*, 6–10.

[39] Elmore, K. L.; Hatfield, J. D.; Dunn, R. L.; Jones, A. D. Dissociation of Phosphoric Acid in Aqueous Solution at 25 °C. *J. Phys. Chem.* **1965**, *69*, 3520-3525.

[40] Camidti, R.; Cucca, P.; Atzei, D. Phosphate–H_2O Interactions in Concentrated Aqueous H_3PO_4 Solutions. *J. Phys. Chem.* **1985**, *89*, 1457-1460.

[41] Turner, D. W.; Baker, C.; Baker, A. D.; Brundle, C. R.; Molecular Photoelectron Spectroscopy. Wiley– Interscience, London (1970).

[42] Baker, A. D.; Brundle, C. R.; Turner, D. W. The Interpretation of Photoelectron Spectra—Especially Those of Benzene and Water. *Int. J. Mass Spectrom.* **1968**, *1*, 443-454.

[43] Palascak, M. W.; Shields, G. C. Accurate Experimental Values for the Free Energies of Hydration of H^+, OH^-, and H_3O^+. *J. Phys. Chem. A.* **2004**, *108*, 3692-3694.

[44] Trasatti, S. The Absolute Electrode Potential: An Explanatory Note. *Pure Appl. Chem*. **1986**, *58*, 955-966.

[45] Reiss, H.; Heller, A. The Absolute Potential of the Standard Hydrogen Electrode: A New Estimate. *J. Phys. Chem*. **1985**, *89*, 4207-4213.

[46] O'Neill, P.; Stevens D. L.; Garman, E. F. Physical and Chemical Consideration of Damage Induced in Protein Crystals by Synchrotron Radiation: A radiation Chemical Perspective. *J. Synchroton Rad*. **2002,** *9*, 329-332.

[47] Purkayastha, S.; Milligan, J. R.; Bernhard. W. A. Correlation of Free Radical Yields with Strand Break Yields Produced in Plasmid DNA by the Direct Effect of Ionizing Radiation. *J. Phys. Chem. B.* **2005,** *109*, 16967-16973.

Chapter 4: Probing the Hydrated Electron Paired with Hydronium Ions in Aqueous Solutions

Chapter 4 Probing the Hydrated Electron Paired with Hydronium Ions in Aqueous Solutions

4.1 Introduction

Since the first identification by transient optical absorption measurements in 1962, the hydrated electron in liquid water was found to be a ubiquitous species in radiation chemistry and photochemistry. Much information on the production, solvation, thermodynamic and structure of the hydrated electron has emerged over the decades as introduced in **Chapter 1**. It displays a broad, featureless absorption band peaking at 715 nm which is mainly attributed to the transitions from *s*-like ground states to three non-degenerate *p*-like excited states.

As the simplest reducing species in aqueous solution, the reactivity of the hydrated electron towards different solutes has been extensively studied. Four types of solute can be distinguished regarding to their reactivity with hydrated electrons: i) scavengers with a rate constant controlled by diffusion; ii) solutes reacting with hydrated electron but with a rate constant lower than that controlled by diffusion; iii) solutes not reacting with hydrated electron but forming an ion pair with it; iv) solutes not interacting with solvated electron.

The study of the effect of water dissolved inorganic salts on the absorption spectrum of e_{hyd}^- began after the discovery of hydrated electron[1,2]. Early systematic experiments by Kreitus[3] in the pulse radiolysis of LiCl aqueous solutions over the range of 0-15 mol L^{-1} showed that the maximum of the e_{hyd}^- absorption spectrum shifts to the higher energy with the increasing of concentration but not in the uniform manner (**Figure 4.1**). The change of hydration energy of hydrated electron is found to be responsible for the observed spectral difference. Several years later, Krebs *et al*[4] carefully revisited the same measurements using the photolysis method. In contrast with the previous reports, the uniform blue shift of e_{hyd}^- spectra was observed by

increasing the concentration while keeping the similar absorption band shape. It was concluded that a favorable spatial distribution of deep traps created by the presence of Li^+ ions would capture the electron.

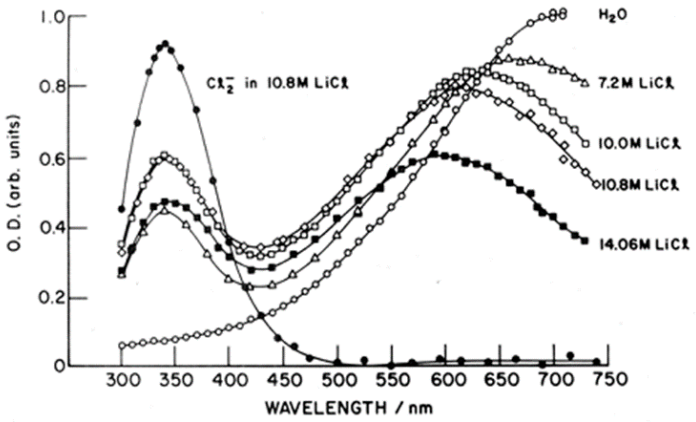

Figure 4.1. *Spectrum of hydrated electron in presence of lithium cations in different concentration*[1].

Molecular dynamics simulations suggested a possible formation of a contact cation-electron pair, denoted as $(M^{n+}, e_{hyd}^-)_{hyd}$, in these aqueous electrolyte solutions[5]. The origin of spectral blue shift was attributed to a stronger stabilization of the *s*-like state than the *p*-like state in the close presence of the cation with the contraction of the cavity (see **Figure 4.2**).

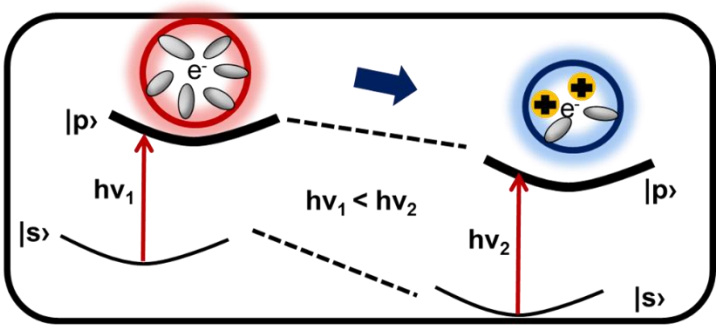

Figure 4.2 *Schematic diagram of hydrated electron in presence of nonreactive cations*

It was also reported that in aqueous solutions, many nonreactive alkaline, earth alkaline metal ions and *f*-block trivalent cations such as Tb^{3+}, form ion pairs with a hydrated electron[6]. The degree of shift is found to be the greatest in the hydrated electron paired with the trivalent cations having the same counter ion at same salts concentration compared to the other nonreactive monovalent or divalent ions. It was then summarized that the spectral shift of hydrated electron depends on the characteristics of the salts solution such as cation size and

charge (through charge densities) or dissociation degree of the salt (partial screening of the cation charge when incomplete dissociation) (**Figure 4.3**).

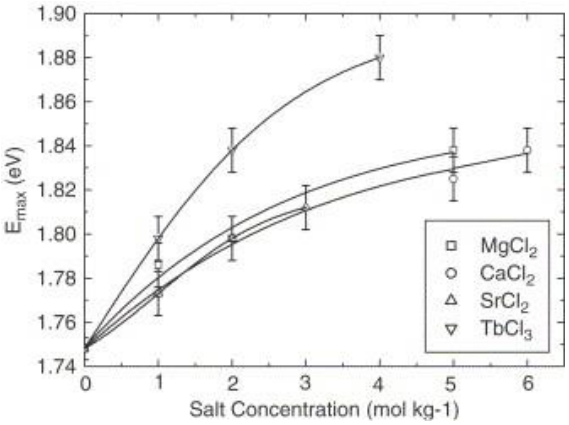

Figure 4.3. *Position of the maximum of the absorption band of the hydrated electron, E_{max}, as a function of the di- and trivalent chloride salt concentration at 10 °C.*[6]

Water radiolysis under extreme condition of temperature, pressure and high energy linear transfer (*LET*) has been a challenging subject for radiation chemists with particular importance in the application of nuclear industry. It has been well known in neat water, the rise of temperature up to 350 °C induced a red shift of absorption spectrum of hydrated electron[7]. The absorbance greatly decreases with the temperature because the water density decrease and decay of e_{hyd}^- is accelerated with increasing temperature (see **Figure 4.4**). With the application of spectral moment theory, Bartels *et al.*[8] estimated the average size of the electron wave function and its kinetic energy. It appears that for water densities from 0.1-0.6 g/cm^3, the average radius of gyration for the electron remains constant at around 0.34 nm, and its absorption maximum is near 0.9 eV. For higher densities, the electron is squeezed into a smaller cavity and spectrum is shifted to the lower energy (red shift).

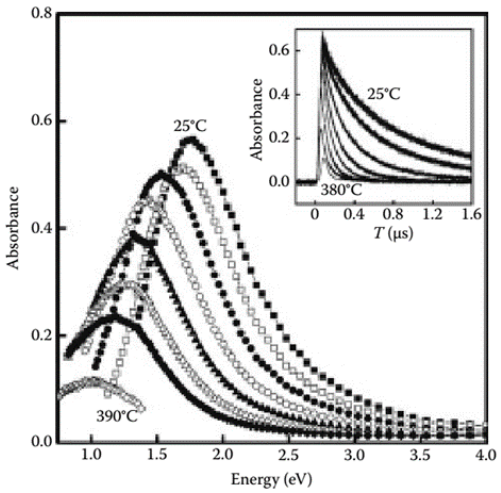

Figure 4.4. *Absorption spectra of hydrated electron in heavy water (D_2O) under a pressure of 25 MPa at temperature:25* °C, 50°C, 100°C, 150°C, 200°C, 250°C, 300°C and 390°C[7].

The redox reaction between a hydrated electron and a hydronium cation H_3O^+ (or D_3O^+) in water forming a hydrogen radical atom is the most elementary chemical processes in liquid. It is well accepted that, during this reaction, due to solvent molecules rearrangement around both electron and H_3O^+, the reaction rate of this process at room temperature is not controlled by diffusion. An activation barrier of ~11 kJ/mol[9] is present to slow down the reduction reaction and an encounter pair is expected to be formed.

$$H_3O^+ + e_{hyd}^- \rightarrow (H_3O^+, e_{hyd}^-)_{hyd} \rightarrow H^\bullet + H_2O \quad k = 2.3 \times 10^{10}\ L\ mol^{-1}s^{-1} \qquad (4.1)$$

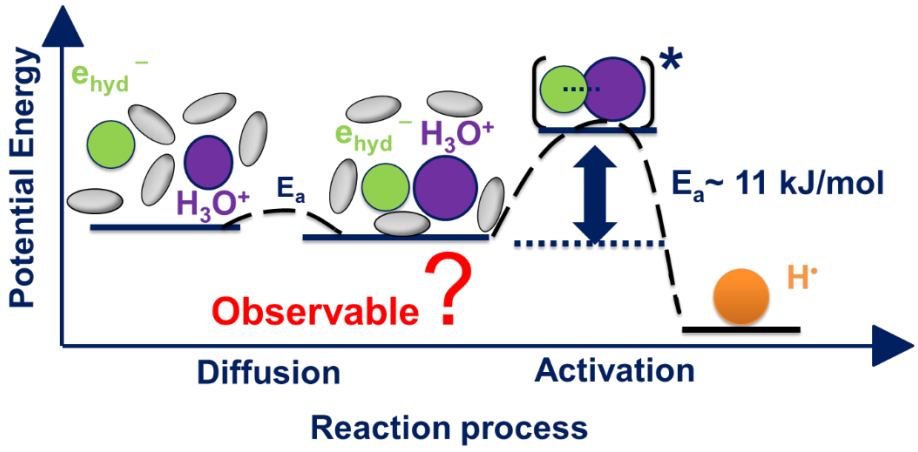

Figure 5. *A schema representing for the reaction of hydrated electron with hydronium ion, H_3O^+.*

The well accepted value of the rate constant (2.3×10^{10} mol^{-1} L s^{-1}) of this reaction in diluted aqueous solution is at least three to five times lower than the one estimated for diffusion

controlled rate constant (1.0×10^{11} mol^{-1} L s^{-1}) at room temperature[10]. Picosecond pulse radiolysis (electron pulse is 30 ps) showed that the rate constant of the reaction (4.1) in concentrated acid solution (1.2×10^{10} mol^{-1} L s^{-1})[11], is somewhat smaller than that obtained from microsecond pulse radiolysis in dilute solutions, due to the change of the solute activity and ionic strength [10,11]. In addition, the rate constant was obtained in very diluted acid solution using nanosecond pulse radiolysis at different temperature up 350 °C. The value of rate constant at different temperature in diluted acidic solutions was given in **Figure 4.6**[12,13,14].

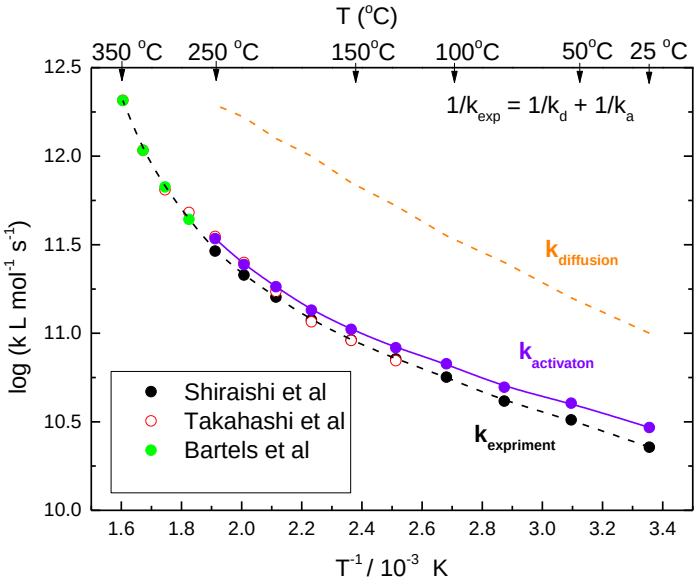

***Figure 4.6**. Arrhenius plot of reaction rate constant of hydrated electron with hydronium ion k_{exp} (black line), $k_{diffusion}$ (orange line) taken from Shiraishi et al and deduced k_{act} (vert line)[12,13,14].*

For a non-diffusion controlled charge recombination reaction, one can write the equation as followed[12]:

$$1/k_{exp} = 1/k_{dif} + 1/k_{act} \qquad (4.2)$$

Where the k_{act} is the activated rate constant, k_{dif} is the diffusion rate constant and k_{exp} is the observed or measured rate constant.

The diffusion rate constant of these two charged species can be described by Smoluchowski-Debye equation[13]:

$$k_{dif} = 4\pi N_A R(D_{e^-} + D_{H^+})F_D \qquad (4.3)$$

$$F_D = \frac{r_c}{R}\left(\frac{1}{e^{r_c/R}-1}\right) \tag{4.4}$$

$$r_c = \frac{e^2}{4\pi\varepsilon_0\varepsilon k_B T} \tag{4.5}$$

Where k_{diff} is written as the Smoluchowski rate times the Debye factor, F_D. The value of e in the definition of r_c is the charge of the electron, D is the relative diffusion coefficient of reactants, referring to hydrated electron and hydronium ion, R is the reaction distance that is assumed to be around 0.5 nm. N_A is Avogadro's number, k_B is Boltzmann's constant, ε_0 is the permittivity of free space and ε is the dielectric constant of liquid water. r_c is so called Onsager radius and estimated as 0.71 nm in water at 25 °C .

The activation rate constant of this reaction can described by Arrhenius Equation:

$$k_{act} = Ae^{\left(\frac{-Ea}{RT}\right)} \tag{4.6}$$

Where E_a is the activation energy that is reported as around 11 kJ mol^{-1}, A is Arrhenius factor and R is the gas constant.

For a given acid solutions, in order to estimate the duration or survive time of the transient encounter pair (H^+, e_{hyd}^-)$_{hyd}$. A very simplified model is considered as below with an equilibrium of the pair complexes formation and a dissociation reaction to H atom.

$$H_3O^+ + e_{hyd}^- \leftrightarrow (H_3O^+, e_{hyd}^-)_{hyd} \rightarrow H^\bullet + H_2O \tag{4.1}$$

For instance, in the acid solutions with 0.01 mol L^{-1} of H_3O^+, assuming the initial concentration of e_{hyd}^- is 1.0 ×10^{-5} mol L^{-1} which is far less than 0.01 mol L^{-1} of H_3O^+, the formation rate constant of pair is then estimated as $k_{diff} \times [H_3O^+]$ obeying the pseudo first order. The first order rate constant of the formation of $H^\bullet$ radical from the pair is k_{act}/K_A, where K_A is equilibrium constant of the formation of pair from hydrated electron according to the model of *Shiraishi et al*[12]. The value of K_A is set as 1 at room temperature.

Therefore, according to an A-B-C reaction model, the equation for all the three species could be expressed as follow:

$$\left[e_{hyd}^-\right]_t = \left[e_{hyd}^-\right]_0 e^{-k_a t} \tag{4.7}$$

$$\left[(e_{hyd}^{-}, H^{+})_{hyd}\right]_t = \left[e_{hyd}^{-}\right]_0 (e^{-k_a t} - e^{-k_b t}) \frac{k_a}{k_b - k_a} \tag{4.8}$$

$$\left[H^{\bullet}\right]_t = \left[e_{hyd}^{-}\right]_0 \left(1 + \frac{k_a e^{-k_b t} - k_b e^{-k_a t}}{k_b - k_a}\right) \tag{4.9}$$

Where k_a is the rate constant of pair formation depending on the concentration of H_3O^+ concentration which equals to $k_{diff} \times [H_3O^+]$, and k_b is the rate constant of collapsing of pair to $H^{\bullet}$ radical that equals to k_{act}/K_A.

At certain time after the radiolysis of acid solution, we have:

$$\left[(e_{hyd}^{-}, H^{+})_{hyd}\right]_t + \left[e_{hyd}^{-}\right]_t + \left[H^{\bullet}\right]_t = \left[e_{hyd}^{-}\right]_0 \tag{4.10}$$

When $t \sim \infty$, the concentration of e_{hyd}^{-} and $(H^+, e_{hyd}^{-})_{hyd}$ tend to zero, and the concentration $H^{\bullet}$ radical equals to initial concentration of e_{hyd}^{-}. An example has been given in the 0.01 mol L^{-1} acid solutions at room temperature. The value of k_a and k_b are calculated as 1.0×10^9 s^{-1}, 3.0×10^{10} s^{-1}, respectively. The decay of hydrated electron is much slow and the lifetime of the encounter pair is very short and its quantity is almost negligible. In this case, it is not likely to observe any absorption signal of $(H^+, e_{hyd}^{-})_{hyd}$ by picosecond pulse or nanosecond pulse.

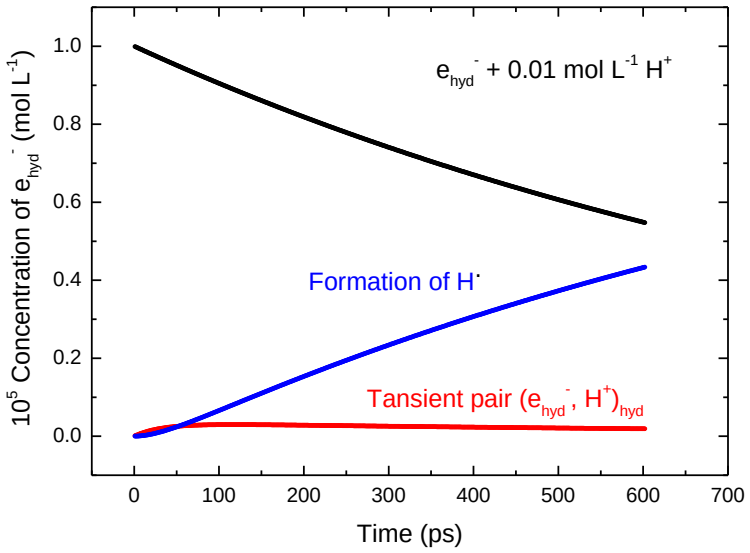

Figure 4.7*. Temporal evolution of the species, e_{hyd}^{-}, $(H^+, e_{hyd}^{-})_{hyd}$ and $H^{\bullet}$ radical in the picosecond radiolysis of acid solution with concentration of 0.01 mol L^{-1}based on the reaction (1)*

However, if we increase the concentration of acid ten times high to 0.1 mol L^{-1} or even higher (0.1 to 1 mol L^{-1}) in **Figure 4.8**, the value of k_a increases rapidly while having almost no effect on the value of k_b at ambient temperature. The hydrated electron decline much faster that is completed less than 400 ps while the duration of transient pair become longer up to 200 ps. The abundance of the encounter pair also increases continuously with increasing of the acid concentration from 0.1 to 1 mol L^{-1} (see **Figure 4.8**). Therefore, it is learned that, it becomes possible to probe the $(H^+, e_{hyd}^-)_{hyd}$ pair using the picosecond electron pulse, only in much concentrated acidic solutions.

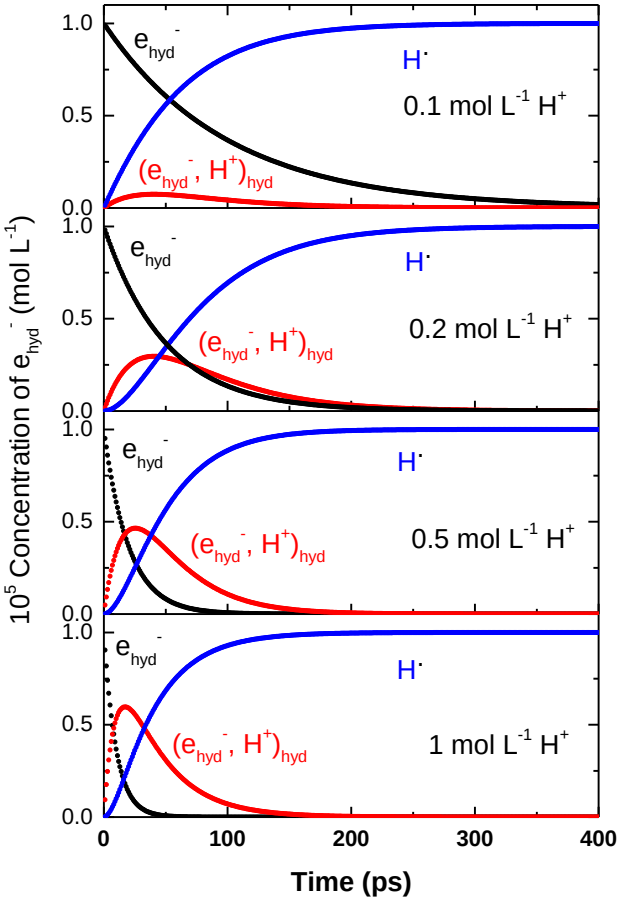

***Figure 4.8**. Concentration dependence of temporal evolution of the species, e_{hyd}^-, $(H^+, e_{hyd}^-)_{hyd}$ and $H^{\bullet}$ radical in the acid solution with concentration ranging from 0. 1 mol L^{-1} up to 1 mol L^{-1} at room temperature based on the reaction (1)*

It should be noted here that, in order to set a model as simple as possible, both the pre-solvated electron scavenging and ionic strength effect on diffusion process have not been

taken into account in this model though it is certain that the rate constant for each process would be modified particularly in highly concentrated solutions.

Table 4.1 Estimated temperature-dependent values of rate constants for each process of reaction [12](4.1).

T	k_{diff}	C (H^+)	k_{act}	k_a	K_A	k_b
(°C)	10^{11} $smol^{-1}L^{-1}$	(mol / L)	10^{10} $smol^{-1}L^{-1}$	10^{10} s^{-1}	$L\ mol^{-1}$	10^{10} s^{-1}
25	1	0.1	3	1	1	3
150	7.1	0.1	10.51	7.1	1.14	9.22
250	19.5	0.1	33.8	19.5	2.1	16.1
350	31.6	0.1	59.2	31.6	3.2	18.5

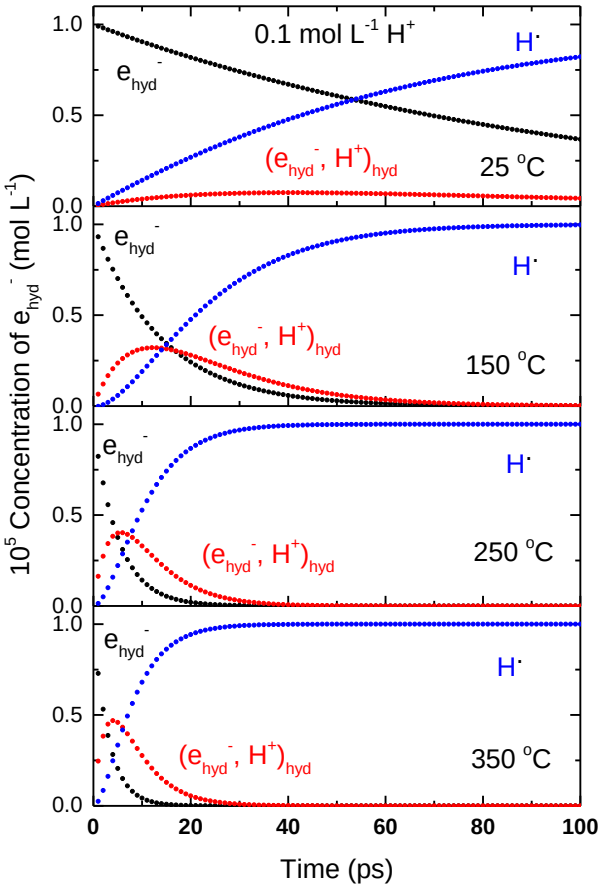

***Figure 4.9**. Temperature dependence of temporal evolution of the species, e_{hyd}^-, $(H^+, e_{hyd}^-)_{hyd}$ and $H^{\bullet}$ radical in the acid solution with concentration of 0. 1 mol L^{-1} based on the reaction (1)*

The ration between k_a/k_b depends also on the temperature since the diffusion process has accelerated and the activation barrier become less important. This change of temperature would directly results in the pair formation and its surviving time at elevated temperatures.

For concentration of 0.1 mol L^{-1} at room temperature, the absorbance of $(H^+, e_{hyd}^-)_{hyd}$ is almost 15 times lower that of hydrated electron. With the increasing of the temperature (**Figure 4.9**), the amount of pair complex increases up to 30% at 150 °C, 45% at 250 °C, and 48% at 250 °C of the initial amount of hydrated electron. However, the survive time or duration of pair, $(H^+, e_{hyd}^-)_{hyd}$ become much short as the temperature increases, around 80 ps at 150 °C, 40 ps at 250 °C and only 20 ps 350 °C. Hence, it suggests that the probabilities of observing the pair with 0.1 mol L^{-1} H^+ presented at the temperature between 150 °C to 250 °C is relative higher compared with that at ambient condition. But when the temperature is above 250 °C, with the picosecond electron pulse, it is impossible to find any $(H^+, e_{hyd}^-)_{hyd}$ absorbing in UV-visible region. Additionally, *ab* initio simulation of electronic and vibrational spectra of the hydrated H_3O radical exhibit striking similarities with the spectral signatures of the hydrated electron which might also be a reason that it is not likely to observe the pair complex in dilute acidic solutions.

From the analysis above, it could be understood that for many years until now, the observation of transient species $(H^+, e_{hyd}^-)_{hyd}$ has not been reported in diluted acid solutions.

Despite the apparent simplicity of the reaction (4.1), it has been debated by several groups.[15] The Bronsted correlation of solvated electron reaction rates observed for an important number of acids suggested firmly that reaction (4.1) is a proton transfer reaction rather than an electron transfer one. A long-lived $H_3O^{\bullet}$ radical intermediate in reaction (4.1) was suggested but no clear evidence was reported by time-resolved transient absorption down to the picosecond time scale and ESR spectroscopy[16,17]. The reaction between hydrated electron and H_3O^+ was also studied by considering temperature effect on the overall rate constant to derive the reaction rate constant at ambient temperature.[18]

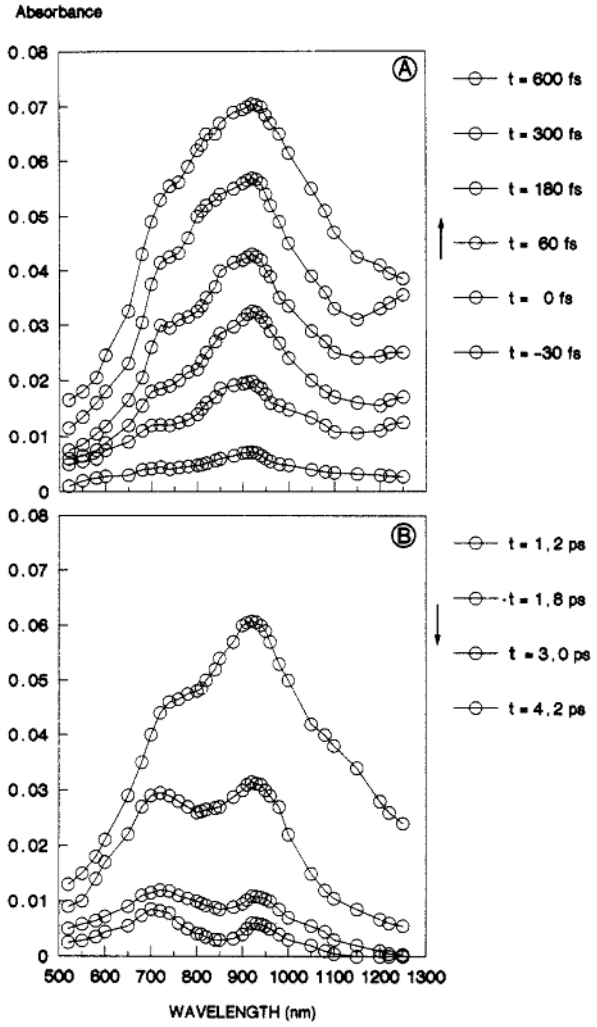

Figure 4.10*. Transient absorption spectra obtained at different times (from -30 fs to 4.2 ps) after femtosecond photoionization of concentrated aqueous solution of HCl at 310 nm (E = 4 eV). The points are calculated from the experimental kinetics and the amplitude of the signal obtained at different wavelengths*[17].

A recent *ab initio* simulation suggests that the $H_3O^{\bullet}$ radical may be present as an intermediate in reaction (4.1). The radical is stable in the gas phase, but in the presence of a few water molecules it is separated and turns out to be a delocalized $H_3O^+ \ldots e^-$ solvent-separated pair.[19] It was also reported that the absorption spectrum of the hydrated electron is not influenced in acidic solution.[20] Normalized absorption measurements showed that the transient species observed in 0.1 up to 3.5 mol L^{-1} $HClO_4$ exhibited the same absorption spectrum of the hydrated electron in neat water with a maximum around 715 nm. The initial radiolytic yield immediately after the electron pulse of hydrated electron was found to be also constant for solutions with concentrations of H_3O^+ up to 2 mol L^{-1}, meaning that the H_3O^+ does not react with the precursor of hydrated electron.[20]

In contrast, femtosecond laser photolysis measurements (Fig. 4.10) showed that the initial transient absorption in the strong acidic aqueous solution is lowered (by 10%) compared to that observed in pure water.[21] Kinetics simulation showed that the probability of the reaction between solvated electron and H_3O^+ in the pair is small and the encounter duration can be on the order of a few picoseconds.[22] It is interesting that a femtosecond photolysis study of 11 mol L^{-1} HCl solution showed that a precursor of hydrated electron could be formed in the solvation shell of H_3O^+, forming a $(H_3O^+, e^-)_{hyd}$ pair displaying an absorption spectrum located around 950 nm.[23] But the authors did not observe the pair between solvated electron and hydronium cation, $(H_3O^+, e_{hyd}^-)_{hyd}$.

In this Chapter 4, using the picosecond pulse radiolysis method, we try to answer the following questions:

I. Is it possible to observe the so called transient encounter pair, $(H_3O^+, e_{hyd}^-)_{hyd}$ based on the spectral changes of e_{hyd}^- , if yes, in which condition we might see it?

II. Can hydronium ion, H_3O^+ serve as a scavenger of pre-solvated electron in acidic solutions?

III. How about this reaction taking place at elevated temperature, especially in highly concentrated acidic solutions?

4.2 Paring of hydrated electron with H_3O^+

The absorption spectra in pure water and in acid solutions with different concentrations are observed at 15 ps after the time zero (see **Figure 4.11**). The solution properties of perchoric aicd for pulse radiolysis are listed in **Table 4.2**.

Table 4.2 *Chemical compositions of perchoric acid ($HClO_4$) solutions with different concentrations. fs, fw represent the electron fraction of solutes and water, respectivity. The density of the solutions d_{sol} is obtained from the ref [24]*

C [M]	f_s	f_w	F	d_{sol} (g/cm^3)	$[H_2O]/[HClO_4]$
0.2	0.019	0.981	1.006	1.008	274.5
0.5	0.044	0.956	1.020	1.025	108.4
1	0.086	0.914	1.045	1.056	53.1
1.5	0.13	0.87	1.067	1.081	34.0
2	0.17	0.83	1.087	1.109	25.2
3	0.24	0.76	1.136	1.168	16.0
4	0.30	0.70	1.183	1.226	11.4
6	0.42	0.58	1.28	1.342	6.9

It is well known that the radicals $ClO_4^{\bullet}$, $SO_4^{\bullet-}$ and $H_2PO_4^{\bullet}$ are formed by the direct radiation effect in perchloric, sulfuric and phosphoric acid solution, respectively.[25,26] They absorb in the UV-visible around 370, 450, and 520 nm, respectively with small extinction coefficients (100-1850 M^{-1} cm^{-1}). Their low contribution has been subtracted from the observed absorption band before spectrum normalization (**Figure 4.12**) for three types of acidic solutions.

At 10 ps, the electron induced by electron pulse in solution is already solvated and the presolvated electron optical signature is not likely to be present in the absorption band. For these three acidic solutions, the blue shift of the absorption band of solvated electron is obvious. The shape of observed spectra does not depend on time; only the intensity decreases with increasing time delay (see **Figure 4.13**). The blue shift is most pronounced for perchloric acid. As the dissociation of perchloric acid is greater than of phosphoric acid, the blue shift for the solution containing 6 mol L^{-1} $HClO_4$ is larger than for that containing 2 mol L^{-1} H_3PO_4 (3 equivalent H_3O^+).[27,28,29]

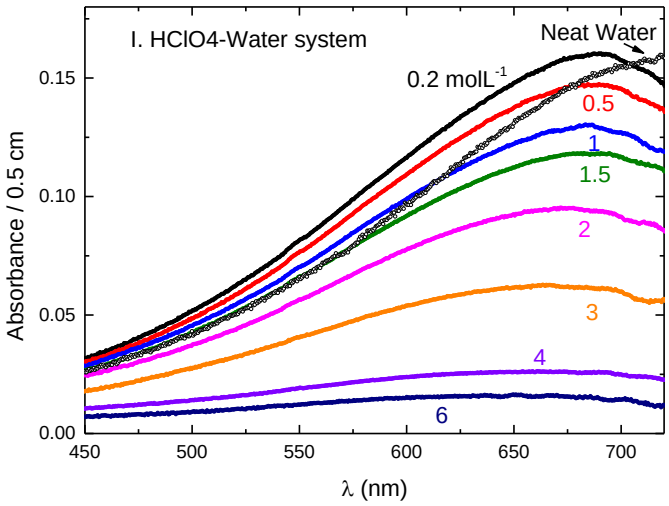

Figure 4.11. *The absorption spectra recorded at 10 ps after the electron pulse in perchloric acid system. The perchlorate radicals ($ClO_4^{\bullet}$) absorbing around at 370 nm from 0.2 mol L^{-1} up to 4 mol L^{-1} is negligible due to its low extinction coefficient and low radiation induced yield. The radiation dose deposited on the solutions is measured with 44.25Gy.*

Even for 0.2 and 0.5 mol L^{-1} $HClO_4$ solutions the shift is not negligible. The maximum of the absorption band for 0.2 and 0.5 mol L^{-1} is located at 696 ± 5 and 692 ± 5 nm, respectively. For the lowest concentrations (0.2 and 0.5 mol L^{-1}) the shift of the absorption band of the solvated electron is clearer observed in the visible part of the absorption band. The variation of the maximum of the electronic transition observed in the case of perchloric acid, exhibits a shift of 0.22 eV from pure water to 6 mol L^{-1} H_3O^+ (**Figure 4.14**). The band shape remain almost unchanged in acid solutions containing different concentrations from 0.2 to 6 mol L^{-1}, and only in the higher wavelength region (long tail part of the absorption spectrum) is slightly different when all the spectrum are normalized by the absorption maximum.

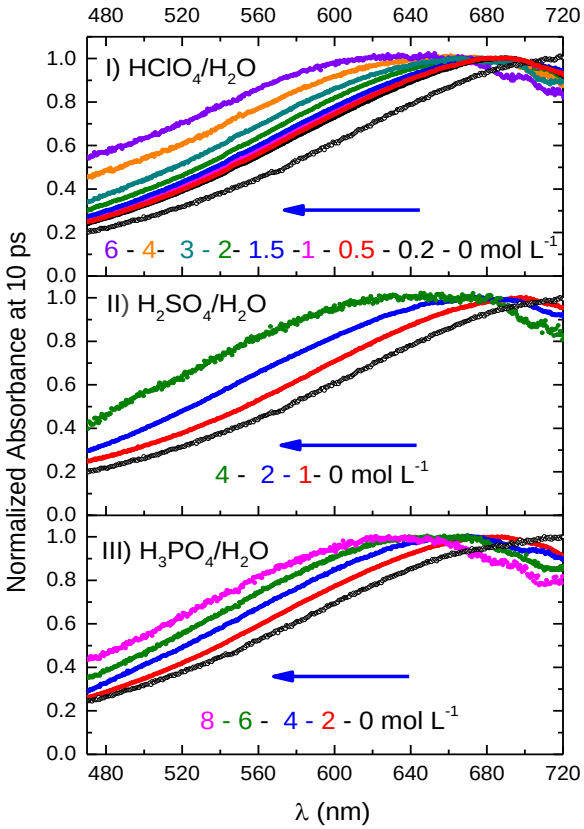

Figure 4.12. *Normalized absorption spectra measured at a delay of 10 ps in three acid solutions (Perchloric, sulfuric and phosphoric acids) at different concentrations.*

The blue shift of the absorption band towards cation concentration is similar than those previously reported with small cations such as Li^+ and Na^+, with ClO_4^- as the counter ion. However, the degree of shifting is lower in the case of H^+ comparing with metal ions. It could be understood that the H_3O^+ has a higher mobility via the hydrogen bond structure of water while the Li^+ or Na^+ is, on average, much closer with the electron in cavity. These observations are in favor of the formation of an intermediate not to be identified as $H_3O^{\bullet}$ radical as suggested before, but a transient solvent separated electron and hydronium pair $(H_3O^+, e_s^-)_{hyd}$.

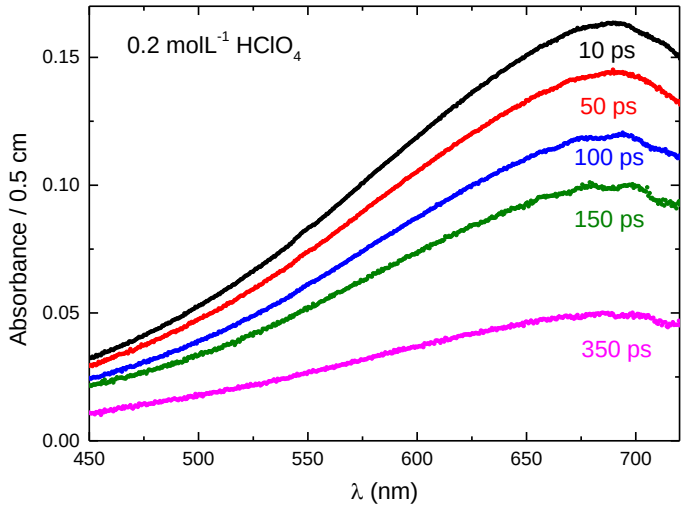

Figure 4.13. *The absorption spectra recorded at different delay time in 0.2* mol L^{-1} *$HClO_4$ aqueous solutions.*

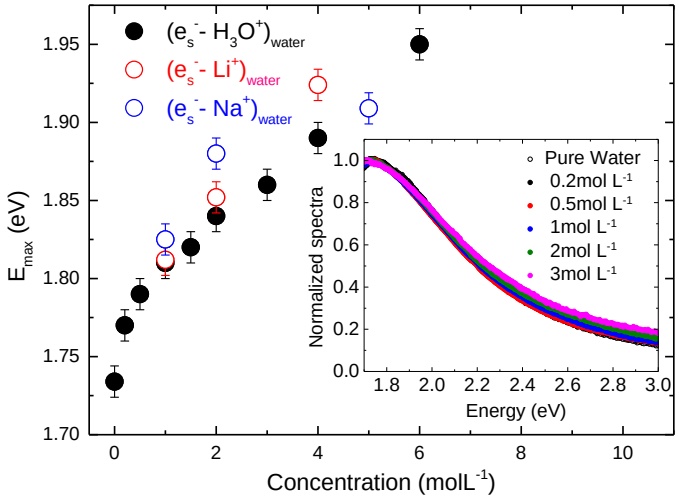

Figure 4.14. *Energetic position of the absorption band maximum of the pairs formed by hydrated electron and H_3O^+ (this work, perchloric acid system), Li^+ and Na^+.[8] Inset: Absorption spectra of hydrated electron and pair $(H_3O^+, e_s^-)_{hyd}$ formed at different concentrations normalized for amplitude and spectral position. The counter ion is ClO_4^- in all cases.*

According to a simple Debye-Smoluchowski model, the rate constant of the pair formation in diluted solution is estimated around 10^{11} mol^{-1} L s^{-1}. Therefore, the formation time of the ion pair is expected to be 50 ps at the lowest concentration solution (0.2 mol L^{-1}). Basically, the time evolution of shifting is supposed to be observed which means the process involving

the transfer of hydrated electron to ion pair should be observed. But our measurements do not display any shift of the absorption between delay time of 10 ps and 100 ps (**Figure 4.13**). That can be explained by the fact that, the relaxation dynamics of electron in highly concentrated acidic solutions is not like the one in neat water. A part of precursor of hydrated electrons could be trapped in the vicinity of H_3O^+ and consequently the solvated electrons are already formed very quickly in close distance of H_3O^+ without any diffusion. The pairs $(H_3O^+, e_s^-)_{hyd}$ are formed within the apparatus function of our experimental setup, picosecond electron pulse radiolysis. Femtosecond measurements, either radiolysis or photolysis have the potential ability to unravel the existence of fully hydrated electron before ion pair formation.[23]

The blue shift of the absorption band was also observed in low polar solvent such as THF and alcohol when the solvated electron is paired with metal cation, even at low concentration of the cation without changing much of the microstructure of solvent.[30,31,32] But in aqueous solutions, it is worth to note that water molecule presents a high dielectric constant at ambient condition which is not in favor of pair complex formation at low concentration of the solutes. That is reason that our time resolved measurements were performed in highly concentrated acid solutions. In highly concentrated solution, the pairing process take place because the distances between solvated electron and H_3O^+ are very short. For example in the case of 6 mol L^{-1} solution, this distance is estimated only a few Å, and the solvated electron is in contact distance with H_3O^+. It should be also noted that the dielectric constant of the highly concentrated solutions is changed compared with that of neat water. In fact, the structure of the solvent is changing by increasing the ionic strength. For example in phosphoric acid solutions, it is reported that the dielectric constant of the solutions decreases from 78 for neat water, to 70, 62, 55, and 44 for 1, 2, 3, and 5 mol L^{-1}, respectively.[33] Therefore, the effect of the ionic strength should be also taken into account for the shift of the absorption band in very concentrated acidic solutions.

We compared the degree of blue shift in these three types of acid solutions as perchloric acid is completely dissociated but not the same cases in sulfuric and phosphoric acid solutions. For instance, the dissociated free H_3O^+ ions concentration are 2, 2.43 and 0.353 mol L^{-1} in the same apparent molar 2 mol L^{-1} $HClO_4$, H_2SO_4 and H_3PO_4 solutions, respectively. With the same amount of H_3O^+ ions, the energetic position of the pair $(H_3O^+, e_s^-)_{hyd}$ are not the same and depends on the type of acid particular at a higher concentration (> 0.5 mol L^{-1}). It could be seen in **Figure 4.15**, in phosphoric acid solution, the pair complexes seem much tighter in contact and present the greatest absorption band blue shift from the neat water. This might be

explained by the charged ions in solution, ionic strength as well as the dielectric constant of acidic solutions particularly in much concentrated media where the properties of water solvent are completely changed by the presence of large amount of solute species. Additionally, the thermalized, relaxation and recombination reactions of ejected electron in these highly concentrated solutions are strongly affected by the surrounding solutes species instead of surrounding water in diluted solutions.

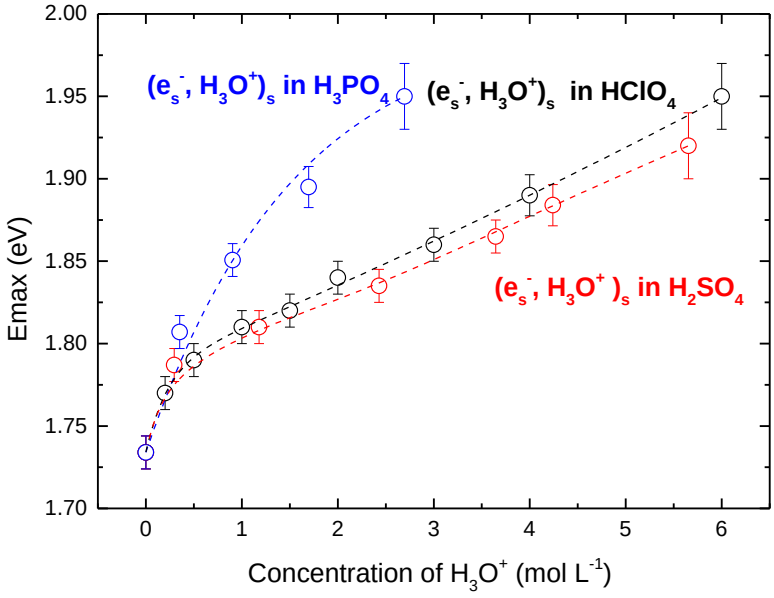

Figure 4.15. *Energetic position of the absorption band maximum of the pairs formed by hydrated electron and H_3O^+ in various acidic solution.*

4.3 Paring of hydrated electron at elevated temperatures

As rising the temperature of water solutions, many physical parameters of liquid water including the density, viscosity and dielectric constant changed rapidly as listed in **Table 4.3**. The coulomb potential between reactants will change significantly which is in favor of the encounter pair formation. Therefore, it is expected that, at elevated temperature, with a relative lower concentration of hydronium ions, the ion pair become more obvious comparing with that at room temperature. On the other hand, both of the diffusion and activation process are accelerated by the rise of the *T (*°C*)* but the diffusion is faster. As shown in **Figure 4.6**, above 300 °C the value of rate constant observed in diluted acid solutions is approaching to the value of diffusion controlled rate constant, implying that from this temperature, the reaction (1) is not activation controlled as the activation barrier become less important. Hence, it is not likely to observe the ion-pair in this condition.

Table 4.3 *Properties of water as a function of water and the rate constant of reaction (1) at different temperature*[34]

Temperature	k $\times 10^{10}$	Density	Dynamic Viscosity	Dielectric constant
(°C)	*L mol^{-1}L^{-1}*	*(g / cm^3)*	*(Pa s, N s/m^2) 10^{-3}*	*ε*
25	2.3	0.997	0.891	80.4
50	3.21	0.988	0.547	72.21
100	5.65	0.958	0.282	55.39
150	9.13	0.917	0.182	43.89
200	16.6	0.865	0.134	34.59
250	32	0.799	0.106	26.75
300	65	0.712	0.086	19.66
350	208	0.575		12.61

Several solutions of different concentration (0.001, 0.01, 0.05, 0.1 mol L^{-1}) of $HClO_4$ in D_2O and H_2O are studied in picosecond pulse radiolysis (University of Tokyo) coupled with high temperature & high pressure cell setup. Deutorated water is specially used to have a lower absorption of OH-bound in water when observing the absorption spectrum. Figure 4.16 shows one example of studied solutions for the absorption band measured in the 0.1 mol L^{-1} D_3O^+ solution, the highest concentration studied, at different temperatures.

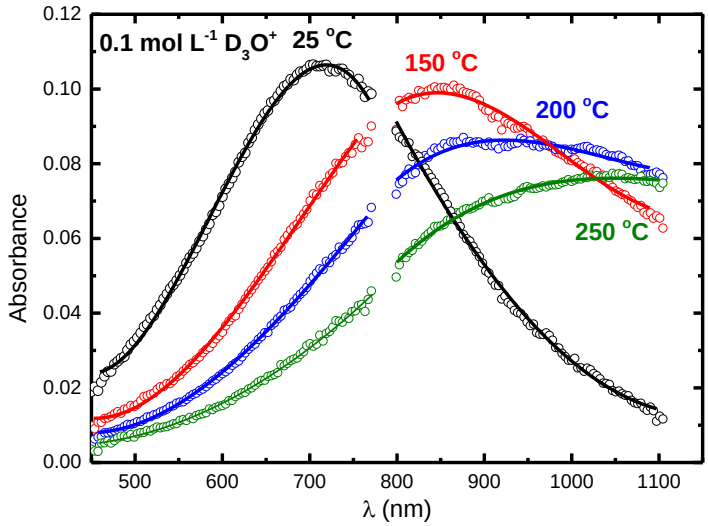

Figure 4.16. *Temperature-dependent absorption spectra of hydrated electron in 0.1 mol L^{-1} acid perchloric solution at 30 ps.*

The absorption band is red shifted by increasing the temperature as the similar cases in neat D_2O. For solutions of 0.01 and 0.001 mol L^{-1} acid, the spectra of e_{hyd}^- is the exactly the same as that in neat water at different temperature from 50 °C up to 350 °C. As expected, at 25 °C the measurements show the same absorption band than in neat D_2O already reported in the literature. As mentioned above, only at high concentration (more than 0.2 mol L^{-1}), an effect of acid on the absorption band can be detected at room temperature. However, the change of acidic D_2O of 0.1 mol L^{-1} is not the same and slightly different with pure D_2O only when the temperature is above 150 °C. For example at 200 °C, the absorption band in neat D_2O with a maximum at 1.31 eV is found at 1.38 eV when 0.1 mol L^{-1} $HClO_4$ is present in solution. The intensity of the absorption band measured from 1.1 to 2.8 eV decreases rapidly with time (**Figure 4.17**) while keeping the same shape. Additionally, the kinetics show that, for this solution at 200 °C, the lifetime of hydrated electron is very short, around 100 ps. For the same absorbed dose per pulse, the maximum of the absorption band in neat D_2O is located at 950 nm but it is shifted to 900 nm for solution containing 0.1 mol L^{-1} D_3O^+ . The shift can also be verified by the kinetics observed at 900 and 950 nm (**Figure 4.17 inset**). In neat D_2O at 200 °C, the absorbance from kinetics at 950 nm is higher than that at 900 nm while the relation gets inversed in the presence of 0.1 mol L^{-1} D_3O^+ . The value of the maximum of the absorption band of hydrated electron in pure D_2O and in acidic solutions at 0.1 mol L^{-1} is presented in **Figure 3.18**. It is clear that the change of the absorption band depends on the

temperature and also on the concentration of hydronium cation. From room temperature up to 150 °C, there is almost no change of the absorption band in the presence of 0.1 mol L^{-1} H_3O^+, but with increasing the temperature in terms of dielectric constant the effect of the presence of hydronium cation becomes more obvious on the absorption band of solvated electron.

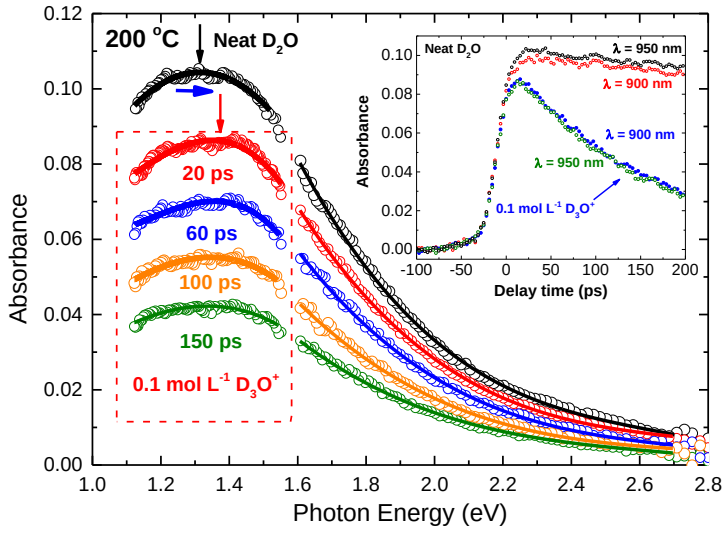

Figure 4.17. *Absorption spectra of hydrated electron in neat heavy water and in 0.1 mol* L^{-1} *perchloric acid aqueous solution at 200 °C. Inset: Kinetics observed at the wavelength of 900 nm and 950 nm in neat and acidic heavy water.*

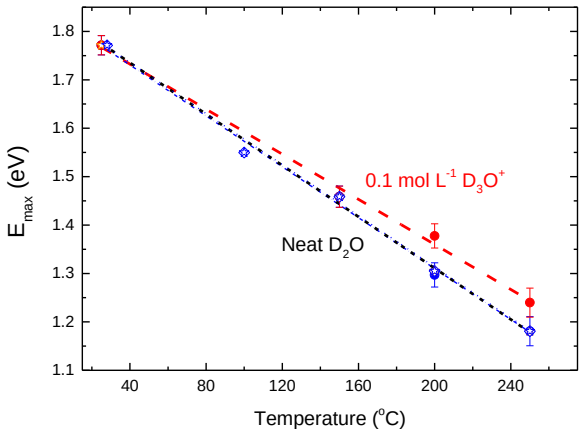

Figure 4.18. *Energetic position of the maximum of the hydrated electron absorption band plotted at different temperature in 0.1 mol* L^{-1} *acidic aqueous solutions 30 ps after the pulse (red) For comparison, previous results in neat* D_2O *(Black) are also given. The dashed lines are guiding eyes.*

At highest temperature, 250 °C, the maximum is located at 1.17, 1.2 and 1.24 eV in neat D_2O and in acidic solutions containing 0.05 and 0.1 mol L^{-1} H_3O^+, respectively (**Figure 4.18**). Due to the ultrafast decay of solvated electron, within our time resolution (30 ps) the measurements at higher temperature were not possible for the concentration above 0.05 mol L^{-1}. At 300 °C, the maximum of the absorption band is beyond our observation windows as shown in **Figure 4.19** and for 0.05 mol L^{-1} H_3O^+ the shift was not observed. Nevertheless, the shape of the absorption band of hydrated electron between 800 and 1100 nm is almost the same in neat water at 300 and 350°C than those measured for the same temperature but in the presence of low amount of H_3O^+.

This observation could be also in agreement with the finding that, at these temperatures, the activation barrier of $H^{\bullet}$ atom formation disappears and the high rate constant of the reaction is almost controlled by diffusion. The absence of the spectral shift can also be explained by the fact that, for these temperatures, the proton tunneling process can be also an important factor for the high rate constant and the absence of the pair observation. In that case the lifetime of the pair is negligible even if it is formed very quickly by fast diffusion.

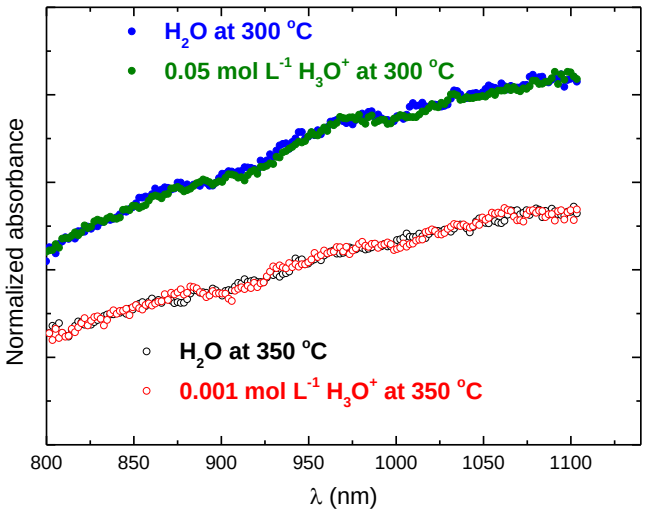

Figure 4.19. *Normalized absorption spectra performed at 300 °C 350 °C in neat light water and in the presence of 0.05 mol L^{-1} and 0.001 mol L^{-1}, respectively. The dash line is best fit of the spectral data showing that the spectrum are almost identical between H_2O and 0.001-0.05 mol L^{-1} H_3O^+ when the temperature is above 300 °C.*

4.4 Scavenging of presolvated electron by H_3O^+

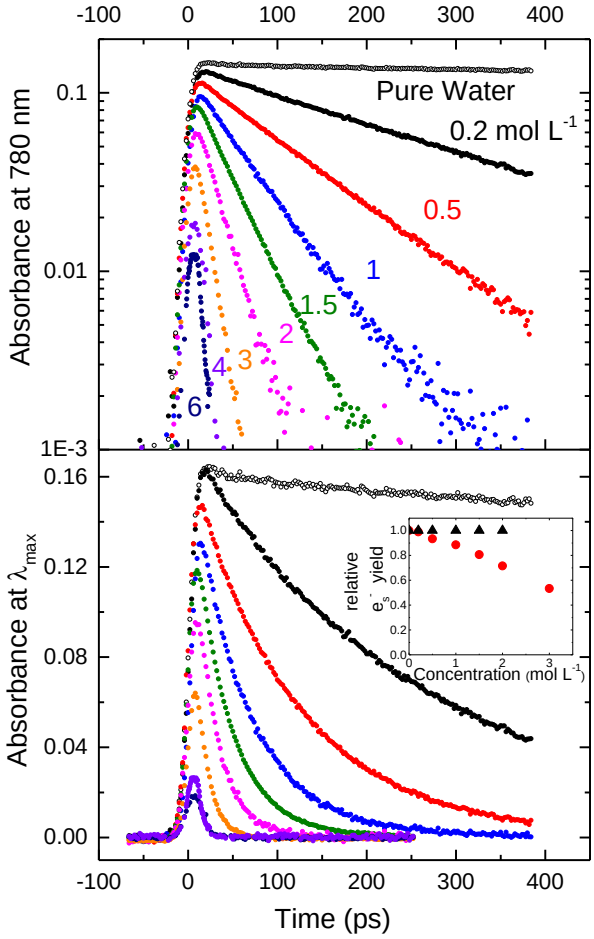

Figure 4.20. *Decay of solvated electron in perchloric acid solution at different concentrations. Upper part: logarithmic scale at 780 nm. Bottom: the absorbance observed at the maximum of the absorption band for each perchloric acid concentration. Inset: relative yield of solvated electron deduced from the absorbance at maximum in this work ●, in reference ▲ by Hunt et al*[20].

The initial absorbance is decreased by 0, 7, 12, 20, 29, and 47% for the perchloric acid solution at concentration of 0.2, 0.5, 1, 1.5, 2, and 3 mol L^{-1}, respectively (**Figure 4.20 inset**). This decrease is due to the scavenging of the presolvated electron by H_3O^+ which was previously considered to be negligible up to 2 mol L^{-1} perchloric acid (**Figure 4.20 inset**, **black triangles**). The reason could be that the shift of the absorption band was not taken into account. We find from the analysis of the kinetics C_{37}, which is defined by a solute concentration that reduces the initial yield of solvated electrons to 1/e, to be around 3.5 mol L^{-1}. This value is much larger than that for efficient scavengers of presolvated electrons such as cadmium, selenite, bipyridine or nitrate suggesting H_3O^+ is in fact not an efficient

scavenger. However, it is shown clearly in this study that H_3O^+ is able to scavenge presolvated electrons. The blue shift of epithermal electron (non-solvated electron) from $\lambda >$ 1300 nm to λ = 930 nm observed by femtosecond spectroscopy[23] showed that the $(H_3O^+, e^-)_{water}$ has the same spectral trend as $(H_3O^+, e_s^-)_{water}$. But the lifetime of $(H_3O^+, e^-)_{water}$ is very short and H• atom is formed in less than 1 ps. This ultrafast reaction is in agreement with our observation that the initial yield of solvated electron observed at 10 ps subsequently decreases by rising the concentration of H_3O^+, showing that the presolvated electron is scavenged partially by H_3O^+. The formation of H• atom via the ultrashort-lived pair $(H_3O^+, e^-)_{water}$ is believed to occur without energy barrier and it can be considered as an intra-electron transfer within the pair. Note that the electron in this pair is not solvated. The lifetime of $(H_3O^+, e_s^-)_{water}$ is much longer and first order kinetics are expected to apply if an intra-electron transfer occurs forming H•. As reported above, the reaction rate of the decay is concentration dependent. In fact, the decay of the pair $(H_3O^+, e_s^-)_{water}$ observed in different solutions and at various concentrations are all pseudo-first order (**Figure 4.19**). That means, contrarily to the case of $(H_3O^+, e^-)_{water}$, the channel of the decay of the pair $(H_3O^+, e_s^-)_{water}$ resulting in a hydrogen atom is not an intra-electron transfer as follow:

$$\left(H_3O^+, e_s^-\right)_{water} \rightarrow H^\bullet + H_2O \qquad (4.10)$$

And this point suggest that the hydrogen atom formation by solvated electron reaction with H_3O^+ is governed by a proton transfer reaction which is regulated by hydrogen network and hopping mechanism of proton from one water molecule to another one. Therefore, the reaction involves H_3O^+ concentration. Consequently, even if the solvated electron is in close contact with H_3O^+, the reaction is not immediate and, as the lifetime of the pair is long enough, even another proton can come in contact and react with solvated electron through the hydrogen network. The difference of energy of the electronic transition between $(H_3O^+, e^-)_{water}$ and $(H_3O^+, e_s^-)_{water}$ shows that the first pair is on an energy level raised by 0.35 eV, which is larger than the activation barrier (0.15 eV) for reaction (4.1). This points out that the reduction reaction giving H• atom could occur via an electron transfer from the presolvated electron, whereas a proton transfer occurs when the electron is fully stabilized by solvation.

The decays are observed at different concentrations and different temperatures at the maximum of the absorption band. The kinetics of hydrated electron for solution containing 0.1 mol L^{-1} H_3O^+ shows that the temperature accelerates the decays but the presolvated

electron is not scavenged at this concentration even at 250 °C. At 300 °C, the decay observed is only limited for 0.05 mol L^{-1} H_3O^+ as the maximum concentration. The decay at 300 °C does not present any scavenging of presolvated electron. It is worth noting that the C_{37}, of H_3O^+ as mentioned above at room temperature is 3.5 mol L^{-1}. At such high temperature, presolvated electron could react very rapidly with H_3O^+ before it becomes solvated. However, the small decrease of the initial absorbance after the pulse is due to the fast reaction within electron pulse at high temperature (**Figure 4.21**).

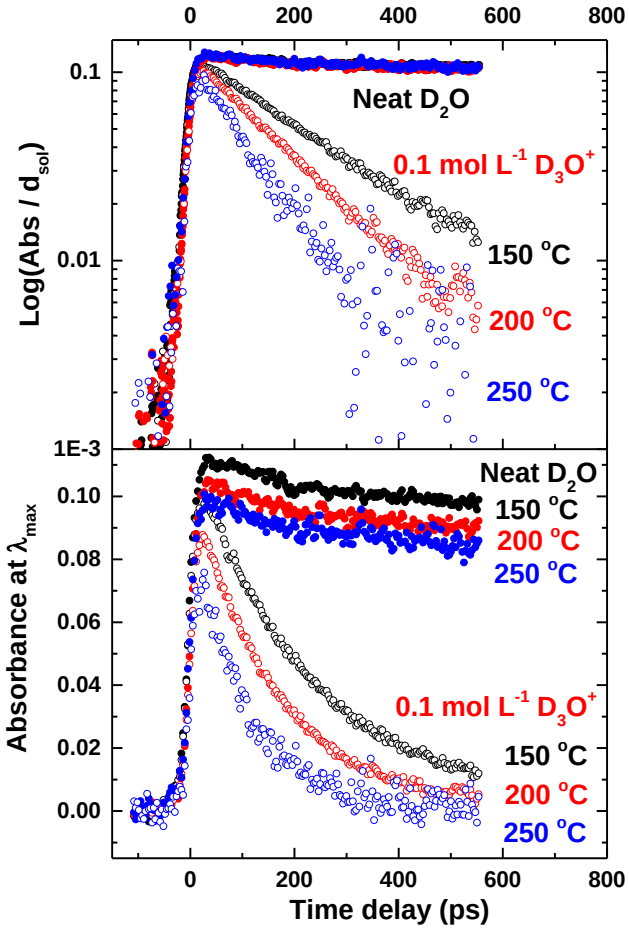

Figure 4.21. *Decay of solvated electron, observed at maximum of the absorption band at different temperature in 0.1 mol L^{-1} acid D_2O solution (Bottom). Decay in neat water and acidic solution at 150, 200 and 250 °C in logarithmic scale.*

Therefore, it can be considered that at 250 °C, C_{37} for presolvated electron scavenging is larger than 0.1 mol L^{-1}. Although a femtosecond pulse is more suitable to be used to clarify the reactivity of presolvated electron in acidic medium, it seems at least this scavenging reaction is not much temperature dependent.

In highly concentrated acidic solutions, the ejected electron is produced partly from the ionizing of the water solvent and partly from the acid solutes. Hydronium ion is believed to be only species in these solutions that could scavenge the excess electron or presolvated electron via electron transfer before the solvation of electron. However, the scavenger efficiency also depends on the microstructure of the acidic solutions. As seen in **Figure 4.22**, the H_3O^+ from the dissociation of sulphuric acid is less reactive to presolvated electron compared with that from perchoric and phosphoric acid. As 1 mol L^{-1} H_2SO_4 could provide more than 1 mol L^{-1} H_3O^+, the ratio between water molecules and acid solutes is the highest in sulphuric, while the lowest value of H_2O/solutes in H_3PO_4 solutions. The fate of excess or hot electron by ionizing radiation of concentrated acid solutions is considered to be influenced by three processes: (1) the thermalized by water or solutes and eventually become solvated before 1 ps; (2) recombination process with hole; (3) reacting with the "free" H^+ that is completed on the time scale of femtosecond.

It is suggested that due to less water hydrogen bond network, the hydrated proton, denoted as H^+ $(H_2O)_n$ is somehow "confined" or "localized" by solutes (ClO_4^-, HSO_4^-, $H_2PO_4^-$) with higher activity with excess electron in contact. Meanwhile, the solvation or mobility of electron is limited. If we assume that the recombination reaction between any electrons and holes is not affected by the change of concentration, therefore, the H^+ react much rapidly or immediately when it is in contact with excess electron where less water molecule is presented to separate the (e^-, H_3O^+) pair. In other words, in acidic solutions the lower value of H_2O/solutes is in favour of scavenging presolvated electron.

Since the initial yield of e^- in pure acid ~ 3.5×10^{-7} J mol L^{-1} in H_2SO_4, or ~ 3.7×10^{-7} J mol L^{-1} in H_3PO_4 is lower than that in neat water (~ 4.5×10^{-7} J mol L^{-1}), the initial yield electron in concentrated acid decreases with increasing the concentration of solutes which has to be taken into account in scavenging electron. However, this changes as shown in **Figure 4.23**, is not much important and cannot stand alone to explain the discrepancy of scavenging efficiency for various types of acid. The initial yield of electron produced in homogenous aqueous system with much solutes could be described as:

$$G(e^-) = f_s G_{solutes}(e^-) + f_w G_{water}(e^-) \qquad (11)$$

In order to better understand the reaction pattern of presolvated electron in acidic media, a detail simulation concerning the micro-picture of acid aqueous solutions especially in highly concentrated is the critical point.

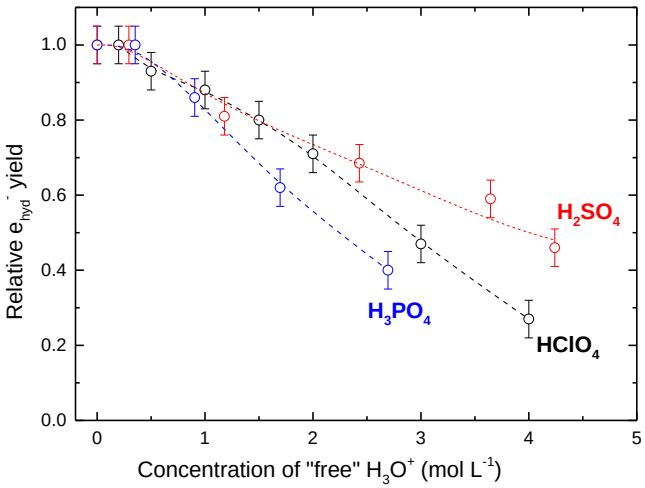

Figure 4.22. *Relative yield of hydrated electron at 15 ps deduced from the absorbance at maximum in different acidic solutions, perchoric acid, sulfuric acid and phosphoric acid. It suggests the presolvated electron was partly scavenged within the electron pulse (7 ps)*

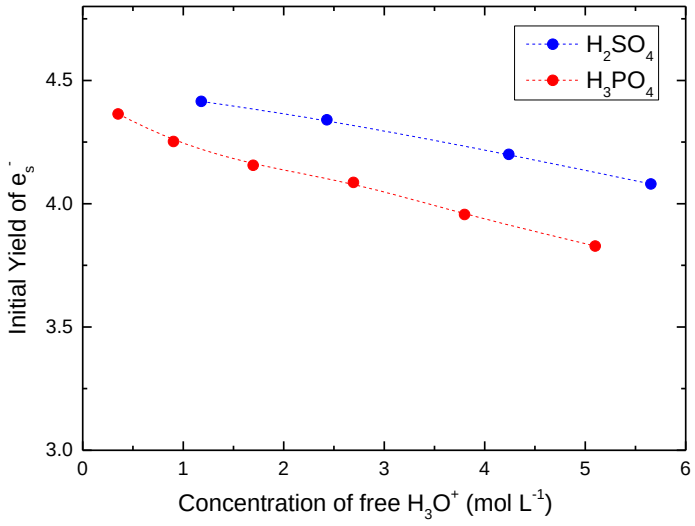

Figure 4.23*. Estimated initial yield of electron produced in highly concentrated acid solutions as a function of dissociated H_3O^+ ion at the same absorbed dose. The reason of this decreasing yield is mainly due to the fact that the direct radiolytic yield of solutes are lower than that in neat water.*

4.5 Reaction of hydrated electron + H_3O^+: Concentration effect

The reaction of hydrated electron + H_3O^+ has been measured in diluted solutions with a preferred value of rate constant of 2.3×10^{10} mol^{-1} L s^{-1} at ambient temperature. It was reported that in the presence of added salts up to ionic strength around 0.05, the rate constant *k* obeys the Brønsted-Bjerrum equation as follow:

$$\log_{10}\left(\frac{k}{k_0}\right) = \frac{2Az_Az_B\sqrt{I}}{1+\sqrt{I}}$$

At room temperature, the *A* is a constant with the value of 0.51 at room temperature. *I* is the ionic strength. As in this Chapter, the reaction occurs in highly concentrated solutions (0.2 - 6 mol^{-1} L s^{-1}) with the purpose of observing hydrated electron pair as well as scavenging the presolvated electron. The value of *I* become important in determining the rate constant of this reaction. Since it has been shown that the pair formation $(H_3O^+, e_s^-)_{hyd}$ as well as the scavenger efficiency of presolvated electron is completely different in three acid solutions. It might be also interesting to give value of the rate constants for each type of acid at different concentration. Previously, several studies have been performed using picosecond radiolysis of perchoric acid solutions for observing the decay of the hydrated electron. The highest concentration of acid was reported to 4 mol^{-1} L.

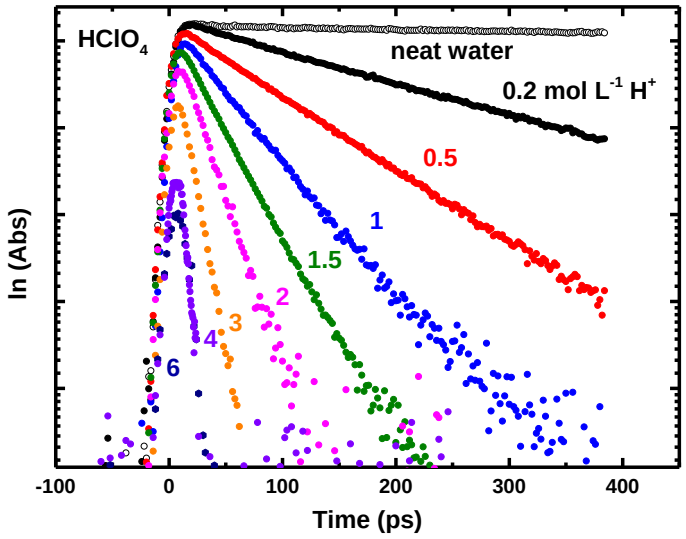

Figure 4.24. *Decay of hydrated electron in the concentrated perchoric acid solutions that is directly observed by 7 picosecond pulse radiolysis with probe light in UV-Visible region.*

It is worthy to note that time-dependence effect of rate constant was considered to be negligible. The lower rate constant was mainly attributed to the change of diffusion process affected by the changes in activities of e_{hyd}^- and H_3O^+.

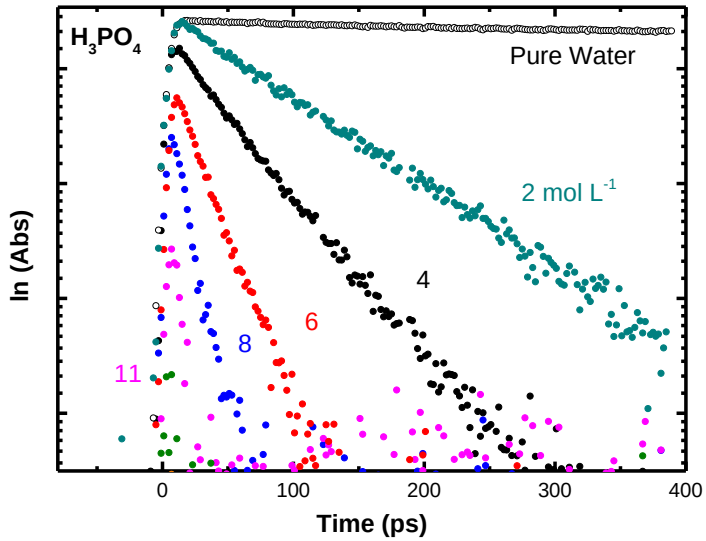

Figure 4.25. *Decay of hydrated electron in the concentrated phosphoric acid solutions that is directly observed by 7 picosecond pulse radiolysis with probe light in UV-Visible region.*

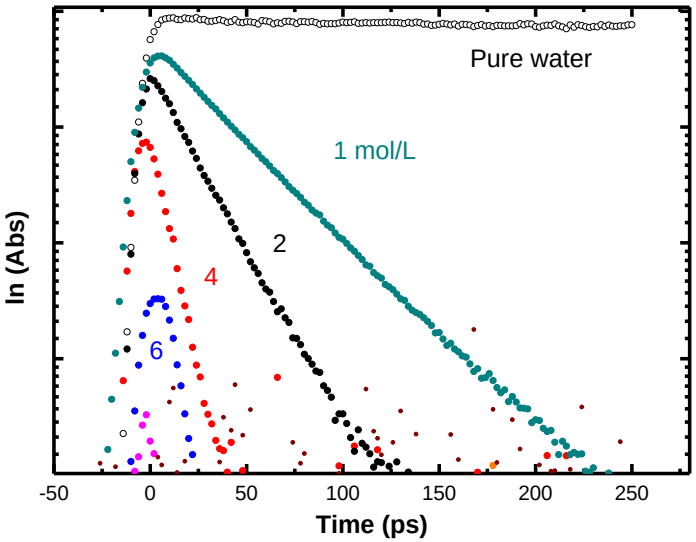

Figure 4.26. *Decay of hydrated electron in the concentrated sulfuric acid solutions that is directly observed by 7 picosecond pulse radiolysis with probe light in UV-Visible region.*

All the original decays of hydrated electron in $HClO_4$, H_3PO_4 and H_2SO_4 acid solutions are presented in **Figure 4.24-4.26**. As could been seen all of kinetics obey the pseudo first order reaction involving the concentration of acid. The value of rate constants for these three acidic solutions are then deduced from these kinetics and they are summarized in **Figure 4.27** comparing to the previous data by Jonah *et al.*[10] and Hunt *et al.* [20] The experimental values in $HClO_4$ solutions by ELYSE (our facility) are overall higher than those from literatures but the trend over the concentration of H_3O^+ is similar. The reason is unknown. For pulse radiolysis of three types of acid under our identical measuring conditions, there is an obvious difference between these acids. It was suggested that the reaction of hydrated electron with H_3O^+ is a proton transfer reaction. Therefore, this difference might be explained by the fact different microstructure of these acidic solutions which has completely different H-network for hopping the proton.

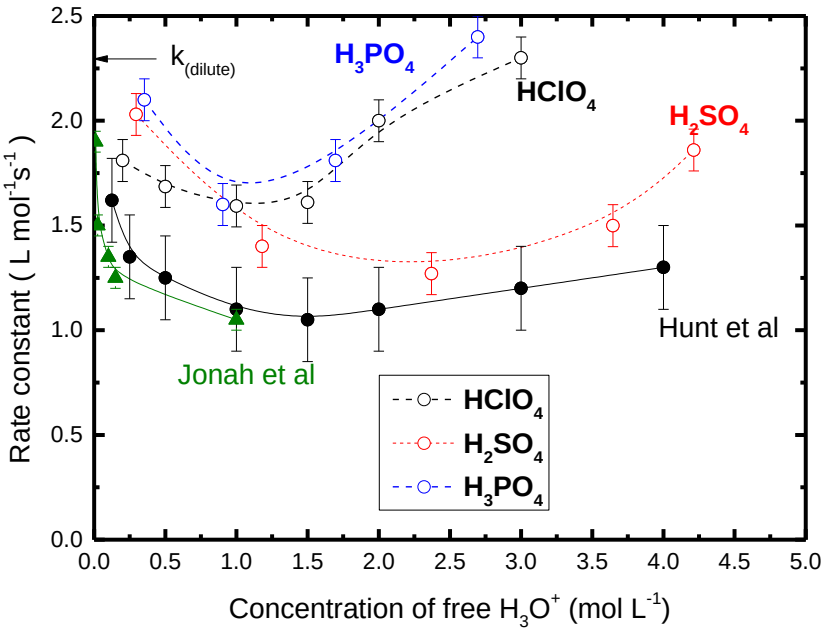

Figure 4.27. *Rate constant of reaction of solvated electron with H_3O^+ deduced from the kinetics in three different acidic solutions ($HClO_4$, H_2SO_4 and H_3PO_4). The previous values measured in HClO4 acid solutions by Jonah et al.[10] and Hunt et al.[20] are also added for the comparison.*

4.6 Reaction of hydrated electron + H_3O^+: Temperature

For a given concentration, the value of A depends strongly to the temperature. The equation given for A is:

$$A = \frac{\sqrt{2}F^2 e}{8\pi\left(\varepsilon(T)RT\right)^{3/2}}$$

F and R, are Faraday and universal gas constants. ε(T) is the dielectric constant of water which depends to the temperature. The value of the dielectric constant of water decreases from 78 to 20 when the temperature is increased from 25 and 250 °C, respectively. By increasing the temperature, ε (T) T is decreasing. Consequently, the value of A in equation (2) increases with temperature[35].

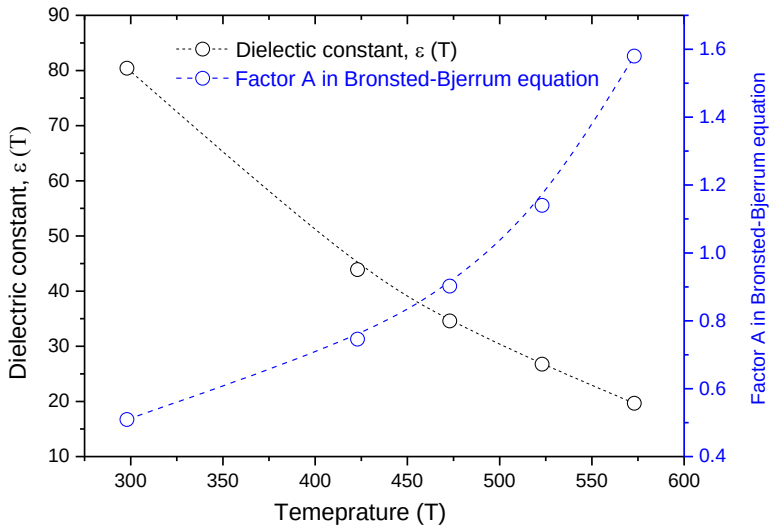

Figure 28. *Dielectric constant of water, ε (T) and factor A in Brønsted-Bjerrum equation as a function of temperature (Kelvin).*

If we take into consideration of the changing of factor *A* in Brønsted-Bjerrum equation, the rate constant of these two charged species at different temperature is still valid for the equation. We also used the modified equation of Debye - Hückel by taking into account the distance of closest approach of the ions (*a*) and temperature dependent of the factor *B*.

$$\log_{10}\left(\frac{k}{k_0}\right) = \frac{2Az_A z_B\sqrt{I}}{1+aB\sqrt{I}}$$

B is proportional to $\sqrt{\varepsilon(T)T}$. At room temperature the value of aB equals to 1 according to the so-called "limiting law" of Debye-Hückel and increase up to 1.12 and 1.29 at 200 and 300 °C, respectively by considering the changes of factor *B* with temperature. By taking into

account the temperature change of B in equation (3), the modified curves (black solid line) are obtained (**Figure 4.29**). The temperature dependent parameter "*B*" does not have much pronounced effect on the rate constant value from Brønsted-Bjerrum equation in the conditions (at 200, 300 °C, 0.001-0.05 mol L^{-1}) that we studied.

Therefore, compared to diluted solutions at the same temperature, increasing the concentration of acid in solution (the effect of ionic strength), decreases considerably the rate constant of reaction between solvated electron and hydronium. As reported in **Figure 4.29**, for a given concentration (a given value of *I*) for instance for 0.05 mol L^{-1}, the effect is more pronounced at 300 °C than at 200 °C. By taking the effect of

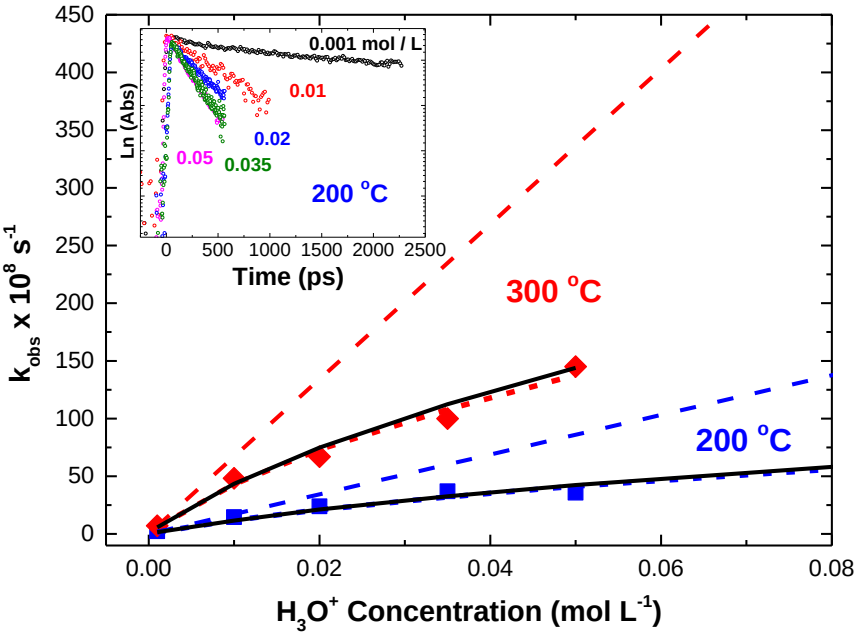

***Figure 4.29**. Pseudo-first order rate constant versus H_3O^+ concentration reported at 200 and 300 °C. For comparison, previous results given by Bartels et al. (dashed lines at 300 and 200 °C)). The dotted lines present the results by using the equation (1) and (2). Inset: the decay of solvated electron at 200 °C at different concentration of H_3O^+. Black solid line is curve from the modified equation (3) by considering the parameter "B".*

4.7 Conclusion and perspectives

4.7.1 Conclusion

The reaction of hydrated electron with hydronium cations is one of the most elementary chemical processes in radiation chemistry. In this Chapter several issues have been addressed using picosecond pulse radiolysis. Firstly, the chemical shift of absorption spectrum over the acid concentration presents a direct evidence of the formation of the transient encounter "ion pair" before producing $H^{\bullet}$ atom. At elevated temperature, this shift could only be observed in a constrained condition with high concentration of acid (0.1 mol L^{-1}) and proper temperature (200- 250 ^{o}C). Second, the substantial decreasing of the initial yield of hydrated electron at 15 ps suggests that the presolvated electrons are able to react with hydronium cation (H_3O^+) before they becomes solvated (< 1ps). For a given concentration of 0.1 mol L^{-1} H_3O^+, however, this presolvated electron scavenged reaction is not, in fact, accelerated by rising the temperature. In addition, the scavenged efficiency varied with the types of acids. As the reaction involves the amount of dissociated H^+ ions, this variation is probably due to the difference in degree of acid dissociation and molar ration between H^+ / H_2O for perchoric, sulfuric and phosphoric acids at a given concentration. Third, the value of the rate constant of this reaction is strongly influenced by the ionic strength that is related to the concentration. The classical Brønsted-Bjerrum model is demonstrated to be valid in the concentration range from 0.01 up to 0.1 mol L^{-1} by considering the ionic strength as well as the temperature. At higher concentration (> 0.5 mol L^{-1}), the measured rate constant value are again different in three types of acid. With such large amount of solutes insider the solution, the "hydrated electron" turns out to be "solvated electron" and the charge recombination reaction in this complex system still needs more experimental and theoretical insights into the microstructure of these acid solutions.

4.7.2 Perspectives

The highly reactive of excess electron or presolvated electron towards hydronium cation is not fully explored in my thesis due to the time resolution of ELYSE facility (7 ps). The time evolution of this reaction is supposed to be several hundreds of femtoseconds accompanying with the relaxation of electron. Indeed, the reactivity of presolvated electron has been one of the most challenging subjects in radiation chemistry and a femtosecond pulse photolysis of aqueous solutions containing 0.5 - 1 mol L^{-1} acid is necessary to possibly observe the time dependent spectral changes with the purpose of in the future.

It was learnt that the reactivity of both of presolvated and solvated electron in electrolyte solutions strongly depends on the microstructure of solution. Another interesting issue is the solvation of electron in highly concentrated aqueous solutions as well as the molecular dynamic simulations of these solutions.

Reference

[1] Anbar, M. Hart E.J. The Effect of Solvent and Solutes on the Absorption Spectrum of Solvated Electrons. *J. Phys. Chem.* **1965**, 69, 1244–1247.

[2] Anbar M. Thomas J.K. Pulse Radiolysis Studies of Aqueous Sodium Chloride Solutions. *J. Phys. Chem*. 1964, 68. 3829–3835.

[3] Kreitus I.V. Effect of Solution Microstructure on the Hydrated Electron Absorption Spectrum. *J. Phys. Chem*. **1985**, 89. 1987–1990

[4] Asaad, A.N. Chandrasekhar, N. Nashed, A.W. Krebs P. Is There Any Effect of Solution Microstructure on the Solvated Electron Absorption Spectrum in LiCl/H2O Solutions? *J. Phys. Chem. A*, **1999**, 103. 6339–6343.

[5] Boutin A., Spezia R., Coudert F.X. Mostafavi M. Molecular Dynamics Simulations of the Temperature and Density Dependence of the Absorption Spectra of Hydrated Electron and Solvated Silver Atom in Water. *Chem Phys Lett.* **2005**, *409*, 219.

[6] Bonin, J. Lampre, I. Soroushian, B. Mostafavi? M. First Observation of Electron Paired with Divalent and Trivalent Nonreactive Metal Cations in Water. *J. Phys. Chem. A*, **2004**, 108. 6818–6820

[7] Wu, G.; Katsumura, Y.; Muroya, Y.; Li, X.; Terada, Y. Hydrated Electron in Subcritical and Supercritical Water. *Chem. Phys. Lett.* 2000, 325, 531–536.

[8] Bartels D.M, Takahashi K, Cline J.A, Marin T.W, Jonah C.D. Pulse Radiolysis of Supercritical Water. 3. Spectrum and Thermodynamics of the Hydrated Electron. *J. Phys. Chem. A*. **2005**, 109, 299-307.

[9] Cercek, B. Formation of H-Atoms from Hydrated Electrons. *Nature Physical Science*, 1971, 234, 159-160.

[10] Jonah, C. D.; Miller, J. R.; Matteson, M. S. The Reaction of Hydrated Electron + Oxonium. Concentration Effects of Acid or Salts. *J. Phys. Chem.* **1977**, *9*, 931-934.

[11] Bronskill, M. J.; Wolff, R. K.; Hunt, J. W. Picosecond Pulse Radiolysis Studies. I. The Solvated Electron in Aqueous and Alcohol Solutions. *J. Chem. Phys*. **1970**, *53*, 4201-4210.

[12] Shiraishi, H.; Sunaryo, G.R.; Ishigure, K. Temperature Dependence of Equilibrium and Rate Constants of Reactions Inducing Conversion between Hydrated Electron and Atomic Hydrogen. *J. Phys. Chem*. **1994**, *98*, 5164–5173.

[13] Takahashi, K. Bartels, D.M. Cline, J.A. Jonah C.D. Reaction rates of the hydrated electron with NO_2^-, NO_3^-, and hydronium ions as a function of temperature from 125 to 380 degrees C. *Chem. Phys. Lett.* 2002, 357, 358–364.

[14] Stanisky, C.M. Bartels, D.M. Takahashi, K. Rate Constants for the Reaction of Hydronium Ions with Hydrated Electrons up to 350 °C. *Radiat. Phys. Chem.* **2010**, 79, 64–65

[15] Han, P; Bartels, D.M. H/D Isotope Effects in Water Radiolysis.4.The Mechanism of $(H)_{aq}$= $(e^-)_{aq}$ Interconversion . *J. Phys. Chem.* **1992**, *96*, 4899-4906.

[16] Ulhilg, F.; Marsalek, O.; Jungwirth, P. From a localized H_3O radical to a delocalized $H_3O^{+\cdots}e^-$ solvent-separated pair by sequential hydration *Phys. Chem. Chem. Phys*. **2011**, *13*, 14003-14009.

[17] Pommeret, S.; Gobert, F.; Mostafavi, M.; Lampre, I. Malocq, J. C. Femtochemistry of Hydrated Electron at Decimolar Concentration. *J. Phys. Chem. A.* **2001**, *105*, 11400 -11406.

[18] Gauduel, Y.; Pomeret, S. Migus, A.; Yamada, N.; Antoneti, A. Femtosecond Spectroscopy of an Encounter Pair Radical (H3O+…e-)hyd in Concentrated Aqueous Solution. *J. Am. Chem. Soc.* 1990, 112, 2925-2931.

[19] Ulhilg, F.; Marsalek, O.; Jungwirth, P. From a localized H_3O radical to a delocalized $H_3O^{+\cdots}e^-$ solvent-separated pair by sequential hydration *Phys. Chem. Chem. Phys*. **2011**, *13*, 14003-14009.

[20] Wolff, R. K.; Bronskill, M. J.; Hunt, J. W. Picosecond Pulse Radiolysis Studies. II. Reactions of Electrons with Concentrated Scavengers. *J. Chem. Phys*. **1970**, *53*, 4211-4215.

[21]Pommeret, S.; Gobert, F.; Mostafavi, M.; Lampre, I. Malocq, J. C. Femtochemistry of Hydrated Electron at Decimolar Concentration. *J. Phys. Chem. A.* **2001**, *105*, 11400 -11406.

[22] Goulet, T.; Jay-Gerin, J. P. On the Reactions of Hydrated Electrons with $OH^{\cdot}$ and H_3O^+. Analysis of Photoionization Experiments. *J. Chem. Phys.* **1992**, *96*, 5076-5087.

[23] Gauduel, Y.; Pomeret, S. Migus, A.; Yamada, N.; Antoneti, A. Femtosecond Spectroscopy of an Encounter Pair Radical $(H_3O^+\ldots e^-)_{hyd}$ in Concentrated Aqueous Solution. *J. Am. Chem. Soc.* **1990**, *112*, 2925-2931.

[24] Markham, A.E. Density of Perchloric Acid Solutions. *J. Am. Chem. Soc.*, **1941**, *63*, 874–875

[25]Katsumura, Y. Radition Chemistry of Concentrated Inorganic Aqueous Solution, in *Radiation Chemistry Present Status and Future Trends.* Eds. C.D. Jonah and B.S.M. Rao. Elsevier Science B.V. Paris, 2001.

[26] Ma, J.; Schmidhammer, U.; Pernot, P.; Mostafavi, M. Reactivity of the Strongest Oxidizing Species in Aqueous Solutions: The Short-Lived Radical Cation $H_2O^{\bullet+}$ *J. Phys. Chem. Lett.* **2014,** *5*, 258-261.

[27] Covington, A. K.; Tait, M. J.; Wynne-Jones, W. F. K. Dissociation of Perchloric Acid in Aqueous Solution at 25 °C. *Proc. R. Soc. Lond. A*. **1965**, *286*, 235-250.

[28] Elmore, K. L.; Hatfield, J. D.; Dunn, R. L.; Jones, A. D. Dissociation of Phosphoric Acid in Aqueous Solution at 25 °C. *J. Phys. Chem*. **1965**, *69*, 3520–3525.

[29] Margarella, A. M.; Perrine, K. A.; Lewis, T.; Faubel, M.; Winter, B.; Hemminger, J. C. Dissociation of Sulfuric Acid in Aqueous Solution: Determination of the Photoelectron Spectral Fingerprints of H_2SO_4, HSO_4^-, and SO_4^{2-} in Water. *J. Phys. Chem. C*. **2013**, *117*, 8131-8137.

[30] Renou, F.; Mostafavi, M.; Archirel, P.; Bonazzola, L.; Pernot, P. Solvated Electron Pairing with Earth Alkaline Metals in THF. 1. Formation and Structure of the Pair with Divalent Magnesium. *J Phys Chem. A*. **2003**, *107*, 1506-1516.

[31] Salmon, G. A.; Sedddon, W. A.; Fletcher J. W. Pulse Radiolysis of Solvated Electrons, Ions Pairs, and Alkali Metal Anions in Tetrahydrofuran. *Can. J. Chem*. **1974**, *52*, 3259-3268.

[32] Ma, J.; Archirel, P.; Schmidhammer, U.; Teuler, J. M. ; Pernot, P.; Mostafavi, M. Reduction of Earth Alkaline Metal Salts in THF Solution Studied by Picosecond Pulse Radiolysis *J. Phys. Chem. A*. **2013**, *117*, 14048-14055.

[33] Christensen, J. H.; Smith, A. J.; Reed, R. B.; Elmore, K. L. Dielectric Properties of Phosphoric Acid Solutions at 25° C. *J. Chem. Eng. Data*. **1966**, *11*, 60–63.

[34] Markham, A.E. Density of Perchloric Acid Solutions. *J. Am. Chem. Soc.*, **1941**, *63*, 874–875

[35]Daniel J. Bradley and Kenneth S. Piker. Thermodynamics of Electrolytes. 12. Dielectric Properties of Water and Debye-Huckel Parameters to 350 "C and 1 kbar

Chapter 5: Reactivity of Solvated Electron in Tetrahydrofuran (THF)

Chapter 5 Reactivity of Solvated Electron in Tetrahydrofuran (THF)

5.1 Introduction

Since 1962, it is known that the solvated electron can be formed in a variety of solvents ranging from high polar liquid like water or alcohol to weakly polar molecule, for example in THF.[1-8] The reactivity, thermodynamic properties, solvation of solvated electron in ester differ much from that in water. One typical example is that the absorption spectrum of solvated electron in terms of peaking wavelength and band shape at room temperature strongly depend on the type of solvent molecules as shown in **Figure 5.1**. The solvents may be classified into three main groups:

(1) Polar protic solvents with hydrogen bonds like water and alcohols. The maximum absorption often located in visible region from 520 nm to 800 nm.
(2) Liquid ammonia, amines and ammonium ionic liquids. The absorption spectrum of solvated electron falls into near infrared domains.
(3) Weakly polar solvents like ester, hydrocarbons and diethyl carbonate. The solvated electron in these solvents present a very broad band and they are observed in infrared region (> 2000 nm).

In general, the maximum absorption band of solvated electron shifts to higher energy as the dielectric constant of liquids decreases and it is mostly governed by molecule structure. The position and shape as indicated by quantum simulations are originated from the transitions from electronic ground *s* like states to three non-degenerated *p* like states together with additional contribution of transitions from bound states to continuum at higher energy. The latter

contribution accounts for the asymmetry of the spectrum. Therefore, the absorbing band of solvated electron is able to provide many information on the depth of potential energy well in which the electron is localized. Over the past decades, it is also not surprise that many theoretical works have been focused on the model picture of electron in liquids, often taking into account these experimental absorption spectrums to verify their proposed models and simulation methods.

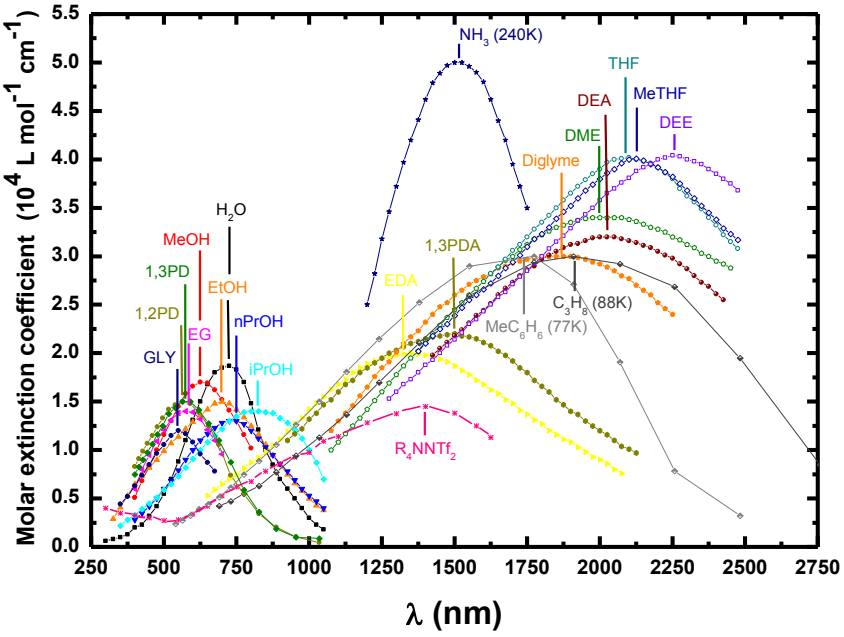

Figure 5.1. *Absorption spectrum of solvated electron in various liquids*[1-5].

In the years of 1970s, some radiation chemists observed that with very small amount of alkali salts inside the non-polar solvents, the absorption spectrum of solvated electron produced by electron pulse has a strong blue shift as shown in **Figure 5.2**[9]. They proposed that reaction of the solvated electron with alkali metal cations forms a variety of absorbing intermediates in a number of weakly polar liquids. The "ion pair" was attributed to these new bands and the pair formation kinetics were studied. Almost thirty years later, *Renou et al*[10], in our group, revisited the nanosecond pulse radiolysis of THF containing alkali earth salts. The absorption spectra of the pairs observed at 50 ns composes two bands and this is interpreted by the *ab* Initio that the three *p*-like excited states of solvated electron are split. Since then, it has been suggested that the blue shift of the absorption spectrum and its band change corresponds to the formation of the pair complexes.

Meanwhile, *Schwartz et al*[11] performed a series of theoretical work using mixed quantum/ classic molecular dynamic simulation to unravel the nature of (e_{THF}^-, Na^+). It was found that the pair exists as a tight contact pair in which the valence electron of sodium, on average, is displaced 1.44 Å from the Na^+ core and four THF solvent oxygen coordinate with Na^+.

In this chapter 5, we use picosecond pulse radiolysis combined with simulations to study the reactivity of e_{THF}^- with a variety of solutes including $HClO_4$, $Mg(ClO_4)_2$ and $LiClO_4$.

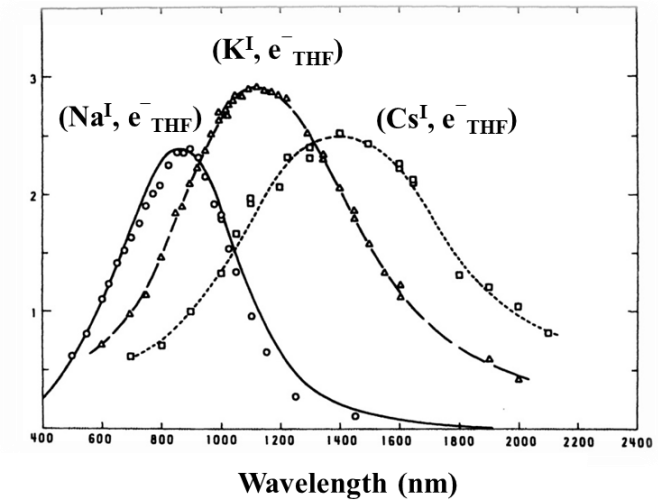

Figure 5.2. *Ion-pair absorption spectra observed immediately after the 1 μs pulse in THF solutions containing $NaBPh_4$, $KBPh_4$ or $CsBPh_4$. The concentration of dissociated salts ranges from $10^{-5} - 10^{-3}$ mol L^{-1}.*[9]

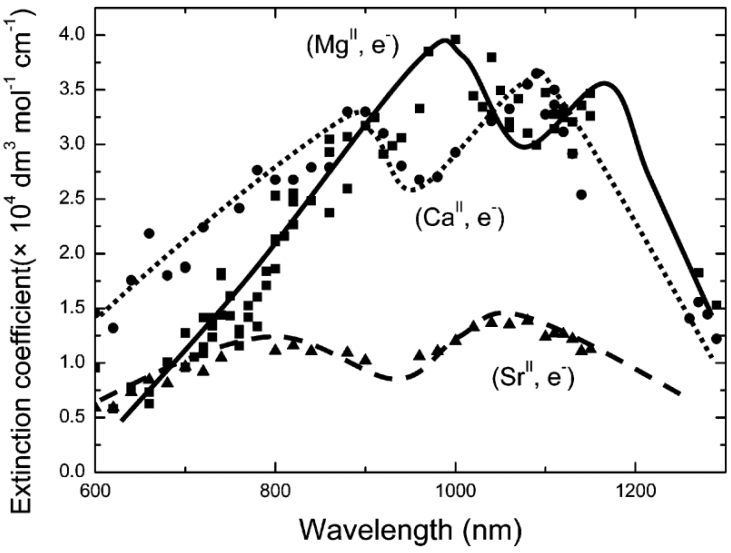

Figure 5.3. *Transition absorption spectrum of the productshe obtained by pulse radiolysis of THF solutions containing 0.01 mol L^{-1} $M^{II}(ClO_4)_2$ at 50 ns*[10].

5.2 Ion association of perchlorates in THF

The knowledge concerning on the ion association of perchlorate salts in THF over the concentration from very dilute to relatively high is essential for understanding the experimental kinetics as well as for theoretical simulations. The conductivity or Raman measurements of THF solutions containing salts are very helpful to provide the information about the abundance distribution of species such as free ions, triple ions in the solutions we have studied. For instance, for THF solutions in presence of lithium perchlorate, it was showed that the conductivity of solutions decrease firstly to the lowest value from dilute (10^{-5} mol L^{-1}) to 0.03 mol L^{-1} (see **Figure 5.4**). This means the dissociation of $LiClO_4$ to Li^+ ion is limited when increasing the concentration. In more concentrated solutions, the conductivity rise up again, which is attributed to the formation of triple ions ($Li_2ClO_4^+$ or Li $(ClO_4)_2^-$)[12].

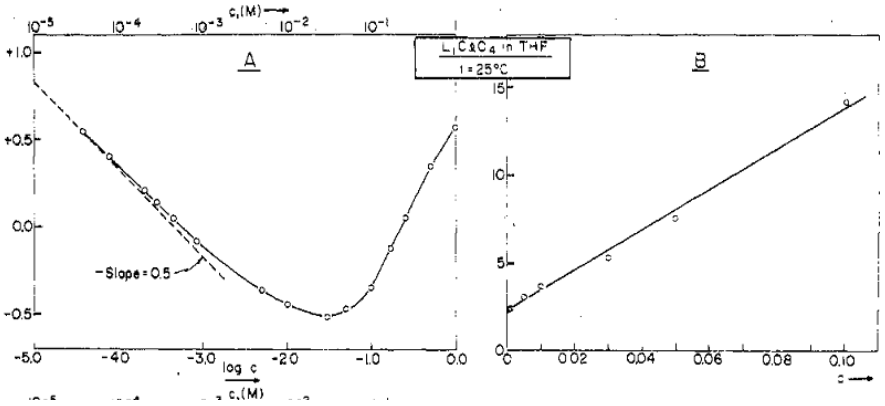

Figure 5.4. *Electrical conductivities as a function of concentration for $LiClO_4$ in THF*[12]

In consequence, according to the Fuoss-Krauss triple-ion theory, the relation between the concentration and conductivity has been described as following equation:

$$\Lambda c^{1/2} = \frac{\Lambda_0}{K_P^{1/2}} + \Lambda_0^T \frac{K_T}{K_P^{1/2}} c. \qquad (5.1)$$

Where c is the apparent molar concentration of solutions, Λ_0 and Λ_0^T are the limiting equivalent conductivities of $LiClO_4$ and of two possible triple ions, $Li_2ClO_4^+$ and $Li(ClO_4)_2^-$. K_p and K_T is the equilibrium constant as below:

$$Li^+ + ClO_4^- \rightarrow LiClO_4 \qquad K_P \qquad (5.2)$$

$$LiClO_4 + Li^+ \rightarrow Li_2ClO_4^+$$
$$LiClO_4 + ClO_4^- \rightarrow Li(ClO_4)_2^- \qquad K_T \qquad (5.3)$$

By fitting the conductivity data with equation, the value of K_P and K_T were fund to be 4.84× 10^7 L mol $^{-1}$ and 153 mol $^{-1}$ by Petrucci *et al*.[11] Very recently, Das modified these constant values to be 6.58 × 10^6 L mol $^{-1}$ and 24.87 mol $^{-1}$, respectively[12]. Therefore, on the basis of this model, the concentration of each species in different solution (0.01− 1 mol L^{-1}) is calculated and given in **Table.5.1**.

Table 5.1 *Chemical compositions of LiClO4 salts in THF ranging from 0.01 to 1 mol* L^{-1}.

Total LiClO4	$Li_2ClO_4^+$	$Li(ClO_4)_2^-$	$LiClO_4$	Li^+
mol L^{-1}	mol L^{-1}	mol L^{-1}	mol L^{-1}	mol L^{-1}
0.01	9.7×10^{-6}	9.7×10^{-6}	9.93×10^{-3}	4.1×10^{-5}
0.05	1.1×10^{-4}	1.1×10^{-4}	0.0496	8.2×10^{-5}
0.1	3.1×10^{-4}	3.1×10^{-4}	0.09895	1.1×10^{-4}
0.5	3.4×10^{-3}	3.4×10^{-3}	0.489	$<4\times10^{-4}$
1	9.7×10^{-3}	9.7×10^{-3}	0.971	$<3\times10^{-4}$

From this table, it is clearly shown that the non-dissociated molecules $LiClO_4$ is predominated species in solution. In 0.01 mol L^{-1} $LiClO_4$ solutions, the amount of triple and Li^+ ions are negligible (< 10^{-5} mol L^{-1}). At highest concentration, comparing with $LiClO_4$ (0.971 L mol $^{-1}$), the concentration of other ions is very low. This point is very important for picosecond pulse radiolysis of lithium perchlorate solutions because in these cases it is not likely to observe the absorbing transient pair species with these ions on the timescale of nanosecond. With such low concentration the reaction of e_{THF}^- to ions or triple ions takes place on the timescale of tens of nanosecond even the reaction is as fast as a diffusion controlled (10^{11} L mol^{-1} s^{-1}) reaction.

In addition, the formation of molecule $LiClO_4$ in THF is believed to be multistep[12]:

$$\begin{aligned} &Li^+ + ClO_4^- \rightleftarrows Li^+\cdot THF\cdot ClO_4^- \rightleftarrows Li^+\cdot ClO_4^-, \\ &2Li^+\cdot THF\cdot ClO_4^- \rightleftarrows Li^+\cdot THF\cdot ClO_4^- \cdots Li^+\cdot THF\cdot ClO_4^-, \\ &2Li^+\cdot ClO_4^- \rightleftarrows (Li^+\cdot ClO_4^-)_2. \end{aligned} \tag{5.4}$$

At higher concentration, the infrared and Raman spectra reveal the non-dissociated molecules $LiClO_4$. In fact, three different type of complexes coexist, the solvent separated dimer (Li^+ $THFClO_4^-)_2$ having a larger proportion, contact dimer (Li^+ $ClO_4^-)_2$ and monomer $LiClO_4$. Apparently, the distribution of these complexes depend on the concentration. Although a detail model for calculating the amount of dimer is lacked in the literatures, it is reasonable to

predicate that at higher concentration like 0.5 or 1 mol L^{-1}, dimerization is the dominating process, while at lower concentration monomer $LiClO_4$ mainly exists in solutions.

The ionic association of perchlorate alkaline earth metal salts ($Mg(ClO_4)_2$, $Ca(ClO_4)_2$ and $Sr(ClO_4)_2$) in solvent THF was previously studied in our lab by Renou *et al.*[13](see **Figure 5.5**) Because of the low polarity of THF, the total dissociation of $Mg(ClO_4)_2$ to Mg^{2+} ion is neglected and it was assumed that the dissociation process could be expressed as:

$$\begin{aligned} M^{II}ClO_4^+ + ClO_4^- &\rightarrow M^{II}(ClO_4)_2 \\ M^{II}(ClO_4)_2 + ClO_4^- &\rightarrow M^{II}(ClO_4)_3^- \\ M^{II}(ClO_4)_2 + M^{II}ClO_4^+ &\rightarrow M^{II}{}_2(ClO_4)_3^+ \end{aligned} \qquad (5.5)$$

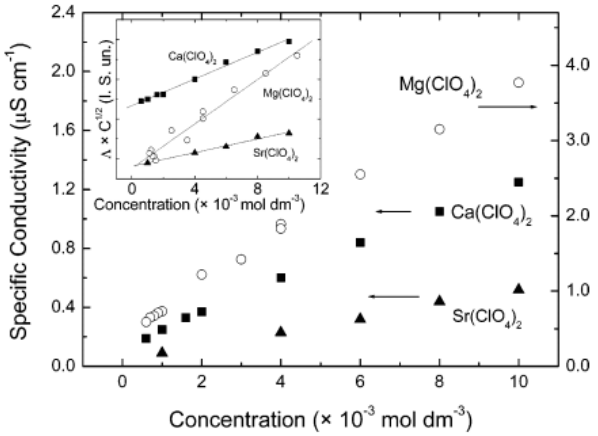

Figure 5.5. *Specific conductivities of $Sr(ClO_4)_2$, $Ca(ClO_4)_2$, and $Mg(ClO_4)_2$ in THF; Inset: Fitting $\Lambda C^{1/2}$ as a function of concentration*[13].

Table.5.2 *Parameters in Fuoss-Krauss triple-ion theory for dissociation of perchlorate salts in THF*

	Λ_0	Λ_0^T	K_P	K_T
	S cm^2 mol^{-1}	S cm^2 mol^{-1}	$10^7 L\ mol^{-1}$	$L\ mol^{-1}$
LiClO4	140.8	93.8	0.65	24.8
$Mg(ClO_4)_2$	200	67	7.0	193
$Ca(ClO_4)_2$	165	55	5.1	221
$Sr(ClO_4)_2$	160	53	3.9	320

Similar to the ion association model of $LiClO_4$, Fuoss-Krauss triple-ion theory was applied to determinate the quantities of ionic species of perchlorates in non-aqueous media.

After fitting the $\Lambda C^{1/2}$ as a function of concentration, the value of equilibrium constant was deduced. For $Mg(ClO_4)_2$, the K_p and K_T were found to be 7×10^7 and 193 L mol $^{-1}$ assuming Λ_0 and Λ_0^T are 200 and 67 S cm^2 mol $^{-1}$, respectively. All the ionic association parameters for each perchlorate salts are summarized in table.5.2

For an initial concentration of 0.01 mol L^{-1} salts of $Sr(ClO_4)_2$ and $Ca(ClO_4)_2$ in THF, the concentration of ionic species for $Ca(ClO_4)_2$ is lower than 5×10^{-6} mol L^{-1} and for $Sr(ClO_4)_2$, lower than 2×10^{-6} mol L^{-1}. This indicates clearly that the reactions between the e_{THF}^- and $M^{II}(ClO_4)_2$ in THF must occur with the neutral form of the metallic salts, which are in huge excess compared to the ionic forms.

5.3 Solvated electron in neat THF

The solvated electron in THF has a broad absorption band from 400 nm to 2500 nm with one signal peak located at around 2150 nm. The radiolytic yield of solvated electron in pure THF is deduced from the decay and the value of the extinction coefficient of solvated electron (**Figure 5.6, inset**). At 15 ps the yield of hydrated electron is around 4.2×10^{-7} mol L^{-1} J^{-1} but in THF it is only 2×10^{-7} mol L^{-1} J^{-1} and at 3.5 ns it decreases to 0.75×10^{-7} mol L^{-1} J^{-1}. The uncertainty on these values is mainly due to the value of the extinction coefficient of solvated electron in THF. The decay in THF is very fast compared with that of hydrated electron and it is mainly due to the reaction with $THF^{\bullet+}$ because of low dielectric constant and lower viscosity of THF than in water. The relative permittivity ε_r (or dielectric constant) of the liquid is an important parameter. The probability P of an electron (e_s^-) which is thermalized at a distance r from its geminate positive ion ($M^{\bullet+}$) escaping recombination with it is:

$$P = e^{(-r_c/r)} \tag{5.6}$$

Where r_c is the distance at which the Coulomb potential between e_s^- and $M^{\bullet+}$, well known as the Onsager radius:

$$r_c = \frac{e^2}{4\pi\varepsilon_0\varepsilon_r k_B T} \tag{5.7}$$

Where e is the elementary charge ($e = 1.6 \times 10^{-19}$ C), ε_0 is the vacuum permittivity ($\varepsilon_0 = 8.854 \times 10^{-12}$ J^{-1} C^2 m^{-1}), k_B is Boltzmann's constant ($k_B = 1.38 \times 10^{-23}$ J K^{-1}) and T is the temperature in Kelvin. In water at 298 K, where ε_r=78.5, r_c~ 0.7 nm, so that the probability of recombination of solvated electron with positive ions is small in water since the r is a few nanometers. In contrast to this, in THF, ε_r=7.6, r_c~ 7.3 nm, most of electron and ions produced recombine.

Due to the time resolution of our setup, there is no access to the decay occurring during the first 15 ps. The value of the rate constant of this recombination reaction:

$$e_{THF}^- + THF^{\bullet+} \rightarrow \text{Products} \tag{5.8}$$

is diffusion-controlled and larger than 10^{12} s^{-1} dm^{-3} mol^{-1}.[14] The nature of the hole, represented here by $THF^{\bullet+}$ is not known and it stands for all radical cations produced by the pulse. If we consider that the initial yield of ionization in solvent by low LET radiation is around 4.5×10^{-7} mol L^{-1} J^{-1} we have to consider that the presolvated electron in THF can react very quickly with the cation parent due to low solvent polarity and high diffusion of excess electron in THF.

Therefore, more than 50% of electrons (presolvated and solvated) produced in THF recombine in less than 15 ps. Very efficient scavenging of precursor of solvated electron by biphenyl was previously reported.[10]

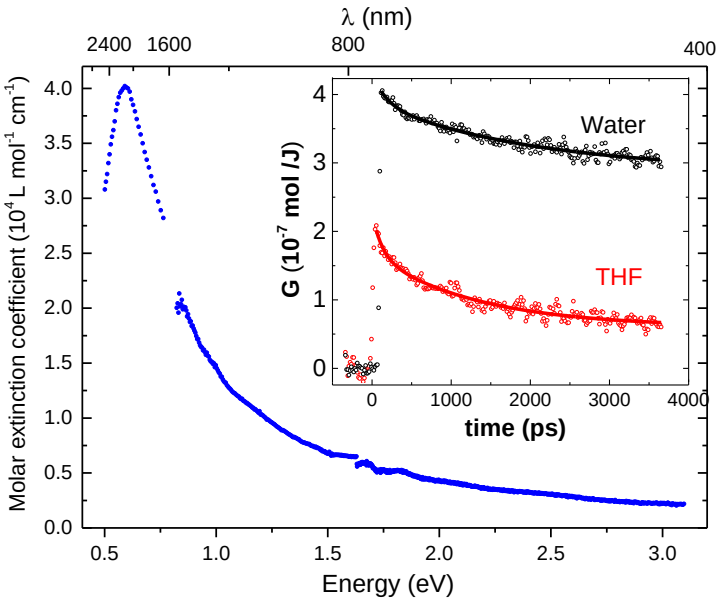

Figure 5.6. *Absorption spectra of solvated electron in THF measured at 20 ps, and scaled in molar extinction coefficient unit. The data from 1600 to 2400 nm are from Jou et al obtained on the microsecond range[8] and those from 1600 nm to 400 nm are deduced from present work which is in agreement with previous results obtained on the microsecond range. Inset: time dependent radiolytic yield of solvated electron in water and in THF[8].*

5.4 Reaction of e_{THF}^- with $HClO_4$

As indicated in Chapter 4, the hydrated electron e_{hyd}^- forms an encounter pairs with hydronium ions on the basis of the spectral changes (blue shift). It is, therefore, quite interesting to find what happened with this reaction in non-polar liquid, THF. First, we observed the absorption band of e_{THF}^- in presence of 0.1 mol L^{-1} as seen in **Figure 5.8**. The shape of the band remain the same and only the absorbance decreases with the delay time which is beyond our expectations at the beginning. It is believed that the low dielectric liquid is in favor of pair formation between electron and acid. This point is certainly true for metal salts ions in THF, a very small amount of ions (10^{-3}–10^{-5} mol L^{-1}) induced a great (400-500 nm) blue shift of the absorption band of e_{THF}^-. In the case of perchoric acid in THF, the dissociation of acid is limited (pK=7.5) which means the acid molecules is solvated by the THF liquid without providing any the "free proton or ions".

$$HClO_4 \rightleftarrows (H^+ClO_4^-)_{THF} \rightleftarrows H^+ + ClO_4^- \qquad (5.9)$$

The kinetics have been investigated in different concentrations of $HClO_4$ solutions (0.01 -0.2 mol L^{-1}). For each concentration, the kinetics are identical and independent on the selected wavelength, suggesting that no transient pairs have been formed. If we plotted the decay in logarithmic form with delay time, it was found that all the decay follow the pseudo first order reaction involving the apparent molar of perchoric acid. The value of the rate constant of this reaction is found to be 7.3×10^{10} L mol^{-1} s^{-1} (**Figure 5.7 Insert**) by linear fitting the kinetics that is much lower a diffusion reaction between two charged species (~10^{11} –10^{12}L mol^{-1} s^{-1}). Given that it is a sort of reaction between the solvated electron and a non-dissociated molecules instead of the mobile charged ions, it was suggested that the rate constant for this reaction high enough to be assigned to a diffusion controlled process. The solvated electron reacts immediately with the acid molecules when they meet with each other without presenting an activation barrier for the formation of an encounter pair.

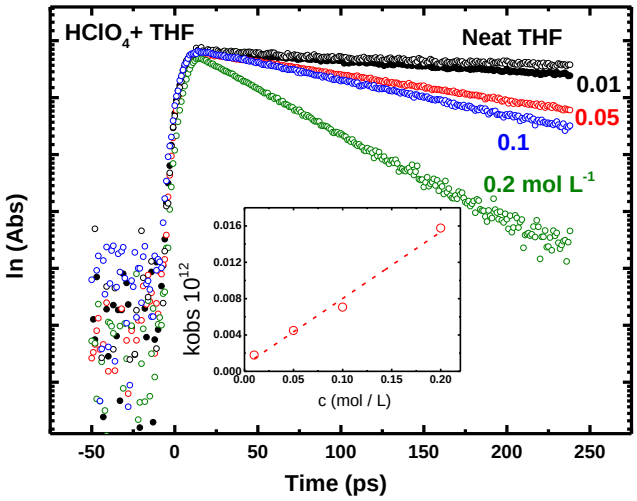

Figure 5.7. *Kinetics of e_{THF}^- observed in THF solutions containing perchoric acid with different concentration from 0.01 up to 0.2 mol L^{-1}.*

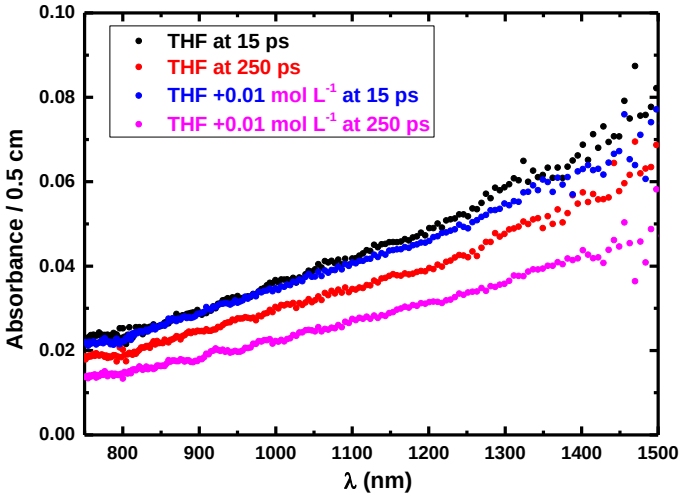

Figure 5.8. *Absorption spectrum of e_{THF}^- observed in THF solutions containing perchoric acid at different delay time.*

5.5 Reaction of e_{THF}^- with $M(ClO_4)_2$ (M: Sr Ca Mg) : Kinetic and Spectra

In solutions containing metal $M^{II}(ClO_4)_2$, the absorption spectra observed at 20 ps are identical to that obtained in pure THF and are due to that of solvated electron in THF. In the presence of Mg^{II} the decay observed at 1500 nm becomes faster with increasing Mg^{II} concentration. The rate constant of the reaction between solvated electron and Mg^{II} deduced from the decay is 1.7×10^{10} mol^{-1} L s^{-1}. By increasing the concentration of Mg^{II} in THF solution, we observe that the kinetics at 730 nm and 1000 nm are also changing (**Figure 5.19**). At 730 nm, in pure THF only decay is observed but this decay is slowed down for 0.01 mol L^{-1} solution and at higher concentration of Mg^{II}, even an increase of the absorbance is observed just after the electron pulse.

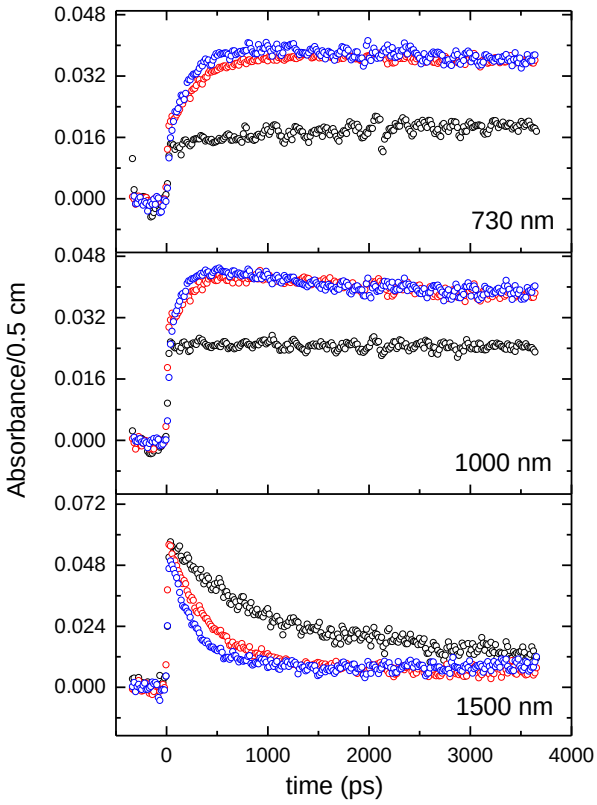

Figure 5.9. *Picosecond pulse radiolysis absorbance measurements at 730 nm, 1000 nm, and 1500 nm in THF with 0.01 mol L^{-1} $Mg(ClO_4)_2$ (black), 0.05 M $Mg(ClO_4)_2$ (red) and 0.1 M $Mg(ClO_4)_2$ (blue)*[15].

The decay at 1000 nm of e_{sol}^- is also slowed down drastically by increasing the Mg^{II} concentration and at highest concentration we observe an increase of the absorbance. The optical absorption spectra measured at 3 ns, show clearly the formation of the new species. The shape of the absorption band recorded at 3 ns depends on the solutions. For solutions containing

Mg^{II}, a large absorption band with a shoulder at 1150 nm, and two bands at around 900 nm and 650 nm are observed (**Figure 5.11**).

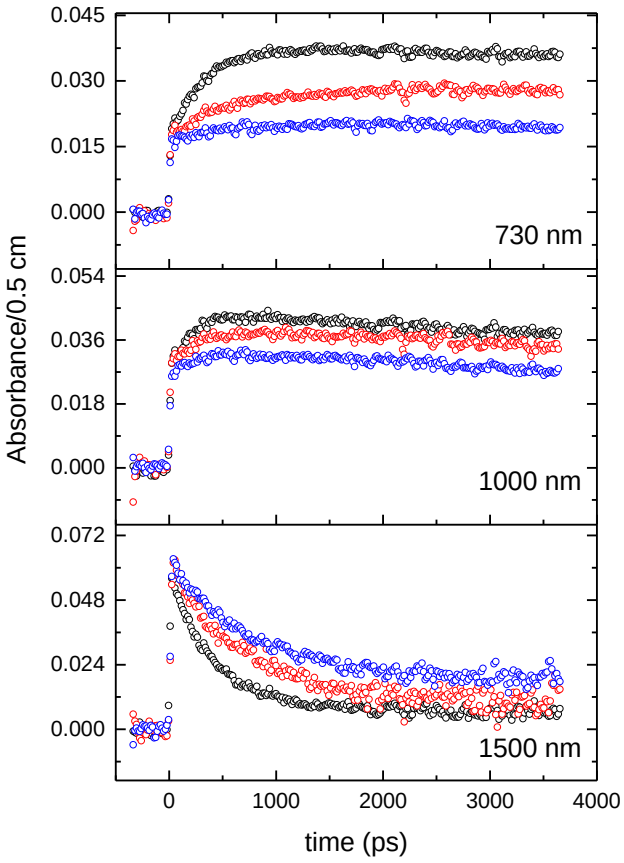

***Figure 5.10**. Picosecond pulse radiolysis absorbance measurements in THF solutions containing 0.05 mol L^{-1} $Mg(ClO_4)_2$ (black), 0.05 M $Ca(ClO_4)_2$ (red) and 0.05 M $Sr(ClO_4)_2$ (blue)[15].*

The reaction occurring between the solvated electron and the cations Ca^{II} and Sr^{II} are slower than what we found with Mg^{II}. Compared to the absorption band of solvated electron, the shift to the visible is more important for the solution containing Mg^{II} and the lowest shift is observed for the solution containing Sr^{II}. The intensity of the absorbance is also more important for solutions containing Mg^{II}. This suggests that the equilibrium between solvated electron and the pair depends on the earth alkaline metal cation. In the case of Mg^{II} due to its lower size, the pairs are more stable than in the two others cases.

It is known that in THF the salt cannot dissociate and even for an initial concentration of 10^{-2} mol dm^{-3} of salt, the concentration of ionic species is very low. This indicates clearly that the reactions between the solvated electron and perchlorates in THF occur with the neutral form of the metallic salts, which is in huge excess compared to the ionic forms.

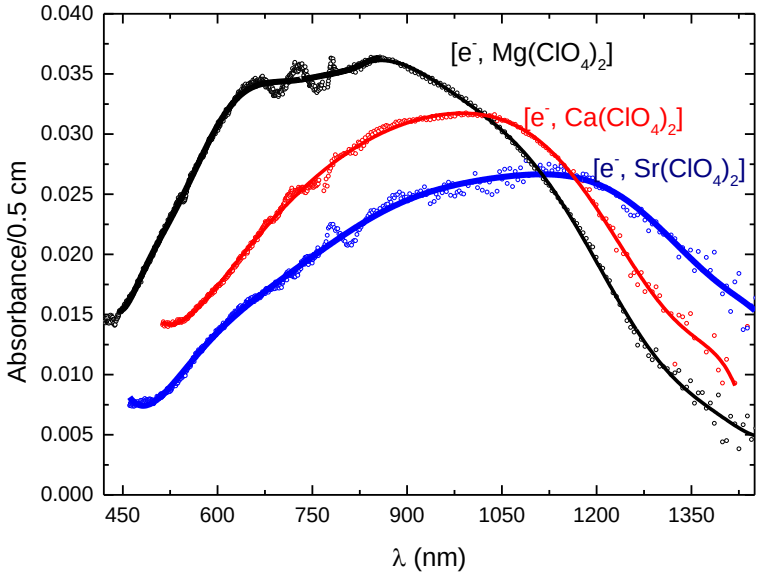

Figure 5.11. *Absorption spectra recorded at 3.5 ns after the electron pulse in THF solution containing 0.05 mol* L^{-1} Mg^{II}, Ca^{II} *and* Sr^{II}. *The oscillations around 780 nm are due to the instability of the laser probe around the fundamental wavelength along the whole translation stage*[15].

5.6 Simulation of transients, (e_{THF}^-, Mg^{II})$_{THF}$

Because of the absorption overlap of the electron and absorbing new species, the number of absorbers was assessed by Singular Value Decomposition of the global matrix, and a MCR-ALS analysis with the corresponding number of species was performed. The analysis of the results show clearly (see **Figure 5.12**) that solvated electron reacts with the earth alkaline metal molecule and the product (e_{THF}^-, Mg^{II})$_{THF}$ has an optical absorption band very different than that of solvated electron in pure THF.

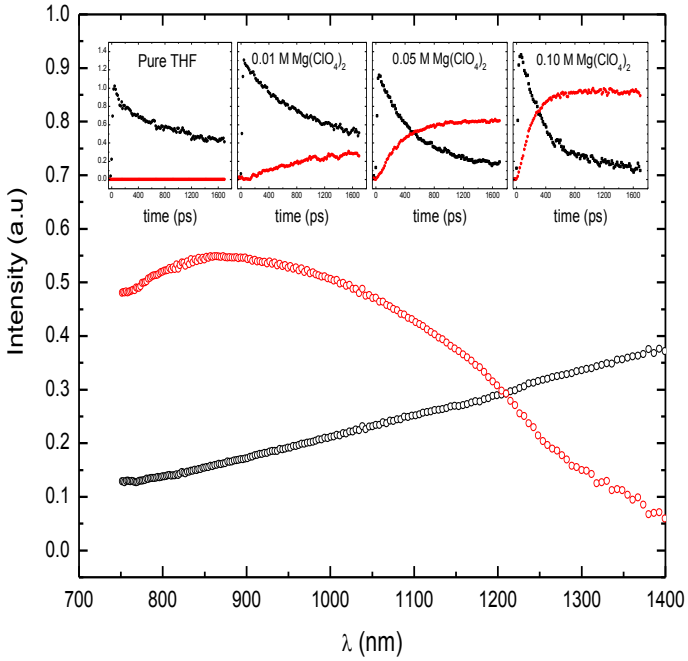

Figure 5.12. *Absorption spectra and kinetics of the two transient species from the global MCR-ALS analysis of all data collected by picosecond pulse radiolysis measurement in pure THF, and solution containing Mg^{II} at 0.01, 0.05 and 0.1 mol L^{-1}.*

In the past we performed Hartree-Fock calculations of the $Mg(ClO_4)_2$ in the presence of an excess electron in a spherical PCM cavity, and found out that the electron did not reduce the solute, but rather stayed in the vicinity of it, forming a so called contact electron-solute pair (noted ($Mg(ClO_4)_2$, e^-)).[16] We also found out that the perchlorate dissociation:

$$\left(Mg\left(ClO_4\right)_2,\ e^-\right) \rightarrow MgO^+\left(ClO_3^-\right)\left(ClO_4^-\right) \qquad (5.10)$$

is very favorable with ΔG = -2.7 eV.[16]

We first tried to determine the structure of the absorbing species. To this aim we tried to optimize the geometry of the anionic solute $[Mg(ClO_4)_2]^-$ and found that the procedure always leads to the dissociated form MgO^+ of equ. (5.10), whatever the (affordable) method used:

B3LYP with large diffuse bases, MP2 with the aug-cc-pvtz basis. We have also supplemented the solute with up to eight explicit THF molecules, and again the geometry optimization lead to the dissociated species.

We have therefore performed Monte Carole simulations with frozen geometries of the perchlorates. We have considered two geometries of these perchlorates, taken in the neutral $Mg(ClO_4)_2$ molecule with two bidentate ligands (its ground configuration) and two monodentate ligands (obtained with the help of a C_3v symmetry constraint. These two perchlorates differ from the isolated perchlorate by one or two elongated ClO bonds, designed to the MgO bonds: the monodentate perchlorate displays short (1.49 Å) and one elongated bond (1.57 Å), the bidentate perchlorate displays two short (1.49 Å) and two elongated bonds (1.57 Å).

The energy fluctuations for three simulations, started with two bidentate (hereafter noted bi – bi) formes, one bi and one mono (bi – mono), and finally two monodentate perchlorates (mono – mono) are shown in **Figure 5.13**.

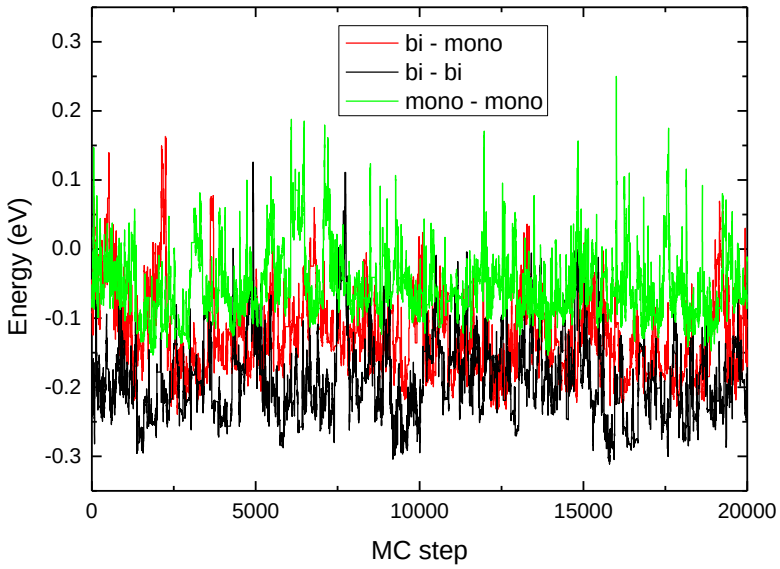

Figure 5.13. *Energy fluctuations of the simulations with mono and bidentate perchlorates (the energy zero is set at -4320. eV). zero is set at -4320. eV)*[15].

It is should be noted that the simulations with the frozen perchlorates preserve their mono *versus.* bidentate binding. This can be seen on **Figure 5.14** where the radial distribution function of MgCl g(r) have been presented. For the bidentate perchlorate g(r) ranges from 2.5 to 3 Å, and in the case of the monodentate perchlorate it ranges from 3 to 3.5 Å. It shows also that the

bi – bi simulation is the most stable one, the mono – mono the less stable one, and that the bi – mono simulation is slightly above the bi – bi simulation, but close to it. The difference of the average energies of the bi – bi and bi – mono simulations amounts to be 0.05 eV.

The absorption spectra corresponding to these three simulations are given in **Figure 5.15** (top). It can be seen that the three simulations result in very different spectra and that the spectra of the bi – bi simulation is very similar to the experimental one, with only a depression between 600 and 700 nm. It is worth noting that this depression is filled up by the spectrum of the bi – mono simulation. Nevertheless the combination of the bi – bi and bi – mono spectra weighed by their Boltzmann factors hardly improves the calculated spectrum (**Figure 5.15**, bottom). In this combination we have multiplied the Boltzmann factor of the bi – mono spectrum by a factor 2, because both bi – mono and mono – bi spectra actually interfere.

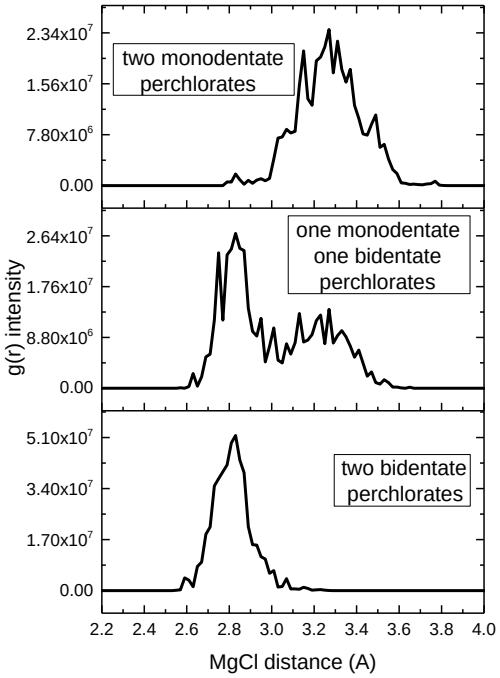

Figure 5.14. *Mg-Cl g(r) functions for the simulations with mono and bidentate perchlorates.*[15]

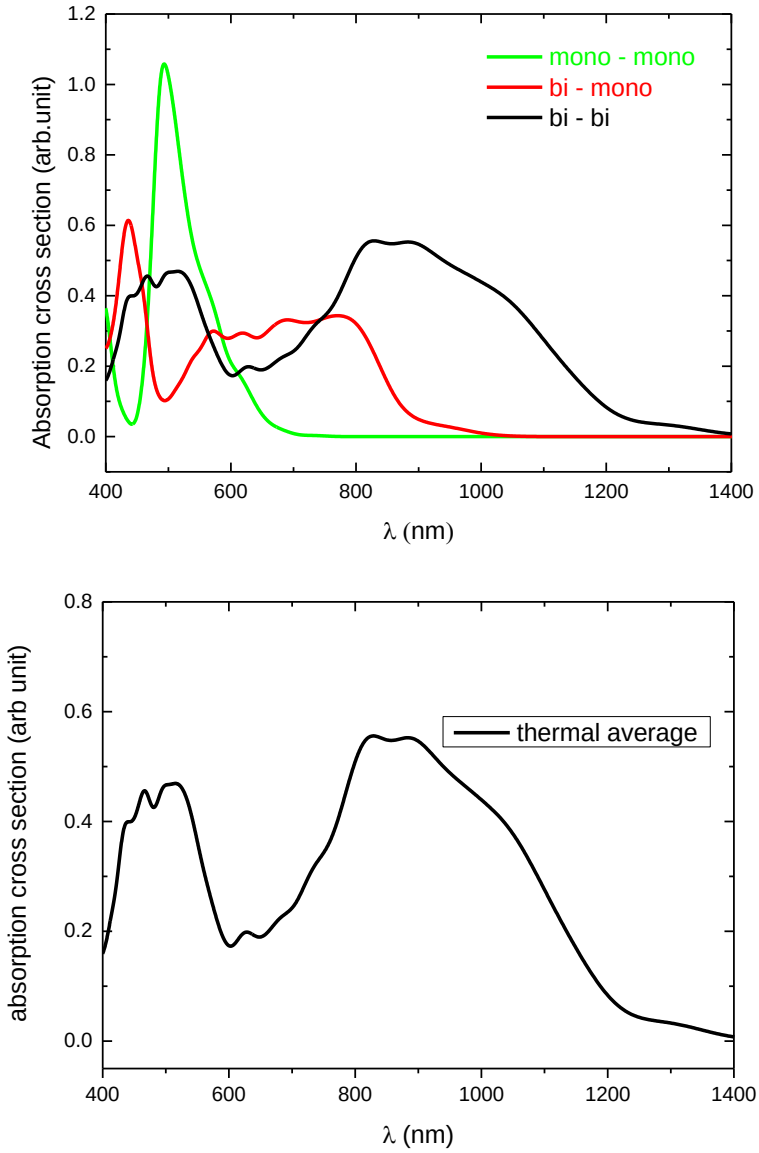

Figure 5.15. *Absorption spectra for the species with mono and bidentate perchlorates*

In **Table 5.3** we give the TDDFT results for the two configurations of the bi – bi simulation, displaying the smallest value (conf. 10450 in the MC list, 1312 nm) and the largest value (conf. 5000 in the MC list, 688 nm) of the first transition energy. The SOMO (singly occupied molecular orbital) and the first three virtual orbitals of these two configurations are shown on **Table 5.3**. It is worth noting that the two SOMOs are somewhat different:

- For the configuration with a large energy transition the orbital is essentially located on the side of the magnesium atom. In this case the solute is exactly what we called in the past *a contact electron solute pair*. In this case we consider that the solute is not reduced by the solvated electron.

- For the configuration with a small transition energy the orbital is located both on the side of the magnesium atom and on the perchlorates. For the sake of simplicity we call this species an reduced *anion*, though the reduction of the solute is only partial.

The present simulations therefore confirm and complement our first insights on this system.[16] The evaluation of the relative weights of these two species, contact pair and anion, is underway. Excitation of the electron from the SOMO toward the first two virtual orbitals (virtual orbitals and 1 and 2 of **Table 5.3**) participates to the broad low energy band of the bi – bi spectrum. Excitation toward the third virtual (virtual orbital 3 of **Table 5.3**) yields the band at 500 nm of the same spectrum. This third virtual is a rather clean *p* orbital of the Mg atom, of A" symmetry with respect of the ClMgCl plane of the solute, for this reason the corresponding band is narrow and depends only slightly of the ligandation mode of the perchlorates, bi or monodentate.

	Conf 5000	**Conf 10450**
virtual 3	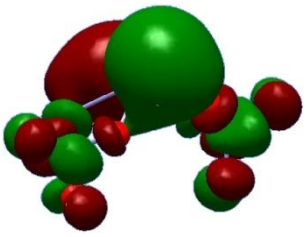	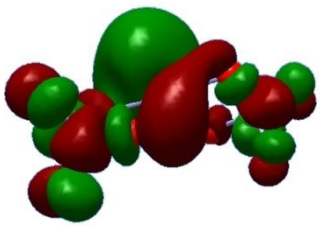
virtual 2	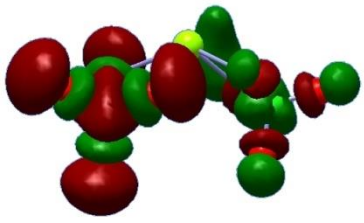	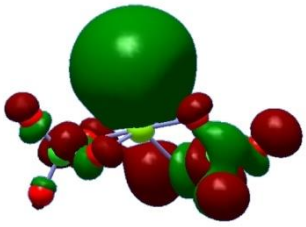
virtual 1	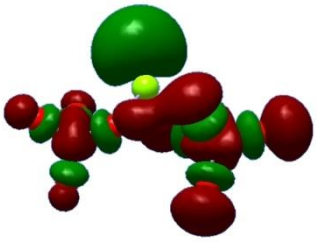	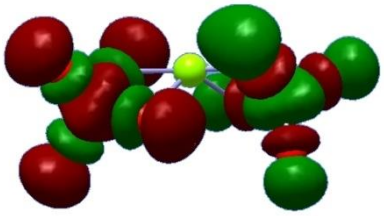
somo	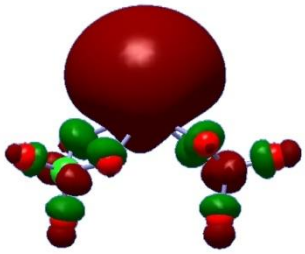	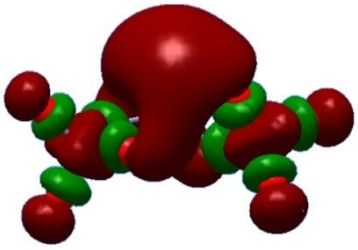

conf. 5000 conf. 10450

transition	ΔE	λ	f	ΔE	λ	f
1	1.802	688	0.1033	0.945	1312	0.1475
2	1.808	686	0.0879	1.148	1080	0.0403
3	1.984	625	0.0911	1.239	1000	0.0953

***Table 5.3**. Top: isodensity surfaces of the SOMO and first three virtuals of the solute for two configurations with a large (conf 5000, on the left) and with a small (conf 10450, on the right) value of the first transition energy. Bottom: transition energies (eV), wavelengths (nm) and oscillator strengths for two configurations with a large (conf. 5000) and with a small value (conf. 10450) of the first transition energy.*

5.7 Reaction of e_{THF}^- with $LiClO_4$: Kinetic and Spectra

First, we present the kinetics observed at in THF solutions containing $LiClO_4$ salts with the concentration from 0.01 up to 1 mol L^{-1} with picosecond pulse radiolysis measurements. Four wavelengths at 730 nm, 1000 nm, 1200 nm and 1400 nm) from Visible to Near IR are selected to probe the decay and formation of the absorbing species after the electron pulse as shown in Fig.5.16 compared with the decay in neat THF, the presence of lithium salts slowed down the decay at each wavelength and a formation process of the new absorbing species was clearly observed at 0.1 mol L^{-1}. However, in more concentrated solutions (0.5 and 1 mol L^{-1}), the kinetics in the near IR region (1200 nm and 1400 nm) differ much from those in visible (730 nm and 1000 nm) with a faster decay with the first 500 ps time delay. More detail information about changing of the transients signal within the initial 250 ps after the pulse was shown in **Figure 5.16**.

Figure 5.17 present the transient absorption spectrums at delay time of 3.5 ns in various $LiClO_4$ salts THF solutions and in neat THF for comparison. A strong blue shift has been observed while displaying two distinct bands, with one peak at around 1200 nm and the other one located at 950 nm. The spectra as the function of delay time in three solutions, 0.01, 0.1 and 1 mol L^{-1} respectively were reported in **Figure 5.18**. With increasing concentration, the initial absorption spectra turns to lower wavelength much faster splitting into several bands and the band at visible part becomes more important at 1 mol L^{-1}.

The overall absorption band of the three cases is large and it is constituted by several absorption bands. It is impossible to understand the existence of the species as well as the corresponding

spectra directly from these observations. However, it can be seen that at least three species including solvated electron are formed after the electron pulse.

In order to ration the reaction pattern, a detail data treatment and dynamic simulations are in progress. The very first results showed that there are four transient species between the electron (both hydrated electron and presolvated electron) and the solutes (monomer and dimer $LiClO_4$) in THF.

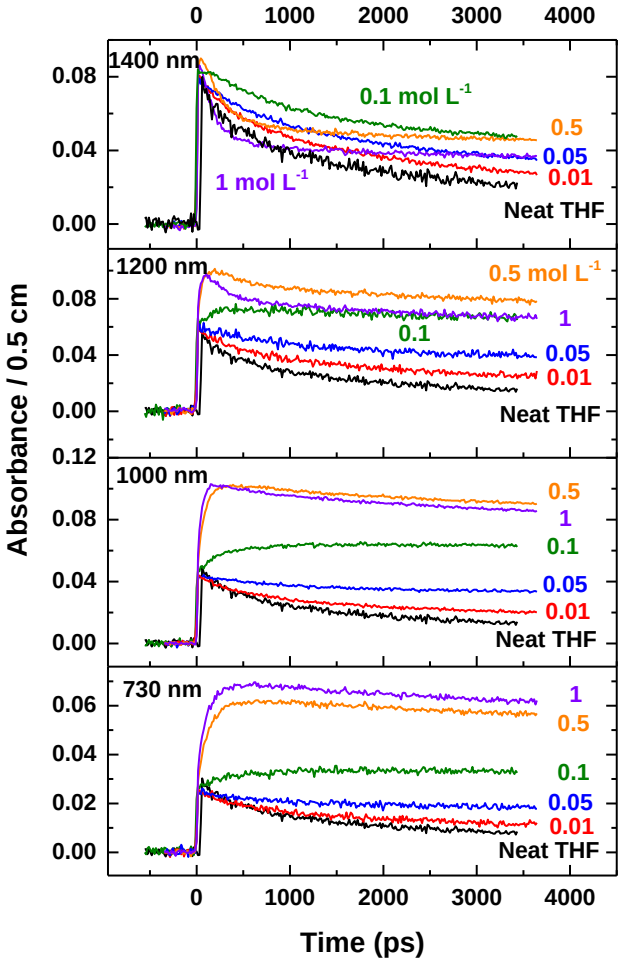

Figure 5.15. *Picosecond pulse radiolysis of kinetics measurements at selected wavelengths (730 nm, 1000 nm, 1200 nm and 1400 nm) in THF solutions containing lithium perchlorate ($LiClO_4$) with different concentration (0.01 – 1 mol L^{-1}).*

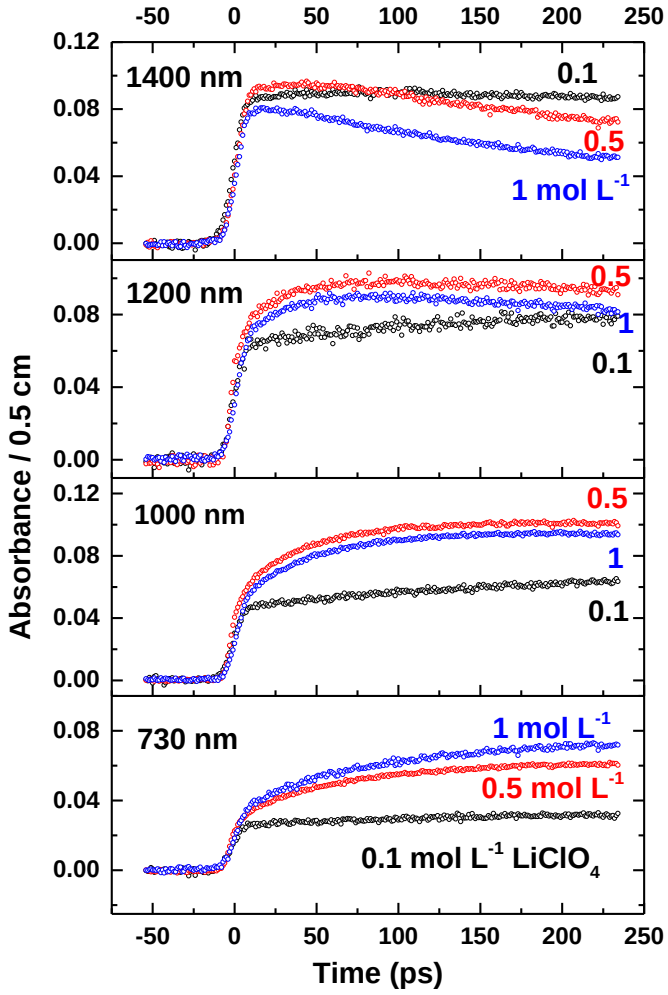

Figure 5.16. *Formation process of intermediates between solvated electron and lithium perchlorate observed at single wavelength.*

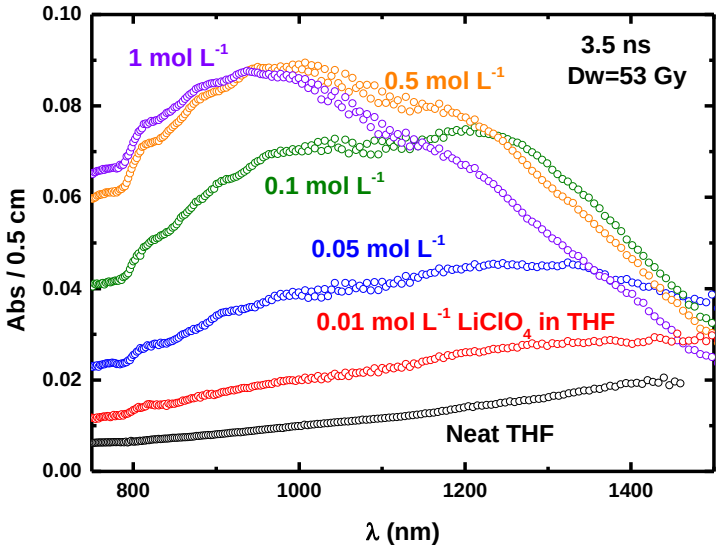

Figure 5.17. *Transition absorption spectrum observed in THF solutions containing $LiClO_4$ salts with different concentrations ranging from 0.01 to 1 mol L^{-1} at delay time of 3.5 ns*

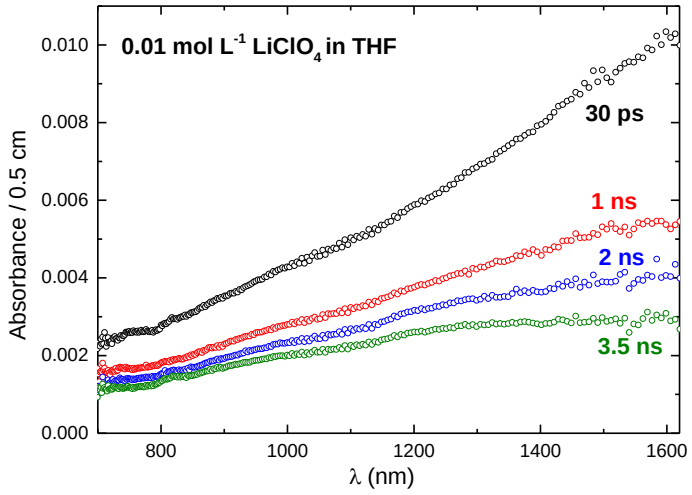

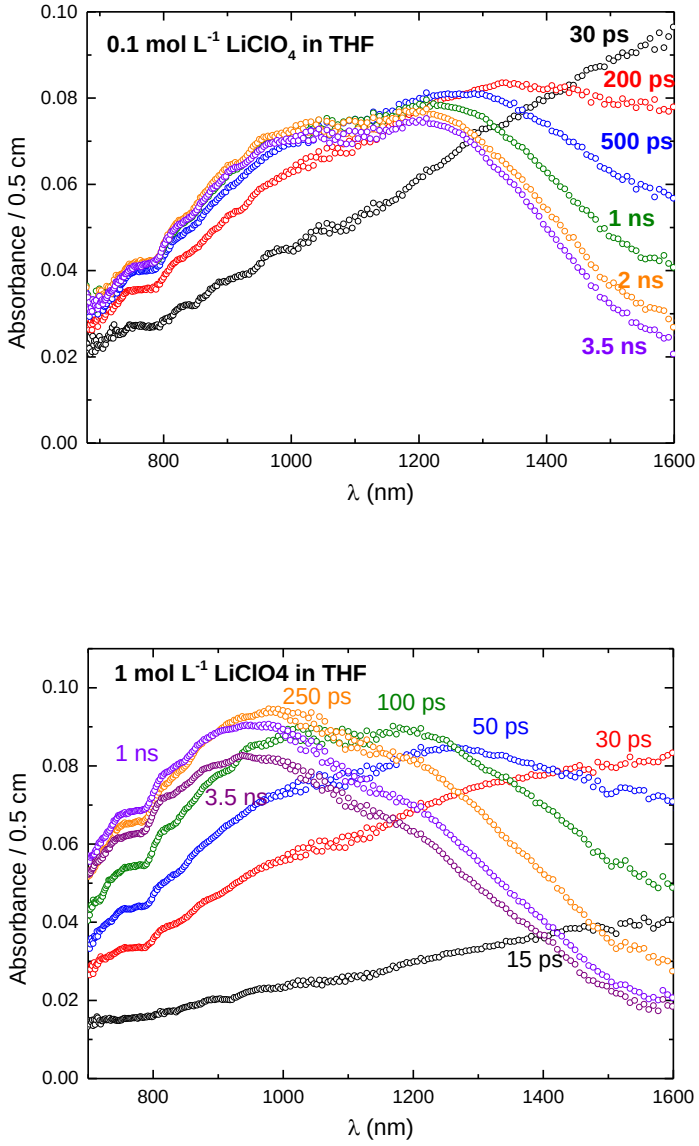

Figure 5.18. *Time-dependent transition absorption spectrum of THF solutions containing 0.01(a), 0.1(b) and 1 mol L^{-1}(c) $LiClO_4$*

5.7 Conclusion and Perspectives

In this chapter, we use picosecond pulse radiolysis coupled with near infrared detection to study the reactivity of solvated electron (e_{THF}^-) in THF towards various perchlorates. The supercontium wavelength is from 730 nm to 1500 nm. It was found the decay of e_{THF}^- in THF is much faster than that in water due to the lower dielectric constant and viscosity. The lower radiolytic yield of e_{THF}^- suggested that the recombination reactions in THF is more efficient. Before subjected to the irradiation, in the THF solutions containing $HClO_4$ with concentration from 0.01 up to 0.2 mol L^{-1}, $LiClO_4$ with concentration from 0.01 up to 1 mol L^{-1}, $M^{II}(ClO_4)_2$ (M: Mg, Ca, Sr) with concentration from 0.01 up to 0.1 mol L^{-1}, the dominating species is non-dissociated molecules. In $LiClO_4$ THF solutions, the dimer species $(LiClO_4)_2$ also formed with the equilibrium with the molecules $LiClO_4$.

In $HClO_4$ THF solutions, the presence of acid molecule has not effect on the absorption spectrum of e_{THF}^-, indicating that the encounter pair between these two reactants is not formed during the reactions. This view is further supported by the kinetics with different concentration of $HClO_4$. The value of rate constant of e_{THF}^- with $HClO_4$ was found to be 7.3×10^{10} L mol^{-1} s^{-1}, which is very similar to the value of a diffusion controlled reaction of solvated electron with an organic molecue in THF.

However, In $M^{II}(ClO_4)_2$ (M: Mg, Ca, Sr)THF solutions, the kinetics show clearly that a transient species is formed within one nanosecond. The absorption spectrum of e_{THF}^- not only has a strong blue shift in presence of Mg^{II} salts but also its shape dramatically changes spitting into two peaks, one at 900 nm, the other one at 650 nm. In order to determine the structure of the absorbing species observed after the electron pulse, Monte Carlo/DFT simulations were carried out in the case of MgII, based on a classical Monte Carlo code and DFT/PCM calculation of the solute. The UV–visible spectrum of the solute is calculated with the help of the TDDFT method. The calculated spectrum is close to the experimental one. It is due to one species, with the fluctuations between a contact pair and an anion.

In $LiClO_4$ THF solutions, the kinetics in different concentrations show that at least three species are formed. The absorption spectrum of e_{THF}^- in $LiClO_4$ solutions is time dependent and also concentration dependent. The theoretical works are in progress for unravelling the complex nature of the reaction of e_{THF}^- towards $LiClO_4$ or its dimers.

Reference

[1] Hart, E. J.; Boag, J. W.Absorption Spectrum of the Hydrated Electron in Water and in Aqueous Solutions *J. Am. Chem. Soc.* **1962**, *84*, 4090−4095

[2] Gould, R. F., ed. *Solvated Electron* Advances in Chemistry Series. NO.50, **1965**.

[3] Baxendale, J. H.; Wardaman, P. Direct Observation of Solvation of the Electron in Liquid Alcohols by Pulse Radiolysis. *Nature*. **1971**, *230*, 449−450

[4] Chase, W. J.; Hunt, J .W. Solvation Time of The Electron in Polar Liquids. Water and Alcohols. *J. Phys. Chem.* **1975**, *79*, 2835−2845

[5] Delaire, J. A.; Delcourt, M. O.; Belloni, J. Mobilities of Solvated Electrons in Polar Solvents from Scavenging Rate Constants. *J. Phys. Chem.* **1980**, *84*, 1186−1189

[6] Holroyd, R. A. The Electron: its Properties and Reactions, in *Radiation Chemistry*, Principles and Applications. Farhaziz and M.A.J. Rodgers (eds), VCH, **1987**, 201

[7] Rossy, P. J.; Schnitker, J. The Hydrated Electron: Quantum Simulation of Structure, Spectroscopy, and Dynamic. *J. Phys. Chem.* **1988**, *92*, 4277−4285

[8] Jou, F. Y.; Freeman, G. R. Shape of Optical Spectra of Solvated Electrons. Effect of Pressure. *J. Phys. Chem.* **1977**, *81*, 909−915

[9] Salmon, G. A. Sedddon, W. A. and Fletcher J. W. Pulse Radiolysis of Solvated Electrons, Ions Pairs, and Alkali Metal Anions in Tetrahydrofuran. *Can. J. Chem.* **1974**, *52*, 3259−3268

[10] Renou, F.; Mostafavi, M.; Archirel, P.; Bonazzola, L.; Pernot, P. Solvated Electron Pairing with Earth Alkaline Metals in THF. 1. Formation and Structure of the Pair with Divalent Magnesium. *J. Phys. Chem. A.* **2003**, *107*, 1506−1516

[11] Jagodzinski, P.; Petrucci, S. Electrical Conductance and Ultrasonic Relaxation for Lithium Perchlorate in Tetrahydrofuran. *J. Phys. Chem.* **1974**, *78* (9), pp 917–925.

[12] Das, D. Ion Association and Solvation Behavior of Some Lithium Salts in Tetrahydrofuran. A Conductivity and Raman Spectroscopic Study. *J. Solution. Chem*, **2008**, 37, 947–955.

[13] Renou, F.; Mostafavi, M.; Archirel, P.; Bonazzola, L.; Pernot, P. Solvated Electron Pairing with Earth Alkaline Metals in THF. 1. Formation and Structure of the Pair with Divalent Magnesium. *J. Phys. Chem. A.* **2003**, *107*, 1506−1516

[14] Cipollini, N. E.; Holroyd, R. A.; Nishikawa, M. Zero Field Mobility of Excess Electrons in Dense Methane Gas. *J. Chem. Phys.* **1977**, *67*, 4636−4639

[15] Ma,J. Archirel, P Uli, S. Pernot, P Mostafavi, M Reduction of Earth Alkaline Metal Salts in THF Solution Studied by Picosecond Pulse Radiolysis. *The Journal of Physical Chemistry A* 2013;117 (51),14048

[16] Renou, F.; Archirel, P.; Pernot, P.; Lévy, B.; Mostafavi, M. Pulse Radiolysis Study of Solvated Electron Pairing with Alkaline Earth Metals in Tetrahydrofuran. 3. Splitting of p-like Excited States of Solvated Electron Perturbed by Metal Cations. *J. Phys. Chem. A.* **2004**, *108*, 987−995

Chapter 6: General Conclusion and Perspectives

Chapter 6: General Conclusion and Perspectives

6.1 General Conclusion

Picosecond Pulse Radiolysis coupled with pump-probe absorption spectroscopy allows us to study the ultrafast electron transfer processes in solutions induced by high energy radiation. The principle of pulse radiolysis is to generate the short-lived species using a pulse of electrons that should be much shorter than the time constants of the subsequent reactions and detect these species by time-resolved optical techniques. The facility ELYSE at Laboratories de Chime Physics composes of a 100 fs femtosecond laser oscillator and a laser – driven radiofrequency gun accelerator delivering the 7 ps electron pulse. The probe light originated from the laser source is covering the wavelength range from 360 nm to 1500 nm to detect the intermediates that absorb in these region. With this tool, it is possible to trace the ultrafast reactions or chemical processes induced by the fast electron taking place on the timescale of picosecond even some on subpicosecond. The picosecond pulse radiolysis setup at University of Tokyo, Tokai, is based on the similar principle but has an electron pulse with much higher energy (20 MeV) than ELYSE (7 MeV). This unique property permits us to further explore the reactions at elevated temperature when the high temperature & high pressure sample setup is coupled with accelerator.

In Chapter 3, picosecond pulse radiolysis techniques were used to observe the kinetics of the $SO_4^{\bullet-}$, $H_2PO_4^{\bullet}$ in highly concentrated sulfuric acid and phosphoric acid solutions over a wide range of concentrations (from 1 mol L^{-1} to neat acid). The experimental results showed clearly that the secondary radical of sulfuric ($SO_4^{\bullet-}$) and phosphoric acid ($H_2PO_4^{\bullet}$) can be formed via two mechanisms: direct electron detachment by the electron pulse (7 ps) and ultrafast electron transfer from the solutes to the radical cation of water $H_2O^{\bullet+}$. The yield of $SO_4^{\bullet-}$ and $H_2PO_4^{\bullet}$ from the direct effect was determined in neat acid as 3.5×10^{-7} and 3.7×10^{-7} mol/J, respectively, which is proportional to the electron fraction of the solutions. After deducing this direct effect for each solutions, the reactivity of the strongest oxidizing species, $H_2O^{\bullet+}$ towards the solutes in highly concentrated aqueous solutions is quantitatively demonstrated and established. The probability of the electron transfer process involving $H_2O^{\bullet+}$ is increasing with the acid concentration and reach a saturated value when the concentration is above 8 mol/L. However, the efficiency of scavenging $H_2O^{\bullet+}$ in sulfuric acid system appears to be greater than that in phosphoric acid solutions. The maximum scavenger yield of $H_2O^{\bullet+}$ in H_2SO_4 system is found to be $5.1 \pm 0.2 \times 10^{-7}$ mol J^{-1} comparing with the lower value of $1.5 \pm 0.2 \times 10^{-7}$ mol J^{-1} in H_3PO_4 system. This difference could be explained by the fact of dimer formation in

phosphoric acid solutions, in which the number of water / solutes contact is considered to be smaller than that of H_2SO_4 solutions. We have also roughly estimated the redox potential value of the couple $H_2O^{\bullet+}/H_2O$ in liquid water to be 3.6 V_{NHE} by assuming the hydration energy of $H_2O^{\bullet+}$ is similar to that of H_3O^+, suggesting that the short-lived radical cation $H_2O^{\bullet+}$ act as a very strong oxidizing species in aqueous solutions.

In Chapter 4, we first presented a direct evidence of the formation of a transient encounter pair between a solvated electron and a hydronium cation (H_3O^+) on the basis of spectral changes (blue shift). The ion pairing $(e_s^-, H_3O^+)_s$ could be only observed in the condition of high concentration (> 0.2 mol L^{-1}) and appropriate temperatures (200-250 °C). The substantial decreasing of the initial yield of hydrated electron at 15 ps in highly concentrated acidic solutions suggested that the presolvated electrons are able to react with hydronium cation (H_3O^+) before they becomes solvated (< 1ps). The scavenging of excess electron is not much temperature dependent in the presence of 0.1 mol L^{-1} from 25 °C up to 250 °C but turn out to be strongly depending on the type of acid and its dissociation in water. For example, in the presence of same amount of H_3O^+ ions, the initial yield of hydrated electron in H_2SO_4 is lower than that in $HClO_4$ solutions followed by H_3PO_4, which means the scavenging efficiency is the greatest in H_3PO_4 system with much less water molecule. The rate constant values of the reaction of hydrated electron with H_3O^+ were measured in a variety of concentrated acidic solutions at ambient temperature as well as elevated temperatures. The ionic strength of the solutions plays an important role in the value of rate constant. The classical Brønsted-Bjerrum model is demonstrated to be valid in the concentration range from 0.01 up to 3 mol L^{-1} by considering the ionic strength as well as the temperature.

In Chapter 5, the reactivity of solvated electron in THF towards a variety of perchlorates are studied by picosecond pulse radiolysis together with theoretical simulations. The dissociation of perchlorates in THF is limited at the concentration ranging from 0.01 to 1 mol L^{-1} and the dominating species are non-dissociated molecules instead of free ions. In $HClO_4$ / THF solutions, the paring of solvated electron was not observed. The reason is attributed to the fast diffusion controlled reactions of solvated electron with $HClO_4$ in THF solutions. However, in $M^{II}(ClO_4)_2$ (M: Mg, Ca, Sr) / THF solutions, the kinetics showed clearly that a transient species is formed within one nanosecond, presenting two distinct peaks in the near infrared region. Monte Carlo/DFT simulations showed in the case of $Mg^{II}(ClO_4)_2$, the intermediate $(Mg^{II}, e_s^-)_s$ is due to one species, with the fluctuations between a contact pair and a reduced anion. In $LiClO_4$ / THF solutions, the kinetics in different concentrations show that at least four transient

species are formed between the electron (both hydrated electron and presolvated electron) and the solutes (monomer and dimer $LiClO_4$) in THF. With primary data analysis and TDDFT (Time dependent DFT) calculations, the species having its own spectra are corresponding to the pairs of electron with $LiClO_4$ monomer, $(LiClO_4)_2$ dimer and $(LiClO_4)_3$ trimer, respectively. This study with the combination of a pulse radiolysis and the DFT simulations provide a new method of using electron as a probe to identifying the nature of salts in non-polar solvent.

6.2 Perspectives

The studied in this thesis are also helpful to some unexplored and challenging topics in radiation chemistry.

6.2.1 Radiation sources

Pulse radiolysis is a well-established time resolved technique to study the chemical reactions (from microsecond to femtosecond) in liquid induced by fast electron with widely used absorption spectroscopy or conductivity detection apparatus. However, it is quite well known that many of radiation induced reactions occur also at the interface and until now time resolved methods have not been applied to address how the presence of solid interface change the spurs reactions of transient species such as hydrated electron and $OH^{\bullet}$ radicals in neat water *etc*. In the near future, the emerging free electron laser technique which uses high energy laser to excite or ionize a sample and meanwhile use the X-rays spectroscopy to probe the chemical changes of the interface, might be a potential way of answering this questions in radiation chemistry.

The type of radiation used in pulse radiolysis is, in fact, the fast electron with very low *LET* value. Unfortunately, not so much effort have been made to develop the other pulsed radiation sources with high *LET* value. In spent nuclear cycling for instance, emission radiation of the fission products, ^{137}Cs, ^{90}Sr or other radioactive elements composes of α, β and γ rays with a wide range of LET. It is well accepted that the geometry of the track structure, free radical reactions, and radiolytic products are strongly dependent on the way of energy deposited and type of radiation. The *LET* effect studied of liquid are mainly underwent using steady state method and model simulations. Therefore, it is also very important to extend the current electron pulse radiolysis to other time resolved techniques using radiation sources with higher LET value.

6.2.2 Issue of $H_2O^{\bullet+}$ water radical cation

The reactivity of H_2O^+ cation in aqueous solutions was demonstrated in aqueous solutions. However, the direct observation of $H_2O^{\bullet+}$ is lack due to the limitation of the time resolution of pulse radiolysis (7 ps). The proton transfer reaction of $H_2O^{\bullet+}$ in neat water is estimated to be around 100 fs or even shorter. $H_2O^{\bullet+}$ probably absorbs in *UV* range (~ 400 nm) with a low extinction coefficient which might be similar with $OH^{\bullet}$ radicals. The femtosecond spectroscopies with a high quality laser pulse (< 30 fs, E > 15 eV) have the possibility of observing this ultrafast reaction. It is also expected the hydration of electron and $H_2O^{\bullet+}$ take place at the same moment. The subtraction of absorption and kinetics of electron is very important to have a clear absorption spectrum of $H_2O^{\bullet+}$ if there is any.

In addition, the excited states of H_2O might also absorb. In order to fully demonstrate the species of $H_2O^{\bullet+}$, the same measurement has to be compared using laser pulse with energy below the ionizing potential even tuning ionizing potential, in which the laser could only excites the water. Theoretical simulations would be very helpful to better understand the nature of $H_2O^{\bullet+}$ in liquid concerning the solvation coordinate number of $H_2O^{\bullet+}$ and having the prediction of absorption spectrum. Delocalization of this positive charge of this water cation over several water molecules has not yet been probed by the simulations.

By using fast electron or laser as the radiation, the ejected electrons are mainly from the valence electron. However, when the radiation energy is around 400-550 eV, $H_2O^{\bullet+}$ might be the complex species since the Auger decay and interatomic columbic decay (ICD) are believed to take place from the ejecting the core-level electrons. The cross section of each events and distribution of each species belonging to the radiation physical issue should be also concerned and discussed in the future.

Concerning the reactivity of H_2O^+, the studies of interfacial oxidation reactions involving H_2O^+ especially towards metal compound (ZrO_2, PuO_2 *etc*) are also relatively rare under irradiation and constitute a challenging subject in radiation chemistry. These possibility of electron transfer is only proposed in my thesis but not yet proven. It is suggested that the picosecond pulse radiolysis of sulfuric acid solutions in the presence of nanoparticles would have different secondary $SO_4^{\bullet-}$ yields comparing with that in sulfuric acid. The idea is that part of water molecules are confined by the nanoparticles that might have a competition effect on the electron transfer to the solutes.

6.2.3 Issue of electron in aqueous

The model of hydrated electron have been a controversial question and the traditional cavity model is repeatly doubted recently by the theoretical scientists. Generally, the water they used for simulations is continuum solvent but the liquid water actually has a special structure of fluctuation with ice like structure and gas like structure as shown by Wernet *et al* . *Science 304 (2004) 995* and many others. These work suggested that in liquid water a statistical distribution of different coordinations can be assumed due to the dynamical motion of the atoms causing the H-bonds to break and reform on a picosecond (*ps*)-time scale. Therefore, the relaxation of electron in water and simulation picture of hydrated electron should take this view into account.

It was found that precursors of hydrated electron react with hydronium ions in my thesis, but this reaction occurs within 1 ps that is on the same timescale of solvation process of electron. In addition, the time evolution of pair formation between hydrated electron and H_3O^+ is missing. The photolysis measurements with femtosecond pulse (100 fs) are invaluable and helpful to explore these questions in depth. The first measurements could be made in 0.5-1mol L^{-1} aicdic solutions because the "blue shift" of the ion pair is more obvious and diffusion reactions is enough slow to be observed within several picoseconds.

The hydration process of electron was extensively studied by femtosecond spectroscopy. The electron is normally produced by direct laser pulse photolysis or indirect charge transfer from ions such as Cl^- in aqueous. The ejected length between the hole and electron would be much different and shorter from that using pulse radiolysis. The statistical energy distribution of excess electron is also considered to be broader than photolysis. The multiply dynamic of relations processes of hydrated electron, therefore, is expected to be modified when the femtosecond electron pulse (80 fs) is applied to this issue.

Publications during my thesis

1. **Jun Ma**, Uli Schmidhammer, Mehran Mostafavi. Picosecond Pulse Radiolysis of Highly Concentrated Phosphoric Acid Solutions: Formation Mechanism of Phosphate Radical. *Journal of Physical Chemistry B* **118**:1-6 (2014). Impact Factor: 3.61

2. **Jun Ma**, Uli Schmidhammer, Mehran Mostafavi. Direct Evidence for Transient Pair Formation between a Solvated Electron and H_3O^+ Observed by Picosecond Pulse Radiolysis. *Journal of Physical Chemistry Letters* 2014; 5:2219-2223. Impact Factor: 6.59

3. **Jun Ma**, Uli Schmidhammer, Pascal Pernot, Mehran Mostafavi. Picosecond Pulse Radiolysis of Highly Concentrated Sulfuric Acid Solutions: Evidence for the Oxidation Reactivity of Radical Cation $H_2O^{\bullet+}$. *Journal of Physical Chemistry A* 2014; 118; 4030. Impact Factor: 2.77

4. **Jun Ma**, Uli Schmidhammer, Pascal Pernot, Mehran Mostafavi. Reactivity of the Strongest Oxidizing Species in Aqueous Solutions: The Short-Lived Radical Cation $H_2O^{\bullet+}$. *Journal of Physical Chemistry Letters* 2014; 5(1):258. Impact Factor: 6.59

5. **Jun Ma**, Pierre Archirel, Uli Schmidhammer, Jean-Marie Teuler, Pascal Pernot, Mehran Mostafavi Reduction of Earth Alkaline Metal Salts in THF Solution Studied by Picosecond Pulse Radiolysis. *The Journal of Physical Chemistry A* 2013; 117 (51),14048. Impact Factor: 2.77

6. Anna Balcerzyk, Uli Schmidhammer, Gregory Horne, Furong Wang, **Jun Ma**, Simon M Pimblott, Aurélien de la Lande, Mehran Mostafavi. Unexpected Ultrafast Silver Ion Reduction: Dynamics Driven by the Solvent Structure. *J Phys Chem B.* 2015 Aug 6;119(31):10096-101.

7. **Jun Ma**, Shinichi Yamashita, Yusa Muroya, Yosuke Katsumura and Mehran Mostafavi. Deciphering the reaction between a hydrated electron and a hydronium ion at elevated temperatures. *Phys. Chem. Chem. Phys.*, 2015, Accepted. Advance Article.

8. **Jun Ma**, Jay A. LaVerne and Mehran Mostafavi. Scavenging the Water Cation in Concentration Acidic Solutions. *The Journal of Physical Chemistry A* 2015. *Submitted*.

Synthèse en Français

Études des Transfer d'électron Ultrarapide en Solutions par la Radiolyse Pulsée Picoseconde

Résumé

Après la découverte des rayons X par W.C Roentgen en 1895, il était important d'étudier et de comprendre la chimie d'interaction entre les rayonnements ionisants (Photon, Particules chargées de grande énergie) et matière. Les formations des radicaux libres et des produits moléculaires par la radiolyse sont caractérisés par leurs courtes durées de vie. Ceci a encouragé les groupes de recherches à développer leurs outils pour qu'ils puissent observer les espèces. La radiolyse impulsionnelle se manifeste comme un outil fondamental permettant de sonder les effets chimiques ainsi que les mécanismes réactionnels dans le milieu étudié.

Le laboratoire de Chimie Physique d'Orsay « LCP » est un laboratoire interdisciplinaire abritant la plateforme « ELYSE » qui est un centre de cinétiques rapides. Grâce au laser femtoseconde et à l'accélérateur d'électrons picoseconde, nous avons eu la possibilité, dans le domaine de la radiolyse, de remonter en temps, en étudiant les effets chimiques dans un milieu réactionnel, jusqu'à ~ 7 ps.

Nous nous sommes intéressés par les transferts d'électron ultrarapide induites par les rayonnements ionisants en solution et ELYSE représentait l'outil principal pour ces études. Les résultats obtenus concernent:

- Etude de l'effet direct du rayonnement ionisant sur les solutions acides concentrées différent ainsi que la vérification de la réaction de transfert d'électron ultrarapide entre le soluté et le trou positif « $H_2O^{\bullet+}$ » issu lors de la radiolyse de l'eau ;
- Etude de le hydratée électron réagit avec hydronium ions dans des solutions aqueuses à température ambiante et aussi à température haut ;

- Etude de l'ionique agrégation de l'électron solvate avec des perchlorates différent en solutions tétrahydrofuranne (THF).

Chapitre I Introduction de la chimie de rayonnement et radiolyse de l'eau

Ce premier chapitre présente une brève introduction des interactions entre les particules chargées de haute énergie et les photons avec la matière, et son effet chimique ultérieure basé sur de nombreuses références. Certaines définitions de la chimie de rayonnement a également été donnés dans ce chapitre. La matière ionisée est dédié à l'eau liquide pour de nombreuses raisons. Premièrement, la plupart de mes recherches de thèse est sur la réactivité de $H_2O^{\bullet+}$ et d'électrons, qui est les espèces ionisées initiales de l'eau; Deuxièmement, radiolyse de l'eau a été étudié pendant près d'un siècle et riche de travaux ont été réalisés autour de lui. Ainsi, il est nécessaire d'introduire quelques notions de base et leur connaissance des travaux antérieurs; troisièmement, l'eau comme un jeu solvant rôle clé commune en radioprotection de la composition humaine et ainsi que l'effet de rayonnement agent de refroidissement dans le réacteur nucléaire.

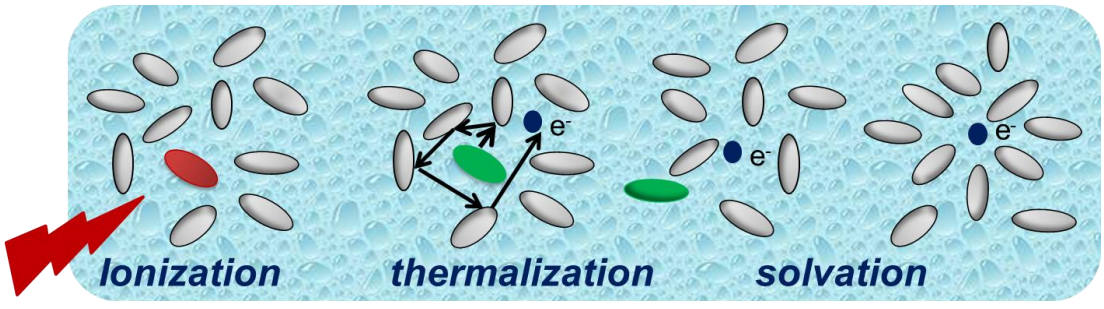

Figure 1.6 Représentation schématique de la formation de l'électron hydraté suivant ionisation de l'eau.

Chapitre II expérimentale Méthodologie: Picosecond Electron radiolyse pulsée

Picoseconde technique impulsion de radiolyse devient une méthode très puissante pour étudier les réactions ultrarapides survenant dans les liquides homogènes induites par les rayonnements ionisants. Haute température et la configuration à haute pression couplée à la picoseconde accélérateur concernent davantage ces études pour être plus réaliste pour l'application de réacteurs nucléaires en tenant compte de l'effet dépend de la température. Le principe de cette technique consiste à utiliser l'accélérateur d'électrons de laser femtoseconde conduit pour délivrer une impulsion d'électrons 7 ps sur l'échantillon et en utilisant la lumière de la sonde pour détecter les changements chimiques induites par l'impulsion. Avec cet outil, les questions de la réactivité des cations de l'eau de courte durée ($H_2O^{\bullet+}$) et électrons presolvaté sont partiellement répondu dans ma thèse, mais ils ont encore besoin d'une impulsion plus de sophistiqué (10-100 fs) d'être clarifiée.

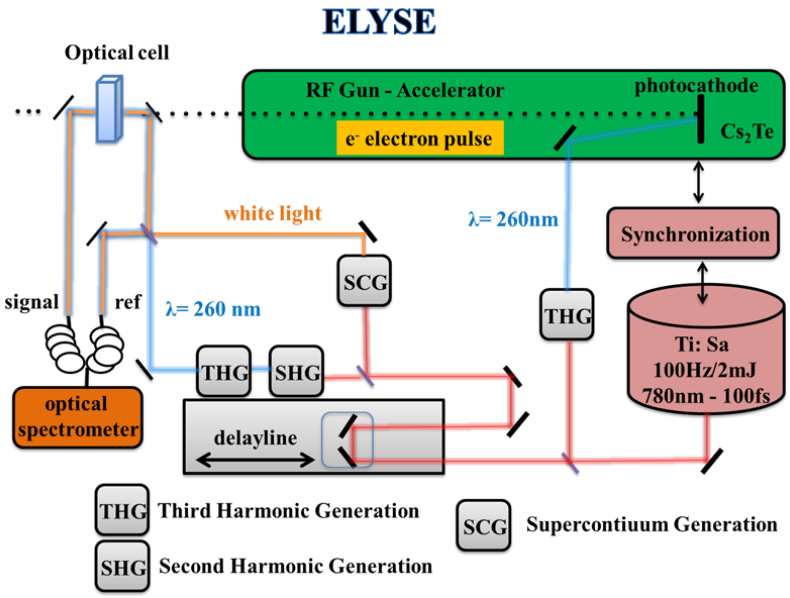

Figure 2. Un schéma général de picosecond electron radiolyse pulsée dans Elyse.

Chapitre III preuve expérimentale de la réactivité de $H_2O^{\bullet+}$ dans des solutions aqueuses

L'interaction de particules énergétiques avec des résultats de l'eau dans l'excitation et l'ionisation des molécules d'eau. Le processus d'ionisation se réfère à la génération des électrons en excès détachés de leurs molécules mères et laissant derrière le trou positive (notée $H_2O^{\bullet+}$). Cela se produit sur l'échelle de temps d'une transition électronique ~ 10-15s. Les processus chimiques plus anciens de $H_2O^{\bullet+}$ suivies eau ionisants en vrac restent encore peu par rapport connu et constitue un sujet difficile dans la chimie de rayonnement. Il est généralement admis que, $H_2O^{\bullet+}$ est une espèce chargée extrêmement instables, qui réagit avec une molécule d'eau voisine de l'échelle de temps de quelques vibrations moléculaires (<100 fs) via le transfert de proton, en formant la H_3O^+ ion et la radical OH.

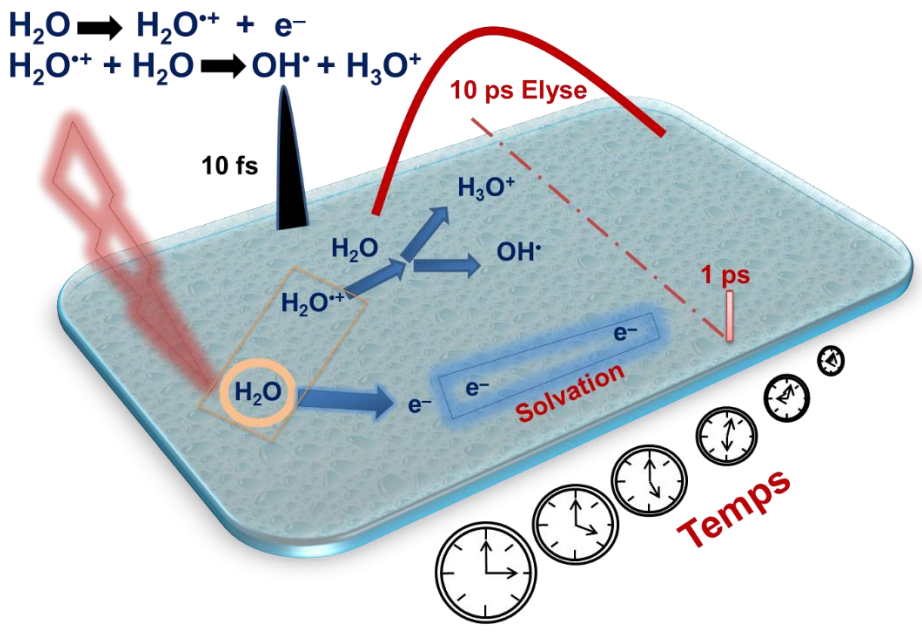

Figure 3. schéma de réactions d'espèces transitoires dans les éperons ou état de distribution homogène produites par irradié dans l'eau, avec du soluté comme un capteur de radicaux.

Il se recombine aussi de retour avec un excès d'électrons sur le site trous avant la détente de l'électron, ce qui donne les états excités de l'eau. Par conséquent, au cours des dernières décennies, il est $OH^{\bullet}$ radicale, au lieu de $H_2O^{\bullet+}$, qui a été pensé comme les principaux intermédiaires oxydants dans indirectement dégâts d'irradiation induite par des matériaux humides ou biomolécules hydratés y compris l'ADN et de nombreuses études cinétiques ont été consacrés à élucider les réactions des opérations impliquant radical $OH^{\bullet}$. Cependant, la réactivité de ce cation $H_2O^{\bullet+}$ radicale, précurseur des radicaux $OH^{\bullet}$ vers la question autre que l'eau environnante, a été une question controversée à long terme et ne sont pas encore entièrement compris.

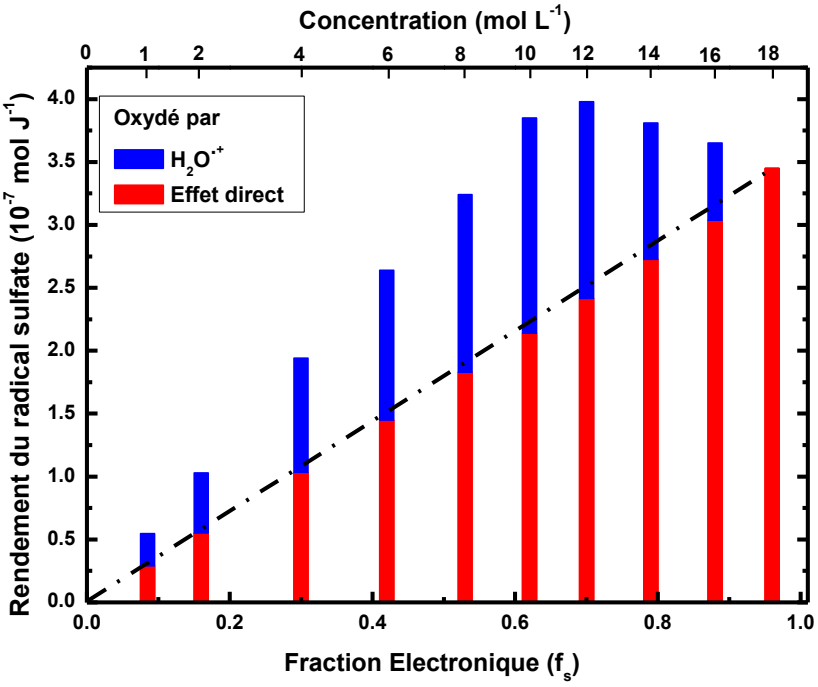

Figure 4. Rendement de la formation de radicaux d'acide sulfurique par rapport à la fraction d'électrons du soluté. La valeur à 18 M est considéré comme le rendement de l'effet direct et est linéairement extrapolée à la concentration zéro. Le rendement supplémentaire est considérée comme étant due à la réaction de transfert d'électrons avec H_2O•+ radical cation.

Les mesures d'impulsion sonde rapportés dans cet ouvrage montrent clairement que le radical d'acide sulfurique et phosphorique peut être formé par deux mécanismes: le détachement d'électrons direct par l'impulsion d'électrons et l'oxydation par le radical cation de l'eau $H_2O^{\bullet+}$. Ce dernier a une durée de vie très courte dans l'eau propre, à savoir moins de 100 fs. Mais en solution très concentrée quand une autre molécule est en contact avec $H2O^{\bullet+}$, le transfert d'électrons devient compétitif contre le transfert de protons avec entourant molécule d'eau. Bien que souvent discuté dans le passé, le rôle de $H2O^{\bullet+}$ dans les processus d'oxydation des systèmes irradiés était surtout un sujet de controverse et de la spéculation. Ici, il a été clairement démontré et quantitativement par la radiolyse de l'impulsion de picoseconde d'acide phosphorique très concentré et d'acide sulfurique que $H2O^{\bullet+}$ peut agir comme un oxydant extrêmement forte. De plus, le rendement radiolytique de $H2O^{\bullet+}$ H2SO4 à se révèle être de 5,3 ± 0,1 x 10-7 mol J-1. Cette valeur est raisonnable et est supérieur au rendement de radiolyse de l'électron solvaté publié à temps très court (1 ps). En fait, dans la première ps, la recombinaison entre géminées électrons presolvaté et radicale cation $H2O^{\bullet+}$ produit et de réduire le rendement de l'électron hydraté. En plus de l'irradiation de solutions concentrées de donateurs forts ou même faibles électrons, le phénomène d'oxydation directe par $H2O^{\bullet+}$ peut effectivement avoir lieu partout où les probabilités de ses voisins les plus proches étant H_2O ou une autre molécule sont comparables. Tel est le cas dans les interfaces lorsque des molécules d’eau irradiée sont en contact avec d'autres molécules.

Cependant, la formation de radicaux phosphate à travers le trou de l'eau de balayage dépend de la concentration de l'acide phosphorique; en général, il est plus faible que le rendement de l'oxydation dans des solutions d'acide sulfurique de la même concentration. La principale raison de cette différence est attribuée à la formation d'espèces dimères dans l'acide phosphorique concentré, en d'autres termes, la géométrie de liaison hydrogène dans la première couche de solvatation de H_3PO_4. Jusqu'à présent, dans le mécanisme d'oxydation seulement $OH^{\bullet}$ et H_2O_2

sont évoqués, mais nos résultats montrent clairement que même si $H_2O^{\bullet+}$ est de courte durée, son implication dans les mécanismes d'oxydation, doit être prise en compte.

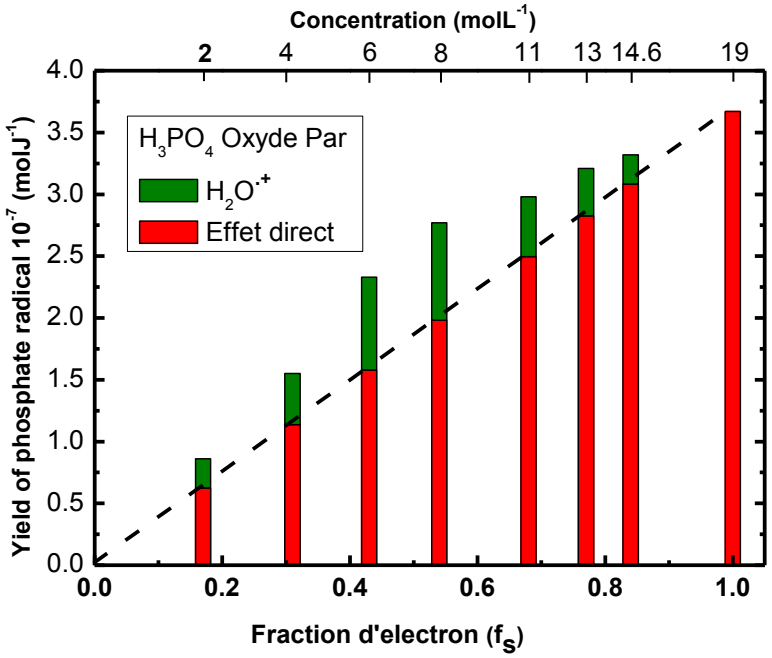

Figure 5. Rendement radiolytique de radical par rapport à la fraction d'électrons du soluté acide phosphorique. Le rendement obtenu à 19 mol L-1 est considéré comme le rendement de l'effet direct qui est linéairement extrapolée au (ligne pointillée) zéro. La contribution de superliner (barres vertes) est due à la réaction de transfert de charge impliquant l'eau radical cation $H_2O^{\bullet+}$.

- La radiothérapie et la radiobiologie: Il est connu que de grandes quantités d'hydratantes molécules d'eau sont en contact direct avec des biomolécules comme l'ADN ou des protéines. Lorsque le rayonnement ionisant est présent, une partie de l'énergie de rayonnement est absorbé directement par ADN et rompt les liaisons des sucres, des phosphates et des bases nucléiques, tandis qu'une partie du rayonnement est également absorbée par l'eau adjacente à l'ADN. Dans ce cas, le généré $H_2O^{\bullet+}$ cations radicales peuvent induire une chimie différente de $OH^{\bullet}$ radicaux et la conséquence est la production de radicaux de biomolécules secondaires qui n'a pas été encore été examinés auparavant. ,

- Traitement et stockage du combustible dans l'industrie nucléaire: Le combustible nucléaire usé est traitée dans des solutions aqueuses d'acide nitrique très concentrées et dans ce cas, le cation H_2O•+ radicale peut réagir avec des ions nitrate pour donner le $NO_3^{\bullet}$ radicale qui est aussi un très espèces oxydants. En variante, lorsque les déchets radioactifs de faible et moyenne est revêtue par du ciment ou de tout autre matériau poreux, l'effet de l'interface est très étendue et la formation du cation radical $H_2O^{\bullet+}$ et ses réactions d'oxydation doit être pris en compte.

- Lorsque le noyau d'une centrale nucléaire entre en contact avec de l'eau, comme cela est arrivé lors de l'incident de Fukushima au Japon, la quantité de rayonnement déposé à l'interface du carburant / eau exposée est important. Bien que nous ne fournissons pas de preuves, le présent travail suggère que, dans cette situation, la corrosion des métaux par $H_2O^{\bullet+}$ peut être impliqué.

Chapitre V Sonder l'hydratée Electron jumelé avec hydronium ions dans des solutions aqueuses

La réaction entre un électron hydraté et d'un cation hydronium H3O + (ou D3O +) dans de l'eau pour former un radical hydrogène atome est procédés chimiques les plus élémentaires en liquide. D'un point de vue pratique, que la H • atome est un des précurseurs de la formation de H2, des informations sur le mécanisme et la constante de vitesse de H • la formation est une question clé pour la chimie se produisant dans les réacteurs nucléaires et les traitements de combustible nucléaire. Cette réaction a fait l'objet de plusieurs études utilisant la méthode impulsion de radiolyse depuis la première observation de l'électron hydraté en 1962 par Hart et Boag. -6 Il est bien reconnu que, au cours de cette réaction, le réarrangement des molécules de solvant autour de deux électrons et ions H3O +, signifie que la vitesse de réaction de ce processus à la température ambiante ne soit pas contrôlé par la diffusion. La réaction peut par modéliser comme le mécanisme suivant:

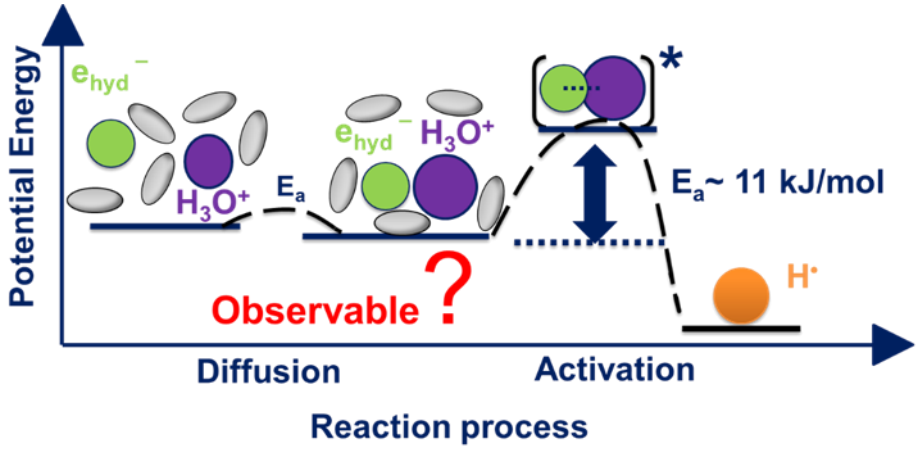

Figure 6. Un schéma représentant pour la réaction d'électron hydraté avec l'ion hydronium, H_3O^+.

La réaction de l'électron hydraté avec des cations hydronium est l'un des procédés chimiques les plus élémentaires de la chimie de rayonnement. Dans ce chapitre, plusieurs questions ont été abordées à l'aide d'impulsions picoseconde radiolyse. Tout d'abord, le déplacement chimique du spectre d'absorption sur la concentration en acide présente une preuve directe de la formation de la rencontre transitoire "de paire d'ions" avant de produire $H^{\bullet}$ atome. A température évaluée, ce changement ne pouvait être observé dans un état contraint à forte concentration d'acide (0,1 mol L^{-1}) et une température (entre 200 et 250 ^{o}C). Deuxièmement, l'importante diminution du rendement initial d'électron hydraté suggère que l'électron presolvaté est capable de réagir avec hydronium cation (H_3O^+) avant qu'il ne devienne solvaté (< 1ps). Pour une concentration donnée de 0,1 mol L-1 H3O +, cependant, cette réaction d'électrons est balayé presolvaté pas, en fait, accéléré par l'augmentation de la température. En outre, l'efficacité balayée varié avec le type d'acides. Comme la réaction implique la quantité d'ions H + dissociée, cette variation est probablement due à la différence dans le degré de dissociation de l'acide et de rapport molaire entre H^+ / H_2O pour perchoric, l'acide sulfurique et l'acide phosphorique pour chaque concentration. Troisièmement, la valeur de la constante de vitesse de cette réaction est fortement influencée par la force ionique qui est liée à la concentration. Le modèle de Brønsted-Bjerrum classique est mise en évidence d'être valable dans l'intervalle de concentration de 0,01 à 0,1 mol L-1 en prenant en compte la force ionique, ainsi que la température. A une concentration plus élevée (> 0,5 mol L^{-1}), la valeur constante de vitesse est à nouveau mesurée dans trois différents types d'acides. Avec une telle grande quantité de solutés initié la solution, le "électron hydraté" se révèle être «électron solvaté» et la réaction de recombinaison de charge dans ce système complexe doit encore plus d'idées dans la microstructure de ces solutions acides.

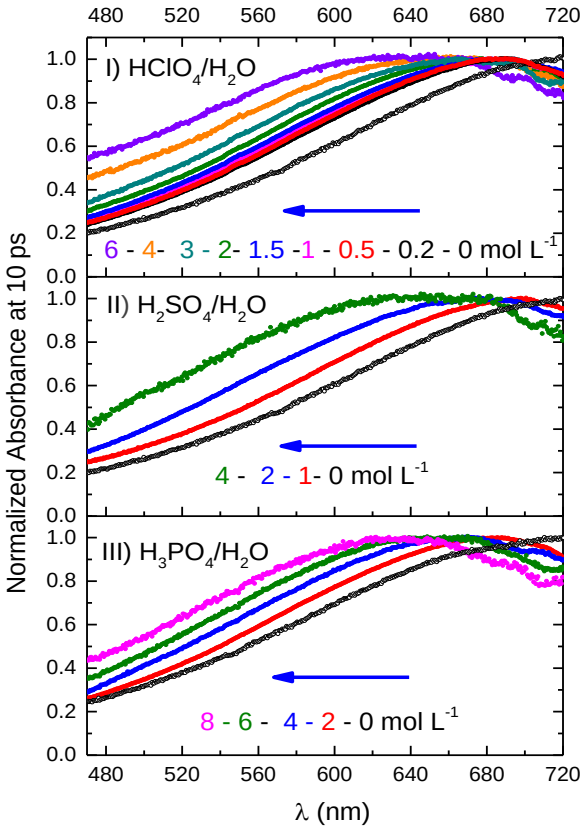

Figure 7. Spectre d'absorption mesuré normalisé à un retard de 10 ps à trois solutions acides (perchlorique, l'acide sulfurique et l'acide phosphorique) à différentes concentrations.

Chapitre V ionique Agrégation des solvatés Electron avec des perchlorates dans le tétrahydrofuranne (THF)

Dans ce chapitre, nous utilisons picoseconde radiolyse pulsée couplée à une détection infrarouge proche pour étudier la réactivité de l'électron solvaté (e_{THF}^-) dans le THF vers divers perchlorates. La longueur d'onde est de 730 supercontium nm à 1500 nm. Il a été constaté le déclin de e_{THF}^- dans le THF est beaucoup plus rapide que dans l'eau en raison de la constante diélectrique et la viscosité plus faible. Le rendement radiolytique inférieur de e_{THF}^- suggéré que les réactions de recombinaison dans le THF est plus efficace. Avant soumis à l'irradiation, dans les solutions contenant du THF avec HClO4 concentration de 0,01 à 0,2 mol L^{-1}, $LiClO_4$ à la concentration de 0,01 jusqu'à 1 mol L^{-1}, $M^{II}(ClO_4)_2$ (M: Mg, Ca, Sr) avec une concentration de 0,01 à 0,1 mol L^{-1}, est l'espèce dominante molécules non dissociées. Dans les solutions $LiClO_4$ THF, les espèces dimères $(LiClO_4)_2$ également formés à l'équilibre avec les molécules $LiClO_4$.

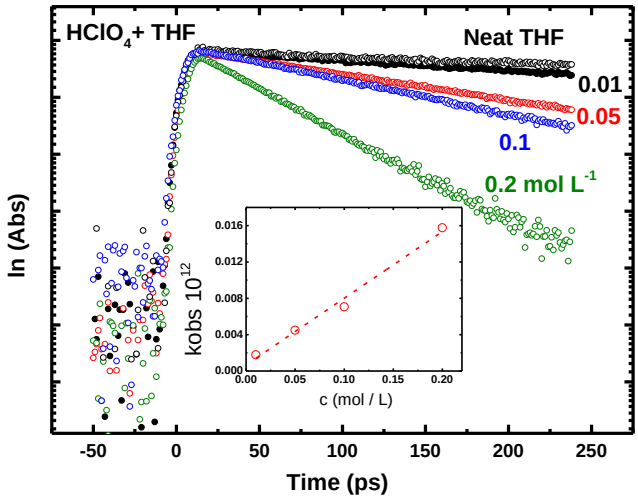

Figure 8. Cinétique de e_{THF}^- observé dans les solutions de THF contenant de l'acide perchoric avec différentes concentrations de 0,01 à 0,2 mol L^{-1}.

Dans les solutions $HClO_4$ THF, la présence de molécule d'acide n'a pas d'effet sur le spectre d'absorption de e_{THF}^-, ce qui indique que la paire de rencontre de ces deux réactifs ne se forme pas au cours de la réaction. Ce point de vue est également soutenu par la cinétique avec une concentration différente de HClO4. La valeur de la constante de vitesse de e_{THF}^- avec $HClO_4$ a été jugée 7,3 $\times 10^{10}$ $Lmol^{-1}$ s^{-1}, ce qui est très proche de la valeur d'une réaction de diffusion contrôlée dans le THF.

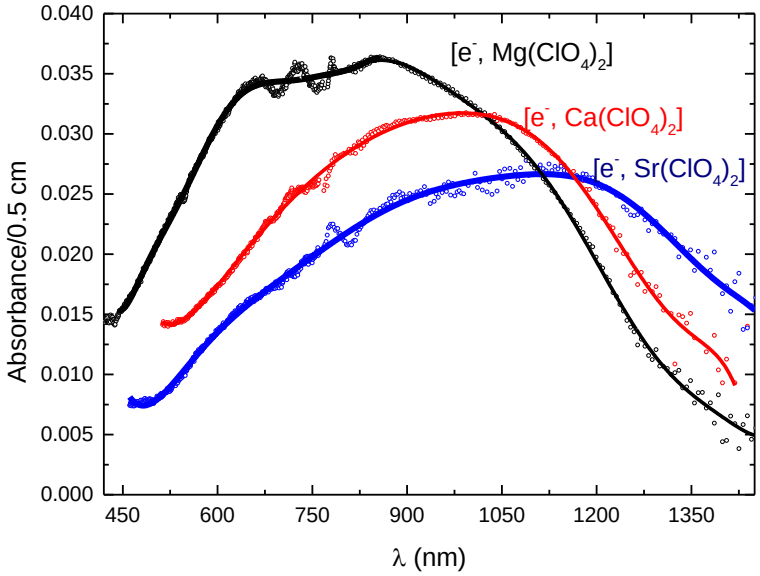

Figure 9. Les spectres d'absorption enregistré à 3,5 ns après impulsion d'électrons dans une solution de THF contenant 0,05 mol L^{-1} Mg^{II}, Ca^{II} et Sr^{II}. Les oscillations autour de 780 nm sont dues à l'instabilité de la sonde laser autour de la longueur d'onde fondamentale le long de toute la phase de traduction

Toutefois, M^{II} $(ClO_4)_2$ (M: Mg, Ca, Sr) des solutions de THF, la cinétique montrent clairement qu'une espèce transitoire est formée à l'intérieur de la nanoseconde. Le spectre d'absorption de e_{THF}^- a non seulement un fort décalage vers le bleu en présence de sels Mg^{II} mais aussi sa forme de façon spectaculaire change cracher dans deux pics, l'un à 900 nm, l'autre à 650 nm. Afin de déterminer la structure des espèces absorbantes observés après l'impulsion d'électrons, des

simulations de Monte Carlo / DFT ont été réalisés dans le cas de Mg^{II}, sur la base d'un code classique de Monte Carlo et calcul de la DFT soluté / PCM. Le spectre du soluté UV-visible est calculé à l'aide de la méthode de TDDFT. Le spectre calculé est proche de l'expérimental. Elle est due à une espèce, avec des fluctuations entre une paire de contacts et un anion.

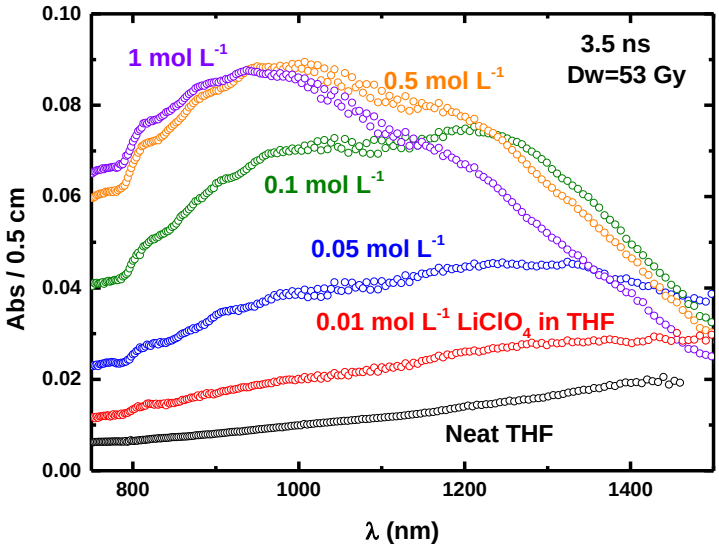

Figure 10. Spectre d'absorption de transition observée dans des solutions contenant des sels de THF LiClO4 avec différentes concentrations allant de 0,01 à 1 mol L^{-1} au temps de retard de 3,5 ns

Dans les solutions de THF $LiClO_4$, la cinétique différente de la concentration montre que les au moins trois espèces sont formés. Le spectre d'absorption dans les solutions de e_{THF}^- $LiClO_4$ dépend du temps et aussi dépendante de la concentration. Les travaux théoriques sont en cours pour démêler la nature complexe de l'agrégation ionique de e_{THF}^- vers LiClO4 ou ses dimères.

université PARIS-SACLAY
ÉCOLE DOCTORALE
Sciences chimiques : molécules, matériaux, instrumentation et biosystèmes

Titre : Étude des Transferts d'électrons Ultrarapides en Solutions par Radiolyse Pulsée Picoseconde

Mots clés : Transferts d'électron, Radiolyse Pulsée Picoseconde, Radicaux de l'eau

Résumé : L'interaction de particules énergétiques avec l'eau peut produire l'excitation et l'ionisation des molécules d'eau. Le processus d'ionisation se rapporte à la génération de l'excès d'électrons détachés de leurs molécules parentes et laissant derrière le trou positive (notée $H_2O^{\bullet+}$). Cela se produit sur le calendrier d'une transition électronique ~ 10^{-15}s. Les processus chimiques plus anciens de $H_2O^{\bullet+}$ et l'excès d'électrons vers autre question suivie de l'eau en vrac ionisants restent encore peu par rapport connu et constitue un sujet difficile dans la chimie rayonnement.
Dans ma thèse, les techniques de radiolyse d'impulsions picoseconde ont été utilisés pour observer la cinétique de la $SO_4^{\bullet-}$, $H_2PO_4^{\bullet}$ dans de l'acide sulfurique très concentré et solutions d'acide phosphorique sur une large gamme de concentrations (de 1 mol L^{-1} à l'acide pur)
Le les résultats expérimentaux montrent clairement que le radical secondaire de sulfurique ($SO_4^{\bullet-}$) et de l'acide phosphorique ($H_2PO_4^{\bullet}$) peuvent être formés par l'intermédiaire de deux mécanismes: détachement d'électrons direct par l'impulsion d'électrons (7 ps) et le transfert d'électrons ultra-rapide des solutés au radical cation de l'eau $H_2O^{\bullet+}$. La réactivité des espèces oxydantes fortes, $H_2O^{\bullet+}$ vers les solutés dans des solutions aqueuses très concentrées est quantitativement démontré.
On a également observé l'excès d'électrons peut réagit avec les cations d'hydronium (H_3O^+) très vite dans l'acide par transferts d'électrons.

Title : Ultrafast electron transfer in solutions studied by picosecond pulse radiolysis

Keywords : electron transfer, water radicals, picosecond pulse radiolysis

Abstract : The interaction of energetic particles with water results in the excitation and ionization of water molecules. The ionization process refers to the generation of the excess electrons detached from their parent molecules and leaving behind the positive hole (denoted as $H_2O^{\bullet+}$). This occurs on the timescale of an electronic transition ~10^{-15} s. The earliest chemical processes of $H_2O^{\bullet+}$ and excess electron towards other matter followed water ionizing in bulk still remain relative little known and constitute a challenging subject in radiation chemistry. Picosecond pulse radiolysis techniques were used to observe the kinetics of the $SO_4^{\bullet-}$, $H_2PO_4^{\bullet}$ in highly concentrated sulfuric acid and phosphoric acid solutions over a wide range of concentrations (from 1 mol L−1 to neat acid).
The experimental results showed clearly that the secondary radical of sulfuric ($SO_4^{\bullet-}$) and phosphoric acid ($H_2PO_4^{\bullet}$) can be formed via two mechanisms: direct electron detachment by the electron pulse (7 ps) and ultrafast electron transfer from the solutes to the radical cation of water $H_2O^{\bullet+}$.
In addition, we observed that the excess electron reacts with the hydronium ions (H_3O^+) very rapidly before its solvation process via electron transfer. The formation of an encounter transient pair between hydrated electron and H_3O^+ was suggested on the basis of spectral changes (blue shift).